SOLUTION-PROCESSABLE CHARGE TRANSPORT LAYERS FOR PHOSPHORESCENT OLEDS

A Dissertation
Presented to
The Academic Faculty

by

Carlos A. Zuniga

In Partial Fulfillment
Of the Requirements for the Degree
Doctor of Philosophy in Chemistry

Georgia Institute of Technology

May 2011

SOLUTION-PROCESSABLE CHARGE TRANSPORT LAYERS FOR PHOSPHORESCENT OLEDS

Approved by:

Dr. Seth R. Marder, Advisor
School of Chemistry & Biochemistry
Georgia Institute of Technology

Dr. Bernard Kippelen
School of Electrical & Computer Engineering
Georgia Institute of Technology

Dr. Jean-Luc Brédas
School of Chemistry & Biochemistry
Georgia Institute of Technology

Dr. Elsa Reichmanis
School of Chemical & Biochemical Engineering
Georgia Institute of Technology

Dr. David M. Collard
School of Chemistry & Biochemistry
Georgia Institute of Technology

Date Approved: March 24, 2011

To my parents

ACKNOWLEDGEMENTS

First and foremost, I am deeply appreciative to my thesis advisor Dr. Seth Marder for providing me with invaluable guidance over the years of my doctoral studies. Furthermore, I'm thankful for his motivation and help in developing my abilities to view scientific problems in new and critical ways. I am grateful to Dr. Stephen Barlow and Dr. Mariacristina Rumi for their invaluable discussions on science related to my projects. I am incredibly indebted to Dr. Yadong Zhang for his expertise and help in overcoming synthetic issues, as well as helping to further develop my skills in the lab. I am thankful to the members of the Marder group for being wonderful labmates and more importantly friends. In particular, I'm grateful to Igor Coropceanu and Jassem Abdallah for their collaboration and assistance with different aspects of my research. I am appreciative of the members of my committee for their time, comments, and assistance during the different stages of my studies. I would also like to acknowledge the Brédas group for providing quantum-mechanical calculations for some of the materials developed. I am especially grateful to Dr. Bernard Kippelen and different members of his group (Dr. Andreas Haldi, Dr. Sung-Jin Kim, and Dr. Dengke Cai) for their invaluable collaboration and expertise in testing organic materials developed during my studies for organic light-emitting diode devices.

Finally, I would like to thank my friends and my family for their incredible support over the last few years. To my parents, words cannot express how truly appreciative I am of their support and understanding when I decided to embark on this journey, and most importantly for their love.

TABLE OF CONTENTS

LIST OF TABLES

LIST OF FIGURES

LIST OF SCHEMES

LIST OF SYMBOLS AND ABBREVIATIONS

AFM Atomic force microscopy

AIBN 2,2′-azo-bis(isobutyronitrile)

Alq_3 Aluminum tris(8-hydroxyquinoline)

BCB Benzocyclobutene

BCP 2,9-dimethyl-4,7-diphenyl-1,10-phenanthroline

CBP 4,4′-(dicarbazol-9-yl)biphenyl

DCC Dicyclohexylcarbodiimide

DFT Density functional theory

DMAP *N,N*-Dimethylaminopyridine

DMSO Dimethylsulfoxide

DSC Differential scanning calorimetry

EA Electron affinity

EQE External quantum efficiency

EML Emissive layer

ETL Electron-transport layer

FIrpic [(bis-4,6-difluorophenyl)-pyridinato-N,C2']picolinate iridium (III)

FPt [2-(4',6'-difluorophenyl)pyridinato-$N,C^{2'}$)](2,4-pentanedionate) platinum (II)

GPC Gel permeation chromotography

HOMO Highest occupied molecular orbital

HTL Hole-transport layer

IC Internal conversion

IP Ionization potential

$Ir(ppy)_3$ *fac* Tris(2,2'-phenylpyridyl) iridium (III)

ISC Intersystem crossing

ITO Indium tin oxide

L Luminance

LE Luminance efficiency

LUMO Lowest unoccupied molecular orbital

M_n Number average molecular weight

M_w Weight average molecular weight

mCP (1,3-di(9H-carbazol-9-yl)benzene

mCPy N,N'-dicarbazolyl-3,5-pyridine

NMR Nuclear magnetic resonance

OLED Organic light-emitting diode

PAG Photoacid generator

PEDOT-PSS

PBD 2-(biphenyl-4-yl)-5-(4-*tert*-butylphenyl)-1,3,4-oxadiazole

PDI Polydispersity index

PE Power efficiency

PVK Poly(*N*-vinylcarbazole)

PL Photoluminescence

rms Root mean square

ROMP Ring-opening metathesis polymerization

RTP Rapid thermal processing

T_c Crystallization temperature

T_g Glass transition temperature

T_m Melting temperature

TAG Thermoacid generator

TFVE Trifluorovinyl ether

TGA Thermogravimetric analysis

THF Tetrahydrofuran

TPA Triphenylamine

TPD *N,N′*-Diphenyl-*N,N′*-bis(3-methylphenyl)-(1,1′-biphenyl)-4,4′-diamine

UV-vis. Ultraviolet visible

SUMMARY

In the last decade, the continued development of phosphorescent organic light-emitting diodes (OLEDs) has permitted great progress in the efficiencies that can be achieved for a variety of colors. Typically, the organic materials used in these highly efficient multilayer devices have been processed by vacuum sublimation. Although sublimation offers many advantages, it has some disadvantages, such as potentially high cost and deposition area limitations. As an alternative, solution-processable polymers such as poly(*N*-vinylcarbazole) and others have been explored in recent years. Despite the potential ease of fabrication of layers (from solution) that can be achieved using polymers, these materials also come with their own disadvantages including difficulty in purification and issues with the fabrication of multilayers. Despite these issues, the limited amount of research has yet to clearly show whether polymers are viable alternatives to vacuum-processed layers for achieving efficient OLEDs.

In this thesis, a series of charge transport moieties were synthesized and converted to side-chain homopolymers. These moieties were specifically incorporated as side groups onto a norbornene polymer backbone with the intention to impart ease of solution processing without resulting in major changes to the properties of the core transport group. In Chapter 3, several types of carbazole containing groups were explored as hole-transport and as host polymers for phosphorescent emitters. In Chapter 4, ambipolar charge-transport molecules containing both hole- (carbazole) and electron-transport moieties (including oxadiazole and triazole) were designed and converted to side-chain polymers, as well. In addition, the design of these ambipolar molecules was undertaken in

such a way as to avoid strong charge-transfer effects that could narrow the optical gap and lower the triplet energy; therefore, these molecules might be candidates for blue phosphorescent OLEDs. Finally, some of these charge transport materials were studied in OLED devices in collaboration with the Kippelen group (School of Electrical and Computer Engineering) and shown to give promising results.

Multilayers fabricated from solution-processed materials can be complicated by issues of layer damage/destruction (upon subsequent processing of additional layers). This issue was addressed in the thesis through the development and evaluation of crosslinkable side-chain copolymers containing both a carbazole-based hole transport group and one of several different crosslinkable co-monomers. In addition, a crosslinkable carbazole-based small-molecule was also synthesized and evaluated. For these materials, the crosslinkable groups chosen for study included thermally and/or photochemically initiated moieties such as benzocyclobutenes, trifluorovinyl ethers, oxetanes, or bis(styrene). Although crosslinking was achieved, for several of these materials the processing times could take several hours. In order to reduce the times needed to crosslink these materials, a study of rapid thermal processing (RTP) in collaboration with Dr. Jassem Abdallah was pursued to further reduce the time required to insolubilize the films from hours to thirty minutes or less; which could be beneficial from a device manufacturing point of view.

CHAPTER 1

An Introduction to Organic Light-Emitting Diodes

1.1. Introduction

In this introductory chapter I will outline the basic processes involved in OLEDs which are central to all chapters of this thesis. In each the chapters that follow I provide a review of the literature pertinent to the subject of each topic of research described in that chapter. Organic light emitting diodes (OLEDs) have been the focus of intense study since the late 1980s, when Tang and VanSlyke[1] at Eastman Kodak reported the first example of an OLED demonstrating an external quantum efficiency of 1%. Since that time, research has continued to demonstrate the potential of OLEDs as viable systems for display and lighting applications. From a fundamental perspective, these devices work by injection of charges (holes and electrons) from metal electrodes into organic semiconducting layers which transport through the device and recombine to form excited states (excitons) that emit light upon relaxation.

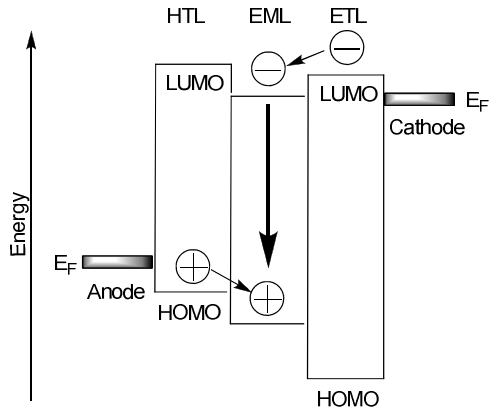

Figure 1.1. Schematic of simple multilayer OLED. HTL = hole transport layer, EML = emissive layer, ETL = electron transport layer, and E_F refers to the Fermi energy of electrodes.

Although progress in OLED research has resulted in improved device performance over the last two decades, this thesis is aimed at addressing the development and study of polymers for use as solution processable charge transport or host layers, the design and study of hosts that combine hole and electron transport moieties, and the development of methods to simplify the fabrication of solution-processed multilayers, which could potentially produce further advancements.

1.2. Organic Light-Emitting Diodes (OLEDs)

1.2.1. Early Work and History of OLEDs

Examples of electroluminescence generated from organic crystals were reported as early as the 1960s. Pope *et al.*[2] observed that single crystal anthracene (when sandwiched between electrodes) would emit light upon application of a voltage of ~ 400 V.

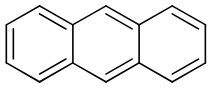

Figure 1.2. Anthracene.

Similarly, Helfrich *et al.*[3] demonstrated a system with electron and hole injecting electrodes to produce electroluminescence from a single crystal of anthracene and showed that the blue light observed originated from fluorescence of the crystal. Although additional research showed that certain organic compounds were capable of light emission from electrically generated excited states, these examples required high voltages that limited their usefulness for such purposes as commercial lighting or displays. For

example, Partridge *et al*.[4] demonstrated electroluminescent devices made with double-layer thin-films of poly(N-vinylcarbazole) with blue emissive properties.

In 1987, Tang and VanSlyke[1] developed a double layer structure that combined a hole transporting diamine layer adjacent to an electron transporting 8-hydroxyquinoline aluminum (Alq_3) layer to afford a device architecture of ITO/diamine/Alq_3/Mg:Ag (10:1). By shifting the recombination zone for holes and electrons away from the electrode to the interface between the transport materials, a dramatic improvement in efficiency was produced. An external quantum efficiency of up to 1.0 % at high brightness levels while operating under a forward bias below 10 V was observed. These results motivated new interest in organic electroluminescence. In 1990. Burroughes *et al*. produced the first example of a polymer-based OLED.[5]

A limitation with early OLEDs resulted from the use of fluorescence-based organic emitters that limited the amount of excitons that could be used to produce emission to a maximum of 25% (see further discussion below). In the late 1990s, Forrest and co-workers[6] reported OLEDs where an organic layer was used as a host for phosphorescent transition-metal organometallic emitters. Such an approach made it possible to theoretically capture up to 100% of the excitons formed in the device to produce light (see further discussion below).

Ongoing research over the last couple of decades has demonstrated the feasibility of these electroluminescent devices for both display and lighting applications.[7] In addition, progress in OLEDs has been built upon new developments in organic charge-transport and host materials, phosphorescent emitters, fundamental studies to comprehend device processes, and the optimization of device fabrication, amongst others.

For example, Kido and co-workers[8] have reported blue phosphorescent OLEDs with an EQE of 25% (46 lm/W at 1,000 cd/m^2) which is one of the best reported blue devices to-date.

1.3. Overview of OLED Processes

For the purposes of introducing OLEDs, the following sections discuss injection, transport and recombination of charges. Specific examples and classes of organic materials (for a variety of functions) and common moieties used are provided further below and in the introductions of subsequent chapters. For these sections, specific examples of organic materials are not discussed, but these materials may be assumed to represent organic semiconductors where π-conjugation that is not extensively delocalized (such as in conjugated small-molecules).

1.3.1. Charge Injection into Organic Semiconductors

The injection of charges from an electrode to an organic layer and can be viewed as arising from redox processes at the metal-organic interface under an applied voltage. In the case of hole injection, the anode oxidizes (removes an electron from) the HOMO of an organic semiconductor producing a radical cation (hole). Conversely, the cathode reduces (adds an electron to) the lowest LUMO of an organic semiconductor producing a radical anion (electron).

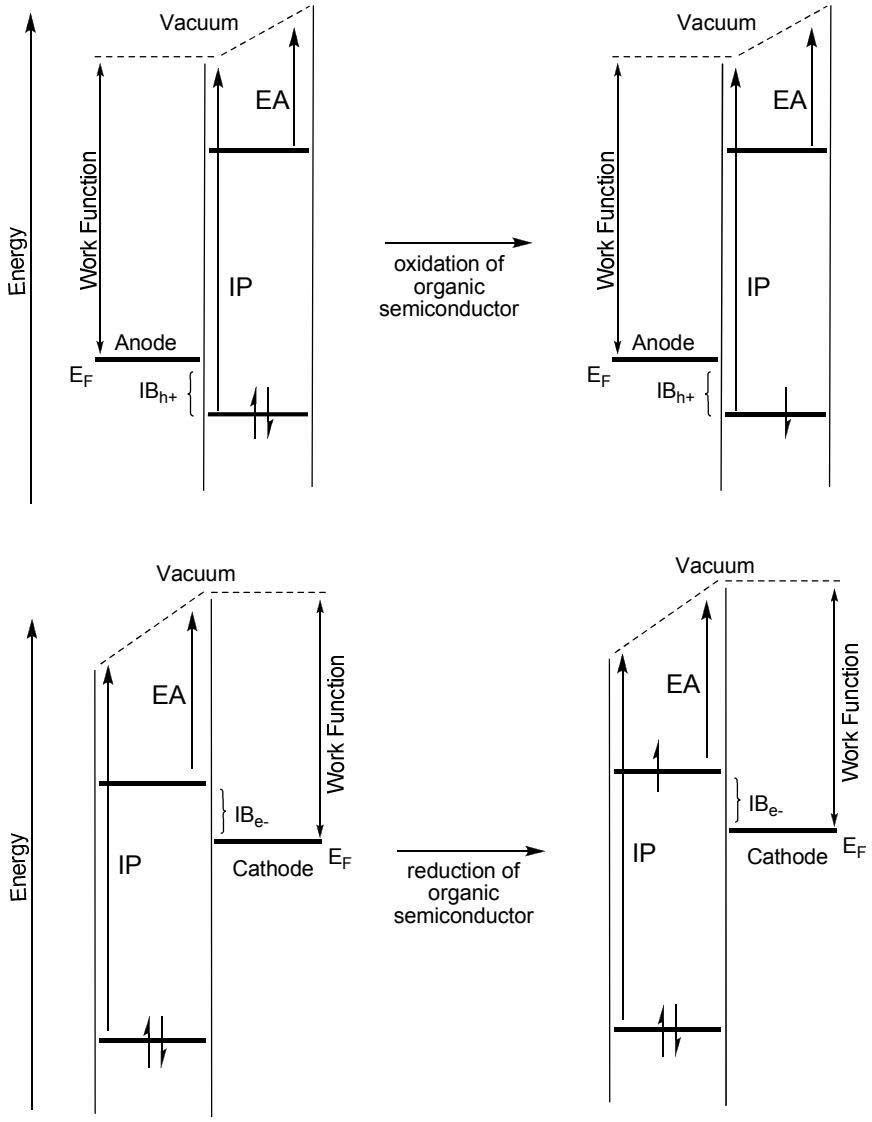

Figure 1.3. Hole (above) and electron (below) injection from metal electrodes into organic semiconductors under the influence of an applied bias (where E_F denotes the Fermi energy of the metal electrodes and IB_{h+} and IB_{e-} denote the injection barriers of the charges).

The energy difference between the Fermi level (E_F) of a metal electrode and the ionization potential (IP) and electron affinity (EA) of an organic semiconductor can be used to estimate the injection barriers for hole or electron injection. Although the relative alignments between the electrode and organic layer are useful in choosing transport materials for interfaces, the process of charge injection may be more complex than

suggested by the diagram above. Studies have shown that behavior at metal-organic interfaces can be complicated by the formation of interface dipole barriers[9,10] (that can originate from several sources; see references) leading to deviations in the barriers from those predicted from the simple vacuum level alignments.

The mechanism of charge injection from the metal electrode into an organic material has been studied by several models including charge tunneling[11,12] or thermionic emission,[13-15] but metal-organic charge injection remains the subject of continued research due to difficulties in studying such processes.

1.3.2. Charge Transport

In the case of structurally disordered (i.e. amorphous) organic materials with highly localized charged states (as can be the case for small-molecules with poor intermolecular overlap to neighboring molecules[16]), studies (theoretical and experimental) have treated charge transport as occurring through a random hopping mechanism.[17-19]

For injected holes and electrons, transport via hopping-type processes can be considered on the basis of donor (D) and acceptor (A) reactions:

$$D + A^{+} \rightarrow D^{+} + A \quad (1.1)$$

$$D^{-} + A \rightarrow D + A^{-} \quad (1.2)$$

which can be treated as electron-transfer reactions and described according to Marcus theory.[20] The rate of electron transfer (k_{ET}) can, therefore, be described by the following equation[21]:

$$k_{ET} = \left(\frac{4\pi^2}{h}\right) {H_{DA}}^2 \left(\frac{1}{(4\pi\lambda kT)}\right)^{1/2} exp\left[\frac{-(\Delta G^0 + \lambda)^2}{4\lambda kT}\right] \quad (1.3)$$

where h is Planck's constant, H_{DA} represents an electronic coupling term (between the donor and acceptor), λ represents the reorganization energy (vide infra), k represents the Boltzmann constant, T is the temperature, and ΔG^0 is the Gibbs free energy difference (between reactant(s) and product(s)).

The process may be considered by looking at the potential energy surfaces for the simultaneous electron transfer between donor and acceptor molecules occurring via a vertical transition (based on the Franck-Condon principle[22,23]).

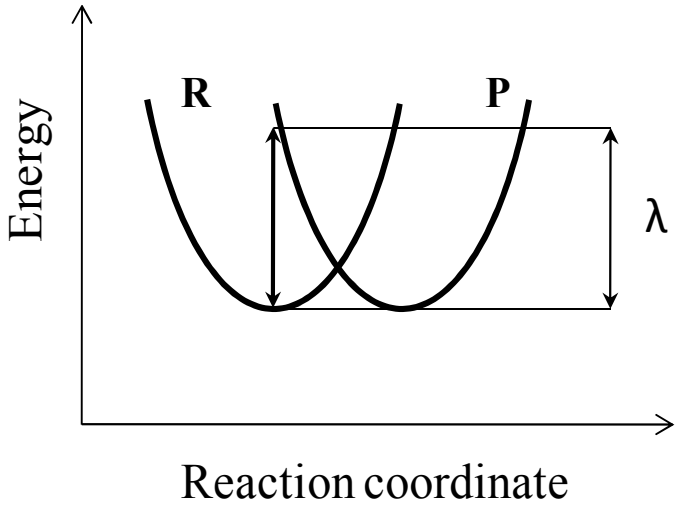

Figure 1.4. Potential energy surfaces of reactants (R) and products (P) for electron transfer process such as those shown in equations (1.1) or (1.2) (where the donor and acceptor are the same species and consequently $\Delta G^0 = 0$). λ represents the reorganization energy.

Following the transition, the product molecules relax to their new minima (bottom of potential wells); the latter process giving rise to the reorganization energy term (λ).[24] The reorganization term, therefore, represents the energy cost necessary to adopt a relaxed geometry following electron transfer. Accordingly, the rate of electron transfer increases as the reorganization term decreases. In the above figure, which

represents a self-exchange process (where the donor and the acceptor are the same molecule) and the ΔG^0 term is consequently zero only the electronic coupling term (H_{DA}) and the reorganization energy (λ) as the primary factors influencing the electron transfer rate.

The speed at which these charge carriers drift under the influence of an applied electric field[25] is described by the magnitude of the charge mobility (denoted μ; measured in $cm^2\ V^{-1}\ s^{-1}$) which is a function of the electron transfer rate.

1.3.3. Charge Recombination

Migrating hole and electron charge carriers that encounter each other within a given radius known as the Coulombic capture radius, r_c, may combine to form a bound electron-hole pair called an exciton.[26] This occurs when the Coulombic binding energy is to equal or greater than the thermal dissociation energy, kT.[13,27] The equation below defines the Coulombic capture radius:

$$r_c = \frac{e^2}{4\pi\varepsilon\varepsilon_0 kT} \qquad (1.4)$$

where e is the electron charge, ε is the dielectric constant, ε_0 is the permittivity of free space, k is the Boltzmann constant, and T is the temperature. From the equation above it can be surmised that as the thermal energy, kT, increases the Coulombic capture radius decreases. As the dielectric constants of organic semiconductors are typically low ($\varepsilon \sim 3$), the capture radius is typically found to be around 20 nm (at room temperature).[16,28] Studies on the rates of recombination[12,27,29] have been treated within the context of recombination of statistically independent opposite charges, as first studied by

Langevin.[30] As such, the bimolecular recombination rate can be specified by the following equation:

$$\text{Recombination rate} = \gamma n_+ n_- \qquad (1.5)$$

where n_+ and n_- represent are the hole and electron densities and γ represents the bimolecular rate constant ($\gamma = e(\mu_+ + \mu_-)/\varepsilon\varepsilon_0$; where e represents the electron charge, μ_+ and μ_- represent the mobilities of the holes and electrons, ε is the dielectric constant, ε_0 is the permittivity of free space.[27]

From the point of view of molecular states, recombination of holes and electrons can generate either singlet or triplet excitons that may form according to spin statistics[26,31] and lead to a one-to-three ratio of these states (although other ratios may be possible[32]). In a simplistic view, four possible excited states may exist:

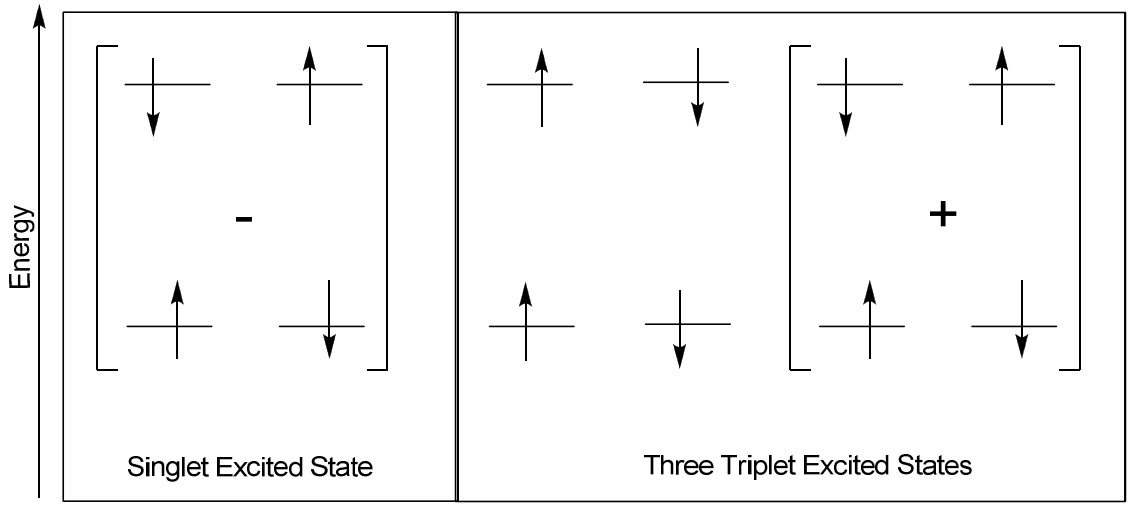

Figure 1.5. Possible exciton states that may be formed upon recombination of holes and electrons. The singly occupied levels denote the ground (S_0) and (S_1) states for the singlet and ground (S_0) and (T_1) states for the three triplet excited states shown.

Although it is possible for excitons to form at states higher[33] than S_1 or T_1, rapid internal conversion to the lowest excited states can be assumed. The bound hole-electron

pair (exciton) formed is stabilized (relative to unbound and charged states) by a Coulombic attraction known as the exciton-binding energy.[16] At temperatures where the exciton-binding energy is greater than the thermal energy *kT*, excitons will not dissociate appreciably after formation. Transition from the exciton state to the ground state is discussed in the following section.

1.3.4. Light Emission in OLEDs

The previous sections showed how charges can inject, transport, and recombine resulting in formation of excitons (of singlet or triplet nature). Light can be generated from the excitons states depending on the type of OLED employed is fluorescent or phosphorescent. The possible pathways for relaxation can be depicted in the Jablonski[34,35] diagram as follows:

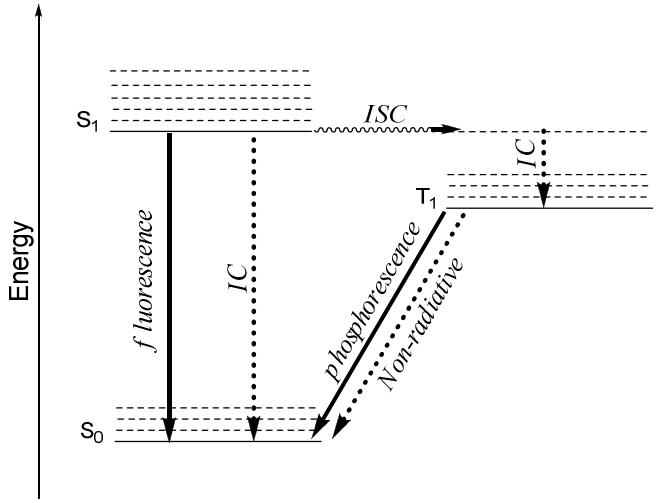

Figure 1.6. Relaxation pathways for singlet excitons (left) and triplet excitons (right) (where IC is internal conversion and ISC is intersystem crossing).

Excluding considerations of allowed transitions or of spin-orbit coupling (vide infra) for the moment, the available decay pathways for a singlet exciton include radiative

fluorescence and/or non-radiative internal conversion. In addition, intersystem crossing from the excited singlet state to the triplet state (which is lower in energy)[34] may occur followed by either radiative phosphorescence and/or non-radiative intersystem crossing to the ground (S_0) state from the triplet state. For the triplet excitons, decay to the ground state can occur via radiative (phosphorescent) and/or non-radiative intersystem crossing.

Early OLEDs were based on fluorescent organic emitters. For fluorescent emitters, decay from the singlet excited state to the singlet ground state is allowed (spin conserved) and produces light via fluorescence. Phosphorescence (at room temperature) is rarely observed for π-conjugated organic emitters due to their typically low rate of intersystem crossing associated with weak spin-orbit coupling.[34] As a consequence, the transition is not spin conserved and therefore a forbidden process. This limitation means that triplet excitons formed on fluorescent emitters do not contribute to the emission of light. Emission in fluorescent OLEDs, therefore can occur only from singlet excitons, which account for only approximately 25% of the total excitons formed.

In the late nineties Forrest and co-workers[6] studied the use of phosphorescent emitters for capturing both singlet and triplet excitons for light emission. Using the red phosphorescent emitter PtOEP (2,3,7,8,12,13,17,18-octaethyl-*21*H,*23*H-porphine platinum) doped into Alq_3 (electron transport material) they observed that energy transfer from the host would occur to the emitter. The ability to capture both singlet and triplet excitons formed on the host and effectively transfer them to the guest showed the potential to utilize up to 100% of the excitons formed. Since that time, other phosphorescent organometallic emitters[36] have been developed that can emit from the singlet and triplet state in a variety of colors.

For organometallic phosphorescent emitters, the ability to emit from the first excited triplet state can be attributed to the incorporation of a transition metal (such as Pt or Ir) with strong spin-orbit coupling. For such systems, the excited states possess mixed singlet and triplet character and the rates of intersystem crossing (ISC) are enhanced.[37,38] As a result the transition rate from $T_1 \rightarrow S_0$ by ISC increases and efficient phosphorescence can be observed.

Despite the usefulness of organometallic emitters to achieve phosphorescence, these materials are not typically deposited as neat layers in devices. Typically, they are doped in organic layers (at levels below 20 wt% of the host) in order to prevent triplet-triplet annihilation[39] processes such as:

$$T_1 + T_1 \rightarrow S_1 + S_0 \quad (1.6)$$

or

$$T_1 + T_1 \rightarrow T_1 + S_0 \quad (1.7)$$

These processes may lead to emission loss by non-radiative transition to the ground state at high concentrations of the emitter. Baldo *et al*.[39] showed that as the doping level of the emitter increases the likelihood of annihilation events also increases.

1.3.5. Energy Transfer in PhOLEDs

For host-guest systems, recombination of charges occurs predominantly on the host, although charge trapping on the guest emitter may also occur.[40] The excitons that recombine on the organic host must then efficiently transfer their energy to the guest. Energy transfer can occur by Förster and/or Dexter processes describing the non-radiative transfer of energy from the excited state of one molecule to another.

Energy transfer via the Dexter process[41] can be viewed as the exchange of the hole and electron between the molecule. For this process, energy transfer may occur as shown in the reactions below (where H = host, G = guest, the 1 or 3 superscripts denote singlet or triplet spin states, and * denotes an excited state).

$$^1H^* + {}^1G \rightarrow {}^1H + {}^1G^* \quad (1.8)$$

$$^3H^* + {}^1G \rightarrow {}^1H + {}^3G^* \quad (1.9)$$

The exchange interaction permits energy transfer from both the singlet or triplet excited states of the host to the guest. The approximate rate of energy transfer can be given by,

$$k_D \sim Je^{2R/L} \quad (1.10)$$

where J is the spectral overlap between the emission and absorption of host and guest molecules, R represents their separation (distance), and L represents the average orbital radius of the host and guest's donor and acceptor states.[28] As a consequence of the requirement for direct overlap between the molecular orbitals and due to the exponential decay dependence of the distance, Dexter energy transfer operates at short distances of 5 – 10 Å between the host and guest.[35]

Energy transfer between the host and guest may also occur by F□rster transfer.[42] For this process, only energy transfer between singlet excited states may occur.

$$^1H^* + {}^1G \rightarrow {}^1H + {}^1G^* \quad (1.11)$$

This process arises from the interaction between the electronic dipoles of the two molecules. For this dipole-dipole coupling, the approximate rate of energy transfer is determined according to the relationship[35]:

$$K_F \sim \frac{D_H^2 \, D_G^2}{R^6} \tag{1.12}$$

where *D* represents the transition dipole moments of the host and guest and *R* represents the distance between them. Therefore, because the dipole moment operator does not affect spin, no triplet energy transfer between host and guest is observed, as a consequence of the spin-forbidden nature of the transition from $T_1 \rightarrow S_0$ for the host (assuming no appreciable spin-orbit coupling).[28] For the Förster process, dipole-dipole interaction may occur up to distances of 100 Å [36] between the host and guest.

Although both types of energy transfer may occur at short distances between the molecules, as the distance, *R*, increases well beyond 10 Å, Förster energy transfer alone can be expected to dominate.[28] For guests doped in hosts, both processes are possible

1.4. Examples of Organic Materials and their Functions in OLEDs

Although there have been a wide variety of organic materials (small-molecule and polymer) developed for use in OLEDs, examples of some well-known materials permit an introduction to the types of moieties generally used for particular device layers.

The materials used at or very near to the interface with the metal electrode fall into the class of hole or electron injection/transport materials. Some well-known examples of these materials include:

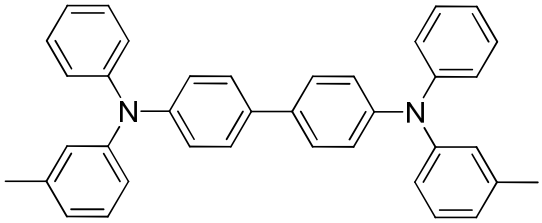

TPD (N,N'-diphenyl-N,N'-bis(3-methylphenyl)-(1,1'-biphenyl)-4,4'-diamine)

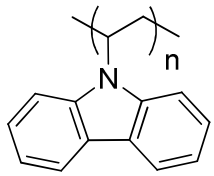

PVK (poly(*N*-vinylcarbazole))

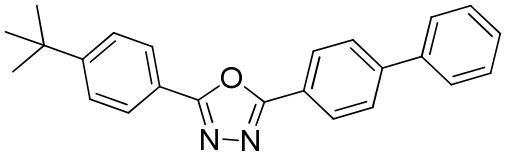

PBD (2-(biphenyl-4-yl)-5-(4-*tert*-butylphenyl)-1,3,4-oxadiazole)

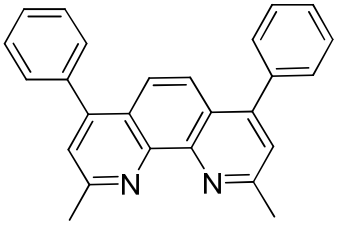

BCP (2,9-dimethyl-4,7-diphenyl-1,10-phenanthroline)

Figure 1.7. Hole transport (**TPD**[43] and **PVK**[44]) and electron transport (**PBD**[43] and **BCP**[45]) examples.

In the case of the hole transport examples, arylamines (such as **TPD** and **PVK**) can be oxidized when used in conjunction with an appropriate anode (i.e. ITO) that permits removal of an electron from their HOMO level with relative ease. For electron transport, electron-deficient moieties such as oxadiazole and phenanthroline (when used in conjunction with an appropriate cathode) permit injection of an electron into the LUMO level. In addition, to injection and transport of charges, these types of layers may sometimes act to block charges as represented schematically.[7]

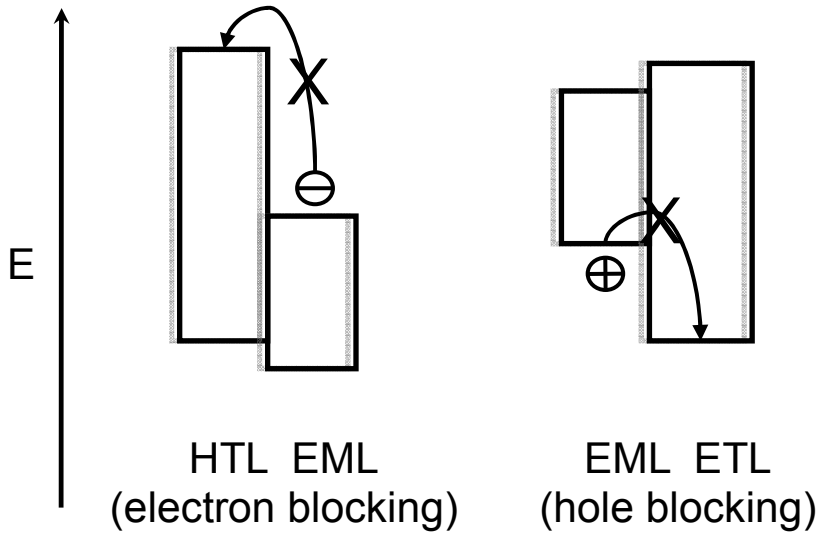

Figure 1.8. Simplified view of charge blocking between the hole-transport layer (HTL) and electron-transport layer (ETL) (where the bottom of the rectangle represents the HOMO and the top represents the LUMO).

If a sufficient energetic mismatch (resulting in a large injection barrier) exists between the HOMOs (or LUMOs) of a given layer vs. that of an adjacent layer, the charge may be blocked from injecting (or escaping) into the other layer. Organic transport materials with blocking properties are useful in defining the recombination zone.

Another important function for organic materials is as host materials for phosphorescent OLEDs. Hosts can include hole-transporting molecules such as the well-studied examples of **CBP** and **mCP**.

CBP (4,4'-di(9*H*-carbazol-9-yl)biphenyl) **mCP** (1,3-di(9*H*-carbazol-9-yl)benzene)

Figure 1.9. Hole transport hosts (**CBP**[46] and **mCP**[47]).

In addition to hole transporting hosts, examples (though more rare) of electron-transport hosts are also known.[48] In recent years, ambipolar hosts, which combine hole and electron transport within the same layer (as a single molecule, copolymer, or blend) have been the subject of increased research (discussed in detail in Chapter 4). Beyond the type (unipolar vs. ambipolar) of host employed, another important consideration is the triplet energy of the host materials. Due to the probability of energy transfer between the triplet states of the host and guest, a requirement for the triplet state of the host to be higher than that of the guest must be considered. This is apparent from the diagram below.

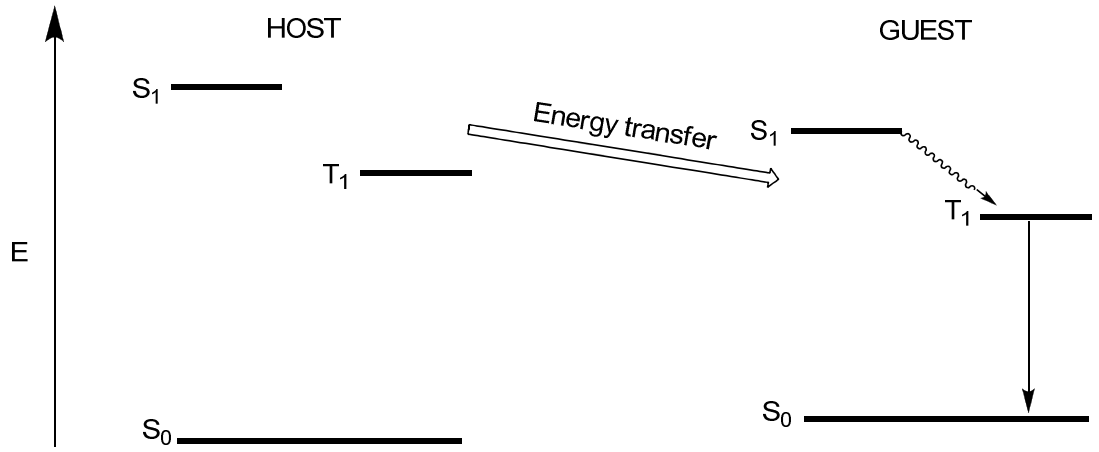

Figure 1.10. Host-guest energy diagram (where the guest is a phosphorescent emitter and energy transfer represents Förster and/or Dexter processes).

In the diagram, the triplet energy of the host is higher than that of the guest. As energy transfer from the guest to the host would be endothermic, it would not observed at an appreciable rate. In the case of poor host-guest matching, when the triplet energy of the host is less than that of the guest, back transfer of energy may occur leading to quenched emission.

1. 5. OLED Devices and Characterization

For OLED devices reported in later Chapters, OLED design, fabrication, and characterization was performed by Dr. Andreas Haldi or Dr. Dengke Cai in the research group of Prof. Bernard Kippelen in the School of Electrical and Computer Engineering. In general, the devices studied possessed the following architecture:

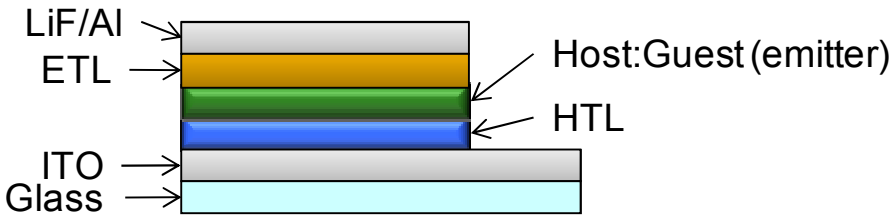

Figure 1.11. Representative architecture employed for study of charge transport materials (where ITO = indium tin oxide, HTL = hole transport layer and ETL = electron transport layer).

Using the above architecture (or variations thereof), materials discussed in Chapters 3, 4, and 5 were evaluated as hole-transport or host layers. The substrate for these devices was glass with a layer of indium tin oxide (ITO) that functioned as the cathode. Furthermore, hybrid devices were pursued that combined solution-processed and vacuum-processed layers. As an example, solution-processable hole-transport polymers could be spin-coated as thin-films onto ITO glass followed by vacuum deposition of the emissive (host:guest), electron-transport and cathode layers. . The use of crosslinkable (see below) solution-processed hole-transport layers further permitted the emissive layer to be processed from solution as well. The electron transport layer was comprised of vacuum-processed bathocuproine, a phenanthroline small-molecule used as both an electron-transport and hole-blocking layer.[45] The cathode was composed of a thin layer of a lithium fluoride and aluminum layer.

With respect to photometric characterization, luminous intensity is defined as the luminous flux emitted from a point source per unit solid angle (1 steradian (sr)) in a given direction.[49] For a source emitting uniformly in all direction, the luminous flux represents the total radiant power emitted by the source weighted against the sensitivity of the human eye to different wavelengths (photopic response; see figure below) and has units of lumens (lm).[50]

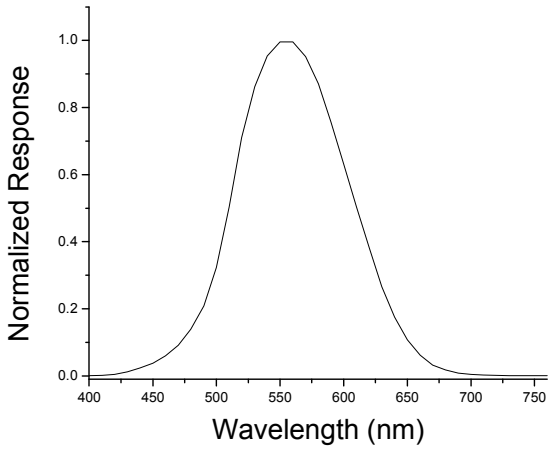

Figure 1.12. Photopic spectral response function of the human eye with maximum response at 555 nm.[50]

Luminous intensity therefore has the derived unit of lm sr^{-1} (which is equivalent to the unit of candela; the SI unit of luminous intensity). Furthermore, the luminous intensity remains the same regardless of the distance from the source because the solid angle does not change. By definition, the intensity of one candela (cd) represents the luminous intensity of an isotropic point source that emits monochromatically at 555 nm with an intensity of 1/683 watts per unit solid angle (1 sr).[51,52] Using the photopic response

function, it is possible to determine the amount of candelas generated at other visible wavelengths.[51]

As OLEDs do not represent point sources, but surface emissive sources, luminance (*L)*, rather than candelas, is used to describe the luminous intensity emitted per unit area (in cd m^{-2}) from a particular direction (such normal to the surface).[50] As such, luminance can be considered a measure of the perceived brightness of the emitting surface of the device. The highest level of luminance that can be achieved efficiently and with good stability is important in determining the application a particular example of an OLED may be suited for, such as for displays or lighting.

For the OLED devices fabricated, performance was evaluated on the basis of the following parameters:[53,54]

- External quantum efficiency (EQE): Ratio of photons emitted in the forward (viewing) direction to the number of electrons injected.

- Luminous efficiency: Comparable to the EQE but with the emitted photons weighted to the photopic response of the human eye (see figure above). It may also be defined as the ratio of the luminance to the current density. This term describes how efficient the device is at converting the applied current into light. This parameter is reported in cd/A.

- Luminous power efficiency: Ratio of the luminous flux emitted in the forward (viewing) direction to the electrical input power (at a particular voltage). This

term represents how efficient the device is at converting applied power into light. This parameter is reported in lm/W.

- Lifetime: For OLED devices lifetime can be limited by impurities, electrochemical, thermal, and environmental concerns, amongst many others.[55] The lifetime of a device is defined as the time it takes for half of the original luminance at a constant operating voltage to be lost.[56]

- Electroluminescence: The visible spectrum produced by the device under operation and determined by the color of the guest emitter.

1.6. Multilayer OLEDs

In general, the best efficiencies obtained for OLEDs have been achieved through vacuum deposition of organic compounds (typically small-molecules); vacuum deposition permits fabrication of well-defined multilayers. Concern about the potential high cost and active area limitations for layers processed by vacuum deposition have motivated research into organic materials (including small-molecules, oligomers, and polymers) that may be processed from solution by spin-coating, inkjet printing, etc.[57] Solution-processing, while potentially more economical, has setbacks as well. The potential for damage from deposition of a solution cast layer onto an existing layer (if soluble in the casting solvent) may damage or destroy the underlying layer. One method to prevent damage is through the use of crosslinkable groups that can be used to insolubilize an organic layer when activated (i.e. via thermal, UV, or chemical treatment, etc.). Crosslinking is introduced in greater detail in Chapter 5.

1.7. Organization of Thesis

The current chapter introduced organic light-emitting diodes and some limited examples of organic materials used in such devices; subsequent thesis chapters focus on matters of molecular and polymer design and review pertinent literature. Chapter 2 summarizes the experimental and characterization details for compounds discussed in Chapters 3 – 5. Chapter 3 explores the functionalization of hole transport materials as side-groups on a polymer backbone to determine effects and explore whether devices made from such materials are viable for OLEDs. Chapter 4 addresses the design of single-molecule ambipolar groups and side-chain derivatives of these moieties. A study of crosslinkable materials by conventional and rapid thermal processing for several types of crosslinking moieties is discussed in Chapter 5. Finally, Chapter 6 provides a synopsis and general conclusions of the work discussed and addresses future directions.

1.8. References

(1) Tang, C. W.; VanSlyke, S. A. *Appl. Phys. Lett.* **1987**, *51*, 913-915.

(2) Pope, M.; Kallmann, H. P.; Magnante, P. **1962**.

(3) Helfrich, W.; Schneider, W. G. *Phys. Rev. Lett.* **1965**, *14*, 229-231.

(4) Partridge, R. H. *Polymer* **1983**, *24*, 748-754.

(5) Burroughes, J. H.; Bradley, D. D. C.; Brown, A. R.; Marks, R. N.; Mackay, K.; Friend, R. H.; Burns, P. L.; Holmes, A. B. *Nature* **1990**, *347*, 539-541.

(6) Baldo, M. A.; O'Brien, D. F.; You, Y.; Shoustikov, A.; Silbey, S.; Thompson, M. E.; Forrest, S. R. *Nature* **1998**, *395*, 151-154.

(7) *Organic Light-Emitting Devices Synthesis, Properties, and Applications*; Mullen, K.; Scherf, U., Eds.; Wiley-VCH Verlag GmbH & Co.: Weinheim, 2006.

(8) Su, S.-J.; Gonmori, E.; Sasabe, H.; Kido, J. *Adv. Mater.* **2008**, *20*, 4189-4194.

(9) Baldo, M. A.; Forrest, S. R. *Phys. Rev. B* **2001**, *64*, 085201.

(10) Kahn, A.; Koch, N.; Gao, W. *J. Polym. Sci. B Poly. Phys.* **2003**, *41*, 2529-2548.

(11) Parker, I. D. *J. Appl. Phys.* **1994**, *75*, 1656-1666.

(12) Malliaras, G. G.; Scott, J. C. *J. Appl. Phys.* **1998**, *83*, 5399-5403.

(13) Scott, J. C.; Brock, P. J.; Salem, J. R.; Ramos, S.; Malliaras, G. G.; Carter, S. A.; Bozano, L. *Syn. Met.* **2000**, *111-112*, 289-293.

(14) Davids, P. S.; Campbell, I. H.; Smith, D. L. *J. Appl. Phys.* **1997**, *82*, 6319-6325.

(15) Scott, J. C.; Malliaras, G. G. *Chem. Phys. Lett.* **1999**, *299*, 115-119.

(16) Hill, I. G.; Kahn, A.; Soos, Z. G.; Pascal, J. R. A. *Chem. Phys. Lett.* **2000**, *327*, 181-188.

(17) Burrows, P. E.; Shen, Z.; Bulovic, V.; McCarty, D. M.; Forrest, S. R. *J. Appl. Phys.* **1996**, *79*, 7991-8006.

(18) Arkhipov, V. I.; Wolf, U.; Baessler, H. *Phys. Rev. B* **1999**, *59*, 7514-7520.

(19) Barth, S.; Wolf, U.; Baessler, H.; Muller, P.; Riel, H.; Vestweber, H.; Seidler, P. F.; RieB, W. *Phys. Rev. B* **1999**, *60*, 8791-8797.

(20) Marcus, R. A. *J.Chem. Phys.* **1956**, *24*, 966-978.

(21) Sakanoue, K.; Motoda, M.; Sugimoto, M.; Sakaki, S. *J. Phys. Chem. A* **1999**, *103*, 5551-5556.

(22) Franck, J. *Trans. Faraday Soc.* **1926**, *21*, 536-542.

(23) Condon, E. *Phys. Rev.* **1926**, *28*, 1182-1201.

(24) Bredas, J.-L.; Beljonne, D.; Coropceanu, V.; Cornil, J. *Chem. Rev.* **2004**, *104*, 4971-5003.

(25) Coropceanu, V.; Cornil, J.; da Silva Filho, D. A.; Olivier, Y.; Silbey, R.; Bredas, J.-L. *Chem. Rev.* **2007**, *107*, 923-952.

(26) Brown, A. R.; Pichler, K.; Greenham, N. C.; Bradley, D. D. C.; Friend, R. H.; Holmes, A. B. *Chem. Phys. Lett.* **1993**, *210*, 61-66.

(27) Bassler, H.; Tak, Y. H.; Khramtchenkov, D. V.; Nikitenko, V. R. *Syn. Met.* **1997**, *91*, 173-179.

(28) Kohler, A.; Bassler, H. *Mater. Sci. Eng. R* **2009**, *66*, 71-109.

(29) Albrecht, U.; Baessler, H. *Chem. Phys.* **1995**, *199*, 207-214.

(30) Langevin, P. *Ann. Chem. Phys.* **1903**, *28*, 289.
(31) Atkins, P.; de Paula, J. In *Physical Chemistry*; W.H. Freeman and Company: New York, 2002, p 395.
(32) Baldo, M. A.; O'Brien, D. F.; Thompson, M. E.; Forrest, S. R. *Phys. Rev. B* **1999**, *60*, 14422-14428.
(33) Beljonne, D.; Shuai, Z.; Ye, A.; Bredas, J.-L. *J. SID* **2005**, *13*, 419-427.
(34) Turro, N. J. *Modern Molecular Photochemistry*; University Science Books: Sausalito, 1991.
(35) Anslyn, E. V.; Dougherty, D. A. *Modern Physical Organic Chemistry*; University Science Books: Sausalito, 2006.
(36) Evans, R. C.; Douglas, P. D.; Winscom, C. J. *Coord. Chem. Rev.* **2006**, *250*, 2093-2126.
(37) Lamansky, S.; Djurovich, P.; Murphy, D.; Abdel-Razzaq, F.; Lee, H.-E.; Adachi, C.; Burrows, P. E.; Forrest, S. R.; Thompson, M. E. *J. Am. Chem. Soc.* **2001**, *123*, 4304-4312.
(38) Baldo, M. A.; Thompson, M. E.; Forrest, S. R. *Nature* **2000**, *403*, 750-753.
(39) Baldo, M. A.; Adachi, C.; Forrest, S. R. *Phys. Rev. B* **2000**, *62*, 10967-10977.
(40) Hartmut, Y. *Top Curr. Chem.* **2004**, *24*, 1-26.
(41) Dexter, D. L. *J. Chem. Phys.* **1953**, *21*, 836-850.
(42) Forster, T. *10th Spiers Memorial Lecture* **1959**, 7-17.
(43) Adachi, C.; Tsutsui, T.; Saito, S. *Appl. Phys. Lett.* **1989**, *55*, 1489-1491.
(44) Kido, J.; Hongawa, K.; Okuyama, K.; Nagai, K. *Appl. Phys. Lett.* **1993**, *63*, 2627-2629.
(45) Lee, J.-H.; Wu, M.-H.; Chao, C.-C.; Chen, H.-L.; Leung, M.-K. *Chem. Phys. Lett.* **2005**, *416*, 234-237.
(46) O'Brien, D. F.; Baldo, M. A.; Thompson, M. E.; Forrest, S. R. *Appl. Phys. Lett.* **1999**, *74*, 442-444.
(47) Adamovich, V.; Brooks, J.; Tamayo, A.; Alexander, A. M.; Djurovich, P. I.; D'Andrade, B. W.; Adachi, C.; Forrest, S. R.; Thompson, M. E. *New J. Chem.* **2002**, *26*, 1171-1178.
(48) Adachi, C.; Baldo, M. A.; Forrest, S. R.; Thompson, M. E. *Appl. Phys. Lett.* **2000**, *77*, 904-906.
(49) Al-Azzawi, A. *Light and Optics: Principles and Practices*; CRC Press: Boca Raton, 2007.
(50) McCluney, W. R. *Introduction to Radiometry and Photometry*; Artech House: Boston, 1994.
(51) Parr, A. C. *J. Res. Natl. Inst. Stand. Technol.* **2001**, *106*, 151-186.
(52) *Organic Light Emitting Materials and Devices*; Li, Z.; Meng, H., Eds.; Taylor and Francis Group: Boca Raton, London, New York, 2007.
(53) Forrest, S. R.; Bradley, D. D. C.; Thompson, M. E. *Adv. Mater.* **2003**, *15*, 1043-1048.
(54) Hung, L. S.; Chen, C. H. *Mater. Sci. Eng. R* **2002**, *39*, 143-222.

(55) Xia, S. C.; Kwong, R. C.; Adamovich, V.; Weaver, M. S.; Brown, J. J. *IEEE 07CH37867 45th Annual international Reliability Physics Symposium Phoenix* **2007**, 253-257.

(56) Aziz, H.; Popovic, Z. D.; Hu, N.-X.; Hor, A.-M.; Xu, G. *Science* **1999**, *283*, 1900-1902.

(57) So, F.; Kido, J.; Burrows, P. *MRS Bulletin* **2008**, *33*, 663-669.

CHAPTER 2

Synthesis, Characterization, and Experimental Details

2.1. Chapter Overview

This chapter provides the synthetic details and characterization data for compounds discussed in the following three chapters. In addition, experimental details for relevant experiments are also given.

2.2. Chapter 3: Carbazole-based Hole Transport Side-Chain Polymers

Starting materials were purchased from commercial sources and used without further purification. Anhydrous solvents were dried either by passage through columns of activated alumina or dried over sodium and benzophenone. ^{1}H NMR and ^{13}C NMR spectra were recorded on 300 or 400 MHz Varian Mercury spectrometers. Electron impact (EI) mass spectrometry data were recorded on a Micromass AutoSpec M. Elemental analyses results were performed by Atlantic Microlab. For polymers, the weight average and number average molecular weights were estimated in chloroform by gel permeation chromatography calibrated with linear poly(styrene) standards on a Shimadzu LC-10AT system. Differential scanning calorimetry (DSC) data was obtained from a TA DSCQ200 in the range of 25 – 300 °C at a heating rate of 10°C min^{-1} under nitrogen atmosphere. Thermogravimetric analyses (TGA) were performed on a NETZSCH STA 449C instrument under nitrogen atmosphere and decomposition was determined by the mass loss of 5% when heating at a rate of 20 °C min^{-1} from 20 °C to 500 °C. UV-vis absorption spectra were measured on Varian Cary 5E spectrometer. Photoluminescence spectra were recorded on a Fluorolog III ISA spectrofluorimeter.

Cyclic voltammetry (CV) was performed on a CH Instruments electrochemical workstation at room temperature in deoxygenated and anhydrous dichloromethane or *N,N*-dimethylformamide with 0.1 M tetrabutylammonium hexafluorophosphate as a supporting electrolyte at scanning rate of 50 mV/s. A platinum wire was used as a working electrode and an Ag/AgCl electrode was used as a reference electrode. Ferrocene/ferrocenium ($Cp_2Fe^{+/0}$) was used as a potential standard for calibration.

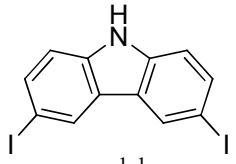

S3.1: Synthesized according to the literature.[1] ^{1}H NMR was consistent with the literature.

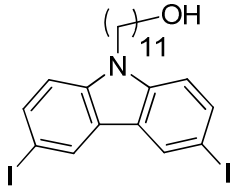

S3.2: To a solution of **S3.1** (10.0 g, 23.87 mmol) and 11-bromo-1-undecanol (7.0 g, 28 mmol) in N,N-dimethyformamide (100.0 mL) was added K_2CO_3 (32.0 g, 230 mmol). The reaction was stirred at room temperature for 24 h. Deionized water (300 mL) was added. The precipitate was filtered. The crude product was purified by column chromatography (silica gel; hexanes:ethyl acetate = 7:3). 12.4 g (87.9 %) of a white product was obtained. ^{1}H NMR (500 MHz, $CDCl_3$) : δ 8.32 (d, J = 1.5 Hz, 2H), 7.71 (dd, J_1 = 1.5 Hz, J_2 = 8.5 Hz, 2H), 7.16 (dd, J_1 = 1.5 Hz, J_2 = 8.5 Hz, 2H), 4.21 (t, J = 6.8 Hz, 2 H), 3.64 (m, 2 H), 3.41 (s, 1 H), 1.81 (m, 4 H), 1.54 (m, 4 H), 1.30 (m, 10 H). ^{13}C{1H} (75 MHz, $CDCl_3$): 139.50, 134.48, 129.35, 123.96, 110.91, 81.77, 63.08, 43.24, 32.77, 29.48, 29.41, 29.39,

29.35, 29.30, 28.80, 27.18, 25.69. MS (EI) m/z : 588.9 [M+]. Anal. calcd. for $C_{23}H_{29}I_2NO$: C, 46.88; H, 4.96; N, 2.38. Found: C, 46.76; H, 5.10; N, 2.22.

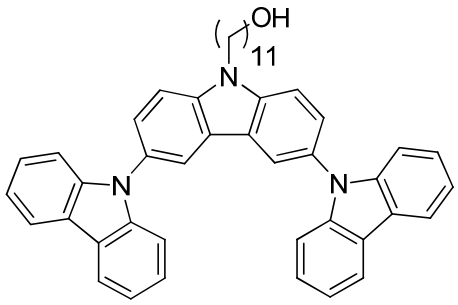

S3.3: To a solution of **S3.2** (8.0 g, 14 mmol), 9*H*-carbazole (6.8 g, 41 mmol) in dimethylsulfoxide (50.0 mL) were added Cu powder (10.0 g, 160 mmol) and Na_2CO_3 (30.0 g, 280 mmol). The reaction was stirred at 180 °C for 12 h. Insoluble inorganic salts were removed by filtration and washed with THF. After removal of THF, water (250 mL) was added. The precipitate was collected by filtration and purified by column chromatography (silica gel; toluene:ethyl acetate = 7:3). 8.1 g (91.0 %) of product was obtained as white solid. ^{1}H (300MHz, $CDCl_3$): δ 8.24-8.13 (m, 5H), 7.71-7.63 (m, 4H), 7.43-7.22 (m, 13H), 4.49 (t, *J* = 6.98 Hz, 2H), 3.62 (t, *J* = 6.34 Hz, 2H), 2.05 (p, *J* = 7.28 Hz, 2H), 1.77-1.23 (m, 18H), 1.18 (s, 1H). ^{13}C{1H} (75 MHz, $CDCl_3$): δ142.09, 140.42, 129.54, 126.19, 126.08, 123.62, 123.35, 123.33, 120.51, 120.07, 119.85, 110.34, 109.97, 63.31, 43.94, 33.02, 29.82, 29.79, 29.71, 29.66, 29.43, 27.66, 25.98. MS (EI) m/z : 667.4 [M+]. Anal. calcd. for $C_{47}H_{45}N_3O$: C, 84.52; H, 6.79; N, 6.29. Found: C, 84.37; H, 6.74; N, 6.29.

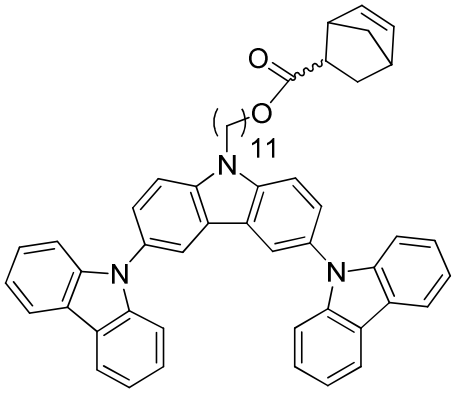

3.28: **S3.3** (1.570 g, 2.35 mmol), 5-norbornene-2-carboxylic acid (0.818 g, 5.92 mmol) and 20 mL of dry THF were combined in a round bottom flask and cooled in an ice bath for 20 min. DCC (1.015 g, 4.92 mmol) and DMAP (0.114 g, 0.93 mmol) were added to flask. The flask was subsequently removed from the ice bath and allowed to return to room temperature. The reaction proceeded overnight. The reaction mixture was filtered to remove insoluble DCC by-product and solvents were removed *in vacuo*. Methanol was added to precipitate the product. The product was recrystallized from hot toluene/hexanes then vacuum filtered and subsequently dried under vacuum to afford a white powder (1.118 g, 60.3%). ^{1}H (300 MHz, $CDCl_3$): δ8.25-8.12 (m, 5H), 7.67 (m, 4H), 7.43-7.34 (m, 7H), 7.34-7.22 (m, 6H), 6.21-6.07 (m, 1H), 5.94-5.88 (m, 1H), 4.49 (t, J = 7.2 Hz, 2H), 4.11-3.93 (m, 2H), 3.19 (s, 1H), 3.02 (s, 1H), 2.97-2.86 (m, 1H), 2.24-2.17 (m, 1H), 2.05 (p, J = 7.5 Hz, 2H), 1.83-1.96 (m, 1H), 1.22-1.69 (m,18H). ^{13}C{1H} (75 MHz, $CDCl_3$): δ 175.11, 142.10, 138.29, 137.99, 132.59, 129.53, 126.20, 126.08, 126.06, 123.35, 123.33, 120.54, 120.52, 119.85, 110.34, 109.94, 64.55, 49.86, 45.96, 43.60, 42.77, 29.80, 29.76, 29.74, 29.48, 29.46, 29.44, 29.40, 28.91, 27.69, 26.19. MS (EI) m/z : 787.4 [M+]. Anal. calcd. for $C_{55}H_{53}N_3O_2$: C, 83.83; H, 6.78; N, 5.33. Found: C, 83.70; H, 6.72; N, 5.28.

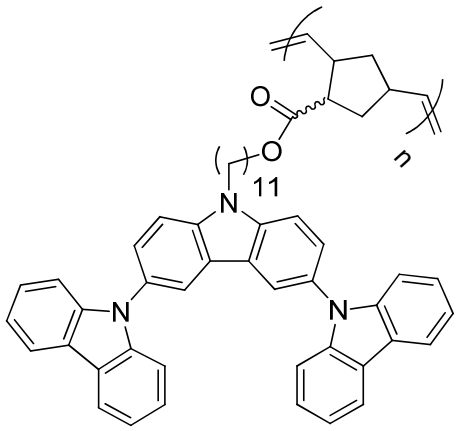

3.29: **3.28** (0.4001 g, 0.51 mmol) was weighed into a bottle. Grubbs' first generation catalyst (0.0046 g, 5.5 x 10^{-3} mmol) was weighed out into separate vial. The bottle and vial were placed into a glovebox. 3 mL of dry and deoxygenated dichloromethane was added to the bottle containing monomer. 1 mL of dry and deoxygenated dichloromethane was added to the vial containing Grubbs' first generation catalyst. Subsequently, the catalyst solution was added to the monomer solution. An additional 1 mL of dichloromethane was added to the catalyst vial and transferred into the monomer bottle. The polymerization reaction was allowed to proceed overnight. The reaction was quenched (outside glovebox) with 3 mL of ethyl vinyl ether and then added (dropwise) into 30 mL of methanol to precipitate polymer. The polymer powder was then vacuum filtered and re-dissolved in dichloromethane (< 3 mL) and 1 mL of ethyl vinyl ether was added. The solution was then added (dropwise) to 30 mL of methanol to precipitate polymer again. The reprecipitation process of isolating, dissolving, and vacuum filtering the polymer was repeated 3 more times. The isolated product was dried under vacuum to give a white/off-white powder (0.21 g, 52.5%). ^{1}H (300 MHz, $CDCl_3$): δ 8.04-8.21 (br m, 5H), 7.54 (br, 4H), 7.10-7.43 (m, 13H), 5.05-5.48 (br m, 2H), 4.32 (br, 2H), 3.94 (br, 2H), 1.62-3.17 (br m, 7H), 0.91-1.59 (m, 18H). Anal. calcd. for $C_{55}H_{53}N_3O_2$: C, 83.83; H,

6.78; N, 5.33. Found: C, 83.64; H, 6.73; N, 5.37. Gel Permeation Chromatography (chloroform): M_w = 49,000; M_n = 25,000; PDI = 1.94.

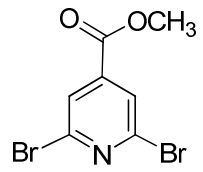

S3.4: Synthesized according to the literature.[2] ^{1}H NMR was consistent with the literature.

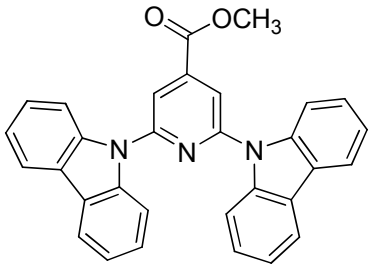

S3.5: To a solution of **S3.4** (5.0 g, 17 mmol), 9*H*-carbazole (6.0 g, 36 mmol), Cu powder (15.0 g, 236 mmol), and 18-crown-6 (0.1 g, 0.4 mmol) in 1,2-dichlorobenzene (50.0 mL) was added K_2CO_3 (20.0 g, 145 mmol) under nitrogen with stirring. The reaction was carried out at 180 °C for 9 hours. After cooling, the reaction mixture was filtrated. The solids were washed with excess dichloromethane and organics combined. Solvents were removed *in vacuo* and then methanol (100.0 mL) was added to produce a dark brown solid. After stirring the mixture for 30 minutes, a yellow solid product was collected by filtration. 6.4 g (81 %) of the pure product was obtained by recrystallization from acetone/methanol. ^{1}H NMR (300 MHz, $CDCl_3$): δ 8.17 (s, 2 H), 8.13 (dd, J = 7.2 Hz, 4H), 8.06 (dd, J = 7.2 Hz, 4H), 7.42 (td, J_1 = 7.2 Hz, J_2 = 1.2 Hz, 4H), 7.35 (td, J_1 = 7.2 Hz, J_2 = 1.2 Hz, 4H), 4.04 (s, 3 H). ^{13}C{1H} (75 MHz, $CDCl_3$): δ 164.67, 152.06, 141.89, 139.06, 126.44, 124.66, 121.55, 120.07, 113.47, 111.99, 53.24. MS (EI) m/z : 467.2 [M+]. Anal. calcd. for $C_{31}H_{21}N_3O_2$: C, 79.64; H, 4.45; N, 8.99. Found: C, 77.49; H, 4.35; N, 8.71. [As elemental analysis failed see ^{1}H NMR spectrum below].

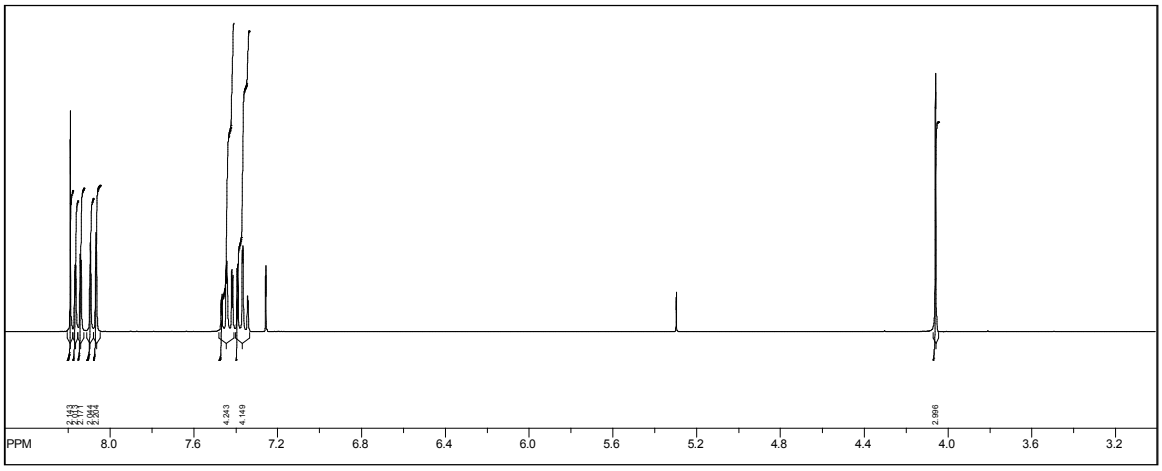

Figure 2.1. ^{1}H NMR (300 MHz, $CDCl_3$) of **S3.5**.

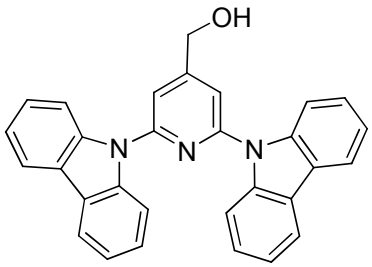

S3.6: **S3.5** (1.002 g, 2.15 mmol) was added to a flask (under N_2 atmosphere) and dissolved in anhydrous THF (50 mL). $NaBH_4$ (0.485 g, 12.8 mmol) was weighed out into a separate vial. Small amounts of $NaBH_4$ were added to the reaction flask. After complete addition of $NaBH_4$, the reaction flask was heated to 70 ºC. Methanol (8 mL) was added to flask (dropwise) over a 15 minute period. Following addition of methanol, saturated NH_4Cl (10 mL) was added to quench the reaction. The reaction solution was then vacuum filtered to remove solids and the filtrate was dried over Na_2SO_4. Solvents were removed *in vacuo* and the crude product was purified by column chromatography (silica gel, toluene:ethyl acetate = 8:2) to produce a white powder (0.575 g, 61.0%). ^{1}H (300 MHz, DMSO): δ 8.25 (m, 2H), 7.93 (m, 3H), 7.76 (m, 4H), 7.42 (m, 4H), 7.32 (m, 4H), 5.77 (t, J = 5.9 Hz, 1H), 4.89 (d, J = 6.0 Hz, 2H). ^{13}C{1H} (75 MHz, $CDCl_3$): 155.18, 151.70, 139.49, 129.07, 128.26, 126.37, 124.54, 121.26, 120.16, 112.24, 112.01, 63.52.

MS (EI) m/z : 439.0 [M+]. Anal. calcd. for $C_{30}H_{21}N_3O$: C, 81.98; H, 4.82; N, 9.56. Found: C, 81.97; H, 4.81; N, 9.31.

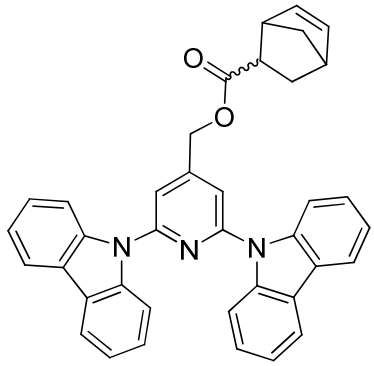

3.30: **S3.5** (0.402 g, 0.91 mmol), 5-norbornene-2-carboxylic acid (0.252 g, 1.82 mmol) and 10 mL of anhydrous THF were combined in a round bottom flask and cooled in an ice bath for 20 min. DCC (0.297 g, 1.44 mmol) and DMAP (0.061 g, 0.50 mmol) were added to the reaction flask which was subsequently removed from the ice bath. After 18 hours, the reaction mixture was filtered to remove insoluble DCC by-product and the filtrate was concentrated *in vacuo* to afford a cloudy white oil that crystallized upon standing. Column chromatography (silica gel, hexanes: ethyl acetate = 8:2) was performed to purify the crude and afforded a white crystalline solid that was isolated by vacuum filtration using methanol. The isolated product was dried in a vacuum oven to produce a white powder (0.402 g, 78.5%). ^{1}H (300 MHz, DMSO): δ 8.26 (m, 4H), 7.94 (m, 4H), 7.77 (m, 2H), 7.43 (m, 4H), 7.33 (m, 4H), 6.21-6.03 (m, 1H), 5.95-5.88 (m, 1H), 5.54-5.35 (m, 2H), 3.26-3.07 (m, 2H), 2.96-2.80 (m, 1H), 2.01-1.88 (m, 1H), 1.52-1.24 (m, 3H). ^{13}C{1H} (75 MHz, DMSO): δ 175.11, 142.10, 138.29, 137.99, 132.59, 129.53, 126.20, 126.08, 126.06, 123.35, 123.33, 120.54, 120.52, 119.85, 110.34, 109.94, 64.55, 49.86, 45.96, 43.60, 42.77, 29.80, 29.76, 29.74, 29.48, 29.46, 29.44, 29.40, 28.91, 27.69,

26.19. MS (EI) m/z : 559.4 [M+]. Elemental analysis calculated for $C_{38}H_{29}N_3O_2$: C, 81.55; H, 5.22; N, 7.51. Found: C, 81.40; H, 5.41; N, 7.44.

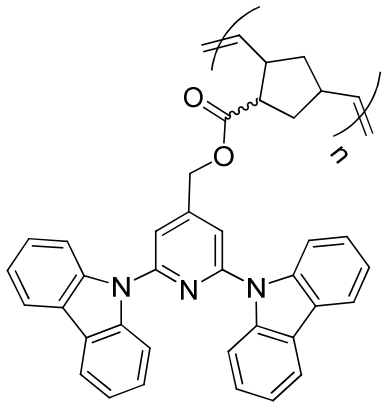

3.31: **3.30** (0.3192 g, 0.57 mmol) was weighed into a bottle. Grubbs' first generation catalyst (0.0058 g, 7.04 x 10^{-3} mmol) was weighed out into separate vial. The bottle and vial were placed into a glovebox. 3 mL of anhydrous and deoxygenated dichloromethane was added to the bottle containing monomer. 1 mL of anhydrous and deoxygenated dichloromethane was added to vial containing Grubbs' first generation catalyst and shaken vigorously. Subsequently, the catalyst solution was quickly transferred to the bottle with monomer. An additional 1 mL of dichloromethane was added to the Grubbs's catalyst vial and transferred into the monomer bottle. The polymerization was allowed to proceed for 18 hours. The reaction was quenched (out of glovebox) with 2.5 mL of ethyl vinyl ether, concentrated *in vacuo* and then added (dropwise) into 30 mL of methanol to precipitate the polymer. The polymer was then vacuum filtered and re-dissolved in minimal (< 3 mL) dichloromethane and 1 mL of ethyl vinyl ether was added. The solution was then added (dropwise) to 30 mL of methanol to precipitate polymer. The reprecipitation process of isolating, dissolving, and vacuum filtering the precipitated polymer was repeated 2 more times. The isolated product was dried under vacuum to

give a white colored powder (0.177g, 55.3%). ^{1}H (300 MHz, $CDCl_3$): δ 8.04-7.74 (br m, 6H), 7.37-7.09 (br m, 12H), 5.46-4.49 (br m, 4H), 3.17-0.39 (br m, 9H). Elemental analysis calculated. for $C_{38}H_{29}N_3O_2$: C, 81.55; H, 5.22; N, 7.51. Found: C, 81.28; H, 5.25; N, 7.39. Gel Permeation Chromatography (chloroform): M_w = 27,000; M_n = 16,000; PDI = 1.69.

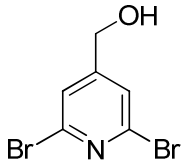

S3.7: To a solution of **S3.4** (10.0 g, 34 mmol) in ethanol (200.0 mL) was slowly added $NaBH_4$ (6.4 g, 170 mmol) at room temperature. The reaction was heated at reflux for 2 hours and then the reaction solution was cooled to room temperature and 2 M HCl (35.0 mL) was added slowly with stirring until bubbling stopped. Solvents were removed *in vacuo*. Solid NaOH was added under stirring until the solution became basic. The solution continued to be stirred, and during stirring the product was precipitated. A white solid product was collected by filtration. After drying, the product was obtained in an amount of 5.0g (55.6%). ^{1}H NMR (300 MHz, $CDCl_3$): δ 7.44 (s, 2H), 4.70 (s, 2 H). ^{13}C{1H} (75 MHz, $CDCl_3$): δ 155.05, 140.70, 124.15, 62.22. MS (EI) m/z : 266.8 [M+]. [Product was found to be consistent with a literature[2] example of the target prepared by an alternate method].

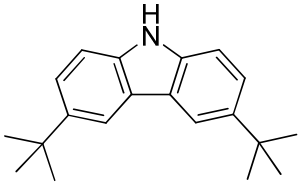

S3.8: Synthesized according to the literature.[3] ^{1}H NMR was consistent with the literature.

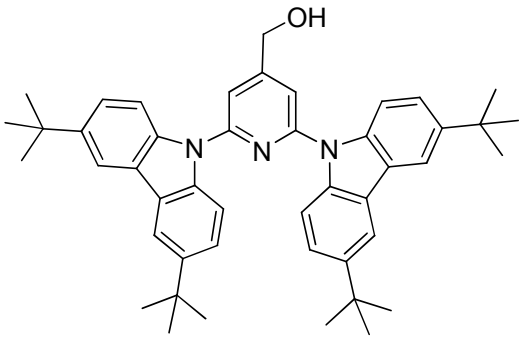

S3.9: To a solution of **S3.7** (1.0 g, 4 mmol), **S3.8** (2.3 g, 8.2 mmol), Cu (2.0 g, 32 mmol) and 18-crown-6 (32 mg, 0.12 mmol) in 1,2-dichlorobenzene (10.0 mL), was added K_2CO_3 (4.0 g, 29 mmol) under nitrogen and stirring. The reaction was carried out at 180 °C for 10 hours. After cooling, the reaction mixture was filtrated and solids were washed with THF. After solvents were removed *in vacuo*, the product was purified by column chromatography (silica gel ; toluene). The pure product was obtained as a white powder in 1.7 g (68.0%) after recrystallization from acetone/methanol/water. ^{1}H NMR (300 MHz, $CDCl_3$): δ 8.12 (d, J = 1.2 Hz, 4H), 7.95 (d, J = 8.8 Hz, 4H), 7.56 (s, 2 H), 7.44 (dd, J_1 = 8.8 Hz, J_2 = 1.2 Hz, 4H), 4.94 (s, 2 H), 1.46 (s, 36 H). ^{13}C{1H} (75 MHz, $CDCl_3$): δ 154.35, 151.82, 143.94, 137.71, 124.45, 123.84, 115.91, 111.68, 110.75, 63.76, 34.84, 32.02. MS (EI) m/z : 663.7 [M+]. Anal. calcd. for $C_{46}H_{53}N_3O$: C, 83.22; H, 8.05; N, 6.33. Found: C, 82.77; H, 8.07; N, 6.31.

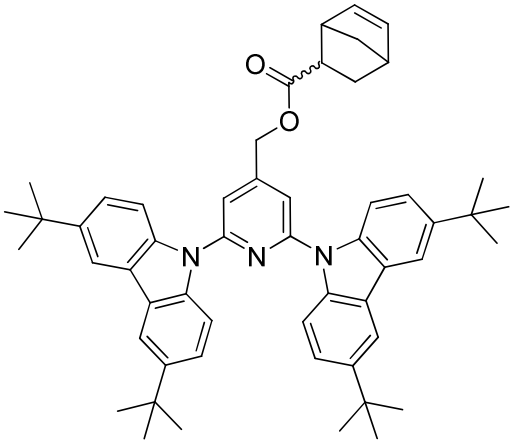

3.32: **S3.9** (0.500 g, 0.75 mmol), 5-norbornene-2-carboxylic acid (0.235 g, 1.70 mmol) and 10 mL of anhydrous THF were combined in a round bottom flask and cooled in an ice bath for 20 minutes. DCC (0.21 g, 1.01 mmol) and DMAP (0.02 g, 0.16 mmol) were added to the reaction flask which was removed from the ice bath. The reaction was allowed to proceed overnight for 18 hours. The reaction mixture was vacuum filtered to remove the insoluble DCC by-product and the filtrate was concentrated *in vacuo*. Methanol was added to the flask to precipitate the product which was isolated by vacuum filtration. The crude product was reprecipitated from dichloromethane with methanol, isolated, and dried overnight to afford a white powder (0.50 g, 85 %). 1H (300 MHz, $CDCl_3$): δ8.20-8.04 (m, 4H), 8.03-7.85 (m, 4H), 7.57-7.35 (m, 6H), 6.21-6.12 (m, 1H), 5.97-5.92 (m, 1H), 5.42-5.19 (m, 2H), 3.31 (s, 1H), 3.19-3.07 (m, 1H), 2.94 (br s, 1H), 2.42-2.36 (m, 1H), 2.06-1.96 (m, 2H), 1.67 (s, 1H), 1.62-1.20 (m, 38H). $^{13}C\{1H\}$ (75 MHz, $CDCl_3$): δ 175.64,162.61, 159.03, 152.32, 144.52, 138.41, 138.06, 124.92, 124.26, 116.29, 112.06 111.66, 64.44, 49.97, 46.04, 42.78, 35.00 32.15, 29.70. MS (EI) m/z: 783.6 [M+]. Elemental analysis calculated. for $C_{54}H_{61}N_3O_2$: C, 82.72; H, 7.84; N, 5.36. Found: C, 82.51; H, 7.85; N, 5.35.

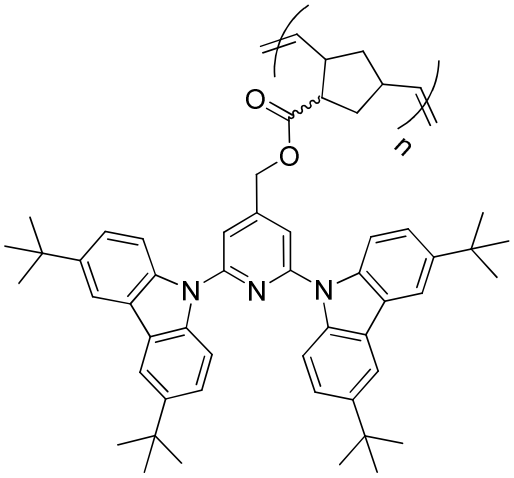

3.33: **3.32** (0.404 g, 0.52 mmol) was weighed into a bottle. Grubbs' first generation catalyst (0.005 g, 6.1 x 10^{-3} mmol) was weighed out into a separate vial. The bottle and vial were placed into a glove box. The bottle and vial were placed into a glovebox. 3 mL of anhydrous and deoxygenated dichloromethane was added to the bottle containing monomer. 1 mL of anhydrous and deoxygenated dichloromethane was added to vial containing Grubbs' first generation catalyst and shaken vigorously. Subsequently, the catalyst solution was quickly transferred to the bottle with monomer. An additional 1 mL of dichloromethane was added to the Grubbs's catalyst vial and transferred into the monomer bottle. The polymerization was allowed to proceed overnight for 16 hours. The reaction was quenched (outside of the glove box) with 3 mL of ethyl vinyl ether and then transferred (dropwise) into 30 mL of methanol to precipitate the polymer. The polymer was then vacuum filtered and re-dissolved in minimal (< 3 mL) dichloromethane and 1 mL of ethyl vinyl ether was added. This solution was then added (dropwise) to 30 mL of methanol to precipitate the polymer. The reprecipitation process of isolating, dissolving, and vacuum filtering the precipitated polymer was repeated 4 more times. The isolated product was dried under vacuum to give a white/off-white powder (0.21g, 52.5%). ^{1}H (300 MHz, $CDCl_3$): δ 8.22-7.97 (br m, 4H), 7.97-7.67 (br m, 4H), 7.62-7.27 (br m, 6H), 5.61-4.44 (br m, 4H), 3.22-1.41 (br m, 7H), 1.35 (s, 36H). Anal. calcd. for $C_{54}H_{61}N_3O_2$: C, 82.72; H, 7.84; N, 5.36. Found: C, 82.35; H, 7.81; N, 5.33. Gel Permeation Chromatography (chloroform): M_w = 44,000; M_n = 22,000; PDI = 1.98.

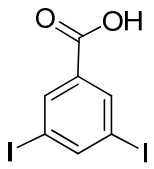

S3.10: Synthesized according to the literature.[4] ^{1}H NMR was consistent with the literature.

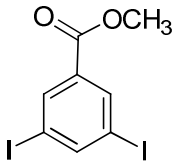

S3.11: To a solution of **S3.10** (6.8 g, 18 mmol) in methanol (200 mL) was added sulfuric acid (0.5 mL). The reaction mixture was refluxed for 7.5 hours, then after cooling concentrated and deionized water (200 mL) was added. A dark-brown solid was collected by filtration and purified by column chromatography (silica gel; hexanes:ethyl acetate = 8:2). The product was obtained as a white powder, 4.2 g (59.2%), by recrystallization from methanol/water. ^{1}H NMR (300 MHz, $CDCl_3$): δ 8.29 (d, J = 1.6 Hz, 2H), 8.20 (t, J = 1.6 Hz, 1H), 3.90 (s, 3H). ^{13}C{1H} (75 MHz, $CDCl_3$): δ 163.97, 148.99, 137.56, 133.08, 94.32, 52.73. [Product was found to be consistent with a literature[4] example of the target prepared by an alternate method].

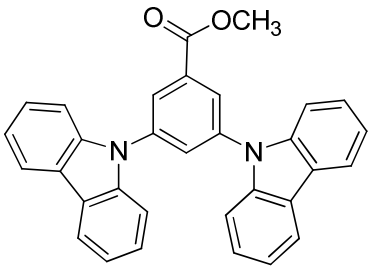

S3.12: To a solution of **S3.11** (3.0 g, 7.73 mmol), 9*H*-carbazole (3.0 g, 17.94 mmol), Cu powder (6.4 g, 100.71 mmol) and 18-crown-6 (65 mg, 0.25 mmol) in 1,2-dichlorobenzene (30.0 mL) was added K_2CO_3 (12.6 g, 91.17 mmol) under nitrogen atmosphere. The reaction was carried out at 180 °C for 10.5 hours. After cooling, the reaction mixture was filtered and solids were washed with THF. After solvent removal *in vacuo*, the product was purified by column chromatography (silica gel ; toluene). The

final product was obtained as a white powder, 2.6 g (71.7%), by recrystallization from acetone/methanol. ^{1}H NMR (300 MHz, $CDCl_3$): δ 8.37 (d, J = 1.6 Hz, 1H), 8.15 (dd, J_1 = 7.2 Hz, J_2 = 0.8 Hz, 4H), 8.02 (t, J = 1.6 Hz, 1H), 7.52 (dd, J_1 = 7.2 Hz, J_2 = 0.8 Hz, 4H), 7.45 (td, J_1 = 7.2 Hz, J_2 = 1.6 Hz, 4H), 7.32 (td, J_1= 7.2 Hz, J_2 = 1.2 Hz, 4H), 3.99 (s, 3H). ^{13}C{1H} (75 MHz, $CDCl_3$): δ 165.39, 140.18, 139.54, 133.63, 129.09, 126.45, 126.20, 123.62, 120.55, 120.43, 109.42, 52.82. MS (EI) m/z : 466.0 [M+]. Anal. calcd. for $C_{32}H_{22}N_2O_2$: C, 82.38; H, 4.75; N, 6.00. Found: C, 82.34; H, 4.66; N, 6.03.

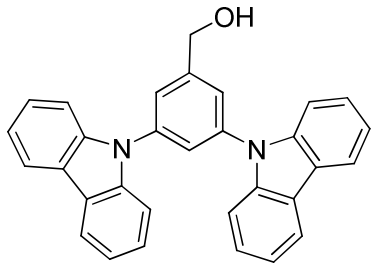

S3.13: **S3.12** (1.002 g, 2.15 mmol) was dissolved (under N_2 atmosphere) in anhydrous THF (30 mL). $LiAlH_4$ (0.438 g, 11.54 mmol) was weighed out into a separate vial. Small amounts of $LiAlH_4$ were progressively added to the reaction flask. After complete addition of $LiAlH_4$, the reaction flask was refluxed overnight. The cooled reaction was quenched by very slow addition of deionized water (dropwise) to the flask until the reaction solution ceased bubbling. Following quenching the reaction mixture was vacuum filtered to remove solids. The filtrate was concentrated *in vacuo* to obtain a white crystalline crude product. Column chromatography (silica gel ; hexanes: ethyl acetate = 7:3) was performed to purify crude product and produced a clear oil that crystallized under high vacuum. The crystalline product was isolated by filtration with deionized water and dried to afford a white powder (0.667 g, 71.0%). ^{1}H (300 MHz, $CDCl_3$): δ 8.16 (d, J = 7.7 Hz, 4H), 7.58-7.50 (m, 3H), 7.45 (m, 4H), 7.32 (m, 4H), 4.96 (d, J = 3.7 Hz,

2H), 1.97 (t, J = 4.5 Hz, 1H). $^{13}C\{1H\}$ (75 MHz, $CDCl_3$): 144.79, 140.55, 139.52, 126.19, 124.15, 123.82, 123.61, 120.48, 120.38, 109.72, 64.47. MS (EI) m/z : 438.0 [M+]. Anal. calcd. for $C_{31}H_{22}N_2O$: C, 84.91; H, 5.06; N, 6.39. Found: C, 84.67; H, 4.90; N, 6.33.

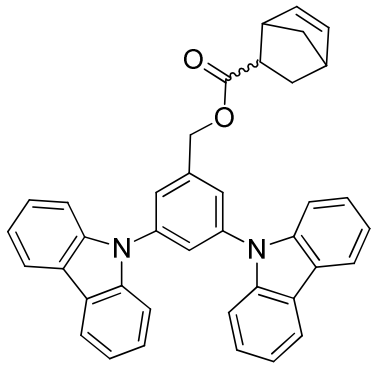

3.34: **S3.13** (0.551g, 1.26 mmol), 5-norbornene-2-carboxylic acid (0.351 g, 2.54 mmol) and 10 mL of anhydrous THF were combined in a round bottom flask and cooled in an ice bath for 20 min. DCC (0.399 g, 1.93 mmol) and DMAP (0.056 g, 0.46 mmol) were added to the reaction flask which was subsequently removed from the ice bath. The reaction was allowed to proceed for ~ 5 h and was then filtered to remove solids. The filtrate was concentrated *in vacuo* and methanol was added to precipitate the product which was isolated by filtration and precipitated from acetone using methanol:water (75:25). Following isolation, the product was dried to produce a white powder (0.502g, 71.6%). ^1H (300 MHz, $CDCl_3$): δ 8.15 (m, 4H), 7.78 (m, 1H), 7.68 (m, 2H), 7.54 (m, 4H), 7.45 (m, 4H), 7.32 (m, 4H), 6.18-6.08 (m, 1H), 5.90 (m, 1H), 5.38-5.26 (m, 2H), 3.30-3.23 (m, 1H), 3.03-3.14 (m, 1H), 2.98-2.89 (m, 1H), 2.04-1.91 (m, 1H), 1.53-1.35 (m, 2H), 1.33-1.23 (m, 1H). $^{13}C\{1H\}$ (75MHz, $CDCl_3$): δ 174.76, 140.68, 140.54, 139.77, 138.40, 138.30, 132.50, 126.44, 124.87, 123.88, 120.72, 120.68, 109.90, 65.22,

49.93, 46.06, 43.67, 42.80, 29.64. MS (EI) m/z : 557.3 [M+]. Anal. Calcd. for $C_{39}H_{30}N_2O_2$: C, 83.85; H, 5.41; N, 5.01. Found: C, 83.59; H, 5.49; N, 5.11.

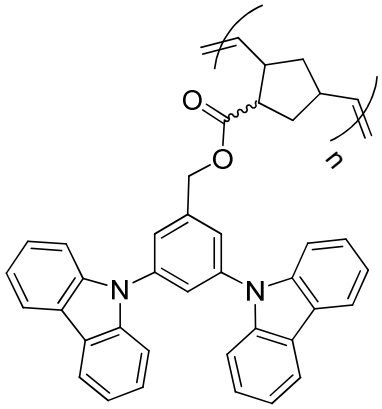

3.35: **3.34** (0.4003 g, 0.72 mmol) was weighed into a bottle. Grubbs' first generation catalyst (0.0065 g, 7.90 x 10^{-3} mmol) was weighed out into separate vial. The bottle and vial were placed into a glovebox. The bottle and vial were placed into a glovebox. 5 mL of anhydrous and deoxygenated dichloromethane was added to the bottle containing monomer. 1 mL of anhydrous and deoxygenated dichloromethane was added to vial containing Grubbs' first generation catalyst and shaken vigorously. Subsequently, the catalyst solution was quickly transferred to the bottle with monomer. An additional 1 mL of dichloromethane was added to the Grubbs's catalyst vial and transferred into the monomer bottle. The polymerization was allowed to proceed for 18 hours. The reaction was quenched (out of glovebox) with 2.5 mL of ethyl vinyl ether, concentrated *in vacuo*, and added (dropwise) into 30 mL of methanol to precipitate polymer. The polymer was then vacuum filtered and re-dissolved in minimal (< 3 mL) dichloromethane and 1 mL of ethyl vinyl ether was added. This solution was then added (dropwise) to 30 mL of methanol to precipitate the polymer. The reprecipitation process of isolating, dissolving, and vacuum filtering the precipitated polymer was repeated two more times. The isolated

product was dried under vacuum to give a cream colored powder (0.240 g, 60.0%). ^{1}H (300 MHz, $CDCl_3$): δ 8.17-7.90 (br m, 4H), 7.78-7.05 (br m, 15H), 5.46-4.73 (br m, 4H), 3.15-0.38 (br m, 9H). Anal. calcd. for $C_{39}H_{30}N_2O_2$: C, 83.85; H, 5.41; N, 5.01. Found: C, 83.55; H, 5.42; N, 4.97. Gel Permeation Chromatography (chloroform): M_w = 40,000; M_n = 22,000; PDI = 1.83.

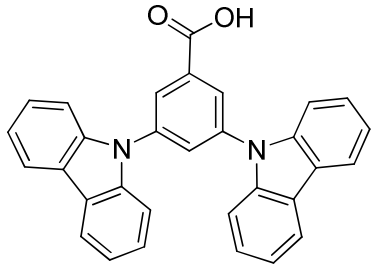

S3.14: To a solution of **S3.12** (1.0 g, 2.14 mmol) in THF and methanol (25.0 mL, 15:10) was added KOH (0.6 g, 10.69 mmol) dissolved in deonized water (2.0 mL) at room temperature. After 4.5 hours, the solvent was removed *in vacuo* and methanol (20.0 mL) was added followed aqueous HCl (80.0 mL; 15.0 mL of 36-38% HCl in 65.0 mL of water). The mixture was stirred for 1 hour and a pale yellow solid product was obtained by filtration. The product was purified by recrystallization from acetone/water to afford a powder, 0.95 g (97.9%). ^{1}H NMR (300 MHz, $CDCl_3$): δ 8.37 (d, J = 2.4 Hz, 2H), 8.21 (dt, J_1 = 7.2 Hz, J_2 = 0.8 Hz, 4H), 8.19 (t, J = 2.4 Hz, 1H), 7.63 (dd, J_1 = 7.2 Hz, J_2 = 0.8 Hz, 4H), 7.47 (td, J_1 = 7.2 Hz, J_2 = 1.2 Hz, 4H), 7.30 (td, J_1 = 7.2 Hz, J_2 = 1.2 Hz, 4H). ^{13}C{1H} (100 MHz, $CDCl_3$): δ 166.04, 141.19, 140.34, 135.14, 130.08, 127.31, 127.11, 124.38, 121.32, 121.17, 110.42. MS (EI) m/z : 452.1 [M+].

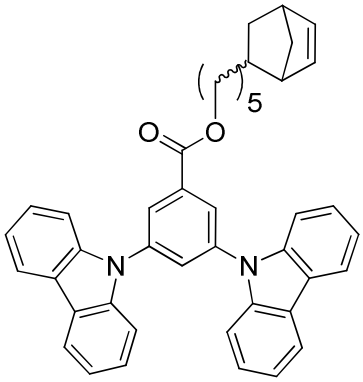

3.36: To a solution of **S3.14** (0.5 g, 1.10 mmol) and 5-(5-bromopentyl)bicyclo[2,2,1]hept-2-ene (0.32 g, 1.32 mmol) in *N,N*-dimethylformamide (6.0 mL) was added K_2CO_3 (4.0 g, 28.94 mmol) at room temperature. After 26.5 hours, deionized water (50.0 mL) was added and a white solid product was obtained by filtration and purified by column chromatography (silica gel ; toluene:hexanes = 6:4). After the removal of solvents *in vacuo*, a glass-like solid was dissolved in acetone (3.0 mL). The acetone solution was dropped into methanol/water (20.0 mL, 75:25) to give a white powder solid. After filtration and drying a white solid, 0.64 g (94.3%), was obtained. ^{1}H NMR (300 MHz, $CDCl_3$): δ 8.37 (d, J = 1.6 Hz, 2H), 8.16 (dd, J_1 = 7.2 Hz, J_2 = 1.2 Hz, 4H), 8.02 (t, J = 1.6 Hz, 1H), 7.53 (dd, J_1 = 7.2 Hz, J_2 = 1.2 Hz, 4H), 7.46 (td, J_1 = 7.2 Hz, J_2 = 1.2 Hz, 4H), 7.33 (td, J_1 = 7.2 Hz, J_2 = 1.2 Hz, 4H), 6.03 (dd, J_1 = 5.6 Hz, J_2 = 3.2 Hz, 1H), 5.96 (dd, J_1 = 5.6 Hz, J_2 = 2.8 Hz, 1H), 4.40 (t, J = 7.2 Hz, 2H), 2.73 (s, br, 1 H), 2.46 (m, 1 H), 1.78 (m, 2 H), 1.44-1.21 (m, 10 H), 1.04 (m, 1 H). ^{13}C{1H} (75 MHz, $CDCl_3$): δ 164.95, 140.19, 139.49, 136.67, 136.01, 134.03, 129.03, 126.43, 126.20, 123.61, 120.54, 120.43, 109.42, 65.99, 46.37, 45.25, 41.90, 38,72, 36.50, 33.10, 28.78, 28.57, 26.37. MS (EI) m/z : 614.2 [M+]. Anal. calcd for $C_{43}H_{38}N_2O_2$: C, 84.01; H, 6.23; N, 4.56. Found: C, 84.03; H, 6.17; N, 4.45.

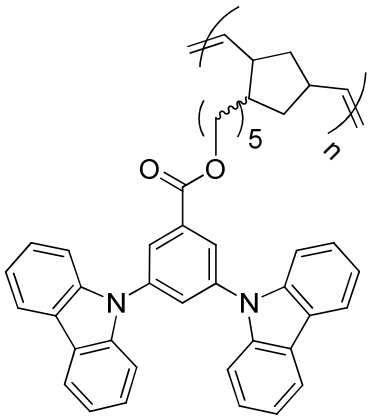

3.37: **3.36** (0.5 g, 0.813 mmol) was weighed into a bottle. Grubbs' first generation catalyst (0.0067 g, 8.13 x 10^{-3} mmol) was weighed out into separate vial. The bottle and vial were placed into a glovebox. The bottle and vial were placed into a glovebox. 6 mL of anhydrous and deoxygenated dichloromethane was added to the bottle containing monomer. 1 mL of anhydrous and deoxygenated dichloromethane was added to vial containing Grubbs' first generation catalyst and shaken vigorously. Subsequently, the catalyst solution was quickly transferred to the bottle with monomer. The polymerization was carried out at room temperature for 15 hours. Ethyl vinyl ether (2.0 mL) was then added. After stirring for 55 minutes, the polymer and dichloromethane solution was added (dropwise) into methanol (60.0 mL) to give a white precipitate. The polymer was then vacuum filtered and re-dissolved in minimal (< 3 mL) dichloromethane. This solution was then added (dropwise) to 30 mL of methanol to precipitate the polymer. The reprecipitation process of isolating, dissolving, and vacuum filtering the precipitated polymer was repeated 5 more times. After filtration and drying in a vacuum, the isolated product was obtained as a white solid, 0.41 g (82.0%). ^{1}H NMR (300 MHz, $CDCl_3$): δ 8.31 (br m, 2 H), 8.06 (br m, 4 H), 7.93 (br m, 1 H), 7.45 (br m, 4 H), 7.37 (br m, 4 H), 7.25 (br m, 4 H), 5.19 (br m, 1 H), 5.08 (br m, 1 H), 4.28 (br m, 2 H), 2.30 (br m, 1 H),

1.72 (br m, 4 H), 1.30 (br m, 8 H), 0.88 (br m, 2 H). Anal. calcd for $C_{43}H_{38}N_2O_2$: C, 84.01; H, 6.23; N, 4.56. Found: C, 83.72; H, 6.17; N, 4.53. GPC (chloroform): M_w = 49,000; M_n = 13,600; PDI = 3.58.

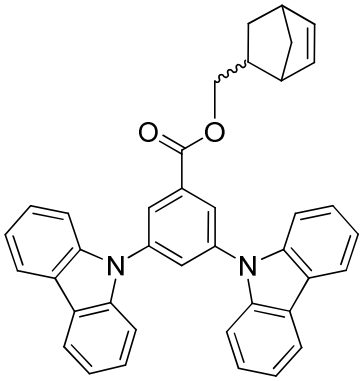

3.38: To a solution of **S3.14** (0.5 g, 1.1 mmol) and 5-(bromomethyl)bicyclo[2,2,1]hept-2-ene (0.3 g, 1.6 mmol) in *N,N*-dimethylformamide (6.0 mL) was added K_2CO_3 (4.0 g, 28.94 mmol) at room temperature. The reaction was then heated at 60 °C for 26 hours. After cooling, deonized water (40.0 mL) was added to precipitate a white solid product collected by filtration. The crude product was purified by column chromatography (silica gel ; toluene:hexanes = 6:4). After removal of the solvents *in vacuo*, a glass-like solid was dissolved in acetone (2.0 mL) and dropped into methanol/water (20.0 mL, 8:2) to give a white powder solid. After filtration and drying, the product was obtained as a white solid, 0.48 g (77.8%). ^{1}H NMR (300 MHz, $CDCl_3$): δ 8.38 (m, 2H), 8.16 (d, J = 7.2 Hz, 4H), 8.19 (m, 1H), 7.53 (d, J = 7.2 Hz, 4H), 7.46 (t, J = 7.2 Hz, 4H), 7.33 (t, J = 7.2 Hz, 4H), 6.19 (dd, J_1 = 5.6 Hz, J_2 = 2.4 Hz, 0.6H), 6.09 (m, 0.66H), 6.00 (dd, J_1 = 5.6 Hz, J_2 = 1.4 Hz, 0.63H), 4.49 (dd, J_1 = 10.4 Hz, J_2 = 6.8 Hz, 0.35H), 4.33 (dd, J_1 = 9.2 Hz, J_2 = 9.2 Hz, 0.35H) 4.18 (dd, J_1 = 10.4 Hz, J_2 = 6.8 Hz, 0.71H), 4.00 (dd, J_1 = 10.8 Hz, J_2 = 9.2 Hz, 0.71H), 2.87 (m, 2 H), 2.53 (m, 1 H), 1.88 (m, 1 H), 1.45 (m, 2 H), 0.67 (m, 1 H). ^{13}C{1H} (75 MHz, $CDCl_3$): δ 164.77, 140.19, 139.50,137.69, 136.85, 135.99, 134.06,

131.95, 129.00, 126.43, 126.20, 123.61, 120.54, 120.44, 109.42, 69.85, 69.21, 49.49, 45.08, 44.04, 43.76, 42.27, 41.68, 38.11, 37.90, 29.70, 29.07. MS (EI) m/z : 558.2 [M+]. Anal. calcd. for $C_{39}H_{30}N_2O_2$: C, 83.85; H, 5.41; N, 5.01. Found: C, 83.89; H, 5.35; N, 4.98.

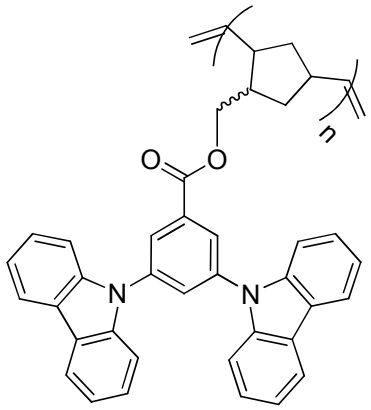

3.39: **3.38** (0.4 g, 0.716 mmol) was weighed into a bottle. Grubbs' first generation catalyst (0.0040 g, 7.2 x 10^{-3} mmol) was weighed out into separate vial. The bottle and vial were placed into a glovebox. The bottle and vial were placed into a glovebox. 5 mL of anhydrous and deoxygenated dichloromethane was added to the bottle containing monomer. 1 mL of anhydrous and deoxygenated dichloromethane was added to vial containing Grubbs' first generation catalyst and shaken vigorously. Subsequently, the catalyst solution was quickly transferred to the bottle with monomer. The polymerization was carried out at room temperature for 15 hours. Ethyl vinyl ether (2.0 mL) was then added. After stirring for 30 minutes, the polymer dichloromethane solution was added to methanol (50 mL) to give a white polymer solid. The polymer was then vacuum filtered and re-dissolved in minimal (< 3 mL) dichloromethane. This solution was then added (dropwise) to 30 mL of methanol to precipitate the polymer. The reprecipitation process of isolating, dissolving, and vacuum filtering the precipitated polymer was repeated 5

more times. After filtration and drying in a vacuum, the isolated product was obtained as a white solid, 0.34 g (85.0%). ^{1}H NMR (300 MHz, $CDCl_3$): δ 8.24 (br m, 2H), 8.01 (br m, 4H), 7.89 (br m, 1H), 7.42 (br m, 4H), 7.31 (br m, 4H), 7.20 (br m, 4H), 5.11 (br m, 2H), 4.06 (br m, 2H), 2.17-1.01 (br m, 7H). Anal. calcd. for $C_{39}H_{30}N_2O_2$: C, 83.85; H, 5.41; N, 5.01. Found: C, 83.62; H, 5.35; N, 4.94. GPC (THF): M_w = 47,000; M_n = 17,000; PDI = 2.78.

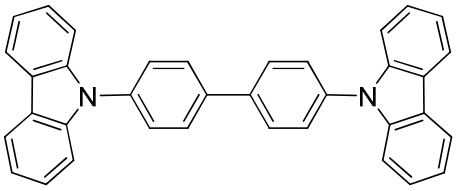

S3.15: Synthesized according to the literature.[5] ^{1}H NMR was consistent with the literature.

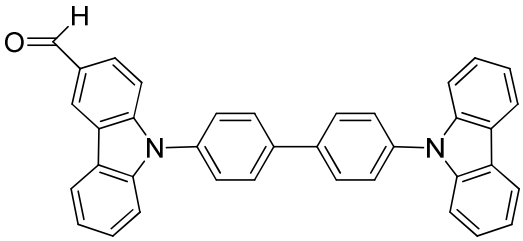

S3.16: DMF (7.2 mL, 93.39 mmol) and $POCl_3$ (8.5 mL, 92.86 mmol) were combined slowly in a flask to give the white Vilsmeier-Haack reagent as a solid that was set aside over ice. **S3.15** (7.60 g, 15.68 mmol) was weighed into a separate flask set-up for reflux (under nitrogen atmosphere). To this second flask dichloroethane (~180 mL) was added and the flask was heated to 80 ºC. The Vilsmeier-Haack reagent was added to the second flask and the reaction was allowed to proceed under reflux. The reaction mixture was slowly added into a beaker half-filled with ice to give a precipitate in a dark green liquid. The flask washed with ice water and subsequently dichloromethane (3 ×) and all fractions were combined. Organic solvents were removed *in vacuo* and the concentrated solution

was purified by column chromatography (silica gel, dichloromethane: toluene = 3:2) but solubility issues resulted in inadequate separation of starting material from monosubstituted product. A second column (same eluent system) was performed and the product (mono-substituted) was isolated and air dried (24 hours) to give a yellow powder (2.08 g, 27.4%). ^{1}H (300 MHz, $CDCl_3$): δ 10.15 (s, 1H), 8.71 (d, *J* = 1.1 Hz, 1H), 8.12-8.29 (m, 3H), 7.86-8.05 (m, 5H), 7.72 (t, *J* = 8.8 Hz, 4H), 7.11-7.60 (m, 11H). ^{13}C{1H}(75 MHz, $CDCl_3$): δ192.03, 144.69, 142.05, 141.00, 140.52, 139.20, 136.40, 129.29, 128.83, 127.78, 127.35, 124.18, 123.97, 123.76, 123.59, 121.61, 121.01, 120.66, 120.39, 110.72, 110.44, 110.04. [Target was prepared according to the patent literature[6]].

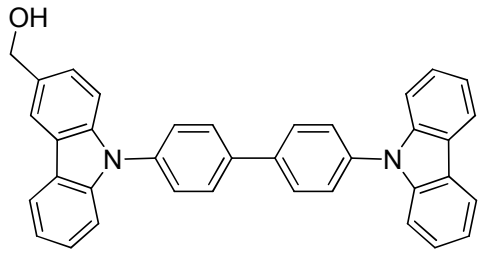

S3.17: **S3.16** (2.071 g, 4.04 mmol) was set up in a flask was placed under nitrogen flow and tetrahydrofuran (~175 mL) was added. $NaBH_4$ (0.903 g, 23.87 mmol) was weighed into a separate bottle and deionized water (~2 mL) was added to the same bottle. The $NaBH_4$ solution was added dropwise to the flask and an additional 1 mL of deionized water was used to wash the $NaBH_4$ bottle. After completion, solvents were reduced *in vacuo* and deionized water was added to yield a white precipitate. The precipitate was vacuum filtered and dried to afford a white powder (1.914 g, 95.3%). ^{1}H (300 MHz, DMSO-d_6): 8.15-8.30 (m, 4H), 8.13-8.01 (m, 4H), 7.81-7.67 (m, 4H), 7.53-7.37 (m, 8H), 7.35-7.24 (m, 3H), 5.23 (t, *J* = 5.6 Hz, 1H), 4.68 (d, *J* = 5.6 Hz, 2H). ^{13}C{1H}(75 MHz, DMSO-d_6): 140.95, 140.74, 139.89, 139.03, 129.20, 129.17, 127.88, 127.04, 123.63, 123.55, 121.31, 120.90, 110.50, 110.46, 64.05. MS (EI) m/z: 514.0 [M+]. Anal. calcd.

for $C_{37}H_{26}N_2O$: C, 86.35; H, 5.09; N, 5.44. Found: C, 84.50; H, 5.32; N, 5.16. [As elemental analysis failed see ^{1}H NMR spectrum below]

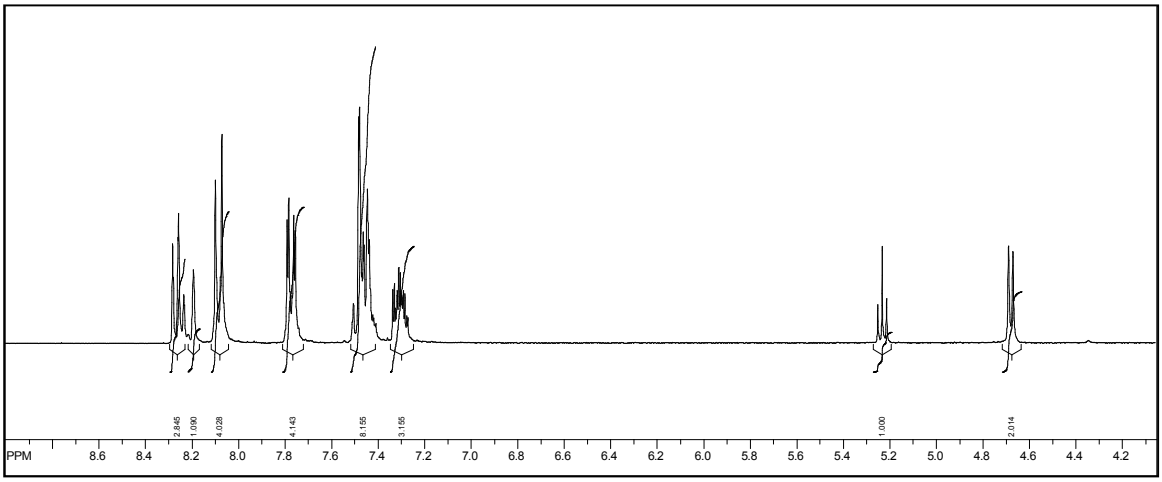

Figure 2.2. ^{1}H NMR (300 MHz, DMSO-d_6) of **S3.17**.

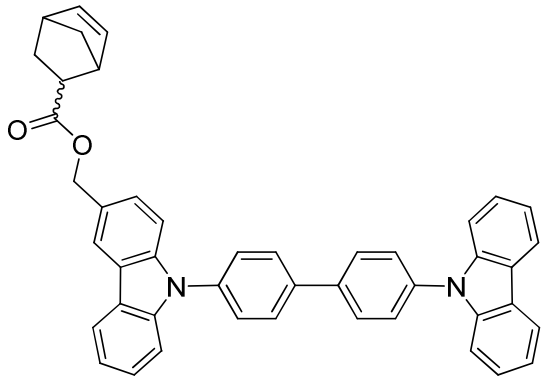

3.40: **S3.17** (0.382 g, 0.74 mmol), 5-norbornene-2-carboxylic acid (0.395 g, 2.86 mmol) and 35 mL of anhydrous THF were combined in a round bottom flask (with stirring). DCC (0.385 g, 1.87 mmol) and DMAP (0.114 g, 0.93 mmol) were added to the reaction flask. The reaction proceeded overnight for 18 hours then the mixture was filtered to remove insoluble solids and the filtrate was concentrated *in vacuo*. Methanol was added to the flask to give a white precipitate that was isolated by vacuum filtration. The crude product was purified by column chromatography (silica gel, hexanes: ethyl acetate = 8:2)

and the product was isolated by vacuum filtration and dried to produce a white powder (0.324 g, 69.2%). ^{1}H (300 MHz, $CDCl_3$): δ 8.18 (d, *J* = 7.9 Hz, 4H), 7.93 (d, *J* = 8.2 Hz, 4H), 7.76-7.66 (m, 4H), 7.56-7.39 (m, 8H), 7.39-7.27 (m, 4H), 6.23-6.07 (m, 1H), 5.94-5.88 (m, 1H), 5.39-5.22 (m, 2H), 3.25 (s, 1H), 3.12-2.99 (m, 1H), 2.92 (s, 1H), 2.35-2.227 (m, 1H), 2.02-1.88 (m, 1H), 1.53-1.34 (m, 2H). ^{13}C{1H} (75 MHz, $CDCl_3$): δ 174.85, 141.03, 140.87, 139.46, 138.34, 138.04, 137.53, 136.02, 132.61, 128.81, 128.77, 128.34, 127.74, 127.68, 127.12, 126.27, 123.73, 120.33, 110.06, 67.01, 49.89, 46.63, 46.09, 46.08, 43.70, 43.51, 42.84, 29.54. MS (EI) m/z : 634.5 [M+]. Anal. calcd. for $C_{45}H_{34}N_2O_2$: C, 85.15; H, 5.40; N, 4.41. Found: C, 84.93; H, 5.35; N, 4.40.

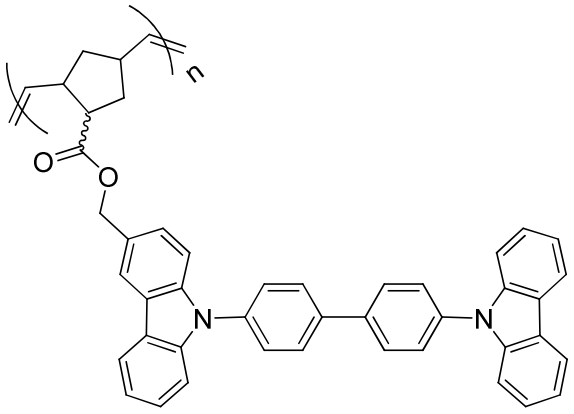

3.41: **3.40** (0.407 g, 0.64 mmol) was weighed into a bottle. Grubbs' first generation catalyst (0.0058 g, 7.0 x 10^{-3} mmol) was weighed out into separate vial. The bottle and vial were placed into a glovebox. 5 mL of anhydrous and deoxygenated dichloromethane was added to the bottle containing monomer. 2 mL of anhydrous and deoxygenated dichloromethane was added to vial containing Grubbs' first generation catalyst and shaken vigorously. Subsequently, the catalyst solution was quickly transferred to the bottle with monomer. The polymerization was allowed to proceed overnight for 18 hours. The reaction was quenched (out of glovebox) with 3 mL of ethyl vinyl ether,

concentrated *in vacuo*, and added (dropwise) into 30 mL of methanol to precipitate polymer. The polymer was then vacuum filtered and re-dissolved in minimal (< 3 mL) dichloromethane and 1 mL of ethyl vinyl ether was added. This solution was then added (dropwise) to 30 mL of methanol to precipitate the polymer. The reprecipitation process of isolating, dissolving, and vacuum filtering the precipitated polymer was repeated 2 more times. The isolated product was dried to give a white colored powder (0.179 g, 44.8%). ^{1}H (300 MHz, $CDCl_3$): δ 8.23-7.94 (br m, 4H), 7.88-7.09 (br m, 20H), 5.46-4.94 (br m, 4H), 3.07-1.02 (br m, 9H). Anal. calcd. for $C_{45}H_{34}N_2O_2$: C, 85.15; H, 5.40; N, 4.41. Found: C, 84.62; H, 5.38; N, 4.53. Gel Permeation Chromatography (chloroform): M_w = 39,000; M_n = 24,000; PDI = 1.63.

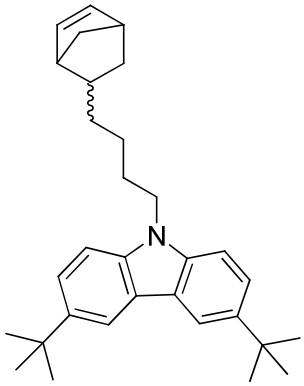

3.42: To a solution of **S3.8** (1.0 g, 3.58 mmol) and 5-(4-bromobutyl)bicyclo[2,2,1]hept-2-ene (0.82 g, 3.58 mmol) in *N,N*-dimethylformamide (16.0 mL) under inert atmosphere was slowly added NaH (0.24 g, 10.00 mmol) at room temperature. After 35 minutes, deionized water (50.0 mL) was added. The solution was extracted with dichloromethane (3 x 40.0 mL). The dichloromethane solution was washed with water (4 x 50.0 mL). After removal of solvents *in vacuo*, the crude product was purified by column (silica gel ; hexanes:ethyl acetate = 95:5). The product fraction was rotovapped to produce a viscous lightly yellow oil that was dried under vacuum overnight to produce a yellowish-brown

crystalline product that was subsequently isolated by vacuum filtration with water and dried overnight under vacuum. The dried product was obtained as an off-white crystalline solid, 1.25 g (81.7%). ^{1}H (300 MHz, $CDCl_3$): δ 8.17-8.10 (m, 2H), 7.57-7.49 (dd, *J* = 6.58, 2.03 Hz, 2H), 7.37-7.29 (m, 2H), 6.17-5.87 (m, 2H), 4.23 (t, *J* = 7.28 Hz ,2H), 2.83-2.17 (m, 2H), 2.04-0.44 (m, 29H). ^{13}C{1H} (75 MHz, $CDCl_3$): δ 141.62, 139.21, 137.30, 132.57, 123.44, 122.90, 116.50, 108.26, 49.83, 45.62, 43.40, 42.76, 38.88, 34.91, 34.77, 32.59, 32.34, 29.57, 26.57. MS (EI) m/z : 427.3 [M+]. Anal. calcd. for $C_{31}H_{41}N$: C, 87.06; H, 9.66; N, 3.28. Found: C, 86.77; H, 9.70; N, 3.16.

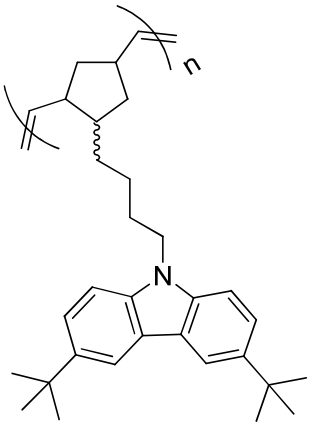

3.43: **3.42** (0.5019 g, 1.17 mmol) was weighed into a bottle. A Grubbs' first generation catalyst (0.0112 g, 1.4 x 10^{-2} mmol) was weighed out into a separate vial. The bottle and vial were placed into a glove box. 10 mL of anhydrous and deoxygenated dichloromethane was added to the bottle containing monomer. 2 mL of anhydrous and deoxygenated dichloromethane was added to vial containing Grubbs' first generation catalyst and shaken vigorously. Subsequently, the catalyst solution was quickly transferred to the bottle with monomer. The polymerization was allowed to proceed overnight for 16 hours. The reaction was quenched (out of glovebox) with 5 mL of ethyl vinyl ether, concentrated *in vacuo*, and added (dropwise) into 50 mL of methanol to

precipitate polymer. The polymer was then vacuum filtered and re-dissolved in minimal (< 3 mL) dichloromethane and 1 mL of ethyl vinyl ether was added. This solution was then added (dropwise) to 50 mL of methanol to precipitate the polymer. The reprecipitation process of isolating, dissolving, and vacuum filtering the precipitated polymer was repeated 5 more times. The isolated product was dried under vacuum to give an off-white powder (0.219 g, 43.8%). ^{1}H (300 MHz, $CDCl_3$): δ 8.14-8.02 (br m, 2H), 7.53-7.31 (br m, 2H), 7.25-6.97 (br m, 2H), 5.45-5.00 (br m, 2H), 4.29-3.91 (br m, 2H), 2.99-2.59 (br m, 1H), 2.59-2.16 (br m, 2H), 2.11-1.58 (br m, 4H), 1.42 (s, 18H), 1.35-0.76 (br m, 6H). Anal. calcd. for $C_{31}H_{41}N$: C, 87.06; H, 9.66; N, 3.28. Found: C, 86.12; H, 9.76; N, 3.15. Gel Permeation Chromatography (chloroform): M_w = 25,000; M_n = 9,000; PDI = 2.90.

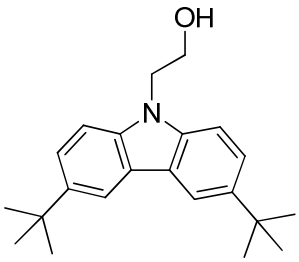

S3.18: To a solution of 9-(2-hydroxyethyl)carbazole (1.65 g, 7.81 mmol) in 2-chloro-2-methylpropane (25.0 mL) was added aluminum trichloride (0.54 g, 4.05 mmol) at room temperature under nitrogen atmosphere. After the addition of aluminum trichloride and the insoluble 9-(2-hydroxyethyl)carbazole dissolved. After 25 minutes, deionized water (20.0 mL) was added. The product was extracted with ethyl acetate (3 x 20.0 mL). The organic layer was washed with water (3 x 60.0 mL), and then ethyl acetate was removed *in vacuo*. The product was purified by column chromatography (silica gel ; ethyl acetate:hexanes = 3.5:6.5) to yield 2.1 g (84.0%) of a white solid after recrystallization

from dichloromethane/hexanes. ^{1}H NMR (300 MHz, $CDCl_3$): δ 8.09 (d, J = 2.4 Hz, 2H), 7.50 (dd, J_1 = 8.4 Hz, J_2 = 2.4 Hz, 2H), 7.35 (d, J = 8.4 Hz, 2H), 4.42 (t, J = 5.6 Hz, 2H), 4.03 (t, J = 5.6 Hz, 2H). ^{13}C{1H} (75 MHz, $CDCl_3$): δ 141.87, 139.02, 123.38, 122.76, 116.22, 108.04, 61.74, 45.65, 34.77, 32.14. Anal. calcd. for $C_{22}H_{29}NO$: C, 81.69; H, 9.04; N, 4.33. Found: C, 81.55; H, 9.15; N, 4.30.

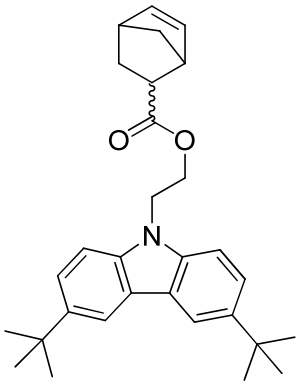

3.44: **S3.18** (1.462 g, 4.51 mmol), 5-norbornene-2-carboxylic acid (1.231 g, 8.91 mmol) and 10 mL of anhydrous THF were combined in a round bottom flask and cooled in an ice bath for 20 minutes. DCC (1.398 g, 6.78 mmol) and DMAP (0.054 g, 0.44 mmol) were added to the reaction flask. The flask was subsequently removed from the ice bath and the reaction proceeded overnight for 18 hours. The reaction mixture was filtered to remove solids and the filtrate was concentrated *in vacuo* to afford a white precipitate. Methanol was used to isolate the precipitate by vacuum filtration. Column chromatography (silica gel, hexanes: ethyl acetate = 9:1) was performed to purify the product. The purified product was isolated by filtration and dried to give a white powder (0.738g, 36.9%). ^{1}H (300 MHz, $CDCl_3$): δ 8.09 (d, J = 2.0 Hz, 2H), 7.56-7.48 (m, 2H), 7.39-7.32 (m, 2H), 6.10-5.98 (m, 1H), 5.63-5.57 (m, 1H), 4.58-4.42 (m, 2H), 4.38 (m, 2H), 2.99 (s, 1H), 2.87-2.76 (m, 2H), 1.85-1.72 (m, 1H), 1.45 (s, 18H), 1.37-1.16 (m, 3H). ^{13}C{1H} (75 MHz, $CDCl_3$): δ 175.04, 142.24, 139.16, 137.96, 132.48, 123.64,

123.12, 116.53, 108.34, 62.34, 49.81, 45.74, 43.45, 42.69, 41.90, 34.91, 32.29, 32.28, 29.40. MS (EI) m/z : 443.3 [M+]. Anal. calcd. for $C_{30}H_{37}NO_2$: C, 81.22; H, 8.41; N, 3.16. Found: C, 81.20; H, 8.50; N, 3.16.

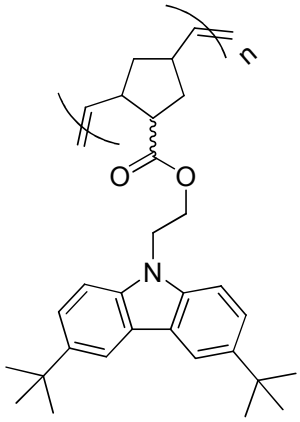

3.45: **3.44** (0.9002 g, 2.03 mmol) was weighed into a bottle. A Grubbs's first generation catalyst (0.0172 g, 2.1 x 10^{-2} mmol) was weighed out into a separate vial. The bottle and vial were placed into a glove box. 18 mL of anhydrous and deoxygenated dichloromethane was added to the bottle containing monomer. 2 mL of anhydrous and deoxygenated dichloromethane was added to vial containing Grubbs' first generation catalyst and shaken vigorously. Subsequently, the catalyst solution was quickly transferred to the bottle with monomer. The polymerization was allowed to proceed overnight for 16 hours. The reaction was quenched (out of glovebox) with 5 mL of ethyl vinyl ether, concentrated *in vacuo*, and added (dropwise) into 75 mL of methanol to precipitate polymer. The polymer was then vacuum filtered and re-dissolved in minimal (< 3 mL) dichloromethane and 1 mL of ethyl vinyl ether was added. This solution was then added (dropwise) to 75 mL of methanol to precipitate the polymer. The reprecipitation process of isolating, dissolving, and vacuum filtering the precipitated polymer was repeated 4 more times. The isolated product was dried under vacuum to

give a cream colored powder (0.408 g, 45.3%). ^{1}H (300 MHz, $CDCl_3$): δ 8.06 (br s, 2H), 7.52-7.35 (br m, 2H), 7.35-7.26 (br m, 2H), 5.46-4.59 (br m, 2H), 4.57-3.91 (br m, 2H), 3.13-2.18 (br m, 3H), 2.03-1.69 (br m, 2H), 1.41 (br s, 18H), 1.23-0.79 (br m, 2H). Anal. calcd. for $C_{30}H_{37}NO_2$: C, 81.22; H, 8.41; N, 3.16. Found: C, 80.44; H, 8.38; N, 3.19. Gel Permeation Chromatography (chloroform): M_w = 46,000; M_n = 21,000; PDI = 2.14.

2.3. Chapter 4: Single-Molecule Ambipolar Transport Hosts

Starting materials were purchased from commercial sources and used without further purification. Anhydrous solvents were dried either by passage through columns of activated alumina or dried over sodium and benzophenone. ^{1}H NMR and ^{13}C NMR spectra were recorded on 300 or 400 MHz Varian Mercury spectrometers. Electron impact (EI) mass spectrometry data were recorded on a Micromass AutoSpec M. Elemental analyses results were performed by Atlantic Microlab. For polymers, the weight average and number average molecular weights were estimated in chloroform by gel permeation chromatography calibrated with linear poly(styrene) standards; in a system consisting of a Water 1515 pump and Waters 2489 UV-vis detector. Differential scanning calorimetry (DSC) data was obtained from a TA DSCQ200 in the range of 25 – 300 °C at a heating rate of 10°C min^{-1} under nitrogen atmosphere. Thermogravimetric analyses (TGA) were performed on a NETZSCH STA 449C instrument under nitrogen atmosphere and decomposition was determined by the mass loss of 5% when heating at a rate of 20 °C min^{-1} from 20 °C to 500 °C. UV-vis absorption spectra were measured on Varian Cary 5E spectrometer. Photoluminescence spectra were recorded on a Fluorolog III ISA spectrofluorimeter. Cyclic voltammetry (CV) was performed on a CH

Instruments electrochemical workstation at room temperature in deoxygenated *N,N*-dimethylformamide with 0.1 M tetrabutylammonium hexafluorophosphate as a supporting electrolyte at scanning rate of 50 mV/s. A platinum wire was used as a working electrode and an Ag/AgCl electrode was used as a reference electrode. Ferrocene/ferrocenium ($Cp_2Fe^{+/0}$) was used as a potential standard for calibration.

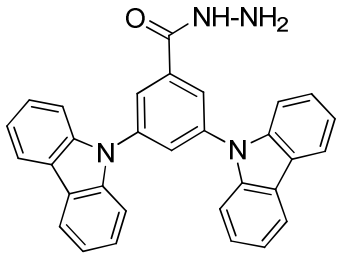

S4.1: To a solution of **S3.12** (10.0 g, 0.5 mmol) in dioxane (100 mL) and ethanol (70 mL) was added hydrazine monohydrate (20 mL). The reaction mixture was reflux for 6 hours. The reaction mixture was cooled down to room temperature and water (380 mL) was added. The solid was collected by filtration, washed with water and dried under vacuum to yield a white solid (10.0 g, 100 %). This compound can be used for next step without any purification. ^{1}H NMR (400 MHz, $CDCl_3$): δ 8.13 (dd, J_1 = 7.6 Hz, J_2 = 0.8 Hz, 4H), 8.05 (d, J = 2.0 Hz, 2H), 7.98 (t, J = 2.0 Hz, 1H), 7.52 (s, br, 1H), 7.50 (dd, J_1 = 7.6 Hz, J_2 = 0.8 Hz, 4H), 7.43 (td, J_1 = 7.6 Hz, J_2 = 0.8 Hz, 4H), 7.31 (td, J_1 = 7.6 Hz, J_2 = 0.8 Hz, 4H), 4.16 (br, 2 H).^{13}C{1H} NMR (100 MHz, $CDCl_3$) δ: 166.85, 140.23, 139.99, 136.14, 128.09, 126.31, 123.85, 123.73, 120.73, 120.55, 109.42. MS (EI) m/z : 466.0 [M+]. Anal. calcd. for $C_{31}H_{22}N_2O$: C, 79.81; H, 4.75; N, 12.01. Found: C, 79.90; H, 4.78; N, 11.82.

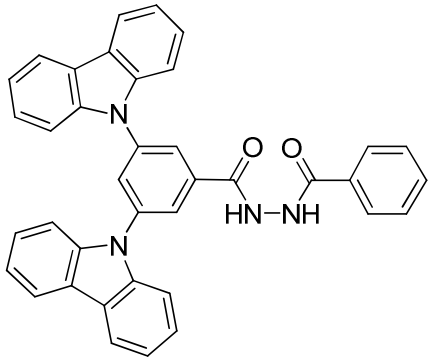

S4.2: To a solution of **S4.1** (1.0 g, 2 mmol) in dry tetrahydrofuran (20.0 mL) benzoyl chloride (0.4 g, 3 mmol) was added slowly at 0 °C under nitrogen. After stirring at room temperature for 21 hours, pyridine (5 mL) was added and stirred for another 1 hour. The reaction mixture was poured into deionized water (200 mL) and a precipitate was collected by filtration, washed with water and dried to afford a white powder (1.2 g, 100 %). ^{1}H NMR (400 MHz, $CDCl_3$): δ 10.92 (s, 1H), 10.67 (s, 1H), 8.31 (d, J = 2.0 Hz, 2H), 8.25 (d, J = 8.0 Hz, 4H), 8.14 (t, J = 2.0 Hz, 1H), 7.91 (m, 2H), 7.64 (m, 1H), 7.63 (d, J = 8.0 Hz, 4H), 7.50 (m, 6H), 7.32 (t, J = 8.0 Hz, 4H). HRMS calcd for $C_{38}H_{26}N_4O_2$ [M+1] 570.2056, found 570.2056. Anal. calcd. for $C_{38}H_{26}N_4O_2$: C, 79.98; H, 4.59; N, 9.82. Found: C, 79.51; H, 4.57; N, 8.91.

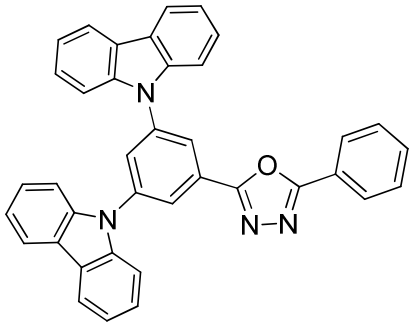

4.30: **S4.2** (1.0 g, 2 mmol) was added to neat $POCl_3$ (20 mL). The reaction was heated to 90 °C for 6 hours. After cooling down, the mixture was poured into ice-water (600 mL). The solid formed was collected by vacuum filtration. The crude product was dried and

purified by silica gel column using dichloromethane/ethyl acetate (9.5:0.5) as eluent. After removal of solvents, pure product as white solid was obtained (0.70 g, 72.7%). ^{1}H NMR (400 MHz, $CDCl_3$): δ 8.49 (d, J = 2.0 Hz, 2 H), 8.17 (dd, J_1 = 8.0 Hz, J_2 = 1.2 Hz, 4H), 8.12 (dd, J_1 = 8.4 Hz, J_2 = 1.6 Hz, 2H), 8.02 (t, J = 2.0 Hz, 1H), 7.57 (d, J = 8.0 Hz, 4H), 7.52 (m, 3H), 7.48 (td, J_1 = 8.0 Hz, J_2 = 1.2 Hz, 4H), 7.34 (td, J_1 = 8.0 Hz, J_2 = 1.2 Hz, 4H), 2.64 (s, 3H). ^{13}C{^{1}H} NMR (100 MHz, $CDCl_3$): δ 165.21, 163.27, 140.49, 140.31, 132.09, 129.15, 127.97, 127.41, 127.09, 126.42, 123.84, 123.67, 123.43, 120.80, 120.60, 109.53. MS (EI) m/z : 552.1 [M+]. Anal. calcd. for $C_{38}H_{24}N_4O$: C, 82.59; H, 4.38; N, 10.14. Found: C, 82.69; H, 4.31; N, 10.17.

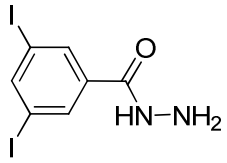

S4.3: To methyl 3,5-diiodobenzoate (5.0 g, 13 mmol) in ethanol (120 mL) hydrazine monohydrate (50 mL) was added and the mixture was refluxed for 18 hours. After cooling to room temperature, deionized water (300 mL) was added and a precipitate was collected by filtration. The product was washed with water and dried to obtain a white solid, 4.6 g (92.0%). ^{1}H NMR (400 MHz, DMSO- d_6): δ 9.92 (s, 1 H), 8.22 (t, J = 1.6 Hz, 1 H), 8.12 (d, J = 1.6 Hz, 2 H), 4.53 (s, 2H). ^{13}C{1H} NMR (100 MHz, DMSO-d_6): δ 163.26, 146.96, 137.04, 135.37, 96.48. MS (EI) m/z = 387.8 [M+]. Anal. calcd. for $C_7H_6I_2N_2O$: C, 21.67; H, 1.56; N, 7.22. Found: C, 21.88; H, 1.44; N, 7.23.

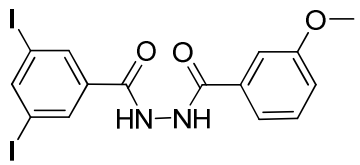

S4.4: To a solution of **S4.3** (4.5 g, 12 mmol) in anhydrous THF and *N,N*-dimethylformamide (100 mL : 10 mL) 3-methoxybenzoyl chloride (2.2 g, 13 mmol) was added slowly at 0 °C under nitrogen. After addition of 3-methoxybenzoyl chloride, the reaction was allowed to return to room temperature and stirred for 19 hours and then pyridine (20 mL) was added and stirred for an additional 45 min. Deionized water (300 mL) was added to reaction mixture and a precipitate formed and was collected by filtration and washed with water. The product was purified by recrystallization from methanol. After drying, the product was obtained as a white powder, 5.05 g (83.3%).^{1}H NMR (400 MHz, DMSO-d_6): δ 10.72 (s, 1H), 10.62 (s, br, 1H), 8.33 (t, J = 1.6 Hz, 1H), 8.23 (d, J = 1.6 Hz, 2H), 7.50-7.41 (m, 3H), 7.15 (m, 1H), 3.81 (s, 3H). ^{13}C{^{1}H} NMR (100 MHz, DMSO-d_6): δ 165.91, 163.57, 159.68, 147.82, 136.23, 135.82, 134.11, 130.18, 120.17, 118.33, 112.99, 96.67, 55.79. MS (EI) m/z = 552.9 [M+H]. Anal. calcd. for $C_{15}H_{12}I_2N_2O_3$: C, 34.51; H, 2.32; N, 5.37. Found: C, 34.78; H, 2.25; N, 5.42.

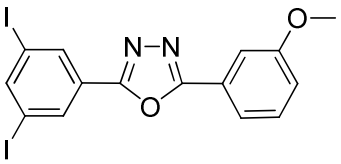

S4.5: **S4.4** (5.0 g, 9.6 mmol) was added to neat $POCl_3$ (60 mL) and the reaction mixture was stirred at 100 °C. After 2 h, the reaction mixture was cooled and was carefully added into ice-water (1000 mL). A white precipitate formed and was collected by filtration and washed with deionized water. After drying, the crude product was purified by column chromatography (silica gel ; dichloromethane:ethyl acetate = 95:5) to afford a white solid that was recrystallized from acetone/water and dried to obtain the product as a white solid, 3.4 g (70.8 %). ^{1}H NMR (400 MHz, $CDCl_3$): δ 8.43 (dd, J_1 = 1.6 Hz, J_2 = 0.8 Hz, 2H), 8.23 (t, J = 1.6 Hz, 1H), 7.71 (d, J = 8.0 Hz, 1H), 7.66 (m, 1H), 7.46 (t, J = 8.0 Hz,

1H), 7.12 (dd, J_1 = 8.0 Hz, J_2 = 2.4 Hz, 1H), 3.92 (s, 3 H). $^{13}C\{^1H\}$ NMR (100 MHz, $CDCl_3$): δ 165.06, 161.67, 159.98, 148.05, 134.63, 130.31, 126.95, 124.44, 119.44, 118.56, 111.66, 94.98, 55.59. MS (EI) m/z = 503.9 [M+]. Anal. calcd. for $C_{15}H_{10}I_2N_2O_2$: C, 35.74; H, 2.00; N, 5.56. Found: C, 35.58; H, 1.92; N, 5.60.

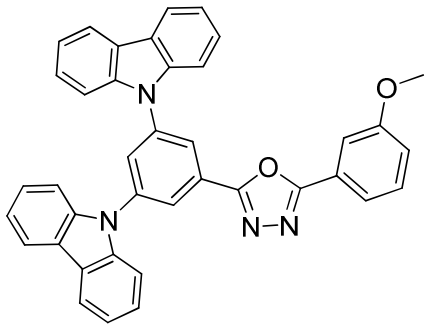

4.31: **S4.5** (1.0 g, 2 mmol), 9*H*-carbazole (1.0 g, 6 mmol), Cu powder (2.0 g, 31 mmol) and potassium carbonate (4.0 g, 29 mmol) were combined in *N,N*-dimethylformamide (20 mL) and stirred at 150 °C for 5 h. After cooling, the reaction mixture was diluted with THF (100 mL) and solids were filtered and washed with THF. The combined filtrate was concentrated *in vacuo* and deionized water (150 mL) was added to produce a brown solid that was collected by filtration. The crude product was purified by column chromatography (silica gel ; dichloromethane:ethyl acetate = 97:3) to afford a white solid that was recrystallized from acetone/methanol and dried to afford a white solid, 0.99 g (86.1%). ^1H NMR (400 MHz, $CDCl_3$): δ 8.47 (d, J = 2.4 Hz, 2H), 8.16 (d, J = 8.0 Hz, 4H), 8.01 (t, J = 1.6 Hz, 1H), 7.69-7.64 (m, 2H), 7.58 (d, J = 8.0 Hz, 4H), 7.45 (m, 4H), 7.41 (t, J = 8.0 Hz, 1H), 7.34 (m, 4H), 7.08 (m, 1H), 3.87 (s, 3H). $^{13}C\{^1H\}$ NMR (100 MHz, $CDCl_3$): δ 165.19, 163.30, 159.98, 140.46, 140.28, 130.31, 128.03, 127.38, 126.43, 124.49, 123.81, 123.72, 120.80, 120.60, 119.48, 118.66, 111.55, 109.52, 55.57. MS (EI)

m/z = 582.2 [M+]. Anal. calcd. for $C_{39}H_{26}N_4O_2$: C, 80.39; H, 4.50; N, 9.62. Found: C, 80.32; H, 4.41; N, 9.60.

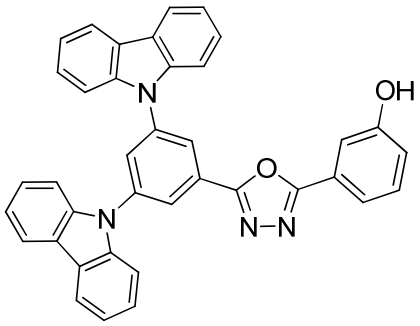

S4.6: BBr_3 (30 mL of a 1.0 M solution in dichloromethane) was added dropwise to a solution of **4.31** (0.95 g, 1.6 mmol) in anhydrous dichloromethane (20.0 mL) at -78 °C (dry-ice/acetone bath) under nitrogen. After addition of BBr_3 solution, the reaction was allowed to return to room temperature and stirred for 6 h. The reaction mixture was then poured into ice-water (100 mL) and dichloromethane was removed *in vacuo* to afford a solid that was collected by filtration. The crude product was purified by recrystallization from acetone/water, filtered and dried to give a white solid, 0.92 g (98.9%).^{1}H NMR (400 MHz, DMSO-d_6): δ 10.01 (s, br, 1H), 8.46 (d, J = 1.6 Hz, 2H), 8.28 (d, J = 8.0 Hz, 4H), 8.17 (t, J = 1.6 Hz, 1H), 7.66 (d, J = 8.0 Hz, 4 H), 7.59 (d, J = 8.0 Hz, 1H), 7.50 (m, 5H), 7.34 (m, 5H), 7.00 (dd, J_1 = 8.4 Hz, J_2 = 2.4 Hz, 1H). ^{13}C{^{1}H} NMR (100 MHz, Acetone-d_6) δ: 166.00, 164.37, 158.90, 141.54, 141.36, 131.55, 129.21, 128.77, 127.45, 125.90, 124.86, 124.72, 121.67, 121.44, 120.11, 119.18, 114.33, 110.79. MS (EI) m/z = 568.2 [M+]. Anal. calcd. for $C_{38}H_{24}N_4O_2$: C, 80.27; H, 4.25; N, 9.85. Found: C, 80.38; H, 4.23; N, 9.79.

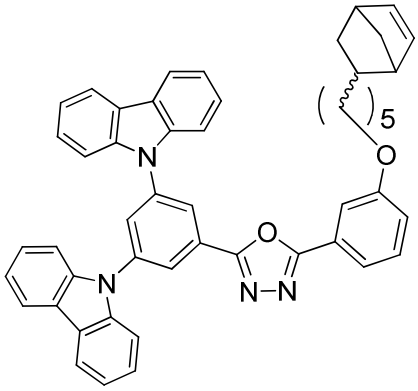

S4.7: To a solution of **S4.6** (0.90 g, 1.6 mmol) and 5-(5-bromopentyl)bicyclo[2,2,1]hept-2-ene (0.5 g, 2 mmol) in *N,N*-dimethylformamide (10 mL) was added K_2CO_3 (5.0 g, 36 mmol) at room temperature. After 24 h, deionized water (150 mL) was added and a solid product was collected by filtration. The crude product was purified by column chromatography (silica gel; toluene:ethyl acetate = 95:5) and produced a glassy material to which acetone (3 mL) was added and after dissolving, started to precipitate as a white solid. Methanol was added into the solution to complete the precipitation and the white product was collected by filtration and dried. The final product was obtained as a white powder, 0.99 g (79 %). ^{1}H NMR (400 MHz, $CDCl_3$): δ 8.48 (d, J = 1.6 Hz, 2H), 8.17 (d, J = 8.0 Hz, 4H), 8.02 (t, J = 1.6 Hz, 1H), 7.68-7.58 (m, 6H), 7.50-7.33 (m, 9H), 7.07 (dd, J_1 = 8.0 Hz, J_2 = 2.0 Hz, 1H), 6.09 (q, J = 2.8 Hz, 0.7H), 6.08 (q, J = 2.8 Hz, 0.3H), 6.00 (q, J = 2.8 Hz, 0.3H), 5.90 (q, J = 2.8 Hz, 0.7H), 4.00 (t, J = 6.4 Hz, 2H), 2.74 (s, br, 1.7H), 2.49 (s, br, 0.3 H), 1.96 (m, 1H), 1.81 (m, 2.5H), 1.46-1.03 (m, 7.5H), 0.47 (m, 1H). ^{13}C{^{1}H} NMR (100 MHz, $CDCl_3$): δ 165.24, 163.26, 159.58, 140.47, 140.31, 136.91, 132.33, 130.23, 128.02, 127.42, 126.42, 124.44, 123.81, 123.72, 120.79, 120.59, 119.25, 118.96, 112.29, 109.52, 68.34, 49.52, 45.37, 42.48, 38.64, 34.63, 32.37, 29.13, 28.34, 26.20. MS (FAB): m/z = 730.4 [M+]. Anal. calcd. for $C_{50}H_{42}N_4O_2$: C, 82.16; H, 5.79; N, 7.67. Found: C, 82.31; H, 5.77; N, 7.68.

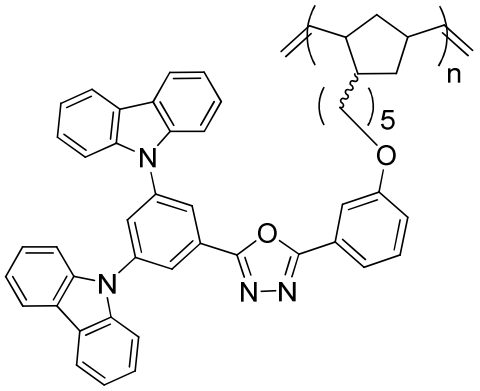

4.32: **S4.7** (0.5 g, 0.7 mmol) was weighed into a bottle. A Grubbs's first generation catalyst (0.0056 g, 6.8 x 10^{-3} mmol) was weighed out into a separate vial. The bottle and vial were placed into a glove box. 6 mL of anhydrous and deoxygenated dichloromethane was added to the bottle containing monomer. 1 mL of anhydrous and deoxygenated dichloromethane was added to vial containing Grubbs' first generation catalyst and shaken vigorously. Subsequently, the catalyst solution was quickly transferred to the bottle with monomer. The polymerization was allowed to proceed overnight for 22 hours. The reaction was quenched (out of glovebox) with 2 mL of ethyl vinyl ether and after 30 min was precipitated into ethanol. The polymer was then vacuum filtered and re-dissolved in minimal (< 3 mL) dichloromethane and 1 mL of ethyl vinyl ether was added. This solution was then added (dropwise) into ethanol to precipitate the polymer. The reprecipitation process of isolating, dissolving, and vacuum filtering the precipitated polymer was repeated 2 more times. The isolated product was dried under vacuum to give an off-white powder (0.38 g, 76.0%).^{1}H NMR(400 MHz, $CDCl_3$): δ 8.39 (br s, 2H), 8.07 (br s, 4H), 7.91 (br s, 1 H), 7.53 (br d, 6 H), 7.39 (br s, 4 H), 7.25 (br s, 5 H), 6.94 (br m, 1 H), 5.21 (br m, 2 H), 3.87 (br m, 2 H), 2.85-2.69 (br m, 1 H), 2.47-2.32 (br m, 2 H), 1.80-1.66 (br m, 6 H), 1.25-1.06 (br m, 6 H). Anal. calcd. for $C_{50}H_{42}N_4O_2$: C,

82.16; H, 5.79; N, 7.67. Found: C, 81.17; H, 5.74; N, 7.58. Gel Permeation Chromatography (chloroform): M_w = 160,000; M_n = 61,000; PDI = 2.60.

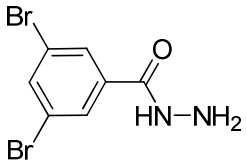

S4.8: Synthesized according to the literature.[7] ^{1}H NMR was consistent with the literature.

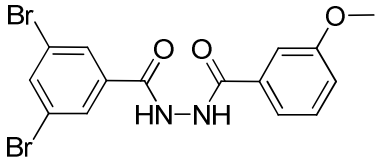

S4.9: **S4.8** (5.002 g, 17.0 mmol) was dissolved in anhydrous THF (40 mL) under inert atmosphere. Due to poor solubility, anhydrous *N,N*-dimethylformamide (40 mL) was added and the mixture cooled to 0 °C in an ice-water bath. After cooling, 3-methoxybenzoyl chloride (3.304 g, 19.4 mmol) was added dropwise. After 24 h, the mixture was added to deionized water and a precipitate formed, was collected, and dried to afford a white powder (2.291 g, 31.5%). ^{1}H (300 MHz, DMSO-d_6): δ 10.75 (s, 1H), 10.61 (s, 1H), 8.14-8.10 (m, 1H), 8.09-8.07 (m, 2H), 7.51-7.39 (m, 3H), 7.18-7.12 (m, 1H), 3.81 (s, 3H). ^{13}C{^{1}H} NMR (75MHz, DMSO-d_6): δ 165.89, 163.53, 159.68, 137.18, 136.38, 134.05, 130.21, 129.88, 123.31, 120.16, 118.37, 112.95, 55.77. MS (EI) m/z = 425.9 [M+]. Anal. calcd. for $C_{15}H_{12}Br_2N_2O_3$: C, 42.09; H, 2.83; N, 6.54. Found: C, 42.28; H, 2.63; N, 6.48.

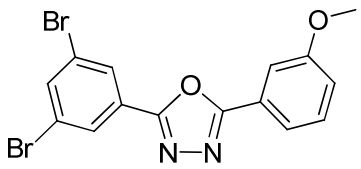

S4.10: **S4.9** (2.365 g, 5.526 mmol) in neat $POCl_3$ (15.0 mL) was stirred under nitrogen atmosphere at 100 °C for 2 hours. Upon cooling, the reaction mixture was poured slowly into *ca*. 400 mL of an ice-water mixture, resulting in the formation of a white precipitate, which was collected by filtration and washed with deionized water. Chromatography of the crude material (silica ; dichloromethane:ethyl acetate = 95:5) yielded the final product as a white solid (1.471 g, 65%).^{1}H (300 MHz, $CDCl_3$): δ 8.18 (d, J = 1.7 Hz, 2H), 7.81 (t, J = 1.7 Hz, 1H), 7.70-7.65 (m, 1H), 7.64-7.60 (m, 1H), 7.41 (t, J = 8.0 Hz, 1H), 7.08 (ddd, J_1 = 8.3, J_2 = 2.6, J_3 = 0.8 Hz, 1H), 3.88 (s, 3H). ^{13}C{^{1}H} NMR (75 MHz, $CDCl_3$): δ 165.14, 162.14, 160.04, 137.05, 130.34, 128.43, 128.40, 126.95, 124.45, 123.71, 119.47, 118.62, 11.71, 55.60. MS (EI) m/z = 409.9 [M+]. Anal. calcd. for $C_{15}H_{10}Br_2N_2O_2$: C, 43.94; H, 2.46; N, 6.83. Found: C, 43.64; H, 2.32; N, 6.75.

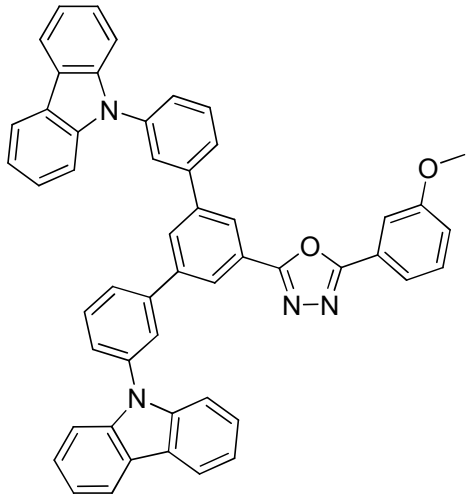

4.33: **S4.10** (1.302 g, 3.175 mmol), 9-(3-(4,4,5,5-tetramethyl-1,3,2-dioxaborolan-2-yl)phenyl)-9H-carbazole (2.815 g, 7.623 mmol), and $Pd(PPh_3)_4$ (0.148 g, 0.128 mmol) were dissolved in a solution of anhydrous toluene (100 mL) and absolute ethanol (50 mL) under nitrogen atmosphere. In a separate flask, K_2CO_3 (13.84 g, 100.1 mmol) was dissolved in deionized water (50 mL) and the resulting solution was added to the reaction

mixture, which was then refluxed with stirring for 24 hours. Upon cooling, the reaction mixture was diluted with 150mL of deionized water, 50 mL of brine were added, and the organic layer was extracted once with 400mL of chloroform, then twice more with 100 mL portions of chloroform. The organic layers were combined, washed with brine (1 x 250 mL) then dried over magnesium sulfate, and concentrated *in vacuo* to yield a dark yellow, oily solid. The oil was purified by column chromatography (silica gel; dichloromethane:ethyl acetate = 95:5) and then precipitated in methanol to afford a white solid (1.648 g, 72%).^{1}H (300 MHz, $CDCl_3$): δ 8.42 (s, 1H), 8.41 (s, 1H), 8.18-8.15 (m, 4H), 8.06 (t, *J* = 1.7 Hz, 1H), 7.93 (t, *J* = 1.7 Hz, 2H), 7.94-7.63 (m, 8H), 7.50-7.39 (m, 9H), 7.33-7.28 (m, 4H), 7.12-7.08 (m, 1H), 3.89 (s, 3H). ^{13}C{^{1}H} NMR (75 MHz, $CDCl_3$): δ 164.90, 164.29, 160.05, 142.08, 141.68, 140.84, 138.56, 130.67, 130.26, 129.32, 126.87, 126.42, 126.09, 126.03, 125.95, 125.36, 124.85, 124.81, 123.47, 120.44, 120.13, 119.47, 118.27, 111.82, 109.74, 55.68. MS (EI) m/z = 734.2 [M+]. Anal. calcd. for $C_{51}H_{34}N_4O_2$: C, 83.36; H, 4.66; N, 7.62. Found: C, 83.22; H, 4.55; N, 7.68.

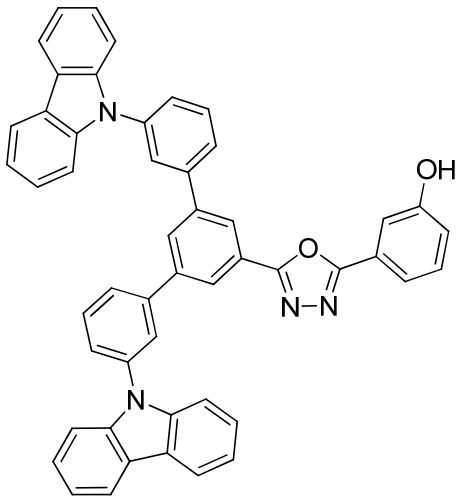

S4.11: BBr_3 (4.20 mL of a 1.0 M solution in dichloromethane) was added to a solution of **4.33** (0.749g, 1.02 mmol) in anhydrous dichloromethane (20 mL) at -78 °C (dry-

ice/acetone bath) under nitrogen atmosphere. The resulting mixture was allowed to warm to room temperature overnight and was then slowly poured unto 50 mL of an ice-water resulting in the formation of a white precipitate, which was collected by filtration. Purification of the crude material was attempted by column chromatography (silica gel ; dichloromethane:ethyl acetate = 90:10) but was hindered by poor solubility. The crude material, 0.499 g, was used in the next step without additional purification. ^{1}H (300 MHz, $CDCl_3$): δ 9.98 (s, 1H), 8.44 (d, J = 1.5 Hz, 2H), 8.38 (t, J = 1.5 Hz, 1H), 8.22 (d, J = 7.6 Hz, 4H), 8.17 (t, J = 1.6 Hz, 2H), 8.07-8.00 (m, 2H), 7.79 (t, J = 7.8 Hz, 2H), 7.69-7.63 (m, 2H), 7.62-7.57 (m, 1H), 7.55-7.52 (m, 1H), 7.47-7.35 (m, 9H), 7.29-7.23 (m, 4H), 7.00 (dd, J_1 = 8.2 Hz, J_2 = 0.8 Hz, 1H). ^{13}C{^{1}H} NMR (75 MHz, DMSO-d_6): δ 164.78, 164.19, 158.37, 141.71, 141.40, 140.60, 138.08, 131.30, 127.05, 126.89, 126.73, 126.00, 125.96, 125.34, 124.93, 124.71, 123.21, 120.95, 120.52, 119.71, 118.09, 113.62, 110.18. MS (EI) m/z = 720.3 [M+]. Anal. calcd. for $C_{50}H_{32}N_4O_2$: C, 83.31; H, 4.47; N, 7.77. Found: C, 82.29; H, 4.58; N, 7.43. [As elemental analysis failed due to inability to purify material see ^{1}H NMR below]

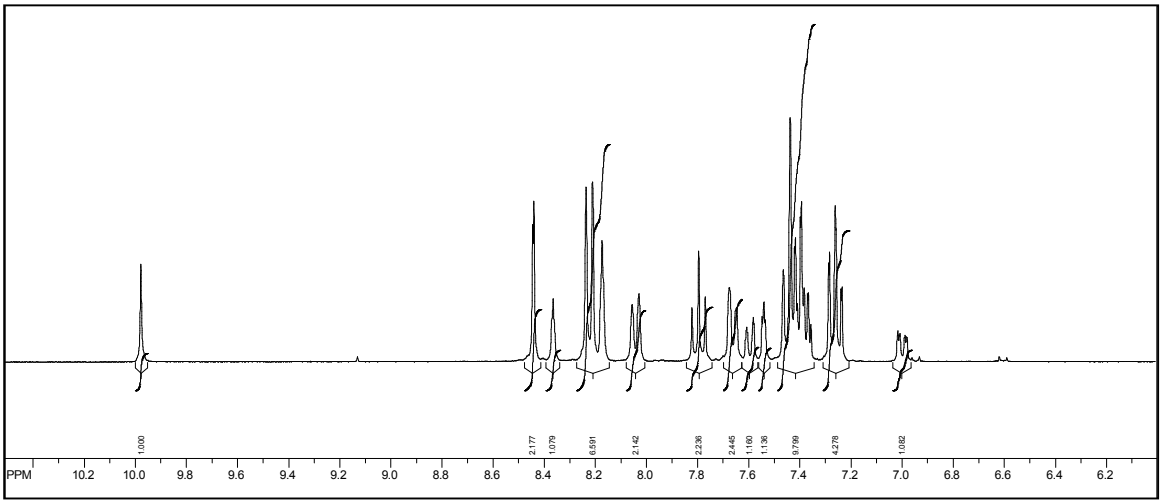

Figure 2.3. ^{1}H NMR (300 MHz, $CDCl_3$) of **S4.11**.

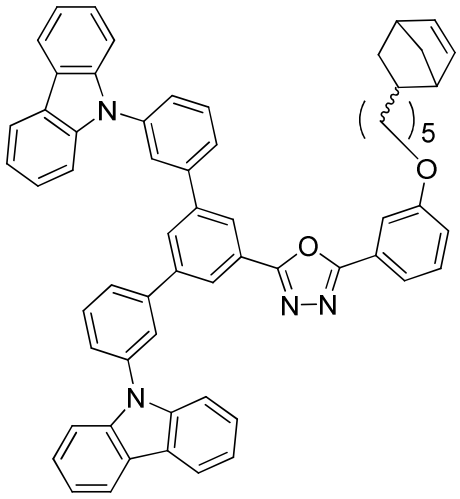

S4.12: To a solution of **S4.11** (0.370 g, 0.514 mmol) and 5-(5-bromopentyl)bicyclo[2.2.1]hept-2-ene (0.177 g, 0.728 mmol) in N,N-dimethylformamide (15 mL) was added K_2CO_3 (0.385 g, 2.786 mmol) and the resulting mixture was stirred at 100 °C for 22 hours. Upon cooling, 200 mL of dichloromethane was added and the mixture was washed with deionized water (2 x 100 mL). The organic layer was dried over magnesium sulfate and concentrated *in vacuo*. The solution was then dissolved in diethyl ether (100 mL) and washed with deionized water (100 mL). The organic layer was then dried over magnesium sulfate and concentrated *in vacuo* to give a waxy yellow solid. The crude material was purified by column chromatography (silica gel ; dichloromethane:ethyl acetate = 95:5) and the product was subsequently precipitated in methanol, collected, and dried to yield the final product as a white solid (0.403 g, 60%). ^{1}H (300 MHz, $CDCl_3$): δ 8.42 (s,1H), 8.41 (s, 1H), 8.16 (dt, J_1 = 7.8 Hz, J_2 = 0.9 Hz, 4H), 8.05 (t, J = 1.8, 1H), 7.93 (t, J = 1.8 Hz, 2H), 7.85-7.62 (m, 8H), 7.49-7.39 (m, 9H), 7.33-7.28 (m, 4 Hz), 7.10-7.06 (m, 1H), 6.12-5.90 (m, 2H), 4.06-4.01 (m, 2H), 2.76-2.75 (m, 2H), 2.05-1.94 (m, 1H), 1.87-1.74 (m, 3H), 1.48-1.03 (m, 8H), 0.52-0.46 (m, 1H). ^{13}C{^{1}H} NMR (75 MHz, $CDCl_3$): δ 164.89, 164.18, 159.55, 142.07, 141.68, 140.83,

138.55, 136.97, 132.39, 130.64, 130.19, 129.30, 126.85, 126.41, 126.07,125.95, 125.38, 124.84, 124.75, 123.46, 120.41, 120.11, 119.25, 118.62, 112.44, 109.71, 68.36, 49.59, 45.43, 42.54, 38.71, 34.70, 32.44, 29.22, 28.42, 26.27. MS (EI) m/z = 882.0 [M+]. Anal. calcd. for $C_{62}H_{50}N_4O_2$: C, 84.33; H, 5.71; N, 6.34. Found: C, 84.04; H, 5.60; N, 6.37.

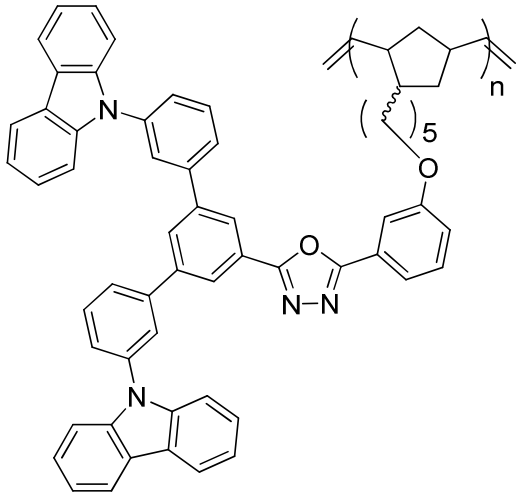

4.34: In a Schlenk tube under nitrogen atmosphere, **S4.12** (0.275 g, 0.311 mmol) was dissolved in 2.0 mL of anhydrous dichloromethane. In a separate flask, Grubbs' first generation catalyst (0.0026 g, 0.0031 mmol) was dissolved in 1.0 mL of anhydrous dichloromethane and the resulting solution was added to the Schlenk tube. The reaction mixture was then stirred for 40 minutes at room temperature and then ethyl vinyl ether (2.0 mL) was added. The solution was concentrated *in vacuo* to yield a brown solid which was then precipitated in methanol to give the product as an off-white solid (0.235 g, 85%). ^{1}H (300 MHz, $CDCl_3$): δ 8.35-8.14 (br m, 2H), 8.12-7.99 (br m, 4H), 7.99-7.74 (br m, 3H), 7.74-7.44 (br m, 8H), 7.43-7.12 (br m, 13H), 7.02-6.78 (br m, 1H), 5.35-5.04 (br m, 2H), 4.00-3.68 (br m, 2H), 2.95-2.63 (br m, 1H), 2.58-2.19 (br m, 2H), 2.09 (br m, 5H), 1.54-0.82 (br m, 7H). Anal. calcd. for $C_{62}H_{50}N_4O_2$: C, 84.33; H, 5.71; N, 6.34.

Found: C, 83.46; H, 5.64; N, 6.24. Gel Permeation Chromatography (tetrahydrofuran): M_w = 37,700; M_n = 19,500; PDI = 1.94.

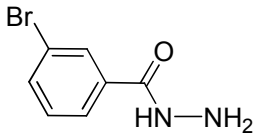

S4.13: Synthesized according to the literature.[8] ^{1}H NMR was consistent with the literature.

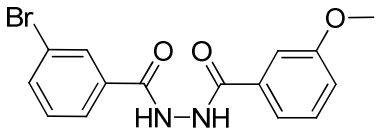

S4.14: **S4.13** (3.990 g, 18.6 mmol) was dissolved in a mixture of THF and *N,N*-dimethylformamide (20 mL: 20 mL) under inert atmosphere. 3-methoxybenzoyl chloride was added dropwise and reaction was stirred overnight. A precipitate that formed overnight was collected by filtration and addition of water to the filtrate produced more solids. Solids were combined and dried to afford a white powder (3.53 g, 54.4%). ^{1}H (300 MHz, DMSO-d_6): δ 10.64 (s, 1H), 10.55 (s, 1H), 8.07 (t, J = 1.7 Hz, 1H), 7.95-7.88 (m, 1H), 7.84-7.77 (m, 1H), 7.53-7.39 (m, 4H), 7.18-7.12 (m, 1H), 3.81 (s, 3H). ^{13}C {^{1}H} (75 MHz, DMSO-d_6): δ 165.9, 164.9, 159.7, 135.1, 134.2, 131.4, 130.6, 130.2, 127.0, 122.3, 120.1, 118.3, 112.9, 55.8. MS (EI) m/z = 348.0 [M+]. Anal. calcd. for $C_{15}H_{13}BrN_2O_3$: C, 51.60; H, 3.75; N, 8.02. Found: C, 51.74; H, 3.67; N, 8.08

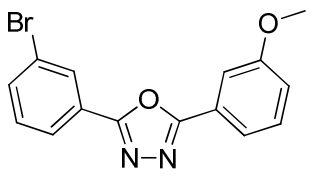

S4.15: **S4.14** (1.501 g, 4.30 mmol) was combined with $POCl_3$ (15 mL) under inert atmosphere and heated to 100 °C overnight. DCM (200 mL) was added to the cooled mixture and phases were separated and solvents removed *in vacuo*. The crude was purified by column chromatography (silica gel ; hexanes:ethyl acetate = 70:30) to afford a white powder (1.039 g, 73.2%). ^{1}H (300 MHz, DMSO-d_6): δ 8.27 (t, J = 1.6 Hz, 1H), 8.14-8.09 (dm, 1H), 7.85-7.80 (dm, 1H), 7.73-7.68 (dm, 1H), 7.64-7.61 (m, 1H), 7.59-7.48 (m, 2H), 7.19 (dd, J = 8.4, 2.6, 0.9 Hz, 1H), 3.85 (s, 3H). ^{13}C{^{1}H} (75 MHz, DMSO-d_6): δ 164.7, 163.3, 160.1, 135.2, 132.0, 131.1, 129.5, 126.2, 125.9, 124.7, 122.9, 119.6, 118.6, 112.1, 56.0. MS (EI) m/z = 330.0 [M+]. Anal. calcd. for $C_{15}H_{11}BrN_2O_2$: C, 54.40; H, 3.35; N, 8.46. Found: C, 54.55; H, 3.22; N, 8.45.

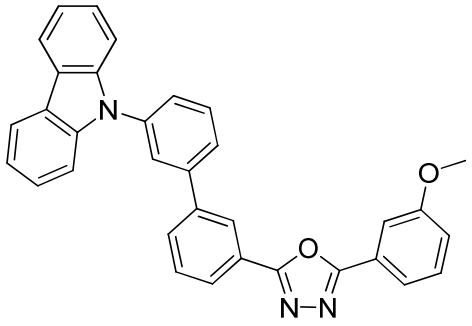

4.35: **S4.15** (0.900 g, 2.72 mmol), 9-(3-(4,4,5,5-tetramethyl-1,3,2-dioxaborolan-2-yl)phenyl)-9H-carbazole (1.206 g, 3.27 mmol), and $Pd(PPh_3)_4$ (0.127 g, 0.110 mmol) were dissolved in a solution of anhydrous toluene (80 mL) and absolute ethanol (40 mL). In a separate flask, K_2CO_3 (11.06 g, 80.0 mmol) was dissolved in deionized water (40 mL) and the resulting solution was added to the reaction mixture, which was then refluxed for 27 hours. Upon cooling, the reaction mixture was diluted with deionized water (150 mL) and brine (50 mL) were added and the organic layer was extracted once chloroform (200 mL) then twice more with 50 mL portions of chloroform. The organic layers were combined, washed with brine (100 mL), dried over magnesium sulfate, and

concentrated *in vacuo* to afford a dark oily solid. The crude material was purified by column chromatography (silica ; dichloromethane:ethyl acetate = 90:10) as a white solid and was then washed with pentane to give the final product (0.945 g, 70%). ^{1}H (300 MHz, $CDCl_3$): δ 8.40 (t, *J* = 1.5 Hz, 1H), 8.19-8.15 (m, 3H), 7.89-7.61 (m, 8H), 7.61-7.41 (m, 5H), 7.34-7.29 (m, 2H), 7.12-7.08 (m, 1H), 3.90 (s, 3H). ^{13}C{^{1}H} NMR (75 MHz, $CDCl_3$): δ 164.83, 164.53, 160.10, 141.97, 141.33, 140.94, 138.58, 130.69, 130.59, 130.37, 129.94, 126.69, 126.38, 126.19, 125.90, 125.68, 125.03, 124.77, 123.59, 120.53, 120.23, 119.52, 118.35, 111.81, 109.86, 55.70. MS (EI) m/z = 492.9 [M+]. Anal. calcd. for $C_{33}H_{23}N_3O_2$: C, 83.31; H, 4.70; N, 8.51. Found: C, 83.01; H, 4.64; N, 8.47.

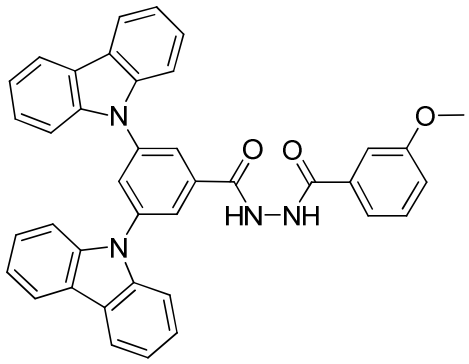

S4.16: **S4.1** (5.007 g, 10.7 mmol) was dissolved in anhydrous tetrahydrofuran (20 mL) and cooled to 0 °C over an ice-water bath under nitrogen atmosphere. 3-methoxybenzoyl chloride (2.056 g, 11.9 mmol) was added dropwise to the cooled solution. The mixture was stirred overnight and then pyridine (8 mL) was added. Then, deionized water (100 mL) was added and the mixture was extracted with dichloromethane (3 x 150 mL). The organic phase was dried over magnesium sulfate, filtered, and concentrated *in vacuo*. The crude product was purified by column chromatography (silica gel; 100% dichloromethane) to afford an oil that formed a precipitate upon addition of methanol. The precipitate was collected by filtration and dried to afford a white powder (3.898 g,

60.5%). ^{1}H (300MHz, DMSO-d_6): δ 10.93 (s, 1H), 10.66 (s, 1H), 8.35-8.30 (m, 2H), 8.25 (d, J = 7.8 Hz, 4H), 8.13 (t, J = 1.8 Hz, 1H), 7.62 (d, J = 8.2, 4H), 7.56-7.39 (m, 7H), 7.32 (t, J = 7.3 Hz, 4H), 7.19-7.12 (m, 1H), 3.80 (s, 3H). ^{13}C{^{1}H} NMR (100 MHz, $CDCl_3$): 166.10, 164.77, 159.68, 140.41, 139.47, 136.60, 134.18, 130.25, 126.98, 125.05, 123.51, 123.44, 121.07, 120.18, 118.33, 112.99, 110.24, 55.75. MS (EI) m/z = 600.2 [M+]. Anal. calcd. for $C_{39}H_{28}N_4O_3$: C, 77.98; H, 4.70; N, 9.33. Found: C, 77.13; H, 4.68; N, 9.53.

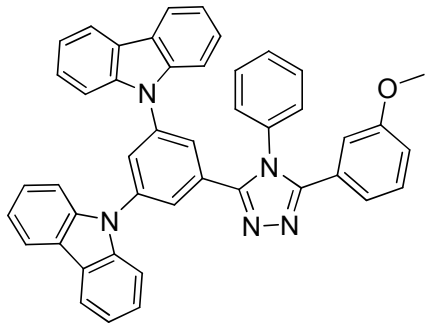

4.36:

Method 1: Aniline (3.793 g, 40.7 mmol) and anhydrous o-dichlorobenzene (50 mL) combined and cooled in ice-water bath under inert atmosphere. After mixture cooled to 0 °C, phenyl phosphorodichloridate (2.334 g, 11.1 mmol) added dropwise and ice-water bath removed. **S4.16** (5.999 g, 9.99 mmol) was added portion-wise and the mixture was heated to 195 °C. After 4h, heating was stopped and 2N HCl (200 mL) was added to cooled mixture. Phases were separated and aqueous layer was extracted with dichloromethane (2 x 100 mL). The combined organic phases were washed with deionized water (200 mL), dried over magnesium sulfate, filtered, and solvents removed *in vacuo* to afford a clear yellowish oil. The crude oil was purified (silica gel; ethyl acetate:dichloromethane = 70:30) and the product was isolated as a white powder (2.061 g, 31.4%). ^{1}H (300 MHz, DMSO-d_6): δ 8.22 (m, 4H), 7.92 (t, J = 2.0 Hz, 1H), 7.79 (d, J

= 1.9 Hz, 2H), 7.75-7.57 (m, 5), 7.47-7.39 (m, 4H), 7.36-7.25 (m, 9H), 7.01-6.94 (m, 2H), 6.87-6.84 (m, 1H), 3.60 (s, 3H). $^{13}C\{^{1}H\}$ (75 MHz, DMSO-d_6): δ 159.3, 154.9, 153.7, 140.1, 139.1, 135.2, 131.0, 130.8, 129.0, 128.4, 127.0, 123.5, 121.2, 121.1, 114.1, 110.1, 55.5. MS (EI) m/z = 657.0 [M+]. Anal. calcd. for $C_{45}H_{31}N_5O$: C, 82.17; H, 4.75; N, 10.65. Found: C, 82.04; H, 4.57; N, 10.52.

Method 2: **4.31** (1.751 g, 3.01 mmol) was added to distilled aniline (15 mL) and sealed in microwave reaction vessel and heated to 200 °C for 6 h (power = 250 W, Temperature = 200 °C, PSI = 250 psi, Run Time = 10 min, Hold Time = 90 min). The reaction solution was mixed with 2N HCl (100 mL) and dichloromethane (100 mL). The phases were separated, dried over magnesium sulfate, filtered, and solvents removed *in vacuo*. The crude product was purified by column chromatography (silica gel; gradient elution from 100% dichloromethane to dichloromethane: ethyl acetate = 80:20) to afford an oil that precipitated upon addition of methanol. The final product was obtained as a white powder (0.603 g, 35.7%). ^{1}H (300 MHz, *DMSO-d_6*): δ 8.22 (m, 4H), 7.92 (t, *J* = 2.0 Hz, 1H), 7.79 (d, *J* = 1.9 Hz, 2H), 7.75-7.57 (m, 5), 7.47-7.39 (m, 4H), 7.36-7.25 (m, 9H), 7.01-6.94 (m, 2H), 6.87-6.84 (m, 1H), 3.60 (s, 3H).

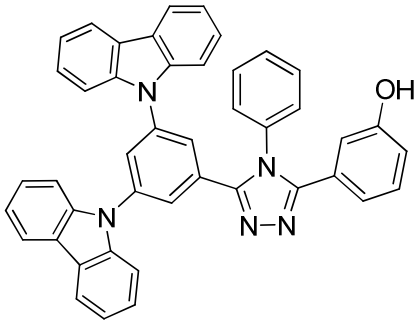

S4.17: **4.36** (1.004 g, 1.52 mmol) was dissolved in anhydrous dichloromethane (20 mL) under inert atmosphere and cooled to -78 °C (dry-ice/acetone bath). 1.0 M BBr_3 (1.574 g, 6.28 mmol) added dropwise and cooling bath was removed. After stirring overnight,

mixture added to ice-water mixture (100 mL) to afford a biphasic solution upon standing. The phases were separated and the aqueous phase was extracted with dichloromethane (2 x 50 mL). The combined organic phase was dried over magnesium sulfate, filtered, and solvents removed *in vacuo*. The crude was purified by column chromatography (silica gel; ethyl acetate:dichloromethane = 70:30) to afford a white powder (0.521 g, 53.3%). ^{1}H (300 MHz, DMSO-d_6): δ 9.70 (s, 1H), 8.22 (m, 4H), 7.92 (t, J = 1.9 Hz, 1H), 7.79 (d, J = 1.9 Hz, 2H), 7.75-7.57 (m, 5H), 7.48 – 7.40 (m, 4H), 7.37-7.26 (m, 8H), 7.13 (t, J = 7.9 Hz, 1H), 6.91-6.88 (m, 1H), 6.82-6.77 (m, 1H), 6.75-6.70 (m, 1H). ^{13}C{^{1}H} (75 MHz, DMSO-d_6): δ 157.7, 155.1, 153.6, 140.1, 139.0, 135.1, 131.1, 130.7, 130.0, 128.9, 128.3, 127.0, 125.8, 123.5, 121.0, 119.5, 115.9, 110.1. MS (EI) m/z = 643.2 [M+]. Anal. calcd. for $C_{44}H_{29}N_5O$: C, 82.09; H, 4.54; N, 10.88. Found: C, 81.97; H, 4.41; N, 10.90.

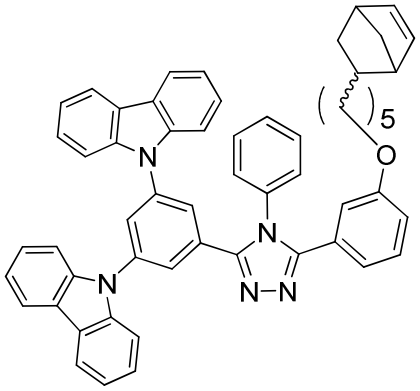

S4.18: To a solution of **S4.17** (0.404 g, 0.62 mmol) and 5-(5-bromopentyl)bicyclo[2.2.1]hept-2-ene (0.214 g, 0.880 mmol) in *N,N*-dimethylformamide (15 mL) was added K_2CO_3 (0.446 g, 3.23 mmol) and the resulting mixture was stirred at 100 °C overnight. Upon cooling, 200 mL of dichloromethane was added and the mixture was washed with deionized water (2 x 200 mL). The organic layer was dried over magnesium sulfate and concentrated *in vacuo*. The crude material was purified by column chromatography (silica gel ; dichloromethane:ethyl acetate = 70:30) and the

product was subsequently precipitated in methanol, collected, and dried to yield the final product as a white solid (0.368 g, 73.6 %). ^{1}H (300 MHz, DMSO-d_6): δ 8.22 (d, J = 7.8 Hz, 4H), 7.93-7.90 (m, 1H), 7.78 (d, J = 2.0 Hz, 2H), 7.74-7.56 (m, 5H), 7.47-7.39 (m, 4H), 7.36-7.22 (m, 9H), 7.00-6.90 (m, 2H), 6.86-6.82 (m, 1H), 6.12-6.05 (m, 1H), 6.02-5.87 (m, 1H), 3.73 (t, J = 6.5 Hz, 2H), 2.75-2.67 (m, 2H), 1.99-1.87 (m, 1H), 1.89-1.74 (m, 1H), 1.64-1.52 (m, 2H), 1.39-0.94 (m, 8H), 0.45-0.37 (m, 1H). ^{13}C{^{1}H} (75 MHz, DMSO-d_6): δ 158.95, 154.87, 154.13, 141.85, 141.00, 140.96, 138.32, 136.96, 135.36, 132.38, 130.47, 130.10, 129.60, 129.38, 128.17, 127.75, 127.69, 126.85, 126.66, 126.18, 126.01, 123.36, 120.82, 120.37, 120.04, 116.97, 114.07, 109.80, 67.98, 49.57, 45.40, 42.52, 38.67, 34.67, 32.41, 29.06, 28.31, 26.16. MS (EI) m/z = 805.4 [M+]. Anal. calcd. for $C_{56}H_{47}N_5O$: C, 83.45; H, 5.88; N, 8.69. Found: C, 83.31; H, 5.85; N, 8.66.

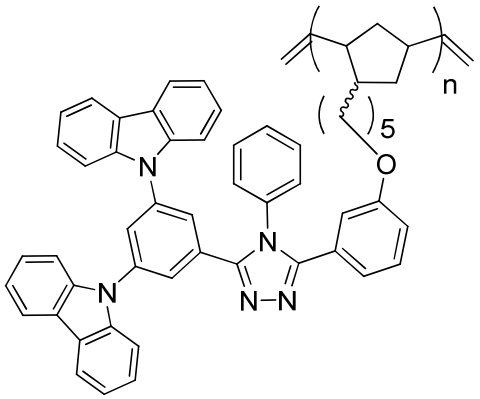

4.37: **S4.18** (0.321 g, 0.398 mmol) was weighed into a bottle. A Grubbs's first generation catalyst (0.0036 g, 4.4 x 10^{-3} mmol) was weighed out into a separate vial. The bottle and vial were placed into a glove box. 2 mL of anhydrous and deoxygenated dichloromethane was added to the bottle containing monomer. 2 mL of anhydrous and deoxygenated dichloromethane was added to vial containing Grubbs' first generation catalyst and shaken vigorously. Subsequently, the catalyst solution was quickly transferred to the bottle with monomer. The polymerization was allowed to proceed 30

min. The reaction was quenched (out of glovebox) with 2.5 mL of ethyl vinyl ether. The solution was concentrated *in vacuo* and precipitated into methanol. The polymer was then vacuum filtered and re-dissolved in minimal (< 3 mL) dichloromethane and 1 mL of ethyl vinyl ether was added. This solution was then added (dropwise) into ethanol to precipitate the polymer. The reprecipitation process of isolating, dissolving, and vacuum filtering the precipitated polymer was repeated 2 more times. The isolated product was dried under vacuum to give an off-white powder (0.126 g, 36.0%).^{1}H NMR(300 MHz, $CDCl_3$): δ 8.03 (br d, 4H), 7.76 (br s, 3H), 7.60-7.40 (br m, 3H), 7.38-7.17 (br m, 15H), 7.11-6.93 (br m, 2H), 6.85-6.67 (br m, 2H), 5.42-5.03 (br m, 2H), 3.85-3.58 (br m, 2H), 2.99-2.22 (br m, 2H), 2.02-1.73 (br m, 3H), 1.62-0.85 (br m, 9H). Anal. calcd. for $C_{56}H_{47}N_5O$: C, 83.45; H, 5.88; N, 8.69. Found: C, 82.76; H, 5.95; N, 8.56. Gel Permeation Chromatography (tetrahydrofuran): M_w = 22,900; M_n = 15,900; PDI = 1.44.

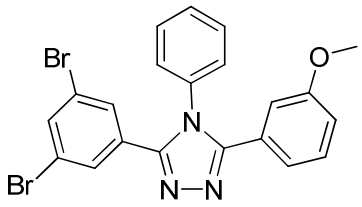

S4.19: Aniline (4.499 g, 11.7 mmol) and anhydrous o-dichlorobenzene (50 mL) were combined and cooled in ice-water bath under inert atmosphere. After the mixture cooled to 0 °C, phenyl phosphorodichloridate (2.508 g, 11.9 mmol) was added dropwise and the ice-water bath removed. **S4.10** (3.759 g, 5.79 mmol) was added portion-wise and then the mixture was heated to 195 °C. Additional o-dichlorobenzene was added (25 mL) to achieve complete dissolution of solids. After 24 h, heating was stopped and 2N HCl (100 mL) was added to the cooled mixture followed by dichoromethane (200 mL). The phases were separated and the aqueous layer was extracted with dichloromethane (2 x 200 mL).

The combined organic phases were washed with deionized water (200 mL), dried over magnesium sulfate, filtered, and solvents were removed *in vacuo* to afford an oil that was purified by column chromatography (silica gel ; gradient from 100% dichloromethane to 100% ethyl acetate). The product was precipitated with deionized water, filtered, and dried to obtain a white powder (2.972 g, 52.4%).^{1}H (300 MHz, DMSO-d_6): δ 7.94 (t, J = 1.8 Hz, 1H), 7.62-7.52 (m, 7H), 7.31 (t, J = 7.9 Hz, 1H), 7.05-6.98 (m, 2H), 6.94-6.92 (m, 1H), 3.65 (s, 3H). ^{13}C{^{1}H} (75 MHz, DMSO-d_6): δ 159.3, 154.8, 152.2, 135.0, 131.0, 130.7, 130.5, 130.2, 128.8, 128.2, 122.9, 121.1, 116.1, 114.2, 55.5. MS (EI) m/z = 486.0 [M+]. Anal. calcd. for $C_{21}H_{15}Br_2N_3O$: C, 51.99; H, 3.12; N, 8.66. Found: C, 51.80; H, 3.04; N, 8.72.

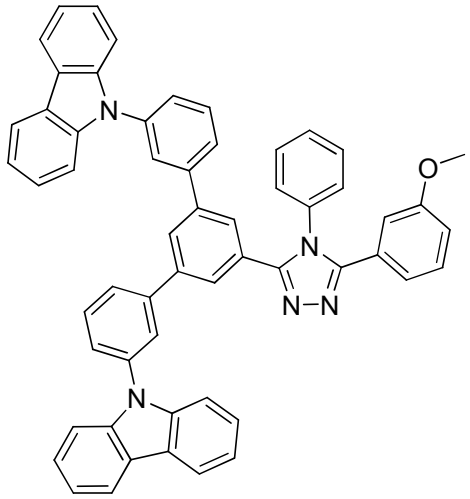

4.38: 9-(3-(4,4,5,5-tetramethyl-1,3,2-dioxaborolan-2-yl)phenyl)-9H-carbazole (2.677 g, 7.21 mmol), **S4.19** (1.412 g, 2.89 mmol), 2.0 M aq. potassium carbonate solution (50 mL), and toluene (100 mL) were combined under inert atmosphere and nitrogen was bubbled through the solution for ~ 30 min. Pd $(PPh_3)_4$ (0.169 g, 0.14 mmol) was added and the mixture was set to reflux overnight. The reaction mixture was cooled, deionized water (200 mL) was added, and then the mixture was extracted with chloroform (3 x 200

mL). The organic phase was washed with brine (1 x 200 mL), dried over magnesium sulfate, filtered, and solvents removed *in vacuo*. The crude was purified by column chromatography (silica gel ; gradient from 100% dichloromethane to dichloromethane:ethyl acetate = 75:25) and recrystallized from acetone to afford a white powder (0.827 g, 35.3%). ^{1}H (300 MHz, DMSO-d_6): δ 8.25 (d, J = 7.4 Hz, 4H), 8.17 (s, 1H), 7.82 (d, J = 7.5 Hz, 2H), 7.76-7.69 (m, 6H), 7.61 (d, J = 7.5 Hz, 2H), 7.48-7.35 (m, 10H), 7.33-7.20 (m, 5H), 7.08 (t, J = 7.5 Hz, 2H), 7.02-6.87 (m, 3H), 6.82 (t, J = 7.5 Hz, 1H), 3.58 (s, 3H). ^{13}C{^{1}H} (75 MHz, DMSO-d_6): δ 159.29, 154.57, 154.39, 141.61, 140.64, 138.04, 135.56, 131.3, 130.18, 130.15, 130.0, 129.91, 128.96, 128.72, 128.44, 126.95, 126.77, 125.65, 123.22, 121.0, 120.56, 115.98, 114.07, 110.20, 55.42. MS (EI) m/z = 809.4 [M+]. Anal. calcd. for $C_{57}H_{39}N_5O$: C, 84.52; H, 4.85; N, 8.65. Found: C, 84.26; H, 4.85; N, 8.58.

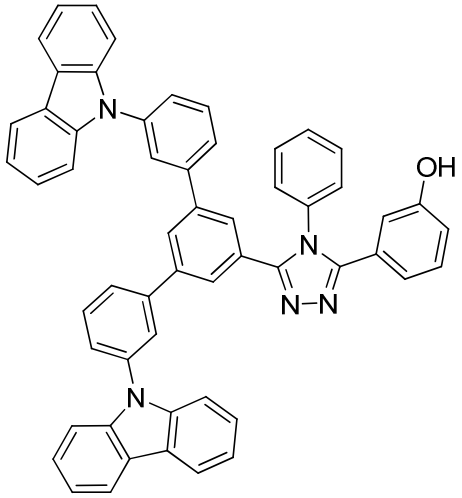

S4.20: **4.38** (0.806 g, 1.52 mmol) was dissolved in anhydrous dichloromethane (15 mL) under inert atmosphere and cooled to -78 °C (dry-ice/acetone bath). BBr_3 (5.0 mL of a 1.0 M solution in dichloromethane) added dropwise and cooling bath was removed. After stirring overnight, mixture added to ice-water mixture (100 mL) to afford a biphasic

solution upon standing. The phases were separated and the aqueous phase was extracted with dichloromethane (2 x 50 mL). The combined organic phase was dried over magnesium sulfate, filtered, and solvents removed *in vacuo*. The crude could not be purified by column chromatography due to solubility issues. The obtained product was used without further purification (0.311 g). ^{1}H (300 MHz, DMSO-d_6): δ 9.65 (s, 1H), 8.26 (d, J = 7.7 Hz, 4H), 8.17 (t, J = 1.4 Hz, 1H), 7.85-7.79 (m, 2H), 7.77-7.69 (m, 6H), 7.65-7.59 (m, 2H), 7.47-7.35 (m, 10H), 7.33-7.25 (m, 4H), 7.07 (td, J_1 = 7.8 Hz, J_2 = 3.2 Hz, 3H), 6.88-6.85 (m, 1H), 6.84-6.66 (m, 3H). ^{13}C{^{1}H} (75 MHz, DMSO-d_6): δ 157.66, 154.79, 154.29, 141.63, 140.64, 140.58, 138.03, 135.54, 131.30, 131.28, 130.10, 129.98, 128.88, 128.80, 128.38, 126.98, 126.95, 126.77, 125.66, 123.21, 120.99, 120.55, 119.46, 115.87, 110.22. MS (EI) m/z = 795.4 [M+]. Anal. calcd. for $C_{56}H_{37}N_5O$: C, 84.51; H, 4.69; N, 8.80. Found: C, 82.62; H, 4.52; N, 8.56. [As elemental analysis failed due to inability to purify material see ^{1}H NMR below]

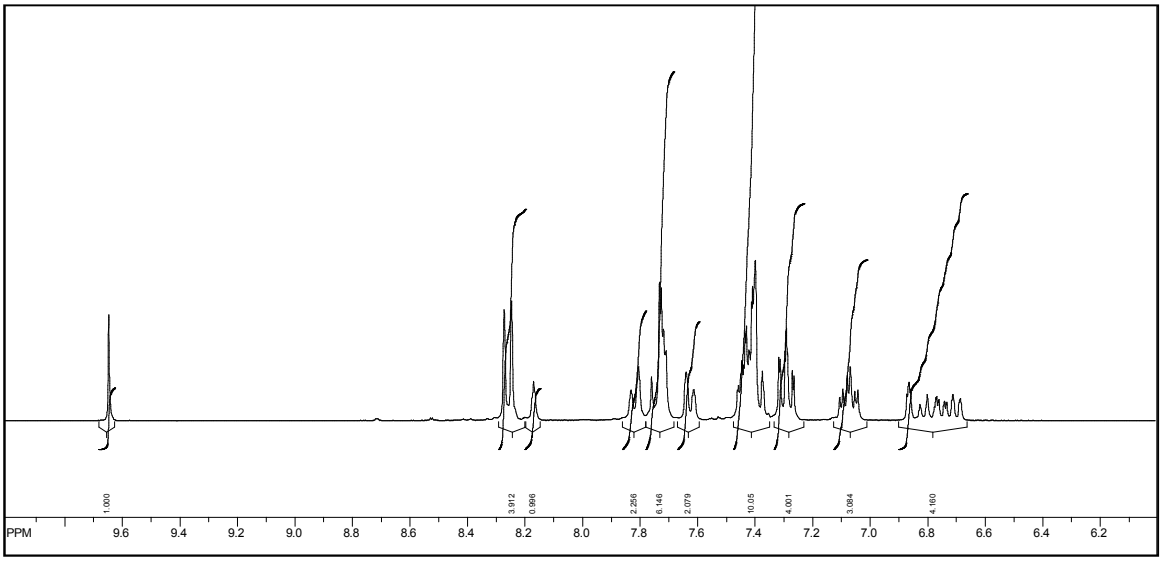

Figure 2.4. ^{1}H NMR (300 MHz, $CDCl_3$) of **S4.20**.

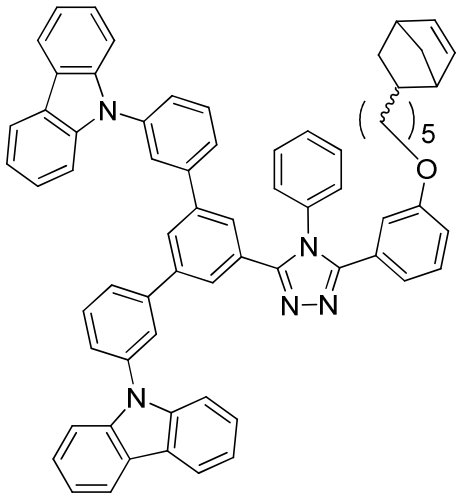

S4.21: To a solution of **S4.20** (0.401 g, 0.50 mmol) and 5-(5-bromopentyl)bicyclo[2.2.1]hept-2-ene (0.171 g, 0.703 mmol) in *N,N*-dimethylformamide (15 mL) was added K_2CO_3 (0.362 g, 2.62 mmol) and the resulting mixture was stirred at 100 °C overnight. Upon cooling, 200 mL of dichloromethane was added and the mixture was washed with deionized water (2 x 200 mL). The organic layer was dried over magnesium sulfate and concentrated *in vacuo*. The crude material was purified by column chromatography (silica gel ; dichloromethane:ethyl acetate = 70:30) and the product was subsequently precipitated in methanol, collected, and dried to yield the final product as a white solid (0.311 g, 64.5 %). ^{1}H (300 MHz, DMSO-d_6): δ 8.25 (d, J = 7.8 Hz, 4H), 8.18-8.15 (m, 1H), 7.85-7.79 (m, 2H), 7.77-7.70 (m, 4H), 7.70-7.67 (m, 2H), 7.65-7.60 (m, 2H), 7.48-7.36 (m, 10H), 7.32-7.25 (m, 4H), 7.21 (t, J = 8.0 Hz, 1H), 7.04 (t, J = 7.8 Hz, 2H), 6.98 (d, J = 7.8 Hz, 1H), 6.89 (dd, J_1 = 7.9 Hz, J_2 = 2.0 Hz, 1H), 6.83-6.79 (m, 1H), 6.75 (t, J =7.5 Hz, 1H), 6.11-6.03 (m, 1H), 6.01-5.86 (m, 1H), 3.68 (t, J = 6.3 Hz, 2H), 2.75-2.67 (m, 2H), 1.97-1.85 (m, 1H), 1.83-1.72 (m, 1H), 1.58-1.45 (m, 2H), 1.34-0.89 (m, 8H), 0.43-0.35 (m, 1H). ^{13}C{^{1}H} (75 MHz, $CDCl_3$): δ 159.27, 155.19, 154.47, 142.16, 141.31, 138.64, 137.27, 136.60, 135.65, 132.70, 130.80, 130.47, 129.95,

129.71, 128.52, 128.09, 127.19, 127.00, 126.48, 126.29, 123.72, 121.20, 120.7, 120.34, 117.35, 114.45, 110.12, 68.39, 49.92, 45.73, 42.84, 39.02, 35.01, 32.75, 29.41, 28.67, 26.48. MS (EI) m/z = 957.4 [M+]. Anal. calcd. for $C_{68}H_{55}N_5O$: C, 85.24; H, 5.79; N, 7.31. Found: C, 84.83; H, 5.74; N, 7.35.

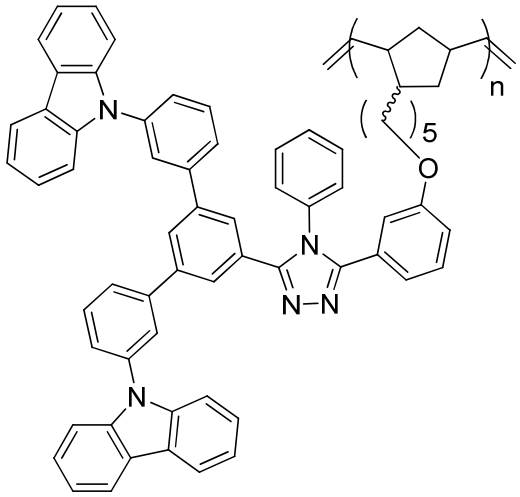

4.39: **S4.21** (0.357 g, 0.373 mmol) was weighed into a bottle. A Grubbs's first generation catalyst (0.0031 g, 3.8 x 10^{-3} mmol) was weighed out into a separate vial. The bottle and vial were placed into a glove box. 2 mL of anhydrous and deoxygenated dichloromethane was added to the bottle containing monomer. 2 mL of anhydrous and deoxygenated dichloromethane was added to vial containing Grubbs' first generation catalyst and shaken vigorously. Subsequently, the catalyst solution was quickly transferred to the bottle with monomer. The polymerization was allowed to proceed 30 min. The reaction was quenched (out of glovebox) with 2.5 mL of ethyl vinyl ether. The solution was concentrated *in vacuo* and precipitated into methanol (20 mL). The polymer was then vacuum filtered and re-dissolved in minimal (< 3 mL) dichloromethane and 1 mL of ethyl vinyl ether was added. This solution was then added (dropwise) into ethanol to precipitate the polymer. The reprecipitation process of isolating, dissolving, and

vacuum filtering the precipitated polymer was repeated 2 more times. The isolated product was dried under vacuum to give an off-white powder (0.196 g, 54.9%). ^{1}H NMR(300 MHz, $CDCl_3$): δ 8.10 (br d, 4H), 7.87-7.76 (br m, 1H), 7.68-7.41 (br m, 8H), 7.39-7.27 (br m, 10H), 7.25-7.16 (br m, 4H), 7.11-6.96 (br m, 4H), 6.94-6.82 (br m, 2H), 6.80-6.66 (br m, 2H), 6.52-6.41 (br m, 1H), 5.36-5.05 (br m, 2H), 3.76-3.55 (br m, 2H), 2.98-2.61 (br m, 1H), 2.60-2.22 (br m, 2H), 2.02-1.171 (br m, 3H), 1.51-0.82 (br m, 9H). Anal. calcd. for $C_{68}H_{55}N_5O$: C, 85.24; H, 5.79; N, 7.31. Found: C, 84.68; H, 5.79; N, 7.30. Gel Permeation Chromatography (tetrahydrofuran): M_w = 29,000; M_n = 19,300; PDI = 1.50.

2.4. Chapter 5: Crosslinkable Solution-Processed OLED Layers

Starting materials were purchased from commercial sources and used without further purification. Anhydrous solvents were dried either by passage through columns of activated alumina or dried over sodium and benzophenone. ^{1}H NMR and ^{13}C NMR spectra were recorded on 300 or 400 MHz Varian Mercury spectrometers. Electron impact (EI) mass spectrometry data were recorded on a Micromass AutoSpec M. Elemental analyses results were performed by Atlantic Microlab. For polymers, the weight average and number average molecular weights were estimated in chloroform by gel permeation chromatography calibrated with linear poly(styrene) standards; in a system consisting of a Water 1515 pump and Waters 2489 UV-vis detector. Differential scanning calorimetry (DSC) data was obtained from a TA DSCQ200 in the range of 25 – 300 °C at a heating rate of 10°C min^{-1} under nitrogen atmosphere. Thermogravimetric analyses (TGA) were performed on a NETZSCH STA 449C instrument under nitrogen

atmosphere and decomposition was determined by the mass loss of 5% when heating at a rate of 20 °C min^{-1} from 20 °C to 500 °C. UV-vis absorption spectra were measured on Varian Cary 5E spectrometer. Rapid thermal processing was performed on a AET model rapid thermal processor/annealer (RTP/RTA).

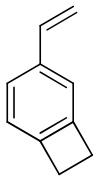

5.33: Potassium vinyltrifluoroborate (1.428 g, 10.7 mmol), 4-bromo-1,2-dihydrocyclobutabenzene (1.507 g, 8.23 mmol), PdCl2 (0.031 g, 0.18 mmol), triphenylphosphine (0.130 g, 0.50 mmol), and cesium carbonate (8.010 g, 24.6 mmol) were combined in a Schlenk tube under nitrogen atmosphere. A (9:1) mixture of THF:water (15.0 mL) was added to the flask and the tube was sealed under nitrogen and stirred at 85 °C for 16 h. After cooling, the reaction mixture was mixed with deionized water (10 mL) and then extracted with dichloromethane (3 x 30 mL). The organic phase was dried over magnesium sulfate and filtered. Solvents were removed *in vacuo* to afford a dark colored oil that was purified by column chromatography (silica gel, 100% pentanes) to give a clear oil (0.591 g, 55.4%). ^{1}H (300 MHz, $CDCl_3$): δ 7.23 (m, 1H), 7.19-7.13 (m, 1H), 7.05-6.98 (m, 1H), 6.78-6.64 (m, 1H), 5.68 (dd, J_1 = 17.57 Hz, J_2 = 0.99 Hz, 1H), 5.16 (dd, J_1 = 10.86 Hz, J_2 = 0.98 Hz, 1H), 3.25-3.09 (m, 4H). [Intermediate was found to be consistent with a literature[9] example of the target prepared by an alternate method].

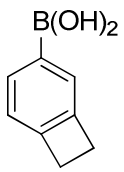

S5.1: In a round bottom flask, 4-bromobenzocyclobutene (1.509 g, 8.244 mmol) was dissolved in anhydrous diethyl ether (10.0 mL) under nitrogen atmosphere and the resulting solution was cooled at -78^{o}C (dry-ice/acetone bath). To the cooled solution, 1.7M *tert*-butyllithium in pentane (6.0 mL, 10 mmol) was added dropwise. To the resulting pale yellow solution was then added 5.70 mL of trimethyl borate (0.80 M solution of in diethyl ether) and the reaction was stirred overnight. The solution was diluted through the addition of 10 mL of diethyl ether and the reaction was quenched by the addition of a dilute HCl (aq) solution. The resulting solution was then washed twice with deionized water (2 x 15 mL) and dried over magnesium sulfate. The solvent was removed *in vacuo* to yield a viscous yellow oil (0.643 g, crude yield = 53.05%).^{1}H (300 MHz, $CDCl_3$): δ 6.89 (d, J = 7.7 *Hz*, 1H), 6.68-6.62 (m, 1H), 6.60-6.57 (m, 1H), 5.71 (br, 1H), 4.62 (br, 1H), 3.09 (s, 4H). [Intermediate was found to be consistent with a literature[10] example of the target prepared by an alternate method].

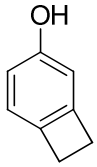

S5.2: **S5.1** (0.623 g, 4.21 mmol), deionized water (18.0 mL), and of 30% aq. hydrogen peroxide (0.88 mL) were mixed in a round bottom flask and the reaction was stirred at room temperature for 24 hours. It was observed that the starting material was only partially dissolved and 5mL of acetone were added to promote further dissolution and the reaction was allowed to proceed at room temperature for an additional 48 hours. The organic layer was then extracted with diethyl ether (30 mL), washed with deionized water (30 mL), and dried over magnesium sulfate. Solvent was removed *in vacuo* to yield a brown oil that was purified by column chromatography (silica gel ; hexanes:ethyl acetate

90:10) to yield a yellow solid (0.194 g, 38.2%).[1]H (300 MHz, $CDCl_3$): δ 6.90 (d, J = 7.8 Hz, 1H), 6.65 (dd, J_1 = 7.8 Hz, J_2 = 2.1 Hz, 1H), 6.59 (d, J = 2.1Hz, 1H), 4.69 (s, 1H), 3.09 (s, 4H). Anal. calcd. for C_8H_8O: C, 79.97; H, 6.71. Found: C, 79.74; H, 6.77. [Intermediate was found to be consistent with a literature[11] example of the target prepared by an alternate method].

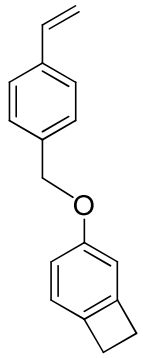

5.34: **S5.2** (0.157 g, 1.31 mmol) was dissolved in N,N-dimethylformamide (20 mL) under nitrogen atmosphere. 1-bromo-4-vinylbenzene (0.204 g, 1.34 mmol) was added dropwise and the resulting solution was cooled to 0 °C. NaH (0.095 g, 3.96 mmol) was then added over a five minute period, producing an intense yellow solution, which was stirred at room temperature overnight. The reaction was quenched by the addition of a saturated aq. NaCl solution (10 mL). The organic layer was extracted with diethyl ether (2 x 50 mL), washed with deionized water (40 mL), and dried over magnesium sulfate. Solvent was removed at reduced pressure to yield an off-white solid that was purified by column chromatography (silica gel; diethyl ether:hexanes 50:50) to yield a white solid (0.240 g, 77.4%). ^{1}H **(**300 MHz, $CDCl_3$): δ 7.42 (d, J = 8.4 Hz, 2H), 7.38 (d, J = 8.4 Hz, 2H), 6.94 (d, J = 8.1 Hz, 1H) 6.81 (dd, J_1 = 8.0 Hz, J_2 = 2.1 Hz, 1H) 6.72 (dd, J_1 = 17.4 Hz, J_2 = 11.1 Hz, 1H), 6.72 (d, J = 2.1 Hz, 1H), 5.75 (dt, J_1 = 17.7 Hz, J_2 = 0.9 Hz, 1H), 5.25 (dt, J_1 = 10.8 Hz, J_2 = 0.9 Hz, 1H), 5.017 (s, 2H), 3.10 (s, 4H). ^{13}C{^{1}H} (75 MHz, DMSO-d_6):

δ 146.71, 137.96, 137.41, 136.70, 127.86, 126.61, 123.72, 114.48, 114.22, 110.0, 70.32, 29.24, 28.98. MS (EI) m/z = 236.2 [M+]. Anal. calcd. for $C_{17}H_{16}O$: C, 86.40; H, 6.82. Found: C, 86.68; H, 6.95.

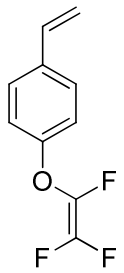

5.35: Potassium vinyltrifluoroborate (1.014 g, 7.57 mmol), 1-bromo-4-(1,2,2-trifluorovinyloxy)benzene (1.894 g, 7.48 mmol), $PdCl_2$ (0.032 g, 0.18 mmol), triphenylphosphine (0.118 g, 0.45 mmol), and cesium carbonate (7.304 g, 22.4 mmol) combined in a Schlenk tube under nitrogen atmosphere. A (9:1) mixture of THF:water (15.0 mL) was added to the flask and the tube was sealed under nitrogen and stirred at 85 °C for 26 h. After cooling, the reaction mixture was mixed with deionized water (10 mL) and then extracted with dichloromethane (3 x 30 mL) and concentrated *in vacuo*. The crude was purified by column chromatography (silica gel ; pentanes) to afford a clear oil. ^{1}H (300 MHz, $CDCl_3$): δ 7.45-7.37 (m, 2H), 7.09-7.02 (m, 2H), 6.69 (dd, J = 17.6, 10.9 Hz, 1H), 5.69 (dd, J = 17.6, 0.7 Hz, 1H), 5.24 (dd, J_1 = 10.9, J_2 = 0.7 Hz, 1H). [Product was found to be consistent with a literature[12] example of the target prepared by an alternate method].

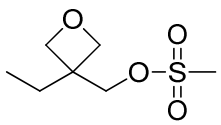

S5.3: Triethylamine (3.266 g, 32.3 mmol), 3-ethyl-3-hydroxymethyl oxetane (3.018 g, 26.0 mmol), and toluene (30.0 mL) were combined under nitrogen atmosphere and

cooled to 0 °C over an ice-water bath. Mesyl chloride (3.243 g, 28.3 mmol) was added to the reaction mixture dropwise over the period of 1 h while maintain the mixture at 0 °C. After 3 h, the reaction was filtered to remove the insoluble salt by-product. The organic phase was concentrated *in vacuo* to afford a clear lightly yellow colored oil (5.192 g). The product was not purified. ^{1}H (300 MHz, $CDCl_3$): δ 4.47-4.42 (m, 4H), 4.38-4.36 (m, 2H), 3.06 (s, 3H), 1.80 (q, *J* = 7.5 Hz, 2H), 0.93 (t, *J* = 7.5 Hz, 3H). [Intermediate was prepared according to the patent literature[13,14]].

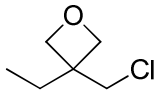

S5.4: Under nitrogen atmosphere, LiCl (1.207 g, 28.5 mmol) and anhydrous THF (20 mL) were combined and heated to 50 °C. **S5.3** (5.192 g) was added into the heated solution dropwise over a period of 1 h. After 5 h, heating was stopped and toluene (50 mL) was added to the reaction flask. The organic layer was extracted with deionized water (3 x 30 mL) and the organic layer solvents were removed *in vacuo* to give a faintly yellow clear oil (2.105 g). The product was used without further purified. ^{1}H (300 MHz, $CDCl_3$): δ 4.41 (s, 3H), 3.79 (s, 2H), 1.83 (q, *J* = 7.5 Hz, 2H), 0.89 (t, *J* = 7.5 Hz, 3H). [Intermediate was prepared according to the patent literature[13,14]].

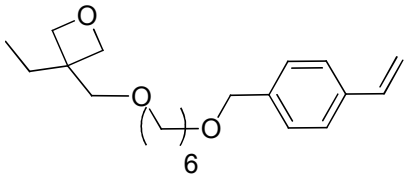

5.36: 3-ethyl-3-((6-(4-vinylbenzyloxy)hexyloxy)methyl)oxetane (3.5 g, 14.9 mmol) was dissolved in anhydrous *N,N*-dimethylformamide (50 mL) under a nitrogen atmosphere and NaH (0.724 g, 30.1 mmol) was added to the reaction in small portions. After three

freeze-pump-thaw cycles the reaction mixture was heated to 50 °C and **S5.4** (2.105 g, 15.6 mmol) was added to the reaction dropwise. The reaction was then heated to 90 °C. After 19 h, the reaction was diluted with ethyl acetate (100 mL) and then washed with deionized water (3 x 200 mL) to remove the DMF. The organic phase was dried over $MgSO_4$ and solvents were removed *in vacuo* to produce a brown colored oil. The oil was purified by column chromatography (silica gel, hexanes:ethyl acetate = 6:4) and concentrated to afford a lightly yellow oil (1.579 g, 31.8%). ^{1}H (300 MHz, CDCl_3): δ 7.41-7.37 (m, 2H), 7.30-7.27 (m, 2H), 6.71 (dd, J_1 = 17.6, J_2 = 10.9 Hz, 1H), 5.74 (dd, J_1 = 17.6, J_2 = 0.9 Hz, 1H), 5.23 (dd, J_1 = 10.9, J_2 = 0.9 Hz, 1H), 4.58-4.31 (m, 6H), 3.51 (s, 2H), 3.45 (dt, J_1 = 6.7, J_2 = 3.8 Hz, 4H), 1.75 (q, J = 7.5 Hz, 2H), 1.67-1.54 (m, 4H), 1.44-1.33 (m, 4H), 0.90 (t, J = 7.45 Hz, 3H). [Product was found to be consistent with a literature[15] example of the target prepared by an alternate method].

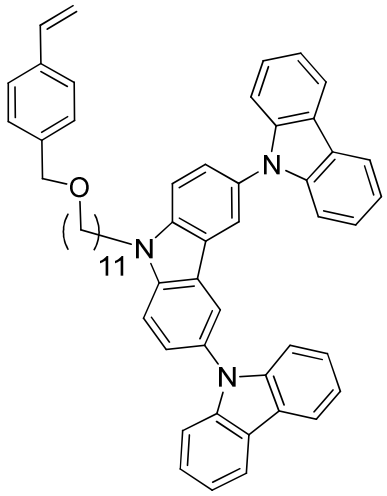

S5.6: Toluene (50 mL) was used to dissolve **S3.3** (2.352 g, 3.52 mmol) in a flask. 50% aqueous sodium hydroxide (98.081 g) and tetrabutylammonium bromide (0.171 g, 0.53 mmol) were added to the flask. Under vigorous stirring, 4-vinylbenzyl chloride (0.601 g, 3.94 mmol) was added and the reaction was heated over an oil bath (50 °C). After one

week, TLC analyses showed starting material was still present. Deionized water (100 mL) was added to the flask and diethyl ether was used to extract the product (3 x 100 mL). The ethereal layers were combined and solvents were removed *in vacuo* to give a yellow/orange crude product. The crude product was purified by silica gel column chromatography (hexanes/ethyl acetate – (8:2)) to give a white powder (1.156 g, 54%). ^{1}H (300 MHz, $CDCl_3$): δ8.19 (ddd, J_1 = 8.7, J_2 = 2.2 Hz, J_3 = 1.3 Hz, 5H), 7.67 (d, J = 0.99 Hz, 4H), 7.48-7.17 (m, 17H), 6.80-6.61 (m, 1H), 5.81-5.65 (m, 1H), 5.29-5.16 (m, 1H), 4.57-4.41 (m, 4H), 3.44 (m, 2H), 2.04 (p, J = 7.1 Hz, 2H), 1.70-1.22 (m, 16H). ^{13}C (75 MHz, $CDCl_3$): δ 142.1, 140.4, 138.6, 137.1, 136.8, 129.5, 128.1, 126.4, 126.2, 126.1, 123.6, 123.3m 120.5, 120.1, 119.9, 114.0, 110.4, 110.0, 72.3, 70.7, 43.9, 30.0, 29.8, 29.7, 29.4, 27.7, 26.5. MS (FAB) m/z = 783.3 [M+]. Anal. calcd. for $C_{56}H_{53}N_3O$: C, 85.79; H, 6.81; N, 5.36. Found: C, 85.90; H, 6.72; N, 5.36.

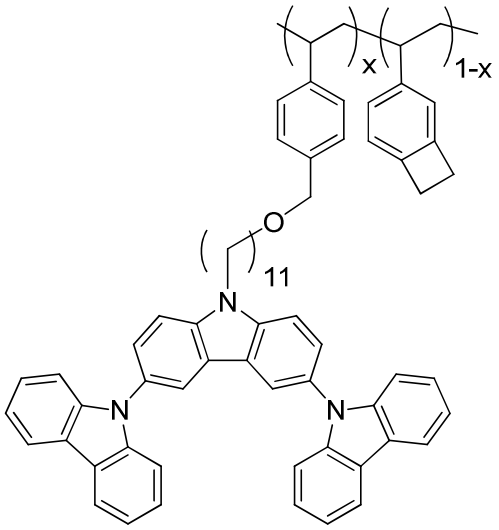

5.37: **S5.6** (0.263 g, 0.34 mmol), AIBN (0.0029 g, 0.018 mmol) and anhydrous tetrahydrofuran (2.4 mL) were combined in a Schlenk tube under nitrogen atmosphere. In a separate flask, **5.33** (0.0099 g, 0.08 mmol) was dissolved in anhydrous tetrahydrofuran (2.0 mL). The **5.33** solution (1.0 mL) was added to the reaction flask to give a 3.4 mL

reaction volume. The mixture was subjected to freeze-pump-thaw (3 x) then placed under static nitrogen atmosphere and heated over an oil bath (60 °C). After 7 days, the solution was concentrated *in vacuo* and precipitated into acetone. The isolated polymer was re-precipitated into acetone (3 x) and then dried to produce a white powder (0.136 g, 51.0%). ^{1}H (300 MHz, $CDCl_3$): δ 8.28-7.98 (br m, 5H), 7.73-7.11 (br m, 14H), 7.08-6.08 (br m, 5H), 4.58-4.10 (br m, 4H), 3.55-3.17 (br m, 2H), 3.11-2.90 (br m, 0.4H), 2.11-1.10 (br m, 18H). Elemental anal. calcd. for copolymer: C, 86.44; H, 6.90; N, 5.36. Found: C, 85.80; H, 6.69; N, 5.25. Gel Permeation Chromatography (chloroform): M_w = 31,100; M_n = 9,200; PDI = 3.38.

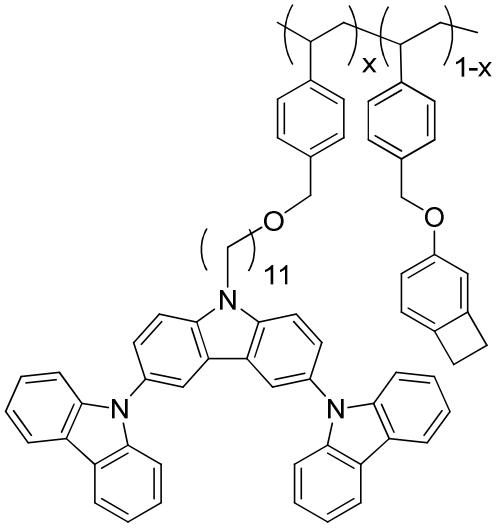

(target x = 0.9)

5.38: **S5.6** (0.649 g, 0.828 mmol), **5.34** (0.0197 g, 0.0834 mmol), and AIBN (0.0070 mg) where dissolved in 8.0 mL anhydrous THF in a Schlenk tube. Freeze-pump-thaw (3 x) was performed and the tube was sealed under static nitrogen afterward. The reaction mixture was then stirred at 60 °C for 2 weeks. The reaction mixture was concentrated *in vacuo*, yielding a pale yellow oily solid that was dissolved in chloroform and precipitated into acetone to yield a white solid (0.555g, 82.8%). ^{1}H (300MHz, $CDCl_3$): δ 8.24-7.95

(br m, 5H), 7.68-7.09 (br m, 14H), 7.09-6.01 (br m, 0.4H), 4.53-4.02 (br m, 4H), 3.50-3.14 (br m, 2H), 3.00-2.87 (br m, 0.4H), 2.06-1.73 (br m, 3H), 1.52-0.84 (br m, 15H). Gel Permeation Chromatography (chloroform): M_w = 24,000; M_n = 10,200; PDI = 2.35. Anal. calcd. for copolymer: C, 85.80; H, 6.81; N, 5.20. Found: C, 85.28; H, 6.83; N, 5.14.

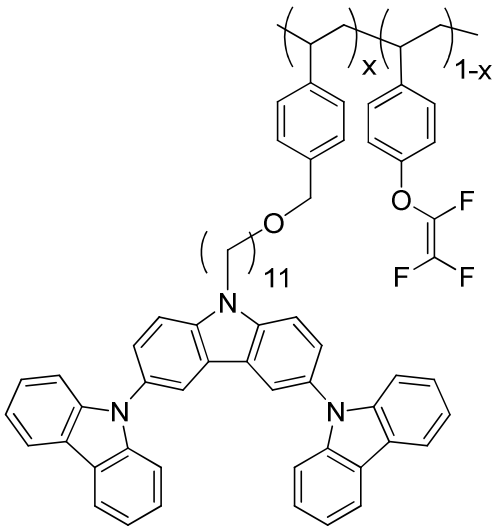

5.39: **S5.6** (0.376 g, 0.48 mmol), AIBN (0.00247 g, 0.015 mmol) and anhydrous tetrahydrofuran (3.75 mL) were combined in a Schlenk tube under nitrogen atmosphere. In a separate flask, **5.35** (0.0192 g, 0.096 mmol) was dissolved in anhydrous tetrahydrofuran (2.5 mL). The **5.35** solution (1.25 mL) was added to the reaction flask to give a 5.0 mL reaction volume. The mixture was subjected to freeze-pump-thaw (3 x) then placed under static nitrogen atmosphere and heated over an oil bath (60 °C). After 8 days, the solution was concentrated *in vacuo* and precipitated into acetone. The isolated polymer was re-precipitated into acetone (3 x) and then dried to produce a white powder (0.232 g, 60.3%). ^{1}H (300 MHz, $CDCl_3$): δ 8.26-7.99 (br m, 5H), 7.70-7.10 (br m, 14H), 7.08-6.12 (br m, 5H), 4.55-4.06 (br m, 4H), 3.53-3.22 (br m, 2H), 2.11-0.99 (br m, 18H). Gel Permeation Chromatography (chloroform): M_w = 22,800 ; M_n = 6,900; PDI = 3.3. Anal. calcd. for copolymer: C, 83.21; H, 6.48; N, 5.36. Found: C, 83.99; H, 6.77; N, 5.23.

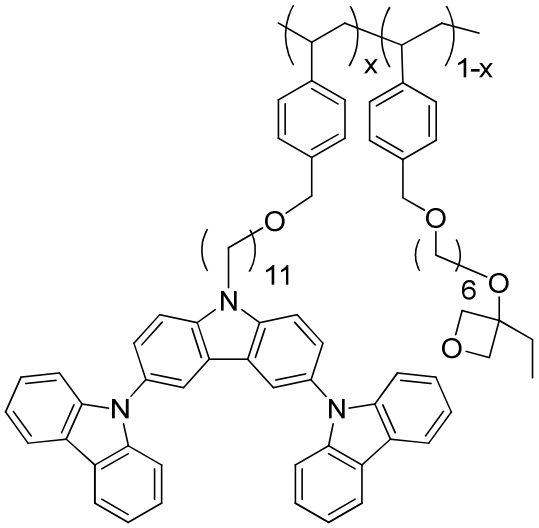

(target x = 0.9)

5.40: **S5.6** (0.373 g, 0.48 mmol), AIBN (0.0027 g, 0.016 mmol) and anhydrous tetrahydrofuran (4.0 mL) were combined in a Schlenk tube under nitrogen atmosphere. In a separate flask, **5.36** (0.01662 g, 0.05 mmol) was dissolved in anhydrous tetrahydrofuran (1.0 mL). The **5.36** solution (1.0 mL) was added to the reaction flask to give a 5.0 mL reaction volume. The mixture was subjected to freeze-pump-thaw (3 x) then placed under static nitrogen atmosphere and heated over an oil bath (60 °C). After 7 days, the solution was concentrated *in vacuo* and precipitated into acetone. The isolated polymer was re-precipitated into acetone (3 x) and then dried to produce a white powder (0.223 g, 57.0%). ^{1}H (300 MHz, $CDCl_3$): δ 8.26-8.00 (br m, 5H), 7.69-7.11 (br m, 14H), 7.08-6.18 (br m, 5H), 4.55-4.12 (br m, 4H), 3.57-3.26 (br m, 2.2H), 2.10-0.78 (br m, 18H). Gel Permeation Chromatography (chloroform): M_w = 25,700; M_n = 7,400; PDI = 3.45. Anal. calcd. for copolymer: C, 84.80; H, 7.10; N, 5.36. Found: C, 84.40; H, 6.86; N, 5.27.

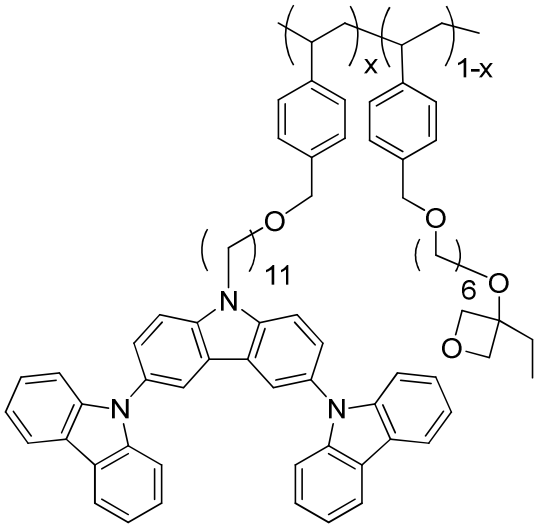

(target x = 0.7)

5.41: **S5.6** (0.294 g, 0.37 mmol), AIBN (0.0036 g, 0.02 mmol) and anhydrous tetrahydrofuran (3.0 mL) were combined in a Schlenk tube under nitrogen atmosphere. In a separate flask, **5.36** (0.052 g, 0.15 mmol) was dissolved in anhydrous tetrahydrofuran (1.0 mL). The **5.36** solution (1.0 mL) was added to the reaction flask to give a 4.0 mL reaction volume. The mixture was subjected to freeze-pump-thaw (3 x) then placed under static nitrogen atmosphere and heated over an oil bath (60 °C). After 7 days, the solution was concentrated *in vacuo* and precipitated into acetone (20 mL). The isolated polymer was re-precipitated into acetone (3 x) and then dried to produce a white powder (0.168 g, 47.9%). ^{1}H (300 MHz, $CDCl_3$): δ 8.26-8.00 (br m, 5H), 7.69-7.11 (br m, 14H), 7.08-6.18 (br m, 5H), 4.55-4.12 (br m, 4H), 3.57-3.26 (br m, 2.2H), 2.10-0.78 (br m, 18H). Gel Permeation Chromatography (chloroform): M_w = 12,700; M_n = 7,500; PDI = 1.7. Anal. calcd. for copolymer: C, 82.88; H, 7.60; N, 3.75. Found: C, 83.87; H, 7.10; N, 4.75. [Elemental analysis data suggests that the ratio may be closer to x = 0.8]

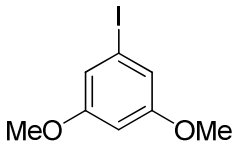

S5.7: Synthesized according to the literature.[16] ^{1}H NMR was consistent with the literature.

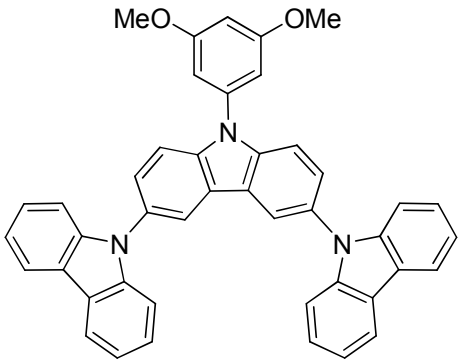

S5.8: **S5.7** (2.415, 9.14 mmol), 3,6-bis(carbazol-9-yl)carbazole (3.507 g, 7.03 mmol), 18-crown-6 ether (0.059 g, 0.21 mmol), copper powder (5.849 g, 92.0 mmol), and o-dichlorobenzene (75 mL) combined in flask under nitrogen atmosphere. Postassium carbonate (11.532 g, 83.4 mmol) was added and reaction heated to 180 °C for 24 h. After cooling, solids were filtered and washed and the filtrate solvents were removed *in vacuo*. The crude was purified by column chromatography (silica gel; hexanes:ethyl acetate = 8:2) to afford an off-white powder after recrystallization from hot dichloromethane/methanol (3.199 g, 71.7%). ^{1}H (300 MHz, $CDCl_3$): δ 8.27-8.26 (m, 2H), 8.16 (dt, J = 7.7 Hz, 4H), 7.75-7.70 (m, 2H), 7.64-7.59 (m, 2H), 7.42-7.37 (m, 8H), 7.31-7.26 (m, 4H), 6.88 (d, J = 2.2 Hz, 2H), 6.66 (t, J = 2.2 Hz, 1H), 3.92 (s, 6H). ^{13}C{^{1}H} (75 MHz, $CDCl_3$): δ 162.1, 141.8, 140.6, 138.8, 130.5, 126.3, 125.9, 124.0, 123.2, 120.2, 119.7, 111.5, 109.7, 105.5, 100.3, 55.7. MS (EI) m/z = 633.2 [M+]. Anal. calcd. for $C_{44}H_{31}N_3O_2$: C, 83.39; H, 4.93; N, 6.63. Found: C, 82.42; H, 4.71; N, 6.49. [As elemental analysis failed see ^{1}H NMR below]

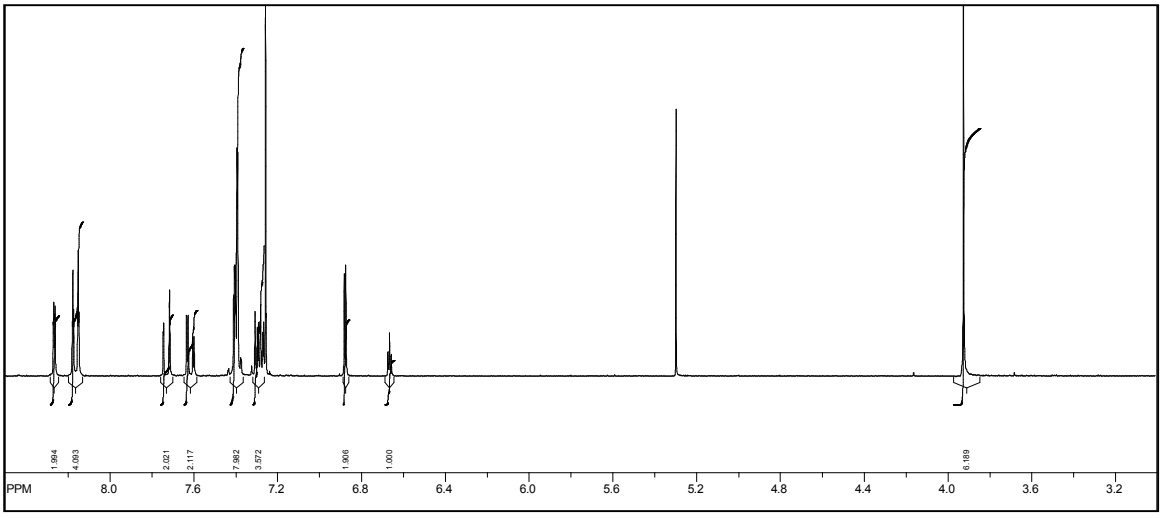

Figure 2.5. ^{1}H NMR (300 MHz, $CDCl_3$) of **S5.8**.

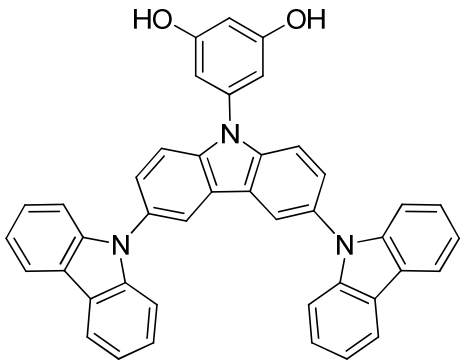

S5.9: **S5.8** (4.011 g, 6.33 mmol) was dissolved in anhydrous dichloromethane (40 mL) under nitrogen atmosphere and cooled to -78 °C (dry-ice/acetone bath). Boron tribromide (50 mL, 1.0 M in DCM) added dropwise to cooled solution and cooling bath removed. After ~4 h, mixture was added into ice-water (150 mL) with stirring. The biphasic mixture was separated and the aqueous phase was extracted with dichloromethane (2 x 100 mL). The combined organic phase was dried over magnesium sulfate, filtered, and solvents removed *in vacuo*. The crude was purified by column chromatography (silica gel; toluene = 100%) and recrystallized from acetone/methanol to afford an grayish white powder (1.551 g, 40.6%). ^{1}H (300 MHz, DMSO-d_6): δ 9.91 (s, 2H), 8.66 (d, J = 1.9 Hz,

2H), 8.27-8.21 (m, 4H), 7.82-7.75 (m, 2H), 7.72-7.66 (m, 2H), 7.46-7.36 (m, 8H), 7.30-7.22 (m, 4H), 6.66 (d, J = 2.1 Hz, 2H), 6.51 (t, J = 2.1 Hz, 1H). $^{13}C\{^{1}H\}$ (75 MHz, DMSO-d_6): δ 160.3, 141.5, 140.2, 138.3, 129.9, 126.6, 126.4, 124.0, 122.9, 120.9, 120.7, 120.2, 112.1, 110.2, 105.1, 102.8. MS (EI) m/z = 605.2 [M+]605.2. Anal. calcd. for $C_{42}H_{27}N_3O_2$: C, 83.29; H, 4.49; N, 6.94. Found: C, 82.64; H, 4.29; N, 6.81. [As elemental analysis failed see ^{1}H NMR below]

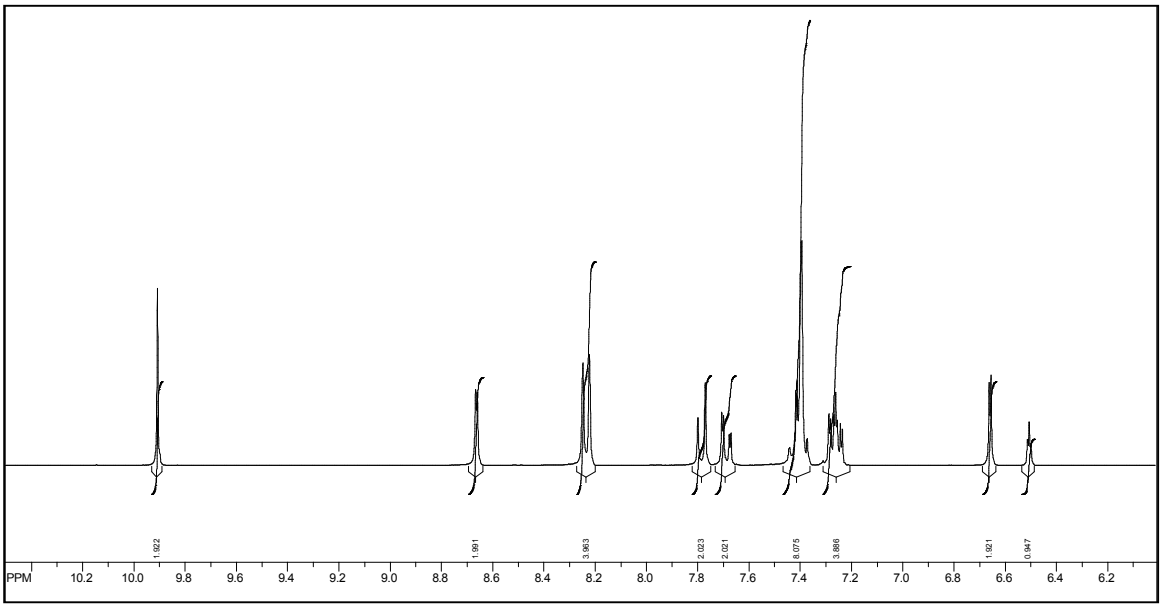

Figure 2.6. ^{1}H NMR (300 MHz, $CDCl_3$) of **S5.9**.

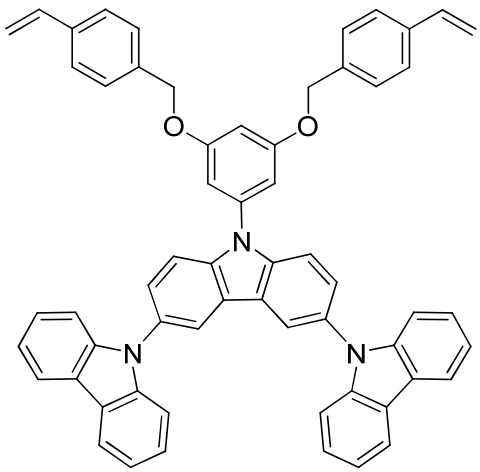

5.42: **S5.9** (1.002 g, 1.65 mmol), DMF (25 mL), and potassium carbonate (2.775 g, 20.1 mmol) combined in a flask. 1-(chloromethyl)-4-vinylbenzene (0.607 g, 3.98 mmol) added dropwise to mixture. After 24h, deionized water (100 mL) added to flask and white precipitate formed. The crude material was isolated by filtration and purified by column chromatography (silica gel ; hexanes: ethyl acetate = 8:2). The resulting oil was precipitated into methanol, collected by filtration, and dried to afford a white powder (0.559 g, 40.5%). ^{1}H (300 MHz, DMSO-d_6): δ 8.64 (d, J = 1.5 Hz, 2H), 8.23 (d, J = 7.7 Hz, 4H), 7.58-7.31 (m, 20H), 7.26 (t, J = 7.4 Hz, 4H), 6.99 (d, J = 2.2 Hz, 2H), 6.91 (t, J = 2.0 Hz, 1H), 6.71 (dd, J = 17.7, 11.0 Hz, 2H), 5.83-5.77 (d, J = 17.6 Hz, 2H), 5.25 (s, 4H), 5.18 (d, J = 10.9 Hz, 2H). ^{13}C{^{1}H} (75 MHz, DMSO-d_6): δ 162.1, 160.8, 141.4, 140.0, 137.2, 136.9, 136.7, 130.0, 128.4, 128.2, 126.8, 126.6, 124.1, 122.9, 120.9, 120.2, 115.0, 110.1, 105.9, 69.8. MS (EI) m/z = 837.2 [M+]. Anal. calcd. for $C_{60}H_{43}N_3O_2$: C, 86.00; H, 5.17; N, 5.01. Found: C, 85.76; H, 5.14; N, 5.08.

2.4.1. UV-vis. Study of Benzocyclobutene-based Thermal Crosslinkable Copolymer **5.37**:

5.37 (0.05007 g) was dissolved in anhydrous toluene (5.0 mL) to provide a 10 mg/mL solution of the copolymer. ~0.5 mL of the polymer solution was filtered (0.2 μm) onto a clean glass slide and spin-coated at 1000 rpm for 1 minute. The thin-films were heated under inert atmosphere (in a glovebox), as follows:

Table 2.1. Crosslinking processing conditions evaluated for **5.37** at 200 °C.

Sample ID	Annealing Time (h) at 170 °C	Heating Time (h) at 200 °C
5.37-control1-d	0	0
5.37-control2-s	0	0
5.37a-d	1	2
5.37b-s	1	2
5.37c-d	2	4
5.37d-s	2	4

where "d" denotes the *dip test* and "s" denotes the *spin coat test*.

The thin-films prepared were evaluated by two methods:

1) *Dip test*: UV-Vis measurements of the sample films were obtained after completely dipping/soaking the slides into chloroform for 0, 10, 60, 90, and 180 s

2) *Spin-coat:* UV-Vis measurements of the sample films were obtained before and after ~0.5 mL of filtered (0.2 μm) chloroform was spin-coated atop the sample at 1000 rpm for 60s.

2.4.2. UV-vis. Study of Benzocyclobutene-based Thermal Crosslinkable Copolymer **5.38**:

5.38 (0.04005 g) was dissolved in anhydrous toluene (4.0 mL) to provide a 10 mg/mL solution of the copolymer. ~0.5 mL of the polymer solution was filtered (0.2 μm) onto a cleaned glass slide and spin-coated at 1500 rpm for 1 minute. The thin-films were heated under inert atmosphere (in a glovebox), as follows:

Table 2.2. Crosslinking processing conditions evaluated for copolymer **5.38** at 175 °C.

Sample ID	Heating time (h) at 175 °C
5.38 – control 1	Control
5.38 – control 2	Control
5.38 – a	0.5
5.38 – b	1
5.38 – c	2
5.38 – d	4

5.38 (0.03010 g) was dissolved in anhydrous toluene (4.0 mL) to provide a 10 mg/mL solution of the copolymer. ~0.5 mL of the polymer solution was filtered (0.2 μm) onto a cleaned glass slide and spin-coated at 1500 rpm for 1 minute. The thin-films were heated under inert atmosphere (in a glovebox), as follows:

Table 2.3. Crosslinking processing conditions evaluated for copolymer **5.38** at 200 or 230 °C.

Sample ID	Heating time (h) at 200 °C	Temperature (°C)
5.38 – e	0.5	200
5.38 – f	1	200
5.38 – g	2	200
5.38 – h	4	200
5.38 – i	0.5	230
5.38 – j	1	230
5.38 – k	2	230
5.38 – l	4	230

5.38 (0.03020 g) dissolved in anhydrous toluene (3.0 mL) to provide a 10 mg/mL solution of the copolymer. ~0.5 mL of the polymer solution was filtered (0.2 μm) onto a cleaned glass slide and spin-coated at 1500 rpm for 1 minute. The thin-films were heated under inert atmosphere (in a glovebox), as follows:

Table 2.4. Crosslinking processing conditions evaluated for copolymer **5.38** at 300 °C.

Sample ID	Heating time (h) at 300 °C
5.38 – m	0.5
5.38 – n	1
5.38 – o	2
5.38 – p	4

All slides thin-films prepared (controls and those heated at 175, 200, 230, and 300 °C) were evaluated for solvent resistance by the *dip test* whereby UV-Vis measurements of the sample films were obtained after completely dipping/soaking the slides into chloroform for 0, 10, 60, and 90 s.

2.4.3. UV-vis. Study of Trifluorovinyl Ether-based Thermal Crosslinkable Copolymer **5.39**:

5.39 (0.05005 g) dissolved in anhydrous toluene (5.0 mL) to provide a 10 mg/mL solution of the copolymer. ~0.5 mL of the polymer solution was filtered (0.2 μm) onto a cleaned glass slide and spin-coated at 1000 rpm for 1 minute. The thin-films were heated under inert atmosphere (in a glovebox), as follows:

Table 2.5. Crosslinking processing conditions evaluated for copolymer **5.39** at 200 or 230 °C.

Sample ID	Crosslinking Time (min)	Temperature (°C)
5.39-control1-d	0	N/A
5.39-control2-s	0	N/A
5.39a-d	40	200
5.39b-s	40	200
5.39c-d	40	230
5.39d-s	40	230

where "d" denotes the *dip test* and "s" denotes the *spin coat test*.

The thin-films prepared were evaluated by two methods:

1) *Dip test*: UV-Vis measurements of the sample films were obtained after completely dipping/soaking the slides into chloroform for 0, 10, 60, 90, and 180 s

2) *Spin-coat:* UV-Vis measurements of the sample films were obtained before and after ~0.5 mL of filtered (0.2 μm) chloroform was spin-coated atop the sample at 1000 rpm for 60s.

5.39 (0.05005 g) was dissolved in anhydrous toluene (5.0 mL) to provide a 10 mg/mL solution of the copolymer. ~0.5 mL of the polymer solution was filtered (0.2 μm) onto a cleaned glass slide and spin-coated at 1000 rpm for 1 minute. The thin-films were heated under inert atmosphere (in a glovebox), as follows:

Table 2.6. Crosslinking processing conditions evaluated for copolymer **5.39** at 230 °C.

Sample ID	**Crosslinking Time (h)**	**Temperature (°C)**
5.39e-d	4	230
5.39f-s	4	230

where "d" denotes the *dip test* and "s" denotes the *spin coat test*.

The thin-films prepared were evaluated for solvent resistance by the same methods (*dip* or *spin coat test*) described above.

2.4.4. UV-vis. Study of Oxetane-based Thermal Crosslinkable Copolymer **5.40**:

A solution (5 mg/mL) of the aryliodonium salt, PAG (see below), was prepared by dissolving 0.02502 g in anhydrous THF (5.0 mL). Two serial dilutions were performed to afford 0.75 mg/mL and 1.0 mg/mL solutions of the PAG in THF.

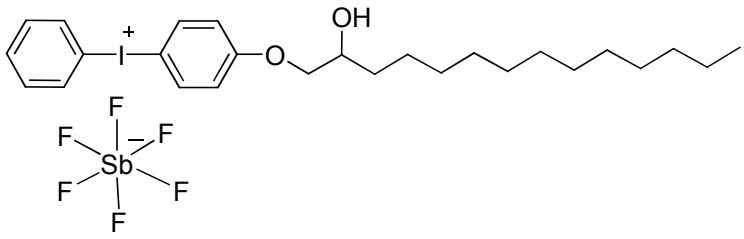

Figure 2.7. 4-((2-Hydroxytetradecyl)oxy)-phenyl)phenyliodonium hexafluoroantimonate, Photoacid Generator (PAG).

To prepare the solutions, the polymer was dissolved in 0.1 mL of the either the 0.75 or 1.0 mg/mL solutions of the PAG (denoted in sample ID) and 0.9 mL of anhydrous THF as summarized in the table as follows:

Table 2.7. Crosslinking processing conditions evaluated for copolymer **5.40** using PAG.

Sample ID	**Polymer (g)**	**PAG Soln (mL) – [0.75 or 1.0 mg/mL]**	**THF (mL)**	**UV exposure (min)**
5.40-control1-d	0.01007	0	1.0	N/A
5.40-control2-s	0.01006	0	1.0	N/A
5.40-0.75a-d	0.01006	0.1	0.9	1
5.40-0.75b-s	0.01009	0.1	0.9	1
5.40-0.75c-d	0.01000	0.1	0.9	3
5.40-0.75d-s	0.01003	0.1	0.9	3
5.40-1.0a-d	0.01000	0.1	0.9	1
5.40-1.0b-s	0.01000	0.1	0.9	1
5.40-1.0c-d	0.01008	0.1	0.9	3
5.40-1.0-3e-s	0.01002	0.1	0.9	3

~0.5 mL of the copolymer solutions (10 mg/mL) were filtered (0.2 μm) onto cleaned glass slides and spin-coated at 1000 rpm for 1 minute. The thin-films were exposed to UV radiation from a hand held UV lamp (Entela model UVGL-58; broad emission with λ_{max} = 366 nm) at a distance of ~1 inch above the films. All samples were subsequently

soft-cured (85 °C for 1 min) and then baked (200 °C for 15 min). The thin-films prepared were evaluated for solvent resistance by two methods:

1) *Dip test*: UV-Vis measurements of the sample films were obtained after completely dipping/soaking the slides into chloroform for 0, 10, 60, 90, and 180 s

2) *Spin-coat:* UV-Vis measurements of the sample films were obtained before and after ~0.5 mL of filtered (0.2 μm) chloroform was spin-coated atop the sample at 1000 rpm for 60s.

2.4.5. UV-vis Study of Oxetane-based Thermal Crosslinkable Copolymer **5.41**:

A solution (2 mg/mL) of the aryliodonium salt, PAG (see below), was prepared by dissolving 0.01008 g in anhydrous THF (5.0 mL). To prepare the solutions, the polymer was dissolved in 0.1 mL of the PAG solution and 0.9 mL of anhydrous THF to afford a 2 wt% level of doping, as summarized in the table as follows:

Table 2.8. Crosslinking processing conditions evaluated for copolymer **5.41** using PAG.

Sample ID	Polymer (g)	PAG Solution (mL)	THF (mL)	UV lamp λ_{max} (nm)	UV exposure (s)
5.41a	0.01001	0.1	0.9	N/A	N/A
5.41b					
5.41c	0.01002	0.1	0.9	253	10
5.41d				253	60
5.41e	0.01003	0.1	0.9	300	10
5.41f				300	60

~0.5 mL of the copolymer solutions (10 mg/mL) were filtered (0.2 μm) onto cleaned glass slides and spin-coated at 1000 rpm for 1 minute. The thin-films were exposed to UV radiation inside a UV photoreactor (Rayonet model) (at λ_{max} = 253 or 300 nm). All samples were subsequently soft-cured (150 °C for 1 min) The thin-films prepared were evaluated for solvent resistance by the s*pin-coat* where UV-Vis measurements of the sample films were obtained before and after ~0.5 mL of filtered (0.2 μm) chloroform was spin-coated atop the sample at 1000 rpm for 60s.

2.4.6. Rapid thermal processing of copolymers **5.37**, **5.38**, **5.39**, **5.40**, and **5.41** and bis(styrene) small-molecule **5.42**:

- Preparation of Solutions:

Solutions of copolymers **5.37**, **5.38**, **5.39** and small-molecule **5.42** were prepared by weighing ~15 mg of the copolymer and dissolving the solids in 1.5 mL of *ortho*-dichlorobenzene (o-DCB) or chlorobenzene. The solution was briefly heated to promote full dissolution of the copolymer and stirred overnight to afford 10 mg/mL solutions. The solutions were filtered (0.2 μm) and subsequently used to spin-coat thin-films (see below).

For oxetane copolymers **5.40** and **5.41**, that were doped with either a photo- or thermoacid generator (see Chapter 5), individual solutions of the copolymer and acid generator were prepared individually and stirred overnight. The solutions were then blended to afford 10 mg/mL concentrations of the copolymer with the appropriate level

of PAG (by wt% with respect to the amount of copolymer). The solutions were filtered (0.2 μm) and subsequently used to spin-coat thin-films (see below).

- Silicon (SiO_2/Si) Substrate Cleaning Conditions:

The silicon substrates were submerged in acetone and were subjected to an ultrasonic bath (5-10 minutes). The substrates were spun at 3000 rpm and rinsed with additional acetone to wash away any residual particulates from the surface. Then, the substrates were dried under a stream of nitrogen.

- Silicon (SiO_2/Si) Substrate Treatment with Phosphonic Acids:

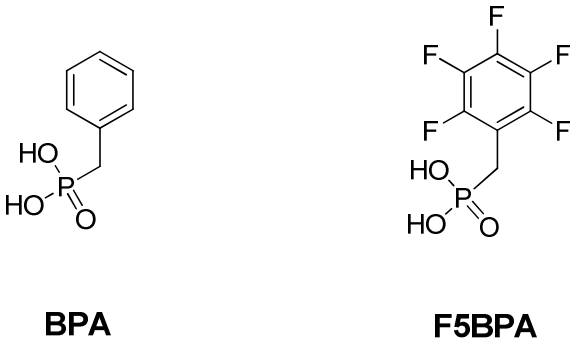

BPA **F5BPA**

Figure 2.8. Surface modifiers (**BPA** and **F5BPA**) used for silicon dioxide substrates.

A 1 mM solution of **BPA** or **F5BPA** was prepared in absolute ethanol. Substrates were sonicated for first in 5% TritonX aqueous detergent, then deionized water, and finally absolute ethanol for 20 minutes at in each solution. The substrates were dried with a stream of nitrogen. Oxygen plasma was performed for 2 minutes at a radio frequency power of 60 W. Immediately following the plasma treatment, the substrates were immersed in the 1 mM solution of the respective phosphonic acid and stored overnight.

The treated substrates were finally sonicated in absolute ethanol for 20 – 30 min, dried, and heated to 180 °C overnight.

- Spin-coating Conditions:

The solutions prepared from the crosslinkable copolymers or small-molecule were dispensed on to silicon substrates and then spin-coated at 1000 rpm for 60 s. Afterward, each sample was placed quickly dried at 90 °C on a hotplate for 5 minutes to evaporate residual solvent.

- Ellipsometry Measurement Conditions:

Thin-films were placed on the ellipsometry stage and psi and delta parameters for the wavelengths 370-1000 nm at the angles of incidence of 65, 70, and 75 degrees were recorded. A Cauchy model was used to perform the initial fitting of the psi and delta values for all angles and wavelengths simultaneously.

- RTP Profiles I-VI:

Table 2.9. RTP Profile I

Step	RTP Description:	Ramp Rate	Δt (min)	Total Time (min)
1	N_2 purge	N/A	5	5
2	Ramp 1	20 °C min^{-1}	11	16
3	Ramp 2	10 °C min^{-1}	5	21
4	Dwell at 300 °C	N/A	10	31
5	Cooling to 160 °C	N/A	5	36
6	Cooling to 110 °C	N/A	5	41

Table 2.10. RTP Profile II

Step	RTP Description:	Ramp Rate	Δt (min)	Total Time (min)
1	N_2 purge	N/A	3	3
2	Ramp 1	150 °C min^{-1}	1.6	4.6
3	Ramp 2	50 °C min^{-1}	0.9	5.4
4	Dwell at 300 °C	N/A	5	10.4
5	Cooling to 180 °C	N/A	2.25	12.7
6	Cooling to 100 °C	N/A	9	19.4

Table 2.11. RTP Profile III

Step	RTP Description:	Ramp Rate	Δt (min)	Total Time (min)
1	N_2 purge	N/A	3	3
2	Ramp 1	150 °C min^{-1}	1.6	4.6
3	Ramp 2	100 °C min^{-1}	0.5	5
4	Dwell at 300 °C	N/A	10	15
5	Cooling to 140 °C	N/A	5.9	20.9

Table 2.12 RTP Profile IV

Step	RTP Description:	Ramp Rate	Δt (min)	Total Time (min)
1	N_2 purge	N/A	3	3
2	Ramp 1	150 °C min^{-1}	2.9	5.9
3	Dwell at 200 °C	N/A	10	20.9
4	Cooling to 110 °C	N/A	3.7	24.6

Table 2.13. RTP Profile V

Step	RTP Description:	Ramp Rate	Δt (min)	Total Time (min)
1	N_2 purge	N/A	3	3
2	Ramp 1	150 °C min^{-1}	0.5	3.5
3	Ramp 2	100 °C min^{-1}	0.1	3.6
4	Dwell at 190 °C	N/A	15	18.6
5	Cooling to 100 °C	N/A	0.8	19.4

Table 2.14. RTP Profile VI

Step	RTP Description:	Ramp Rate	Δt (min)	Total Time (min)
1	N_2 purge	N/A	3	3
2	Ramp 1	150 °C min^{-1}	1	4
3	Ramp 2	100 °C min^{-1}	0.5	4.5
4	Dwell at 200 °C	N/A	15	19.5
5	Cooling to 140 °C	N/A	5.8	25.3

2.5. References:

(1) Maegawa, Y.; Goto, Y.; Inagaki, S.; Shimada, T. *Tetra. Lett.* **2006**, *47*, 6957-6960.

(2) Amb, C. M.; Rasmussen, S. C. *J. Org. Chem.* **2006**, *71*, 4696-4699.

(3) Xu, T.; Liu, X.; Zheng, X.; Qui, X.; Zhao, Y. *Org. Lett.* **2007**, *9*, 797-800.

(4) Endres, A.; Maas, G. *Tetrahedron* **2002**, *58*, 3999-4005.

(5) Low, P. J.; Paterson, M. A. J.; Yufit, D. S.; Howard, A. K.; Cherryman, J. C.; Tackley, D. R.; Brook, R.; Brown, B. *J. Mater. Chem.* **2005**, *15*, 2304-2315.

(6) Jen, K.-Y.; Liu, S. M.; Niu, Y.-H. US Patent 0153021A1, 2009.

(7) Tsai, L.-R.; Chen, Y. *J. Polym. Sci. A Polym. Chem.* **2007**, *45*, 4465-4476.

(8) Ashiq, U.; Ara, R.; Mahroof-Tahir, M.; Maqsood, Z. T.; Khan, K. M.; Khan, S. N.; Siddiqui, H.; Choudhary, M. I. *Chem. Biodiver.* **2008**, *5*, 82-92.

(9) Blomberg, S.; Ostberg, S.; Harth, E.; Bosman, A. W.; Van Horn, B.; Hawker, C. J. *J. Polym. Sci. A Polym. Chem.* **2002**, *40*, 1309-1320.

(10) Yang, J.-X.; Ma, K.-Y.; Zhu, F.-H.; Chen, W.; Li, B.; Zhang, L.; Xie, R.-G. *J. Chem. Res.* **2005**, *3*, 184-186.

(11) Tan, L.-S.; Venkatasubramanian, N. *Synth. Commun.* **1995**, *25*, 2189-2195.

(12) Spraul, B. K.; Suresh, S.; Jin, J.; Smith, D. W. *J. Am. Chem. Soc.* **2006**, *128*, 7055-7064.

(13) Hirotsu, K.; Takebayashi, K.; Kaneko, T. Patent JP 19990304909199910 27, 2001.

(14) Hirotsu, K.; Murakami, T. Patent JP6137420070605, 2007.

(15) Bacher, E.; Bayerl, M. S.; Rudati, P.; Reckefuss, N.; Müller, C. D.; Meerholz, K.; Nuyken, O. *Macromolecules* **2005**, *38*, 1640-1647.

(16) Mariampillai, B.; Alberico, D.; Bidau, V.; Lautens, M. *J. Am. Chem. Soc.* **2006**, *128*, 14436-14437.

CHAPTER 3

Carbazole-based Hole-Transport Side-Chain Polymers

3.1. Introduction

A series of carbazole-functionalized side-chain homopolymers were synthesized based on literature small-molecule hole transport groups. The thermal, photophysical, and electrochemical properties of these polymers were evaluated. Based on these studies selected polymer candidates were used to fabricate phosphorescent OLEDs (PhOLEDs) wherein the polymers functioned as either a hole-transport or host layer. The incorporation of these carbazole-based materials, as side groups on a norbornene polymer backbone was intended to impart ease of solution processing without causing major changes in the photophysical or electrochemical properties of the core transport group.

3.2. Introduction and Background

The majority of hole-transport small-molecules for organic light emitting diodes (OLEDs) fall into two main types: 1) arylamine-based (i.e. triphenylamine) and 2) carbazole-based. These moieties have been the focus of intense research for OLED applications for various reasons (vide infra), but most importantly as a result of the relative ease of anodic oxidation. This feature allows for relatively easy injection of radical cations (or holes) into an OLED device from an anode (typically indium tin oxide (**ITO**)). This introduction will examine selected examples of hole-transport materials (including small-molecule and side-chain polymer-based) as reported in the literature. While many additional examples of hole-transport materials are reported in the literature,

those that are discussed should provide a brief review of the literature, based on their relevance to the work discussed in this chapter.

The relative ease of oxidation of arylamines has been central to their use as hole-transport materials. Nonetheless, the potential exists for reactions between radical cation species that could result in formation of by-products of arylamine-based materials; with potentially detrimental effects on charge-carrier mobility and overall device stability. Oxidative pathways of arylamine radical ions were studied by Seo *et al*.[1] in 1966 and the representative reactions and processes for triphenylamine (**TPA** (**3.1**)) and tetraphenylbenzidine (**TPB** (**3.2**)) were reported as follows:

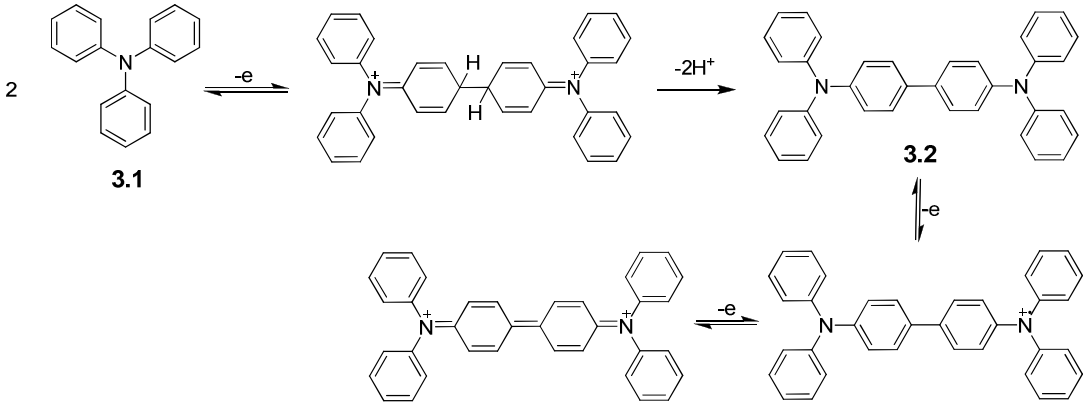

Figure 3.1. Reaction pathways for radical cations of triphenylamine (**TPA** (**3.1**)) and tetraphenylbenzidine (**TPB** (**3.2**)).

It was found that the radical cation formed by oxidation of **TPA** was highly unstable and dimerized (with loss of two protons) to quickly form **TPB**. **TPB**, itself was shown to have a lower oxidation potential than **TPA**, and additional oxidation processes can lead to the formation of quinoidal or partially quinoidal-type dication (as the precise nature of the species is unknown) were reported. Although such processes raise potential

concerns regarding the stability of **TPA**-based materials under oxidative processes, the **TPB** product should nonetheless be capable of hole transport. Therefore, a more practical issue with respect to hole transport for OLEDs may relate to the creation of new species that could act as charge traps (at sufficiently low concentrations) with detrimental effects on hole mobility. It should be noted that blocking of the *para*- position(s) of **TPA**, by substitution with certain moieties (e.g. methoxy or *tert*-butyl), provides a strong stabilizing effect on the radical-cation species that can prevent dimerization.[1]

For the purposes of introducing important parameters of relevance for identifying and/or designing hole-transport materials, we first consider *N,N'*-diphenyl-*N,N'*-bis(3-methylphenyl)-(1,1'-biphenyl)-4,4'-diamine (**TPD** (**3.3**)) as reported by Adachi *et al.*[2-6] for OLED use and considered an archetype for other arylamine-based materials studied by other research groups.[7,8]

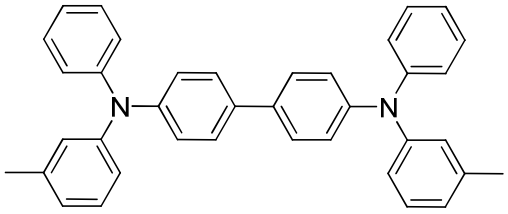

3.3

Figure 3.2. *N,N'*-diphenyl-*N,N'*-bis(3-methylphenyl)-(1,1'-biphenyl)-4,4'-diamine (**TPD** (**3.3**)).

TPD was selected on the basis of studies by Pai and co-workers of hole injection in **TPD**-doped polycarbonate films.[9] Although various arylamine analogues have been shown to possess low oxidation potentials (that permit ease of hole injection from the

anode) and good hole transport mobilities,[10] issues of thermal instability and their effects on OLED device performance as a function of time and operating temperature have been reported. For example, crystallization of **TPD** was noted in studies by Han *et al.*[11] and Sheats *et al.*[12] This was postulated to be a consequence of the low glass transition temperature (65 °C)[7] of the molecule and it was suggested that crystallization of **TPD** lead to degradation the performance of the OLED. In other studies on **TPD** and higher weight oligomers of **TPD** reported by Tokito *et al*.[13] it was observed that the critical temperature at which a device failed showed a dependence on the glass transition temperature of the material. As the molecular weight increased across the series of TPD-like oligomers resulting in higher glass transition temperatures, so did the critical temperature for device breakdown. Examination of the layers by optical microscopy revealed high levels of crystallization for devices operated above their glass transition (T_g). A study by Fenter *et al*.[14] on a **TPD**/Alq_3 bilayer structure (on a silicon wafer) showed that heating above the T_g of **TPD** ($T \geq 83$ °C) produced no detectable crystallization (as measured by X-ray reflectivity). An alternative explanation to the device degradation suggested by the authors was that the thermal expansion (change in layer thickness) of **TPD** above and below its respective T_g produced failure due to strain in the device layers. Adachi *et al*.[8] postulated that the formation of crystals within a given amorphous hole-transport layer may lead to hole trapping sites that negatively affect device performance. Therefore, the development of high T_g materials could be useful in avoiding such issues.[7] As the work described in this chapter concerns polymers anticipated to be amorphous and possessing glass transitions higher than small-molecules, the design of amorphous small-molecules is not addressed. A report by

Yasuhiko Shirota[15] describing the requirements of molecular design for achieving amorphous small-molecules provides good insight for those interested.

The hole-transport small-molecule, *N,N'*-di(1-naphthyl)-*N,N'*-diphenyl-(1,1'-biphenyl)-4,4'-diamine (**α-NPD** (**3.4**)) was developed by Tang and co-workers[16] and has become one of the most widely utilized hole transport materials to-date.

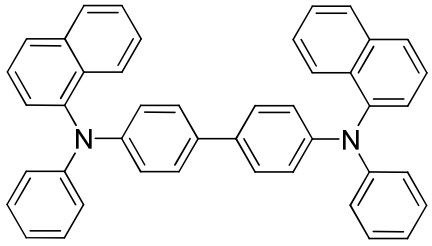

3.4

Figure 3.3. *N,N'*-di(1-naphthyl)-*N,N'*-diphenyl-(1,1'-biphenyl)-4,4'-diamine (**α-NPD** (**3.4**)).

With respect to redox processes, fully reversible first and second oxidations (as studied by cyclic voltammetry) were observed which suggested electrochemical stability of the species under testing conditions. Similar reversibility has been reported for **TPD** and TPD-like derivatives.[17] The notable improvement of **α-NPD** was evident in its higher glass-transition temperature of 95 °C; attributed to the greater bulk of the naphthyl substituents. It could be said that the main advantages of **TPD** and **α-NPD**, at least as compared to unsubsituted triarylamines (NAr_3), lie with their enhanced radical-cation stability.

Numerous additional examples of arylamine-type small-molecules have been synthesized and reported in the literature (and in patents) for OLED use and a complete

review is not practicable for the purposes of this chapter. Therefore, the focus shall center upon relevant side-chain polymers functionalized with arylamine-type groups. One of the earliest known examples of such a system was reported by Kolb *et al.*[18] in 1996.

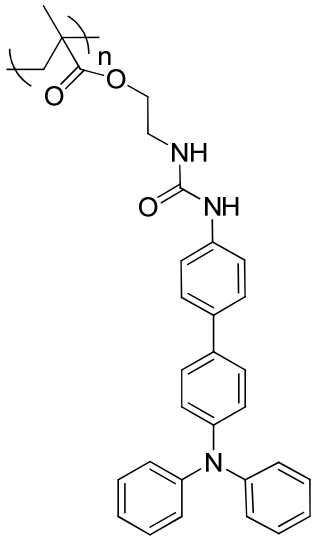

3.5

Figure 3.4. Arylamine-type side-chain polymer **3.5**.

Polymer **3.5** was studied as a solution-processable hole-transport material (with a secondary function as the fluorescent emitter) in single and double-layer polymer OLED architectures (ITO/**3.5**/Al or ITO/**3.5**/poly(methyl(2-(1-pyrenyl)ethyl)siloxane)/Al) to afford a maximum internal quantum efficiency of 0.20%. Cyclic voltammetry showed oxidation of **3.5** to be irreversible and likely lead to the formation of dimer products based on the observation of insolubilization of the films of the oxidized polymer. The authors postulated that the dimerization may actually function as a cross-linking mechanism for the polymer layer, but did not investigate any further. The potential for dimerization products presents issues of layer instability as on-going reactions serve not

only as competing processes to charge transport but also change the redox properties of the layer as the process continues over time. The authors did not adequately address these concerns for their polymer.

Bellmann *et al.*[19] and Shaheen *et al.*[20] demonstrated various examples of side-chain polymers containing TPD-like derivatives (as well as a TPA-like derivative).

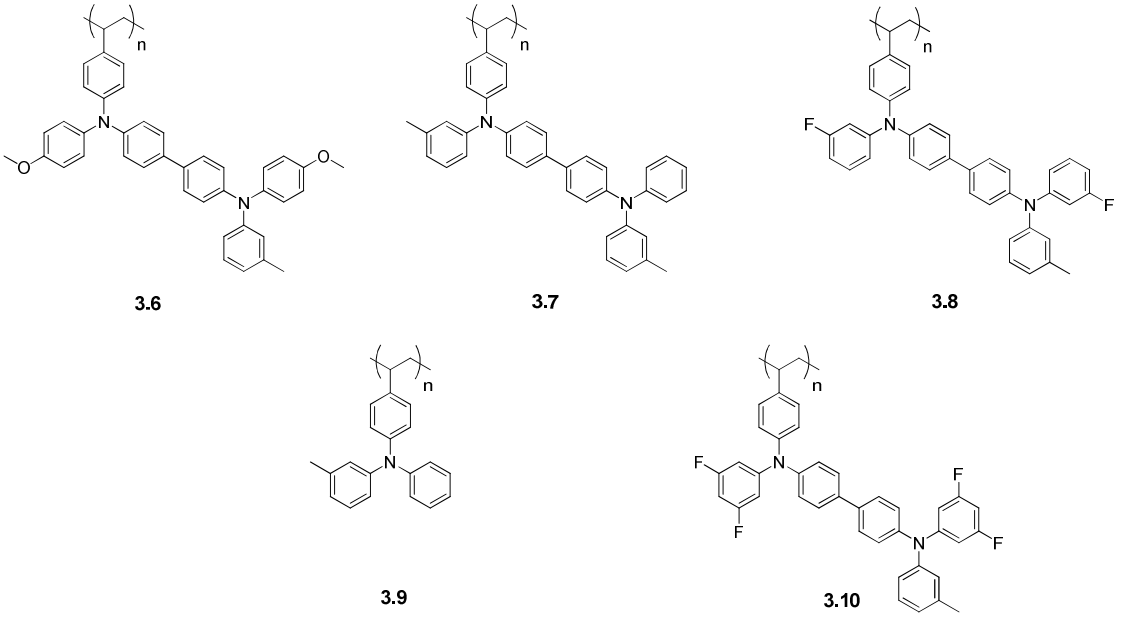

Figure 3.5. Hole transporting polymers **3.6** – **3.10**.

Table 3.1. Selected Polymer **3.6**– **3.10** Properties

polymer	T_g (°C)	IP (eV)[a,b]
3.6	132	5.06
3.7	151	5.38
3.8	147	5.56
3.9	104	–
3.10	140	–

[a] IP estimated from small-molecule analogues via UPS.
[b] reference 19

These reports showed that functionalization onto a side-chain effectively increased the glass-transition temperature above 100 °C for all polymer examples. More importantly, it was shown that modification of the TPD-like core molecule with different electron donating or withdrawing substituents could successfully modify the redox properties for use in polymer OLEDs. A comparative study by cyclic voltammetry (not shown) of the polymers vs. small-molecule analogues showed very small differences in redox properties between the two and for all cases (except **3.9**) the oxidation events were found to be fully reversible, suggesting less likelihood of dimerization events. The ionization potentials (IP) of three polymers (estimated from ultraviolet photoelectron spectroscopy (UPS) of small-molecule analogues) supported the conclusion that the IP could be increased or decreased relative to the TPD-like model polymer **3.7**. Examples of prepared OLEDs (ITO/**3.6** – **3.8**/Alq_3:quinacridone(0.5 wt%)/LiF/Al) demonstrated a maximum EQE of 4.5% and 20 lm/W (at 15 cd/m^2) using polymer **3.8**. The polymer series showed that increasing the IP plays a role in hole injection between layers.[20] In all, these reports demonstrated that careful molecular design could be used to produce a variety of solution-processable side-chain polymers. Judicious energy-level engineering must always be employed as energy-level manipulations leading to improvement of charge injection to some neighboring layer may still adversely affect charge injection or charge blocking ability to another.

Two additional examples containing arylamine-based side-chain polymers were reported by Feast *et al*.[21] and Tamada *et al*.[22]

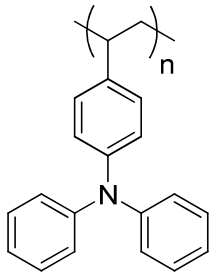

3.11

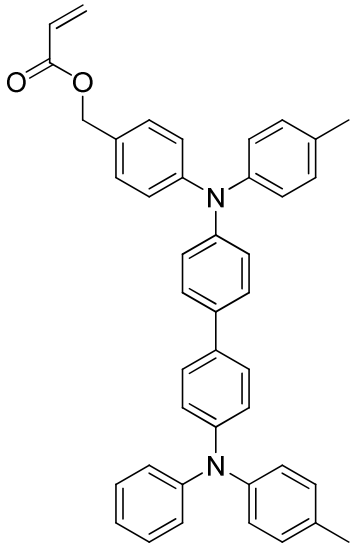

3.12

Figure 3.6. Hole transporting polymer **3.11** and hole transport monomer **3.12**.

Polymer **3.11** was utilized by Feast *et al*. as a solution-processable hole-transport layer and compared with vapor-deposited **TPA** and **TPD** devices. Within a device architecture composed of ITO/**3.11** or **TPA** or **TPD**/ 10 or 11-methoxy-7-H-benzimidazo(2,1-a) benz(de)isoquinolin-7-one (isomer mixture)/Al, the polymeric device gave the best results with higher brightness and an maximum quantum efficiency of 1.05% (surpassing the efficiencies of the small-molecule devices (<<1%)). For the **TPA** devices, the authors conjectured that crystallization (due to low T_g) played a role, whereas the polymer (T_g = 146 °C) would not experience such effects. The **TPD** device efficiency was potentially limited by exciplex formation that competed with emission from the perinone dye mixture (10 or 11-methoxy-7-H-benzimidazo(2,1-a) benz(de)isoquinolin-7-one) as observed by electroluminescence. The authors did not study the redox properties of the TPA-based polymer for evidence of likely dimerization.

Tamada *et al*. used a different approach to obtain a polymeric hole-transport layer. Vapor deposition of monomer **3.12**, followed by *in situ* polymerization (via UV irradiation and subsequent thermal treatment; with conversion levels > 95%) was used to achieve high levels of polymer layers. Devices (ITO/**3.12** or polymer equivalent/Alq_3/Mg:Ag (10:1)) showed that efficiencies with a polymerized layer (vs. unpolymerized control layer) were approximately three times greater. Although the approach yielded superior devices (vs. the control), several issues were not addressed. Among them were the effects of the UV and thermal treatments and their likelihood to produce side-reactions and/or decomposition products, potential changes to the photophysical and redox properties, and what advantages the approach offered as compared to processing the layer directly from the polymer form. Additional examples of side-chain polymers containing arylamine-type hole transport moieties are known but incorporate additional co-monomers such as carbazole (vide infra) or crosslinking groups (see Chapter 5). We discuss these polymers elsewhere.

A change in research focus from fluorescent to phosphorescent OLEDs (see Chapter 1) occurred in the late 1990s, after the introduction phosphorescent transition metal-based emitters (doped in organic hosts). These emitters led to considerable improvements in the efficiency of OLEDs (see Chapter 1). Research by Kido and co-workers[23] and Forrest and co-workers[24] helped to develop and establish phosphorescent OLEDs (PhOLEDs). In 1999, O'Brien *et al.*[25] reported the first use of 4,4'-*N,N'*-dicarbazolyl-biphenyl (**CBP** (**3.13**)), previously developed by Forrest and co-workers as a wide optical-gap molecule for blue organic lasers,[26] as a host material for the platinum emitter 2,3,7,8,12,13,17,18-octaethyl-21*H*23*H*-porphine platinum(II) (PtOEP). This early

host-guest system produced poor energy transfer from the **CBP** host to the PtOEP guest resulting in low device efficiency.

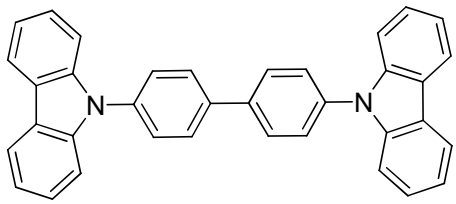

3.13

Figure 3.7. 4,4'-*N,N'*-dicarbazole-biphenyl (**CBP** (**3.13**)).

Subsequent work by Baldo *et al.*[27] with **CBP** and the emitter *fac* tris(2,2'-phenylpyridyl) iridium (III) ($Ir(ppy)_3$) demonstrated a marked improvement resulting from improved energy transfer from **CBP** to the guest emitter. With a device architecture comprised of ITO/α-NPD/**CBP**:$Ir(ppy)_3$ (6 wt%) /bathocuproine (BCP)/Alq_3/Mg:Ag (25:1), a maximum EQE of 7.5% (26 cd/A and 19 lm/W) at 4.3V were reported. Further study of **CBP** by Adachi *et al*.[28] showed that in addition to functioning as a hole-transport material, evidence of electron transport implying a degree of ambipolarity was exhibited. Numerous examples of devices using **CBP** as a host for $Ir(ppy)_3$ have since appeared in the literature. A report by Kido and co-workers[29] demonstrated a device with a maximum EQE of 27% (95 cd/A and 97 lm/W) at 100 cd/m^2 for a device with the architecture ITO/MCC-PC1020 (commercial HIL polymer)/ 1,1-Bis-(4-bis(4-tolyl)-aminophenyl)cyclohexene (TAPC)/$Ir(ppy)_3$ (3 wt%) doped in 4,4',4''-tris(*N*-carbazolyl)-triphenylamine (TCTA) and **CBP**/BCP/BCP:Cs (1:1 molar ratio)/Al. Despite demonstrating the highest known efficiency for a **CBP**/$Ir(ppy)_3$ system, the apparent

complexity of their device design precludes ease of fabrication. The need for such complex vacuum-processed multilayer architectures in order to achieve the highest possible external quantum efficiencies possible, continue to be an area of concern for the development of low cost PhOLEDs.

In the same manner as arylamines, the hole carrier species of carbazoles is the corresponding radical cation. Like arylamines, carbazoles are also known to be reactive in this state. A thorough investigation of carbazoles (**Cbz** (**3.14**)) under oxidative conditions was reported by Nelson and co-workers.[30,31]

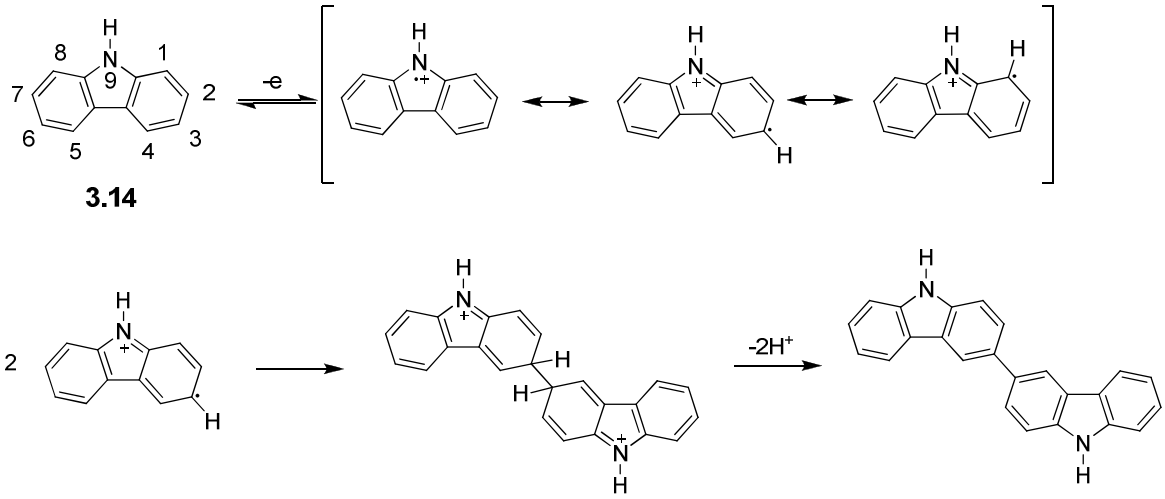

Figure 3.8. Reaction pathways for radical cations of carbazole (**Cbz** (**3.14**)).

The radical cation of carbazole was noted to be highly unstable and that dimerization could proceed at high rates to form a variety of species called bicarbazyls. For example, for *N*-phenylcarbazole the measured bimolecular rate constant for the coupling reaction was found to be $9 \pm 6 \times 10^6$ mol^{-1} sec^{-1}. Dimerization reactions at 3,3' and 6,6' positions were found to be the predominant couplings with loss of two protons.

The 1,1' and 8,8' couplings were not observed due to likely steric hindrance, but 9,9' couplings were observed in some examples. Careful consideration of the electrochemical stability of radical cations must be taken when designing carbazole-based hole-transport materials. It should be noted that unlike **TPD** and **α-NPD**, which exhibit reversible oxidation behavior (vs. **TPA**), the **CBP** radical cation does not show improved stability (vs. the carbazole radical cation).

9H-carbazole has a reported triplet energy of ~ 3.0 eV,[32,33] as measured from phosphorescence data. **CBP**, on the other hand, possesses a lower measured triplet energy of 2.62 eV.[34] Although the X-ray structure of **CBP** has been reported[35] and showed that the carbazoles were twisted (non-planar) with the biphenyl core, the decreased triplet energy suggests the core itself affects the triplet energy of the molecule. He *et al.*[32] reported several CBP-like targets that inhibited conjugation in order to prevent lowering of the triplet energy. Although earlier examples of such an approach[36] have been reported in the literature, this work presented several interesting examples that showed such an approach could result in higher triplet energies (closer to that of carbazole).

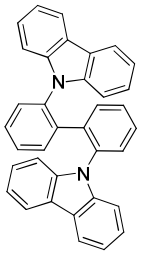

3.15

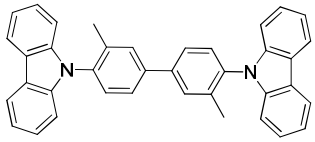

3.16

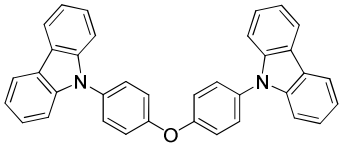

3.17

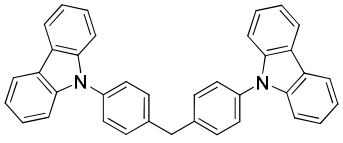

3.18

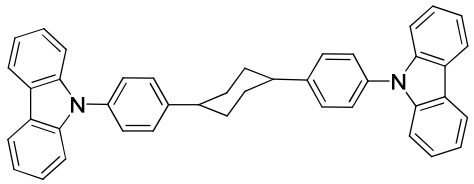

3.19

Figure 3.9. Hole-transport small-molecules **3.15** – **3.19**.

Table 3.2. Adiabatic Triplet Energies

Molecule	E_T (eV)[a]
CBP (3.13)	2.6
3.15	3.0
3.16	2.7
3.17	3.0
3.18	3.0
3.19	3.0
Cbz (3.14)	3.0

[a] estimated from onset of phosphorescence at 77K

Based on the triplet energies measured, it is possible to conclude that interruption of the π-system by twisting or introduction of a heteroatom or non-aromatic linker was sufficient to prevent lowering the triplet energy. For **3.16**, the methyl groups seemed to have a minor effect in producing twist of the biphenyl core and consequently the triplet energy was not raised to the same extent as in the other examples, supporting the possibility that the biphenyl core influences in the triplet energy. Although for molecule **3.15**, the carbazoles could be considered conjugated, across the biphenyl bridge, it is likely that sufficient twist is induced to inhibit the conjugation resulting in the high triplet energy observed. In all cases, the modified molecules also exhibited higher T_gs in the range of 78 – 115 °C. For blue PhOLED devices (ITO/α-NPD/host:FIrpic/BCP/Alq_3/LiF/Al), the authors noted a near doubling in luminance and

power efficiency when using **3.18** or **3.19** versus a **CBP** control device. As a side note, it is worth mentioning that arylamines, such as **TPD** and **α-NPD**, have generally found less use as host materials owing to their relatively low triplet energies (i.e. E_T (**TPD**) = 2.3 eV[37]). Host triplet energies lower than those of a guest emitter produce less efficient OLEDs (see Chapter 1). The most common green and blue emitters used to-date have triplet energies greater than those of arylamine-type hosts effectively limiting their use.

Another commonly used carbazole-based host material studied in the last decade has been *N,N'*-dicarbazolyl-3,5-benzene (**mCP** (**3.20**)) first reported by Thompson and co-workers.[38] **mCP** has a high triplet energy of ~ 2.9 eV (close to carbazole) that can be considered suitable for blue phosphorescent emitters.

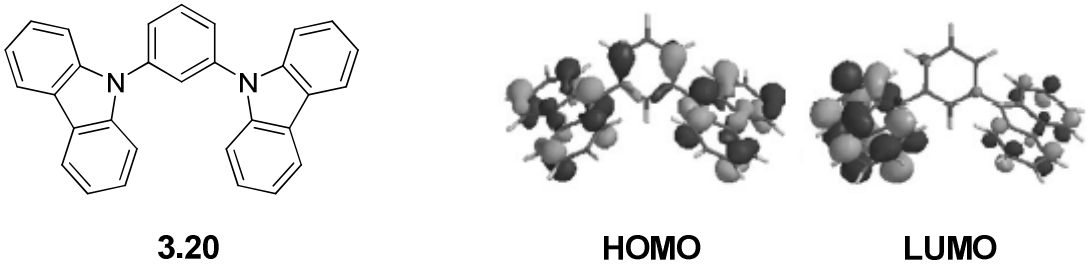

Figure 3.10. *N,N'*-dicarbazolyl-3,5-benzene (**mCP** (**3.20**)) and DFT calculated HOMO and LUMO surfaces (Reproduced with permission from ref. 43. Copyright Wiley-VCH Verlag GmbH & Co. KGaA. Reproduced with permission.).

mCP was first studied as a host candidate for several blue platinum (II) emitter guests, one of which was the emitter platinum(II)[2-(4',6'-difluorophenyl)pyridinato-$N,C^{2'}$)](2,4-pentanedionato) (FPt), which exhibits excimer-type emission in the solid-state affording near white emission.[38-40] In a device architecture composed of ITO/NPD/*fac*-tris(1-phenylpyrazolato-$N,C^{2'}$)iridium(III) (Irppz)/**mCP** or **CBP**:FPt/BCP/Alq_3/LiF/Al, it was found that **mCP** was a good host material with a

maximum quantum efficiency of 4.3% (11.3 cd/A and 8.1 lm/W) at 500 cd/m^2 versus a **CBP** device with a maximum efficiency of 2.3% (5.2 lm/W) at 500 cd/m^2. This was explained as a consequence of more efficient energy transfer from the **mCP** host to the guest as compared to **CBP**. This was reasonable if one considered the triplet energy of FPt (reported to be 2.8 eV[40]) vs. the triplet energies of the hosts. Another emitter for which **mCP** has been used as a host was the blue-green phosphor iridium(III) (bis-4,6-difluorophenyl)-pyridinato-*N,C*$^{2'}$] picolinate (FIrpic) with a triplet energy of 2.65 eV.[41] Lee *et al*.[42] reported a maximum power efficiency of 13.3 lm/W (at < 10 cd/m^2) for an **mCP**:FIrpic device, which to the best of our knowledge, was the highest achieved for such a system but a rather complex device architecture was necessary (see reference).

A variant of **mCP** was reported by Williams *et al*.[43] in 2007 that replaced the substituted the central benzene ring with a pyridine.

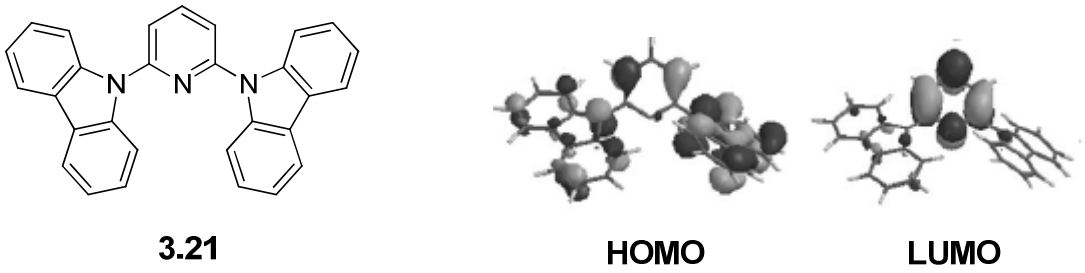

Figure 3.11. *N,N'*-dicarbazolyl-3,5-pyridine (**mCPy** (**3.21**)) and DFT calculated HOMO and LUMO surfaces (Reproduced with permission from ref. 43. Copyright Wiley-VCH Verlag GmbH & Co. KGaA. Reproduced with permission.).

The calculated HOMO and LUMO levels of **mCPy** were reported to be localized on different portions of the molecule which the authors postulated could have an effect on such properties as charge transport without further explanation. For a device structure with architecture ITO/NPD/*fac*-tris(1-phenylpyrazolato-*N,C*^{2})iridium(III) (Irppz)/**mCP** or

mCPy:FPt/BCP/ LiF/Al at 500 cd/m^2, a maximum quantum efficiency of 6.8% for **mCPy** and 5.7% for **mCP** were reported showing a modest improvement from the new host. No studies of the photophysical or redox properties of **mCPy** were reported in the paper, therefore, little can be concluded about the effects on the pyridyl group substitution. Formation of a charge-transfer state might be possible if one considers the connectivity of the carbazole and pyridyl unit. In addition, the authors do not study the possibility that the pyridine may impart some degree of electron transport capability on the molecule. However, it is worth noting that work by Kido and co-workers[44] demonstrated that 2,6-bis(3-(carbazol-9-yl)phenyl)pyridine (which introduced phenyl rings as spacers between the pyridine and the carbazoles) possessed ambipolar transport properties.

Substitution of carbazoles at the 3 and 6 positions has also been studied. Attachment of diphenylamino or carbazolyl groups was reported by Zhang *et al.*[45] 2003 (see **3.22** and **3.23**). In a similar fashion, Tsai *et al.*[46] studied a series of carbazole derivatives (see **3.24** and **3.25**).

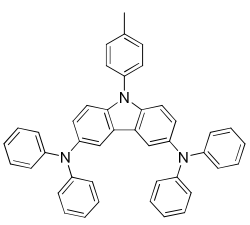

3.22

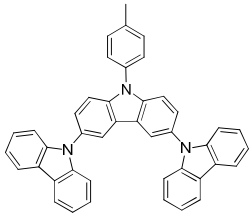

3.23

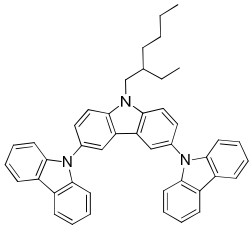

3.24

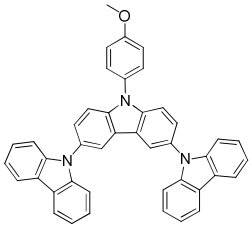

3.25

Figure 3.12. Additional carbazole-based small-molecule examples **3.22** – **3.25**.

The oxidation potentials of compounds **3.22** and **3.23** were evaluated by cyclic voltammetry. It was found that both possessed reversible oxidations suggesting that the

redox event likely occurred on the central carbazole (as the *para*- positions were blocked) and implying greater electrochemical stability of the radical cation species formed. Although not a one-to-one comparison, Kondakov *et al*.[47,48] has reported on degradation products produced from poorly reversible carbazole species (i.e. **CBP**) through dimerization of radicals produced during device operation. Therefore, reversibility by cyclic voltammetry may imply a greater likelihood for stability under device operation. In an ITO/**3.22** or **3.23**/Alq_3/LiF/Al device, both compounds were found to behave as good hole-transport materials. As the devices fabricated were of the fluorescent type, the authors did not consider their use as host materials. Compounds **3.24** and **3.25** were studied as host materials for FIrpic. It was found 3,6-substitution had a very minor effect on the triplet energy which was only 0.1 eV lower than *9H*-carbazole. For devices with architecture ITO/PEDOT: PSS/4,4',4"- tris(*N*-carbazolyl)triphenylamine (TCTA)/**3.24** or **3.25**:FIrpic (8 wt%)/3-(4-biphenyl)-4-phenyl-5-(4-*tert*-butylphenyl)-1,2,4-triazole (TAZ)/LiF/Al, at 1000 cd/m^2 efficiencies of 10.2% (9.4 lm/W) for **3.24** and 8.3% (5.8 lm/W) for **3.25**. No explanation was given for the minor difference. Cyclic voltammetry (which was not reported) would have been useful in elucidating the effects of the branched alkyl vs. p-methoxyphenyl on the oxidation potential of the compounds. Differences between the two would likely affect charge injection/transport between layers which might be responsible for the different efficiencies obtained.

With regard to side-chain polymers, poly(*N*-vinylcarbazole) (**PVK** (**3.26**)) was recognized as a blue electroluminescent material long before it found use in OLEDs.[49] Kido and co-workers recognized the potential of this solution-processable polymer and employed it as a hole transport and fluorescent emissive layer in 1993.[50] In 2000, **PVK**

was first used as a host material for $Ir(ppy)_3$ as reported by Yang *et al*.[51] with a maximum EQE of 7.5% (5.8 lm/W) being measured for the device architecture: ITO/**PVK**:$Ir(ppy)_3$(6.8 wt%)/1,3-bis[(4-*tert*-butylphenyl)-1,3,4-oxadiazolyl] phenylene (OXD-7)/Mg:Ag.

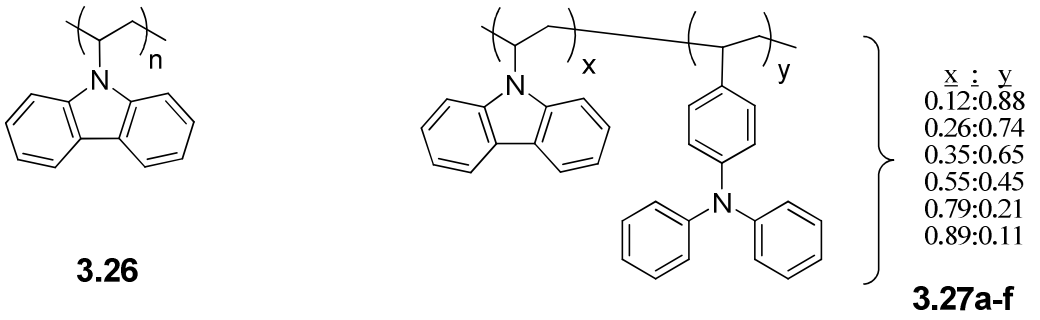

3.26 **3.27a-f**

Figure 3.13. Poly(*N*-vinylcarbazole) (**PVK** (**3.26**)) and PVK-TPA copolymers (**3.27a-f**).

Forrest and co-workers[52] demonstrated relatively low efficiency (1.3%; 0.8 lm/W) in a device with architecture ITO/PEDOT:PSS/**PVK**:FIrpic (5 wt%)/BCP/Alq_3/Mg:Ag/Mg. **PVK** has a measured triplet energy of ~2.5-2.6 eV[33,36] which is considerably lower than that of *9H*-carbazole and may be due to higher interaction between carbazoles within the polymer; this may also explain the low efficiency when used as host for the blue emitter FIrpic. An example of *N*-vinylcarbazole copolymerized with a vinyl **TPA** afforded a series of copolymers (with varying compositions; see **3.27a-f**). This approach showed that introduction of the **TPA** moiety could be used to modify the HOMO level (estimated from electrochemical data) of the copolymers in the range of -5.1 to -5.4 eV (vs. **PVK**; HOMO = -5.8 eV). Such changes can affect charge injection/transport to other layers. Cyclic voltammetry revealed that for all copolymers oxidations were irreversible (suggestive of the possibility of dimerization events). Triplet energies for all copolymers

were also found to be higher (2.6 – 2.7 eV) than that of **PVK**. For devices based on ITO/PEDOT:PSS/**3.28a-f**:$Ir(ppy)_3$(4 wt%):PBD(40 wt%)/BCP/Ca/Al, **3.27d** was demonstrated to be the best host, but all copolymers gave higher device performances than **PVK**.

Other examples of **PVK** as a host[33,53,54] or hole-transport material[55], or of *N*-vinylcarbazole copolymerized with other groups (i.e. crosslinkable, electron transporting, or both) have also been reported. Some of these examples are discussed elsewhere in the thesis as appropriate. **PVK** remains one of the most common solution-processable hole-transport/host polymers in use to-date.

3.3. Goals of Chapter 3

The research aims of this chapter were to study the effects of functionalization of different carbazole-based transport moieties as side-groups on a polymeric backbone. Development of synthetic approaches and studies of the photophysical, thermal, and electrochemical properties were undertaken. Selected polymers were also evaluated in OLED devices.

3.4. Design Rationale and Synthesis of Norbornene-based Carbazole Side-Chain Homopolymers

Several carbazole-based hole transport groups, motivated by literature reports on related small-molecules, were chosen for study as solution-processable polymeric analogues with potential for hole-transport or host-material purposes. In this section we focus on the design rationale and specifics of synthesis of these polymers. For all cases, side-chain functionalization to form a norbornene-type monomer was chosen due the well-established nature of ring opening metathesis polymerization (ROMP) of norbornenes.[56,57] Specific experimental details are given in Chapter 2. Discussions of thermal, photophysical, and electrochemical properties in addition to evaluation of polymers in OLED devices are included in subsequent sections of this chapter.

The first polymer synthesized was based on a triscarbazole design inspired by Zhang *et al.*[45] published in 2003 for hole transport in a fluorescent OLED. The potential for triscarbazole to function as a high triplet-energy host, was recognized by our collaborators in the Brédas group based on theoretical calculations (not shown), (adiabatic E_T (calc) = 3.19 eV by DFT (B3YLP/6-31G*)) and corroborated by a report Tsai *et al*.[46] where the triscarbazole moiety was shown to effectively host the blue phosphor FIrpic. It was also hypothesized that for the first oxidation, the radical cation would form on the central carbazole and might show reversible redox behavior. Such electrochemical studies were not reported by Zhang *et al.* or Tsai *et al*. Scheme 3.1 reveals the synthetic approach used to attain polymer **3.30**.

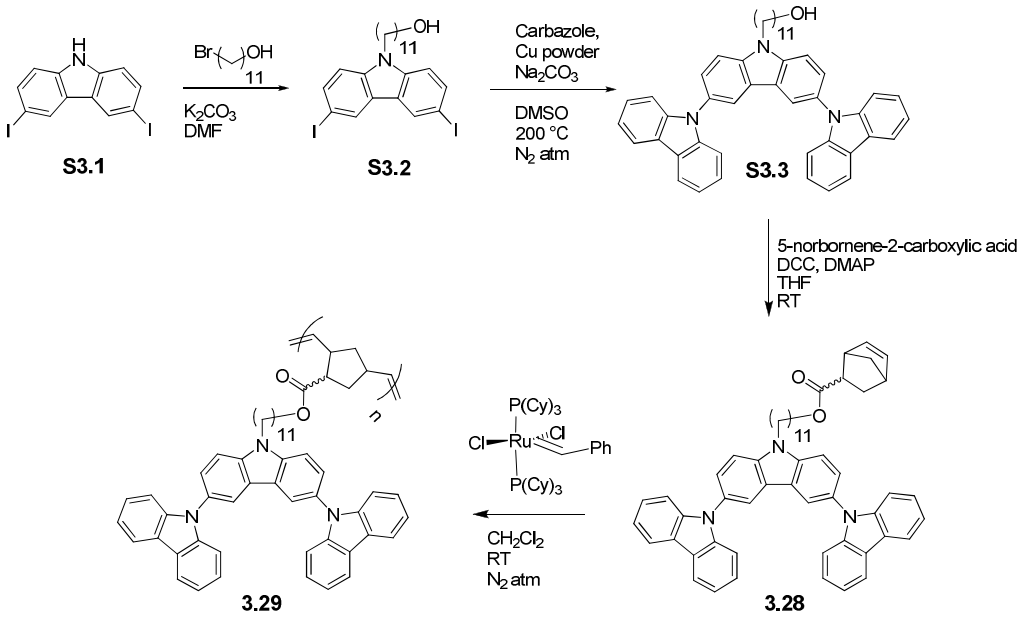

Scheme 3.1. Synthesis of triscarbazole-type functionalized norbornene monomer **3.28** and polymer **3.29**.

Following iodination of carbazole, functionalization at the *9H* position on carbazole with 11-bromoundecanol was performed. Ullmann coupling was performed to obtain the triscarbazole group. The monomer was formed by reaction with 5-norbornene-2-carboxylic acid, the product of which, was polymerized with Grubbs' first generation initiator.

Jabbour and co-workers reported on the development of the small-molecule **mCPy** in 2007 as a host for the blue phosphor FPt.[43] In order to obtain a polymeric analogue, a two step conversion of 2,6-dihydroxyisonicotinic acid was performed by first brominating the hydroxyl positions and then converting the carboxylic acid into the methyl ester.

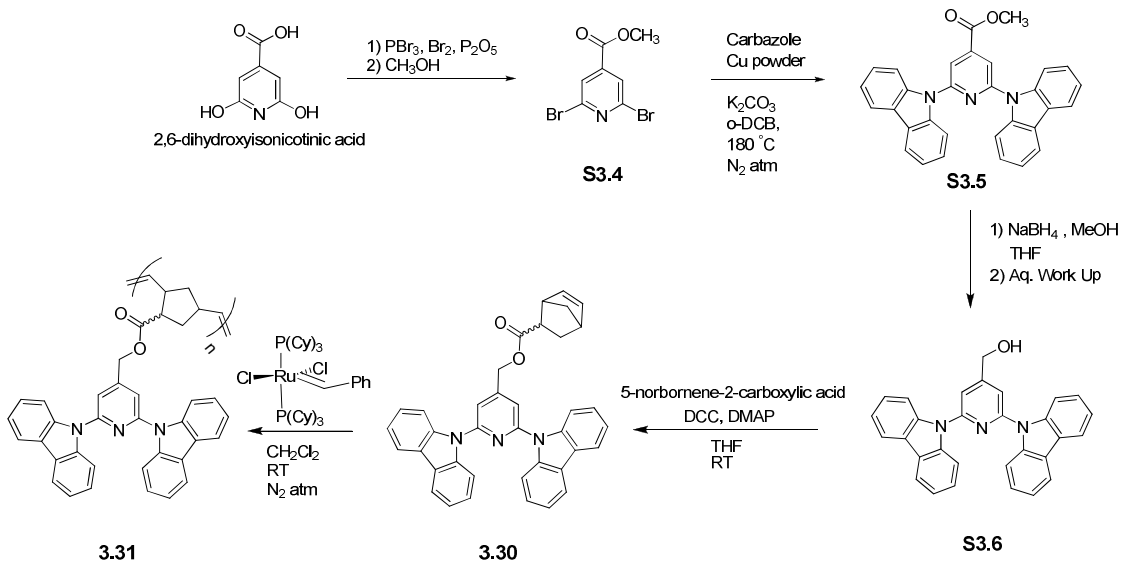

Scheme 3.2. Synthesis of mCPy-type functionalized norbornene monomer **3.30** and polymer **3.31**.

Ullmann coupling with carbazole was then used to convert the intermediate (**S3.4**) into the mCPy-analogue. Reduction to the primary alcohol was achieved with sodium borohydride followed by reaction of the alcohol with 5-norbornene-2-carboxylic acid. ROMP with Grubbs' initiator was used to obtain the polymer.

A second **mCPy** variant was synthesized incorporating *tert*-butyl groups at the carbazole 3,6-positions. This was pursued in order to prevent coupling reactions. It has been well-established that the when the carbazole 3 and/or 6 positions are unsubstituted, high radical cation character at these positions may result in dimerization events[31]; unless these positions are appropriately protected/blocked. The substituent was chosen due to the absence of hydrogen at the α-carbon of the *tert*-butyl group. In studies of methyl- or ethyl- substituents on carbazole 3 or 6 positions, it has been observed that abstraction of a proton on the α-carbon positions (when hydrogens are available) that can lead to couplings.[30] Synthesis was commenced by reduction of **S3.4** with sodium borohyride.

The product was coupled to 3,6-di-*tert*-butyl-*9H*-carbazole (produced via Friedel Crafts alkylation of carbazole) to afford the mCPy analogue.

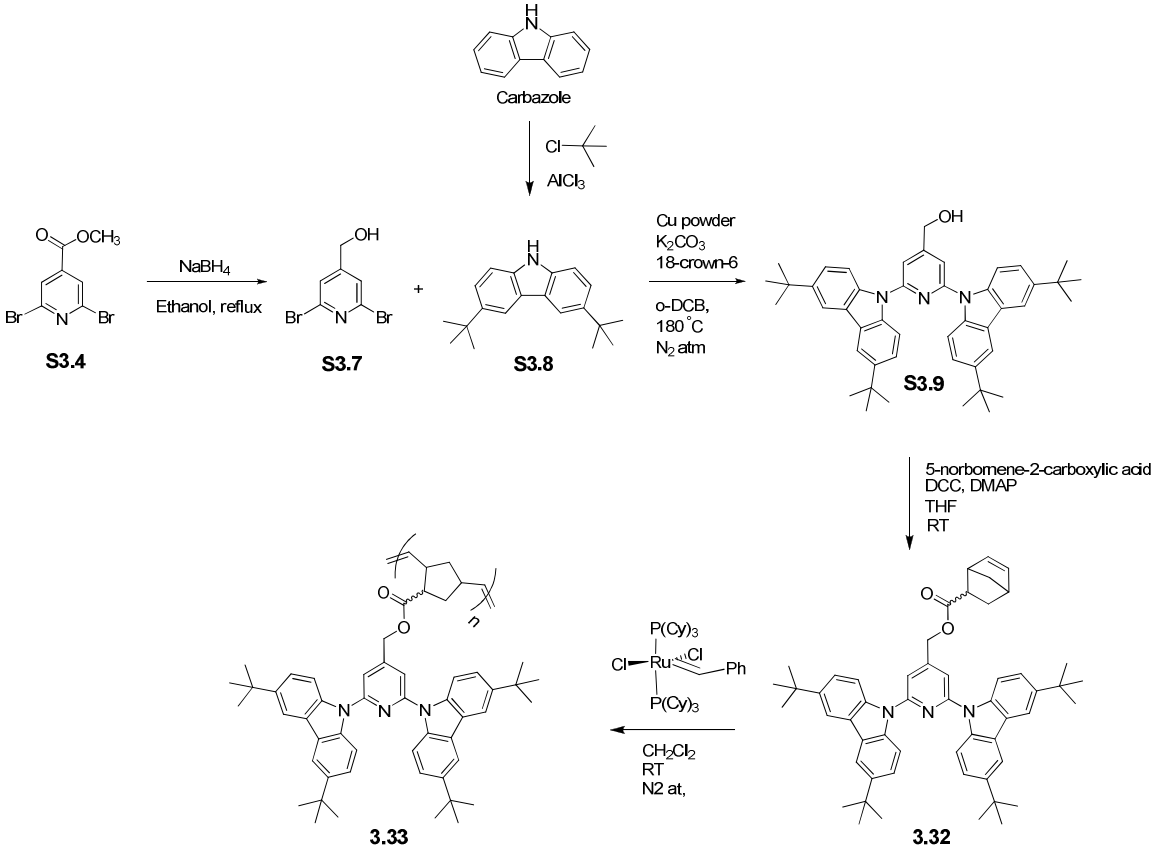

Scheme 3.3. Synthesis of mCPy-type functionalized norbornene monomer **3.32** and polymer **3.33**.

Coupling to 5-norbornene-2-carboxylic acid and polymerization of the resulting monomer with Grubbs' first generation catalyst were subsequently performed.

The **mCP** small-molecule host was first reported by Thomspon and Forrest *et al*.[38] as a good host for the blue phosphor FPt. In order to attach a derivative of this group onto a side-chain polymer we started with iodination of 3,5-diaminobenzoic acid with potassium iodide. The resulting intermediate was converted to the methyl ester with methanol under acidic conditions and then coupled with carbazole (Ullmann conditions).

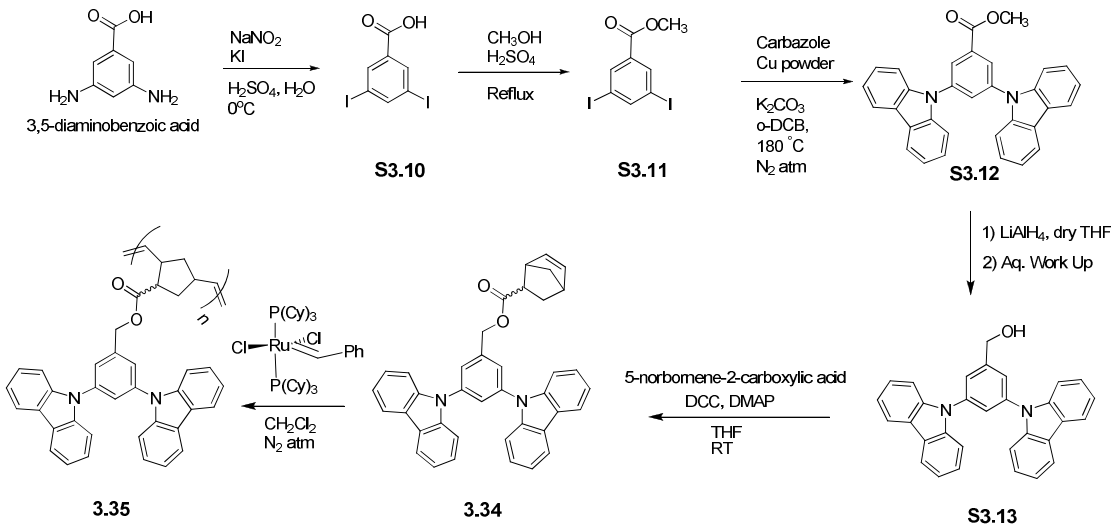

Scheme 3.4. Synthesis of mCP-type functionalized norbornene monomer **3.34** and polymer **3.35**.

Reduction of the methyl ester to the primary alcohol with lithium aluminum hydride was followed by coupling to 5-norbornene-2-carboxylic acid. The monomer was polymerized with Grubbs' first generation initiator via ROMP.

In order to study the effects (if any) of the linker on the properties of the transport moiety two variants of the mCP-type analogues were synthesized. The first, shown in the scheme below, was commenced by conversion of **S3.12** to the carboxylic acid followed by reaction with 5-norbornene-2-(5-bromopent-1-yl) under basic conditions to afford the monomer.

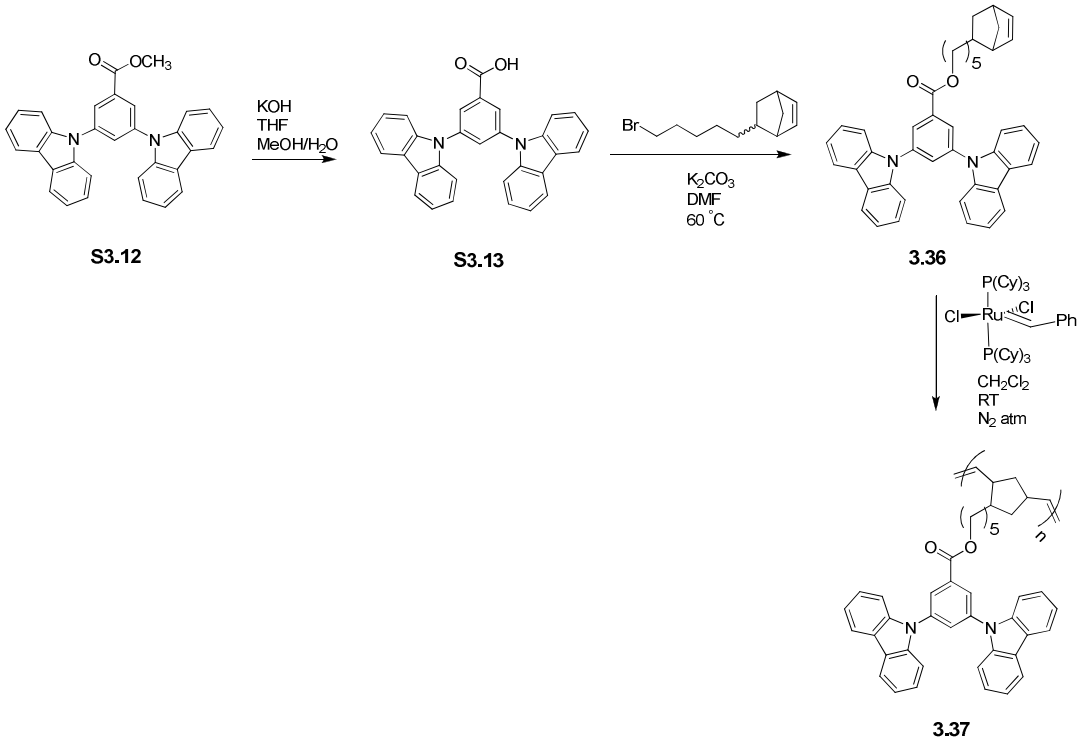

Scheme 3.5. Synthesis of mCP-type functionalized norbornene monomer **3.36** and polymer **3.37**.

The polymerization was subsequently carried out via ROMP using Grubbs' first generation initiator. The third mCP variant monomer and polymer were synthesized in the same manner as above but substituting a shorter linker length on the norbornene (C_1 here vs. C_5 for **3.36**).

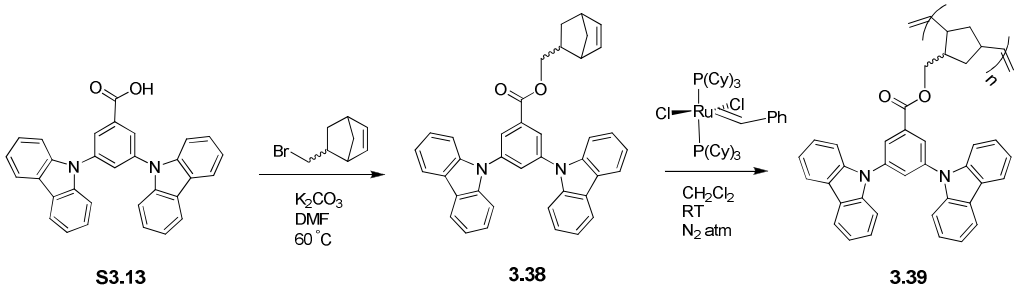

Scheme 3.6. Synthesis of mCP-type functionalized norbornene monomer **3.38** and polymer **3.39**.

As discussed in the introduction, **CBP** has been used as a host for various phosphors[34,58] (i.e. $Ir(ppy)_3$) and has been reported to exhibit ambipolar charge-transport properties[28] (although its transport should be predominantly of the hole type and why it is included in this chapter). Synthesis was started by Ullmann coupling of carbazole to 4,4'-diiodobiphenyl. The Vilsmeier-Haack reaction was used to formylate **S3.14** followed by reduction of the formyl group to the primary alcohol with sodium borohydride.

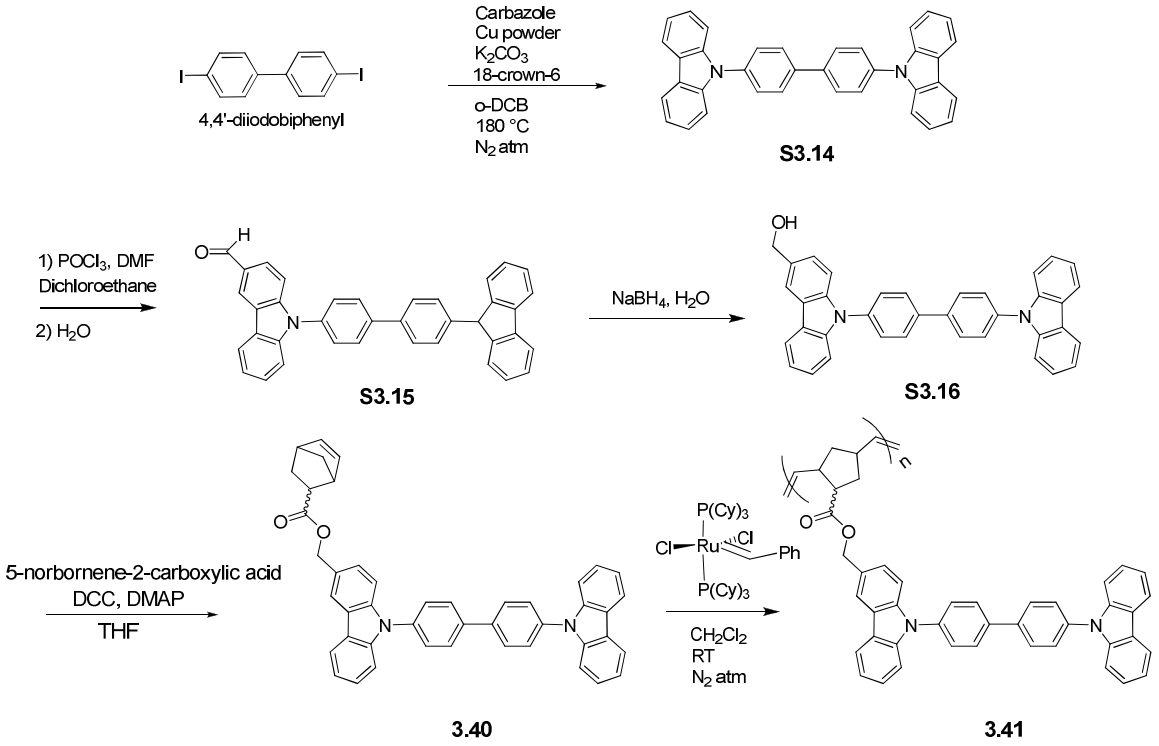

Scheme 3.7. Synthesis of CBP-type functionalized norbornene monomer **3.40** and polymer **3.41**.

The alcohol was reacted with 5-norbornene-2-carboxylic acid to yield the monomer which was polymerized via ROMP.

Finally, two targets were synthesized with some similarity to the well-studied **PVK** polymer. These targets incorporate 3,6-di-*tert*-butyl-*9H*-carbazole in an attempt to prevent dimerization side-reactions as discussed previously. In the first target, 3,6-di-*tert*-

butyl-*9H*-carbazole was reacted with 5-norbornene-2-(4-bromobut-1-yl) to give the monomer, which was then polymerized by ROMP.

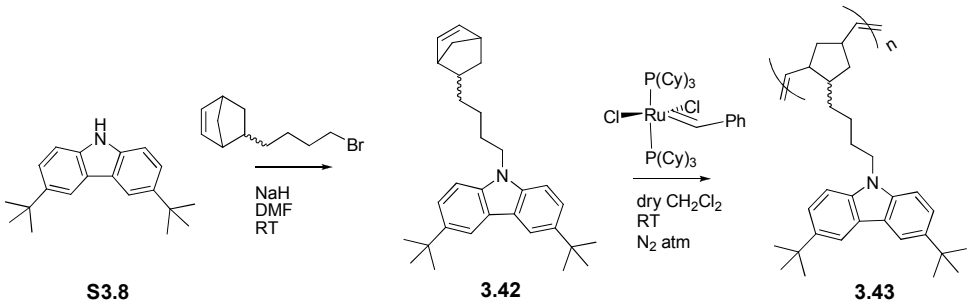

Scheme 3.8. Synthesis of carbazole-type functionalized norbornene monomer **3.42** and polymer **3.43**.

The second target incorporated a different linker for purposes of comparison. Friedel Crafts alkylation of 2-(*9H*-carbazol-9-yl)ethanol followed by coupling to 5-norbornene-2-carboxylic acid afforded the monomer which was subsequently polymerized.

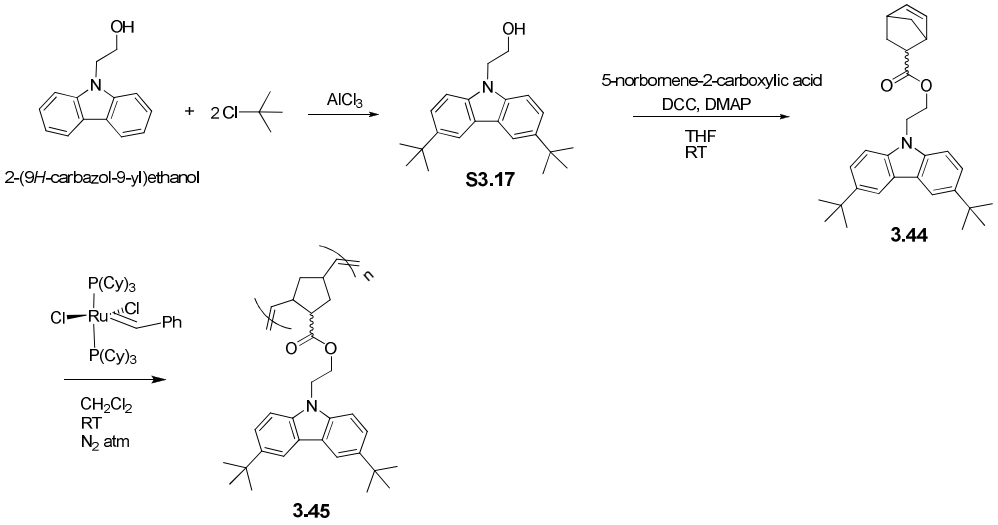

Scheme 3.9. Synthesis of carbazole-type functionalized norbornene monomer **3.44** and polymer **3.45**.

All polymers discussed in this were purified by multiple precipitations (> 3×) into a poor solvent (typically methanol). All polymers were characterized by ^{1}H NMR, gel

permeation chromatography, elemental analysis. Insofar as purity is concerned, it is recognized that these polymers will not possess the level of purity achievable for sublimed small-molecules. It was a primary goal of our studies to determine whether such side-chain polymer systems, regardless of this limitation, could achieve reasonable performance in OLED devices. For ease of comparison in the subsequent sections and discussions, the following figure shows all the polymers synthesized.

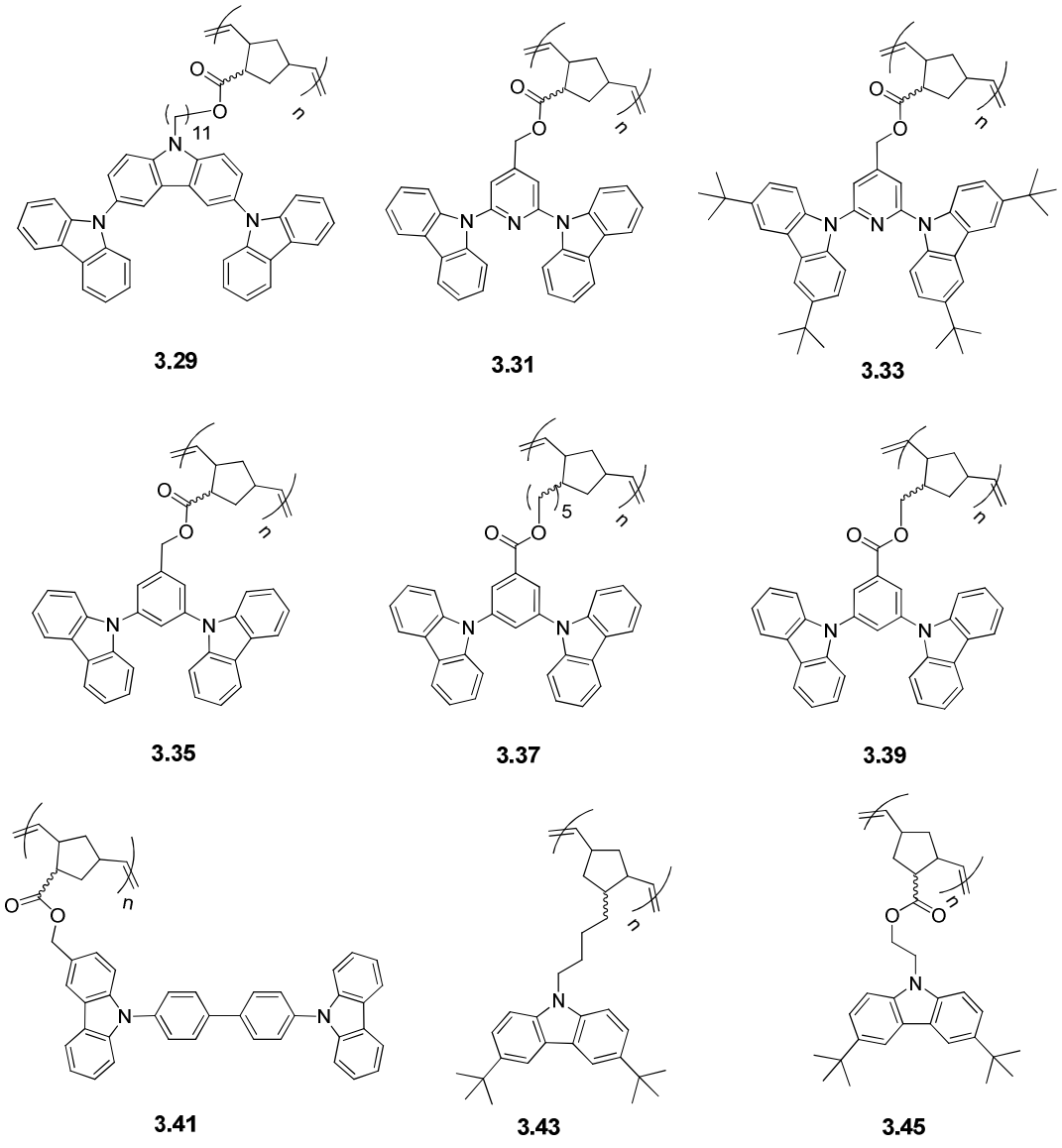

Figure 3.14. Hole-transport side-chain polymers.

3.4.1 Polymer Properties

Table 3.3. Polymer Properties

Polymer	M_w (kDa)[a]	M_n (kDa)[a]	PDI[a]	T_g (°C)[b]	T_d (°C)[c]
3.29	49	25	1.94	149	424
3.31	44	22	1.98	–	–
3.33	25	9	2.9	238	–
3.35	46	21	2.14	175	–
3.37	40	22	1.83	127	396
3.39	27	16	1.69	197	381
3.41	39	24	1.63	212	–
3.43	49	13.6	3.58	132	385
3.45	47	17	2.78	153	373

[a] Calculated from gel permeation chromatography (in chloroform) vs. polystyrene standards

[b] Determined from differential scanning calorimetry

[c] Determined from thermogravimetric analysis (at 5% weight loss)

"–" Denotes the measurement was not obtained

ROMP yielded homopolymers with molecular weights in the range of 25 – 50 kDa, with the majority of the homopolymers closer to the 40 – 50 kDa range. The polydispersity indices (PDIs) obtained were in the range of 1.6 – 3.6, which implied the polymerization was not well-controlled, in contrast to what would be expected from the near living nature of ROMP. A study by Pollino *et al*.[59] on *exo/endo* isomer mixtures of norbornene esters and similar alkyl norbornenes suggested some possible reasons for these observations. For the former (norbornene esters), the relative rates of reaction have shown that the *exo* isomer reacts more quickly than the *endo*, and for alkyl norbornenes poor control of polymerization has also been observed.

Differential scanning calorimetry and thermogravimetric analyses were performed for selected polymers. Functionalization onto a polymeric backbone resulted in glass transition temperatures above 100 °C for the polymers examined. Frequently, small-molecules demonstrate low glass transition temperatures (i.e. **mCP** (T_g = 55 °C)[32], **CBP**

(T_g = 65 °C)[60] which can be detrimental to device performance. The wide range of glass transition temperatures observed (127 – 238 °C) suggested effects due to the linker or side-group attached. For example, comparison of polymers **3.37** and **3.39** (where the linker of the former polymer is longer by four carbons) showed that the former possessed a T_g that was significantly lower by approximately 70 °C. This is consistent with a study of polynorbornene copolymers reported by Kaita *et al*.[61] where increasing the length of the aliphatic side-chain produced notable reductions in the T_g. Polymer **3.33**, with bulky *tert*-butyl groups produced the highest glass transition (238 °C). Comparison to polymer **3.35**, which is similar but lacking these groups showed a difference in T_g of approximately 60 °C suggesting the bulkiness of the side-group can also have pronounced effects. The decomposition temperatures, for those polymers that were evaluated, were found to be in the upper 300 °C or above range which suggests that the polymers should be stable for the purposes intended.

3.5. Photophysical Properties

3.5.1. UV-vis. Absorption Studies

The following figures show the normalized absorption at room temperature of the monomers (on the left) and the thin-film of the respective polymer on the right. Due to the absorption of glass in the deep ultraviolet, the thin-film absorptions are cutoff around 250 nm and close peaks were disregarded. Table 3.4 and 3.5 summarize the absorption maxima of the spectra acquired.

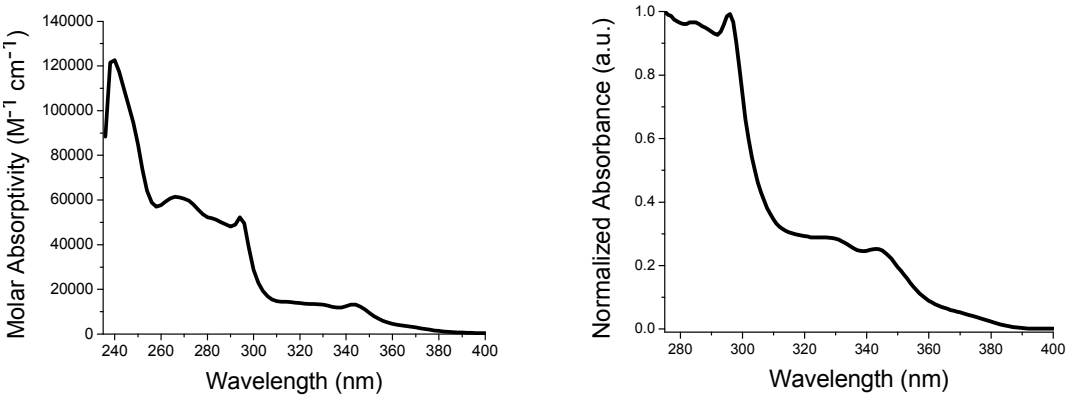

Figure 3.15. Room temperature molar absorptivity (in $CHCl_3$) and thin-film absorption on glass of polymer **3.29**.

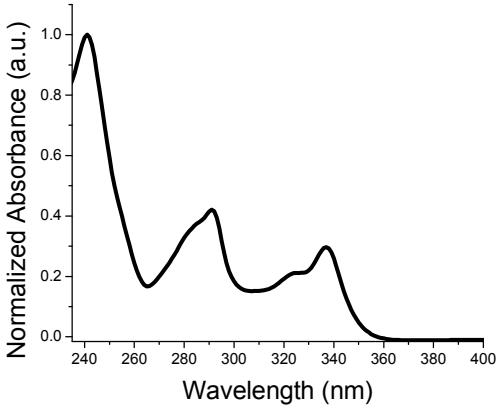

Figure 3.16. Room temperature UV-vis. absorption of monomer **3.30** (in $CHCl_3$) (thin-film of polymer **3.31** unavailable (see below).

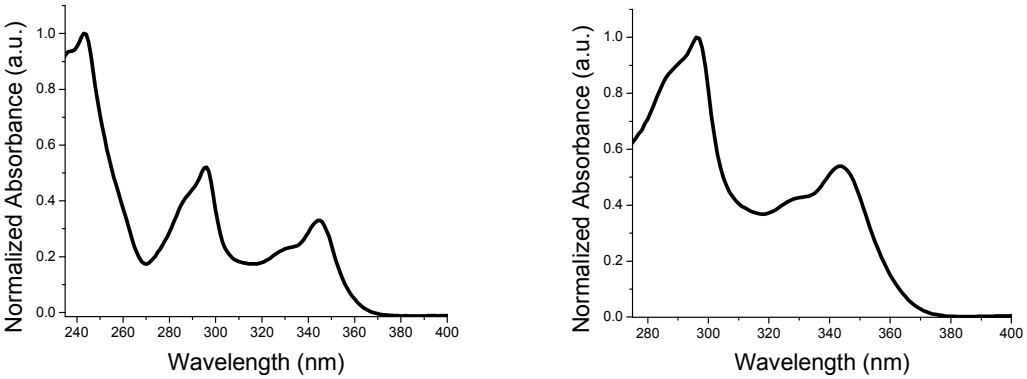

Figure 3.17. Room temperature UV-vis. absorption of **3.32** (in $CHCl_3$) and thin-film on glass of polymer **3.33**.

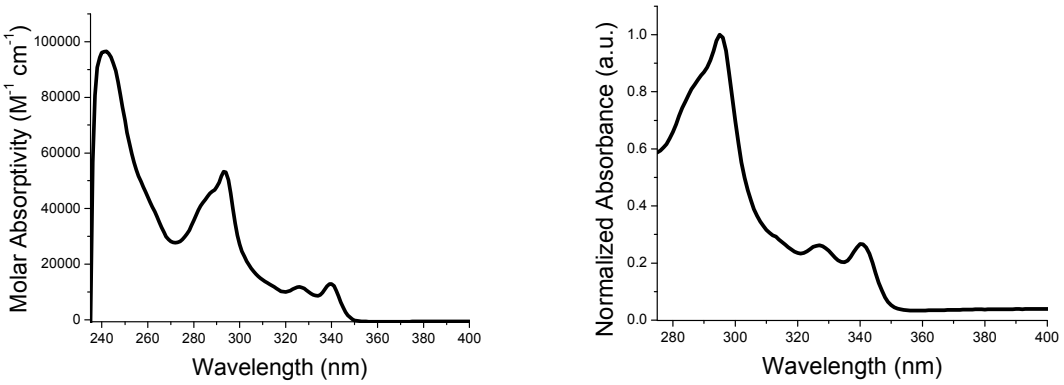

Figure 3.18. Room temperature molar absorptivity (in $CHCl_3$) and thin-film absorption on glass of polymer **3.35**.

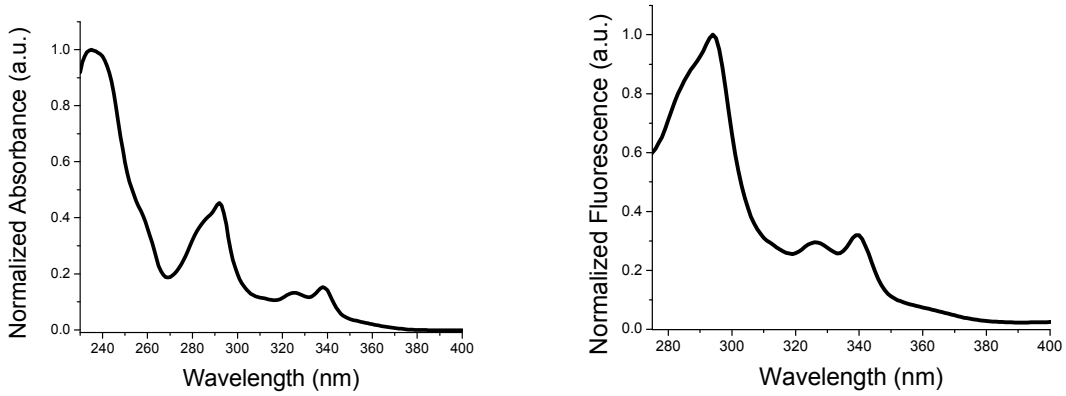

Figure 3.19. Room temperature UV-vis. absorption of **3.37** (in CH_2Cl_2) and thin-film on glass of polymer **3.37**.

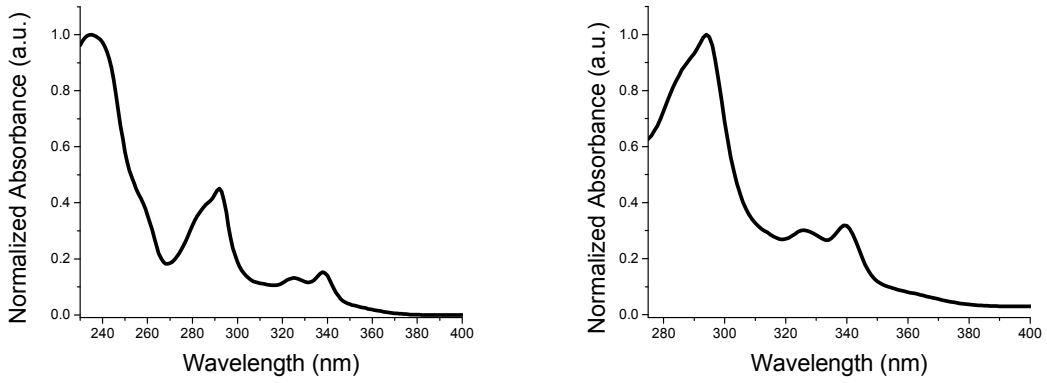

Figure 3.20. Room temperature UV-vis. absorption of **3.39** (CH_2Cl_2) and thin-film on glass of polymer **3.39**.

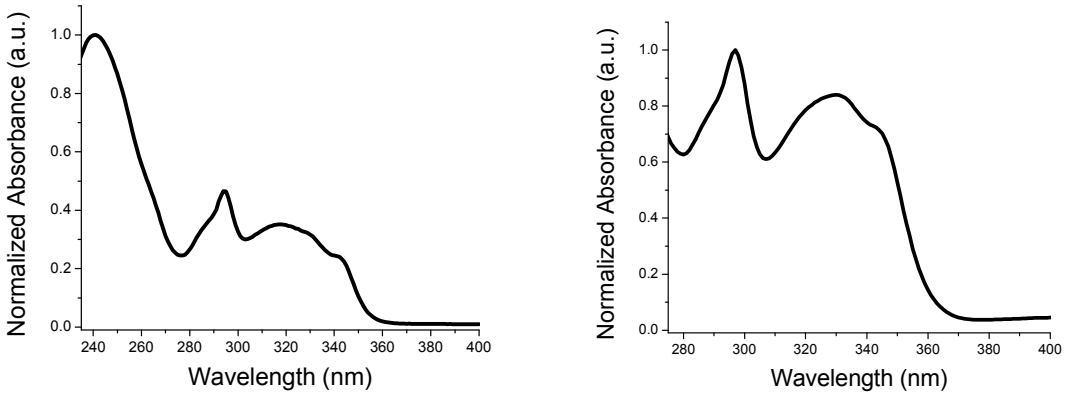

Figure 3.21. Room temperature UV-vis. absorption of **3.40** (in CH_2Cl_2) and thin-film on glass of polymer **3.41**.

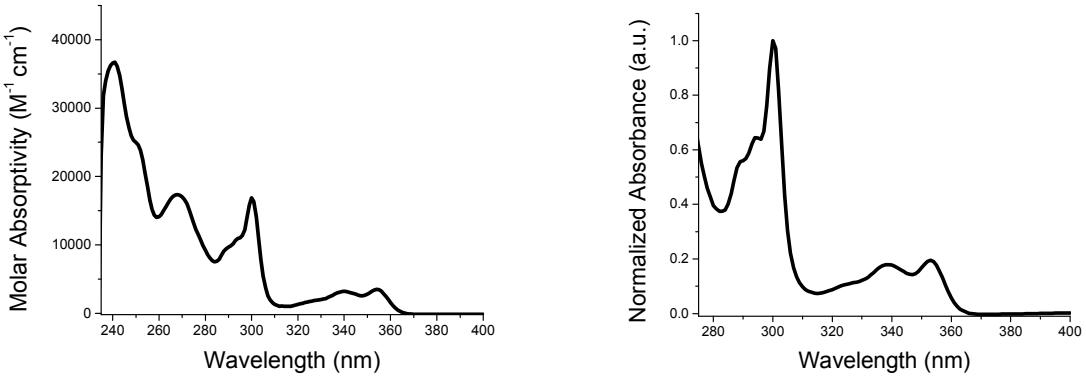

Figure 3.22. Room temperature molar absorptivity (in $CHCl_3$) and thin-film absorption on glass of polymer **3.43**.

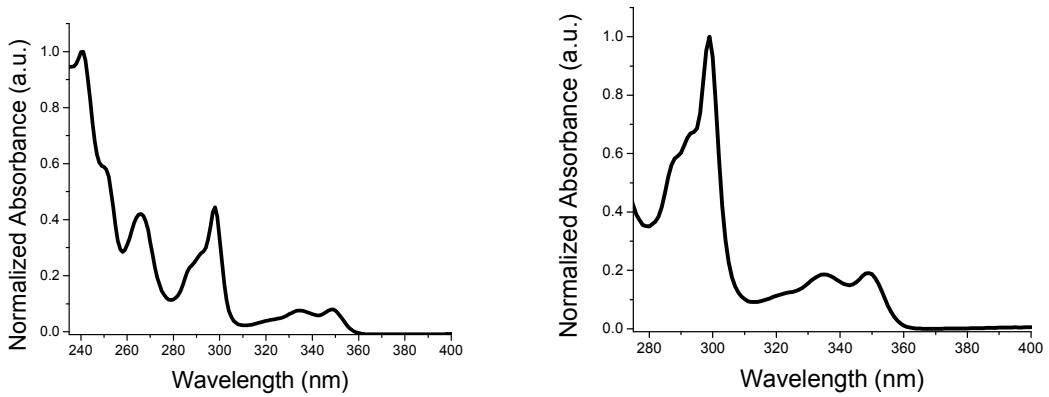

Figure 3.23. Room temperature UV-vis. absorption of **3.44** (in $CHCl_3$) and thin-film on glass of polymer **3.45**.

Table 3.4 UV-Vis Absorption (in solution)

Sample	λ_{max} (nm)[a]	Approx. Abs. Onset (nm)
3.29	239, 263, 294, 342	382
3.30	241,291, 337	366
3.32	243, 296, 345	376
3.35	241, 293, 325, 339	354
3.37§	235, 292, 325, 338	381
3.39§	235, 292, 325, 338	389
3.40§	241, 294*	365
3.43	241, 269, 299, 338, 352	368
3.44	241, 266, 298, 334, 348	360

[a] Measured at room temperature in chloroform or dichloromethane (§)

* A broad absorption peak observed between 300 - 350 nm

For polymer **3.29** (triscarbazole), comparison to the known small-molecule examples (see figure 3.12) showed absorption peaks consistent with the reported values of 239, 294, and 344 nm[45,46] for small-molecule examples. The absorption data for **3.40** (CBP-type) was consistent with the structural shape of the thin-film absorption of **CBP**.[62] Comparison to the solution absorption peaks to those of 3,6-di(*tert*-butyl)carbazole revealed similar absorptions with only minor shifts for monomers **3.43** and **3.44**. It would seem that the for the above materials, at least with respect to the maxima, the incorporation of the transport groups onto polymers does not significantly affect their absorption properties.

For the mCPy-type monomers (**3.30** and **3.32**), absorption cannot be compared to the **mCPy** small-molecule as its absorption was not reported. It was noted that the peak maxima are consistent with other samples evaluated; with peaks at *ca.* 240, 290 and 340 nm. In fact, a study of carbazole and carbazole-derivatives by Bonesi *et al*.[63] demonstrated (in solution and solid-state) absorptions resulting from $\pi \rightarrow \pi^*$ transitions at or very close these particular wavelengths. Therefore, these maxima (for all samples

evaluated) likely originated from the carbazoles. **3.32** was noted to have slightly red-shifted absorption and onset of absorption which may be attributed to the electron-donating effect of the *tert*-butyl substituents.

Comparison of the mCP-type samples (**3.35**, **3.37**, and **3.39**) revealed similar absorption maxima amongst the samples. The maxima were also quite consistent with the absorption spectra (in solution) reported for **mCP**.[64] The most notable difference on comparing these samples were noted in the onset of absorption. It seems that for samples **3.37** and **3.39**, where an ester was attached to the benzene, the onset was red-shifted by approximately 30 nm (a weak absorption event can be observed). This weak event may suggest a charge-transfer event originating from the presence of the ester group and that the LUMO of these samples might be lowered. For **mCP** and **3.35**, the onsets were both around 350 nm.

Thin-film absorption maxima of the polymers (see below) as thin-films on glass demonstrated effectively the same absorption maxima as the dilute solutions of the monomers (in the range above 275 nm).

Table 3.5 UV-Vis Properties of Polymers (thin-films)

Polymer	λ_{max} (nm)[a]
3.29	296, 342
3.33	296, 344
3.35	295, 326, 340
3.37	294, 326, 339
3.39	294, 325, 339
3.41	297*
3.43	267, 300, 338, 352
3.45	265, 299, 335, 348

[a] thin-films on glass

* A broad absorption peak observed between 300 - 350 nm

3.5.2. Thin-film Photoluminescence and Doping Studies

Photoluminescence measurements were taken on thin-films of the polymers on glass substrates. The spectra were as follows:

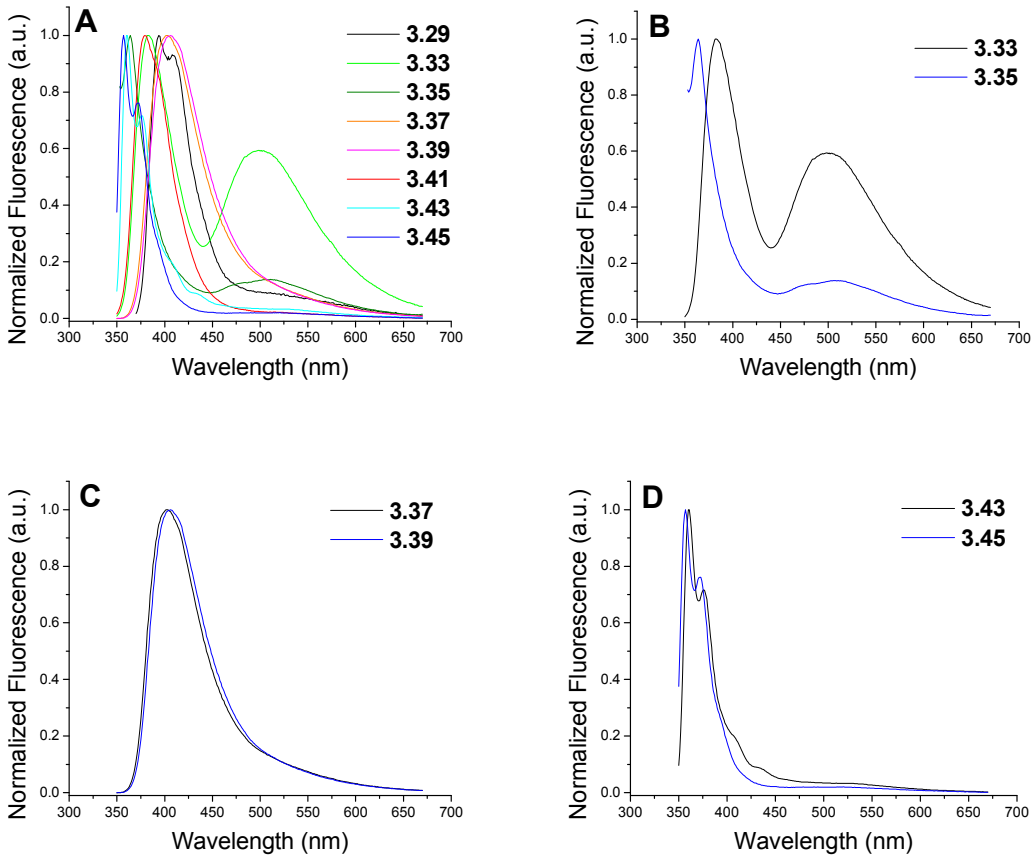

Figure 3.24. Room temperature fluorescence of polymer thin-films on glass (excitation at 340 nm). **A**) All polymers **B**) **3.33** and **3.35** comparison **C**) **3.37** and **3.39** comparison **D**) **3.43**, **3.45**, and **3.29** comparison.

Table 3.6 Fluorescence of Polymers (thin-films)

Polymer	λ_{max}fluo. (nm)[a]
3.29	394, 408
3.33	383, 498*
3.35	366, 511*
3.37	403
3.39	406
3.41	379
3.43	361, 377
3.45	357, 373

[a] thin-films on glass; excitation at 300 nm

* broad emission peak

All polymers demonstrated emission peaks in the blue region of the spectrum, consistent with carbazoles.[63] Polymer **3.29** emitted around 400 nm which is similar to the reported literature examples of triscarbazole. Polymers **3.43** and **3.45** showed deeper blue emission which was consistent with fluorescence observed from small-molecule *9H*-carbazole.[63] The bathochromic shift in going from the PVK-like polymers to triscarbazole can be said to be a product of the extension in conjugation. The same effect can be observed in the CBP-like polymer **3.41** which possessed an emission maximum around 380 nm, which also corresponds well to the small-molecule emission of **CBP**. [65]

The thin-film fluorescence maximum of **mCP** small-molecule has been reported to be around 360 nm.[66] Polymers **3.37** and **3.39** demonstrated a bathochromic shift of approximately 0.4 eV relative to **mCP**. Notably for **3.37** and **3.39** an ester group (with carbonyl attached to the benzene) was used to link the hole-transport moiety to the norbornene. Although an inductive effect from the ester might affect the LUMO level and reduce the optical gap, such an effect would unlikely account for a 0.4 eV shift. A more reasonable explanation could be that **3.37** and **3.39** possess LUMOs that are possibly

located closer to the ester substituted benzene core (but no theoretical calculations have been performed to support this). Polymer **3.35** (which possessed the same **mCP** group) did not have such an electron withdrawing group attached to the central phenyl and had an emission maximum of 366 nm (much closer to small-molecule emission). A shallow and broad emission peak around 500 nm was observed for **3.35** and presumed to be due to aggregation effects. To confirm this, fluorescence of the polymer in dilute solution (dichloromethane) was obtained that showed no lower energy emission.

The thin-film of polymer **3.33** displayed a blue emission peak *ca*. 380 nm but also showed a significant and broad emission peak around 500 nm. In order to determine if the lower energy emission was from aggregation, solution emission was taken of the polymer (in dichloromethane) and the low energy emission was not observed. Unfortunately, the emission spectrum of polymer **3.31** was unavailable (due to sample loss), so comparison to another mCPy-type polymer was not possible.

Studies were carried out using the blue phosphor FPt (known to emit white light due to excimer emission at certain doping concentrations) doped in polymers **3.29** or **3.35**. Photoluminescence of doped systems can be used to qualitatively screen organic materials for hosting ability (for a given guest emitter) despite the fact that electroluminescence can originate by different pathways than those leading to photoluminescence. The following figure shows the emission spectra for FPt doped polymer **3.29**.

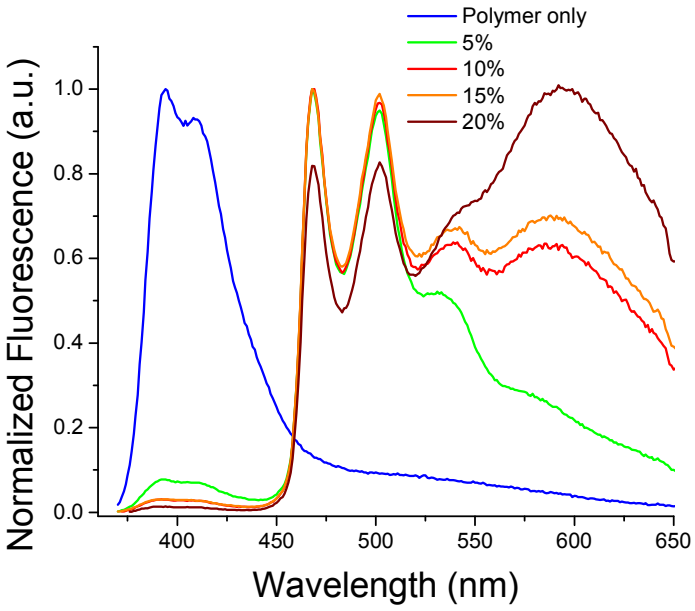

Polymer only (blue), 5 wt% (green), 10 wt% (red), 15 wt% (orange), 20 wt% (wine)

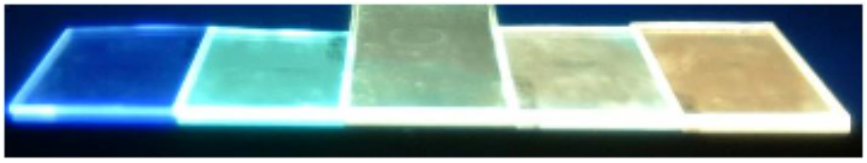

Polymer 5% 10% 15% 20%

Figure 3.25. Fluorescence spectra and images of doped polymer (**3.29**) thin-film slides (under UV lamp excitation) doped with FPt emitter.

The spectra and thin-film slides show effective suppression of the host polymer emission peak. At 5 wt% doping, some host emission can be observed and the FPt emission was mostly strongly from its monomeric blue emission peaks. This concentration was found to be too low and prevented the formation of excimers leading to give more balanced emission for white light. At 10 wt%, the host emission was further suppressed and the excimer emission peak increased, but emission was still mostly from the monomeric form of FPt. 15 wt% demonstrated the most balanced emission while 20

wt% exhibited too strong emission from the excimer and took on a orange-red color. Some very minor amount of polymer emission was noted for all the samples and only at 20 wt% did essentially all the emission disappear.

Polymer **3.35** was evaluated in a similar manner and exhibited a deeper blue emission peak than that of the triscarbazole polymer. At 15, 18, and 20 wt%, no emission from the host was observed, which suggested more efficient singlet energy transfer to the guest emitter (due to better overlap of the absorption of FPt and the emission of the host). Near-white emission was obtained for the 18 and 20 wt% samples.

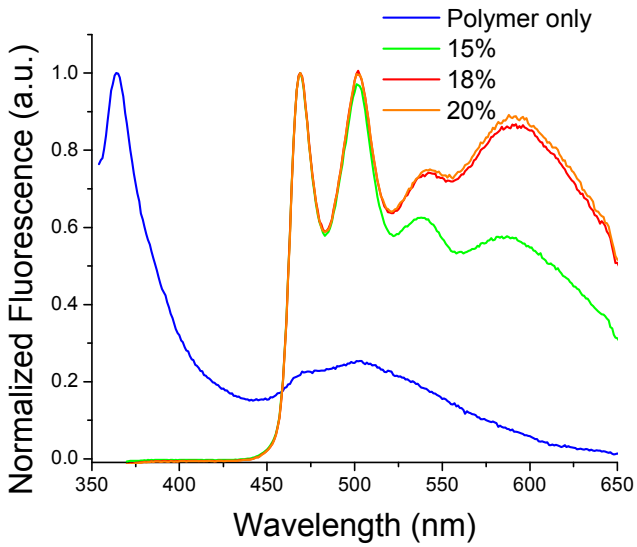

Polymer only (blue), 15 wt% (green), 18 wt% (red), 20 wt% (orange)

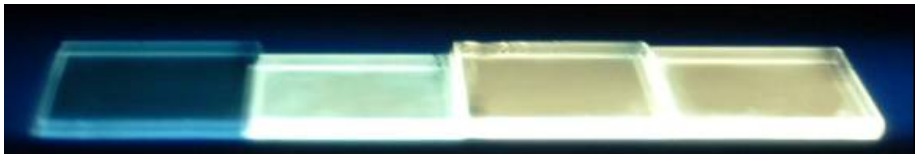

Polymer 15% 18% 20%

Figure 3.26. Fluorescence spectra and images of doped polymer (**3.35**) thin-film slides (under UV lamp excitation) doped with FPt emitter.

3.6. Electrochemical Studies and Energy Level Estimations

Cyclic voltammetry was performed in methylene chloride (0.1 M nBu$_4$NPF$_6$) and referenced to the ferrocene/ferrocenium redox couple as an internal standard for monomers (except where noted otherwise).

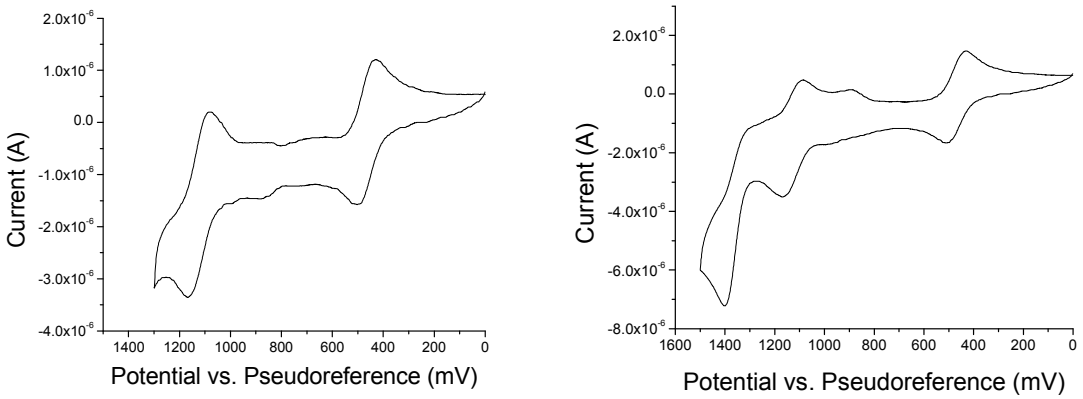

Figure 3.27. Cyclic voltammograms of **3.28** in CH_2Cl_2 (vs. $FeCp_2^+$/ $FeCp_2$). Left: Up to 1300 mV ; Right: Up to 1500 mV.

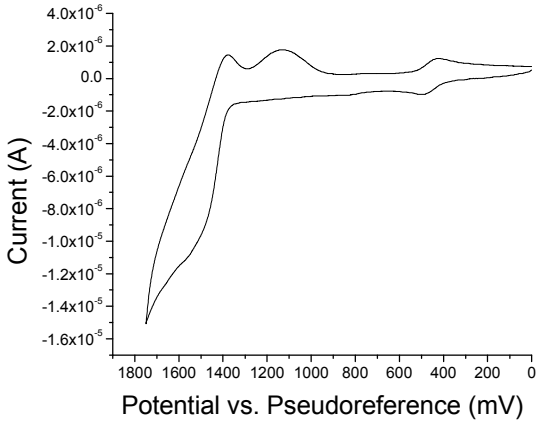

Figure 3.28. Cyclic voltammogram of **3.30** in CH_2Cl_2 (vs. $FeCp_2^+$/ $FeCp_2$).

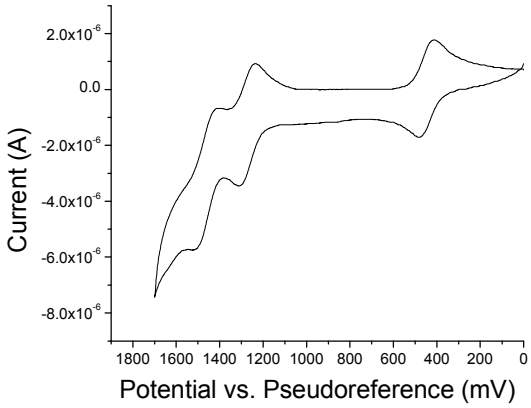

Figure 3.29. Cyclic voltammogram of **3.32** in CH_2Cl_2 (vs. $FeCp_2^+$/ $FeCp_2$).

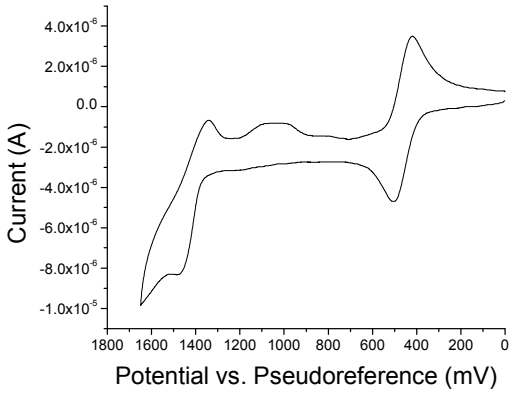

Figure 3.30. Cyclic voltammogram of **3.34** in CH_2Cl_2 (vs. $FeCp_2^+$/ $FeCp_2$).

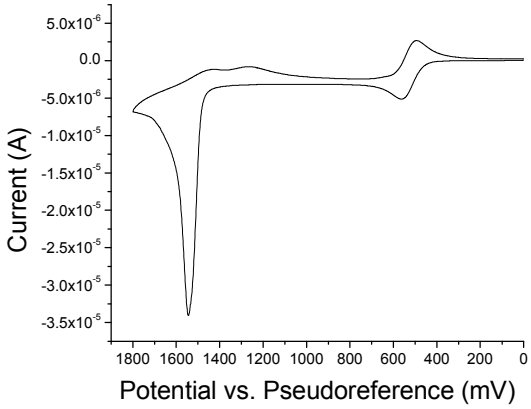

Figure 3.31. Cyclic voltammogram of polymer thin-film of **3.37** in DMF (vs. $FeCp_2^+$/ $FeCp_2$).

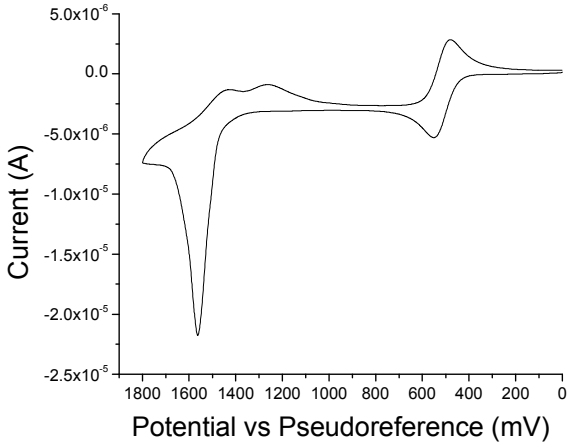

Figure 3.32. Cyclic voltammogram of polymer thin-film of **3.39** in DMF (vs. $FeCp_2^+$/ $FeCp_2$).

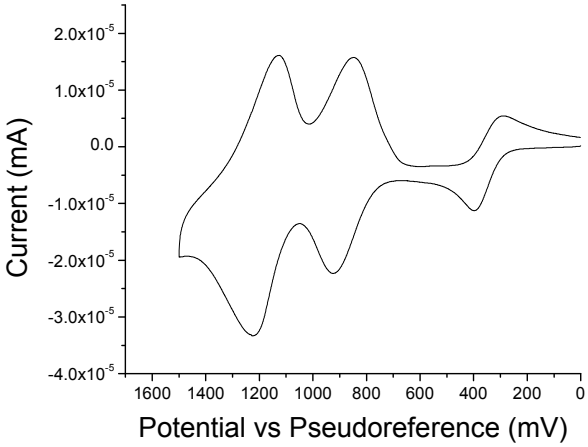

Figure 3.33. Cyclic voltammogram of **3.40** in CH_2Cl_2 (vs. $FeCp_2^+$/ $FeCp_2$).

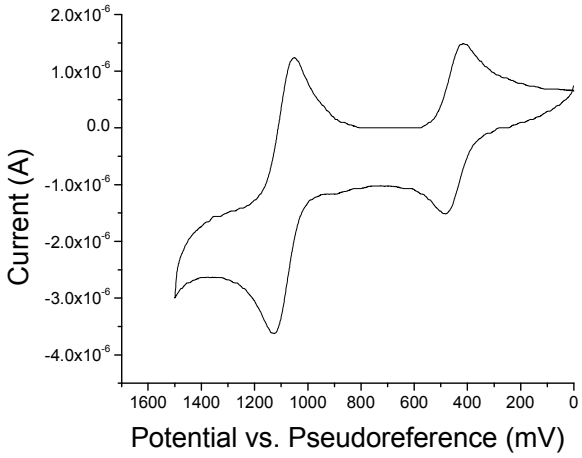

Figure 3.34. Cyclic voltammogram of **3.42** in CH_2Cl_2 (vs. $FeCp_2^+$/ $FeCp_2$).

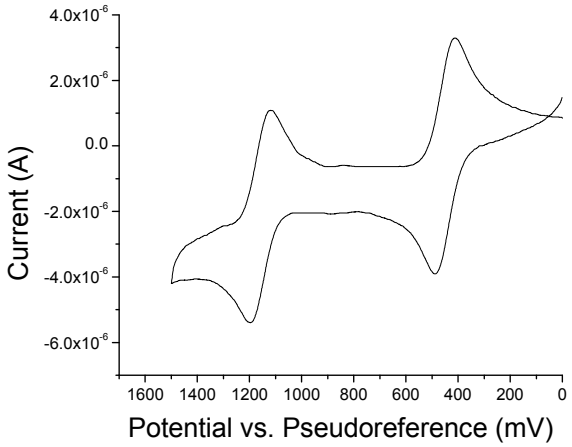

Figure 3.35. Cyclic voltammogram of **3.44** in CH_2Cl_2 (vs. $FeCp_2^+$/ $FeCp_2$).

For all samples, $E_{1/2}^{+/0}$ (vs. ferrocenium/ferrocene) was calculated from E_{ox} and $E_{red,}$ as determined from the maxima or minima for the monomer (or polymer) oxidation-reduction potential wave (in mV) scanned at 50 mV/s. For some compounds oxidation was found to be irreversible and E_{ox} was assumed to be approximately equal to $E_{1/2}^{+/0}$.

Measurements on monomer **3.28** showed that the first oxidation was reversible. We suspect that the oxidation occurred on the central carbazole which has carbazole

blocked 3 and 6 positions. We expected that further oxidation would be irreversible as it would occur at one the peripheral carbazoles. Indeed, in a sweep to higher potential, a second irreversible oxidation was observed. Anderson *et al*.[67] reported the first oxidation of **PVK** oligomers at 0.56 V and found the process to be irreversible. For **3.28**, $E_{1/2}^{+/0}$ was calculated to be 0.66 V, so one might conjecture that the triscarbazole polymer, at least from a redox perspective, might act similarly to **PVK** only with better electrochemical stability for its first oxidation. Similarly, monomers **3.42** and **3.44** with *tert*-butyl substituents at the 3 and 6 positions also demonstrated reversible first oxidation potentials with $E_{1/2}^{+/0}$ values of 0.64 V and 0.71 V respectively.

Comparison of the voltammograms mCPy-type monomers **3.30** and **3.32** showed that for the former the oxidation event was irreversible. The voltammogram of the latter showed two oxidation events, the first of which looked reversible and a second close oxidation which seemed, if not reversible at least quasireversible. The *tert*-butyl groups on **3.32** that block the 3,6 positions on carbazole account for the observed reversibility. Interestingly, $E_{1/2}^{+/0}$ for **3.32** was found to be approximately 0.23 V lower than that of **3.30**, which suggested an electron donation effect from the *tert*-butyl groups decreased the IP of the moiety.

For the mCP-type materials (**3.34**, **3.37**, and **3.39**), the first oxidations were all found to be irreversible; similar to **mCP** where the first oxidation has been observed to be irreversible.[68] In addition, all materials demonstrated an $E_{1/2}^{+/0}$ of *ca*. 1.0 V. It was evident that the linker type used to attach the norbornene to the mCP moiety did not modify the oxidation potential to any appreciable extent. For **3.37** and **3.39**, the electrochemical data

was obtained for thin-films of the polymer due to the lack of availability of the monomers of these compounds.

Monomer **3.40**, based on the **CBP** molecule, had a calculated $E_{1/2}^{+/0}$ of ~ 0.5 V under the assumption that the process was reversible/quasireversible. Issues with the measurement of the oxidation potential(s) of **CBP** have been reported. Low *et al*.[35] observed two irreversible oxidation events (vs. $FeCp_2^+$/ $FeCp_2$ in THF (0.1M nBu_4PF_4) at 1.03 and 1.50 V. Thompson and co-workers[69] reported broad oxidation peaks for **CBP**, that were assumed to be irreversible. The reversibility of the redox processes observed for the CBP monomer (**3.40**) are in contrast to prior reports to the electrochemistry of the CBP small-molecule. It is possible that the formation of the radical cation occurs on the norbornene-subsituted carbazole and that electron-donating effects from the substituent might might explain an increase in the stability of this species against dimerization. Further studies would be needed to confirm this possibility.

Table 3.7. Redox Data and Energy Level Estimates

Sample	$^1E_{1/2}$ (V)[a]	~ IP (eV)[c]	E_{op} (eV)[d]	~ EA (eV)[e]
3.28	0.66	5.5	3.2	-2.3
3.30	1.05[b]	5.9	3.5	-2.4
3.32	0.82	5.6	3.4	-2.2
3.34	1.02[b]	5.8	3.6	-2.2
3.40	0.54	5.3	3.4	-1.9
3.42	0.64	5.4	3.4	-2.0
3.44	0.71	5.5	3.5	-2.0
3.37*	1.05[b]	5.9	3.2	-2.7
3.39*	1.02[b]	5.8	3.2	-2.6

[a] determined by cyclic voltammetry (versus ferrocenium/ferrocene) in CH_2Cl_2;
[b] Irreversible redox (assumed $E_{ox} \approx E_{1/2}^{+/0}$)
[c] calculated from IP = $E_{1/2}^{+/0}$ + 4.8 eV
[d] calculated from onset of absorption
[e] calculated from EA = E_{op} (sample) - IP
* taken from polymer thin-film

The redox data was used to estimate the ionization potential (IP) using the approximation that the solid state ferrocenium/ferrocene couple relative to the vacuum level is 4.8 eV.[70] The electron affinity (EA) was estimated from equation (1),

$$EA = E_{op} - IP(\text{monomer or polymer}) \quad (1)$$

where the optical gap was calculated using the onset of absorption obtained from the absorption data using the relationship E_{op} (eV) = 1240/λ_{onset} (nm). It is noted that the EA values calculated from the optical gap are overestimated by an amount near or equal to the exciton binding energy. The values given offer insight into effects on the energy levels from different modifications of a particular core transport group. For ease of comparison, they are shown relative to each other in the figure below.

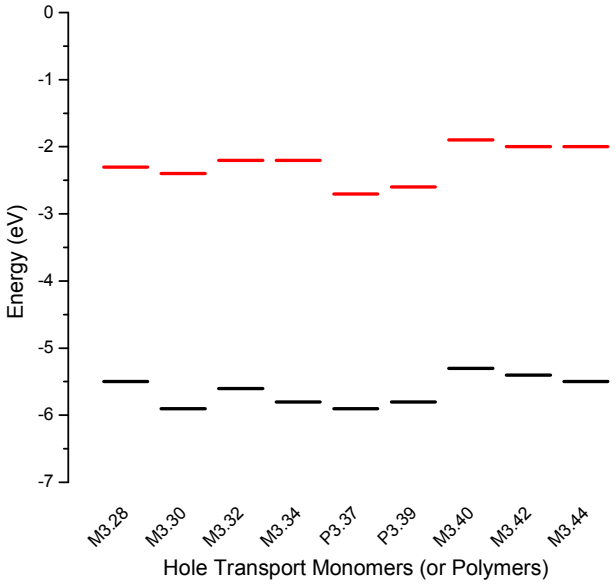

Figure 3.36. Energy diagram showing estimated IP(−) and EA(−) of monomers (denoted M) and polymers (denoted P).

Qualitative comparison of the triscarbazole-based (**3.28**) and carbazole-based (**3.42** and **3.44**) materials revealed they had similar ionization potentials of ~ 5.5 eV. The greater EA of **3.28** may imply an inductive effect from the peripheral carbazoles. The CBP-like monomer, **3.40**, showed IP and EA levels near those of the compounds above. Based on the estimated IPs, these materials

The *tert*-butyl groups on mCPy-like monomer **3.32** decreased the IP and EA, as compared to the unsubstituted mCPy-like analogue **3.30,** presumably due to destabilization of the orbitals from electron donating effects of the substituents. Comparison of **3.30** and **3.34** (**mCPy** vs. **mCP**) revealed minor increases in the IP and EA of **3.30** *vs*. **3.34**, which might be attributed to the electron withdrawing stabilization from the electron deficient pyridine core.

Comparison of the mCP-like targets revealed that the EA level was affected by the nature of the linker. For polymers **3.37** and **3.39**, lower EA levels were observed (*vs*. **3.34)**. This difference could be attributed to the linker attached to the central phenyl group. For **3.37** and **3.39**, an ester group with an electron withdrawing carbonyl group *alpha* to the ring was employed, while the linker on **3.35** had the same linker but with a methylene group *alpha* to the core ring, which should act as a weakly electron donating substituent.

3.7. OLED Devices Incorporating Selected Polymers

Devices reported were fabricated by Dr. Andreas Haldi of the Kippelen group in the School of Electrical and Computer Engineering. The following polymers were evaluated as either hole transport or host materials.

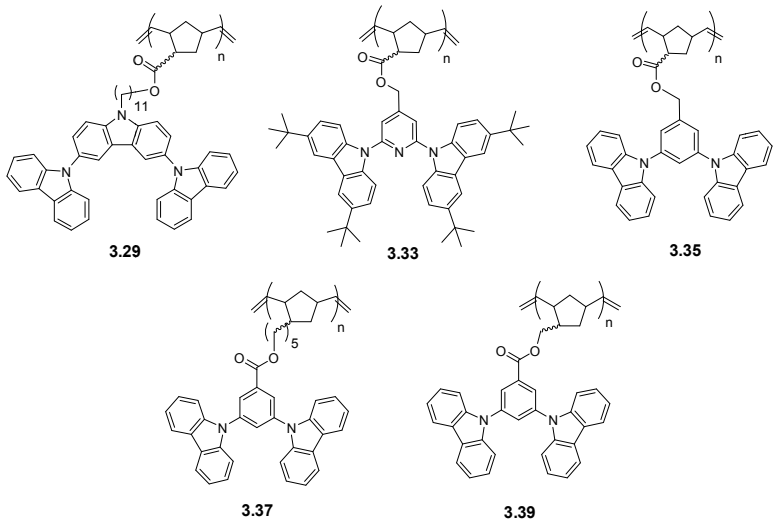

Figure 3.37. Carbazole-based hole-transport polymers examined in OLEDs.

3.7.1 Hole Transport Layers

Three polymers (**3.29**, **3.33**, and **3.39**) were examined in PhOLED devices with the following architecture:

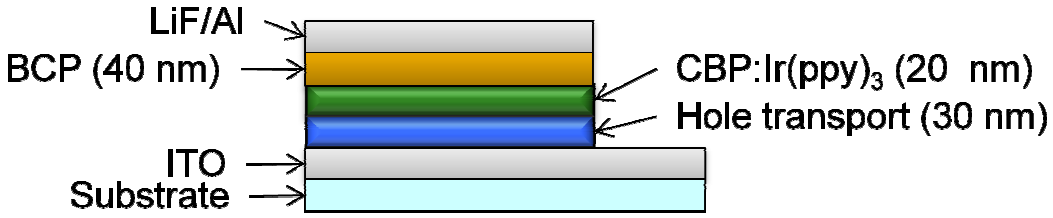

Figure 3.38. OLED device architecture III for study of hole-transport polymers **3.29**, **3.33**, and **3.39**.

For this hybrid architecture, only the hole-transport layer was solution-processed (from chlorobenzene) and the remaining layers were deposited via vacuum sublimation (see Chapter 2 for full processing details).

The well-known homopolymer poly(*N*-vinylcarbazole) (**PVK**) was used for comparison to our carbazole-based homopolymers. The following table summarizes the findings of the Kippelen group.

Table 3.8. Hole Transport Polymer Devices

Device	Polymer	EQE (%)[b]	LE (cd/A)[b]	Turn on (V)[c]
I	**PVK**	12.5 ± 1.1	21 ± 2	~ 4.2
II	**3.29**	13.3 ± 2.0	20 ± 3	~4
III[a]	**3.29**	18.5 ± 0.9	64 ± 3	~4
IV	**3.33**	9.4 ± 0.3	32 ± 3	~7.5
V	**3.39**	10.3 ± 1.1	11 ± 2	~7

[a] optimized device

[b] at luminance of 1,000 cd/m^2

[c] approximate turn on voltages taken from *L*-*V* curves at luminance of 10 cd/m^2

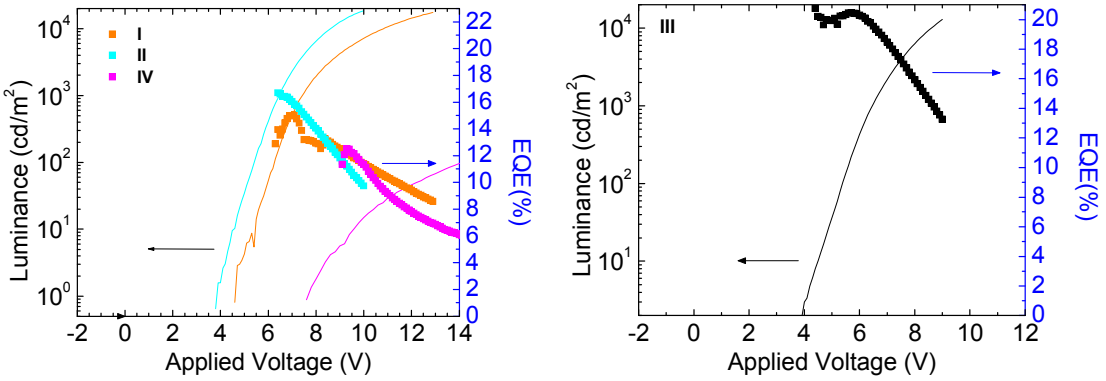

Figure 3.39. Luminance and external quantum efficiency as a function of applied voltage for devices I, II, & IV (left) and optimized device III (right). Data courtesy of Dr. Andreas Haldi (Kippelen group).

The performance of the devices are summarized in Table 3.8 and the luminance and EQE as a function of driving voltage are shown in the figure below. Compared to **PVK** devices, the new polymers demonstrated comparable or even superior device behavior. Devices IV (**3.33**) and V (**3.39**) showed the lowest efficiencies at 9.4% and 10.3%, respectively. They also demonstrated the highest turn-on voltages, which may be a consequence of their higher oxidation potential (as compared to triscarbazole) implying a greater charge injection barrier for holes from the anode. Device II (**3.29**) demonstrated a moderately higher efficiency than the **PVK** device (I) with a slightly lower turn-on voltage. Device III was optimized by variation of the emitter doping level and showed the best efficiency of 18.5%. The oxidation potentials between PVK and polymer **3.29** are relatively similar at 0.56 V for **PVK** (as an oligomer)[67] and 0.66 V for **3.29**. Therefore, the superior performance of polymer **3.29** could be due to a hole-mobility difference. Attempts to compare the hole mobilities of **PVK** and **3.29** were an intended goal of the studies of the polymers, but several attempts to measure hole mobilities have proven unsuccessful. Furthermore, with respect to **PVK**, studies have shown that the radical cation formed on carbazoles have a likelihood of dimerizing (see introduction) and may affect device stability and lifetime. One possible advantage of polymer **3.29** over **PVK** may be a reduction in the probability of dimerization. Indeed, cyclic voltammetry showed that for the triscarbazole monomer (**3.28**), the first oxidation was reversible. Lifetime studies are planned to establish whether polymer **3.29** may provide superior device lifetimes than comparable devices incorporating **PVK**.

3.7.2. Host Polymer Layers

Polymers **3.29**, **3.33**, **3.37** and **3.39** were examined as host layers in PhOLED devices with the following architecture:

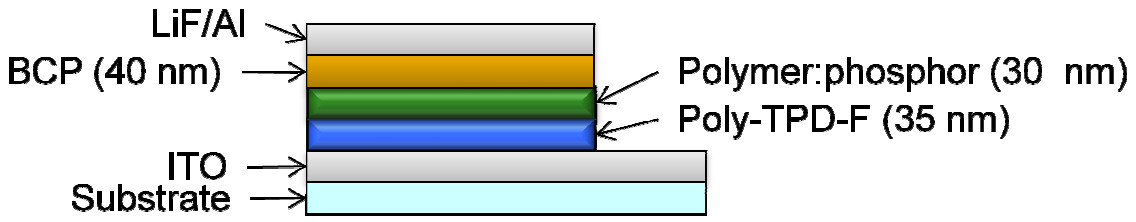

Figure 3.40. OLED device architecture III for study of hole-transporting host polymers **3.29**, **3.33**, **3.37**, and **3.39**.

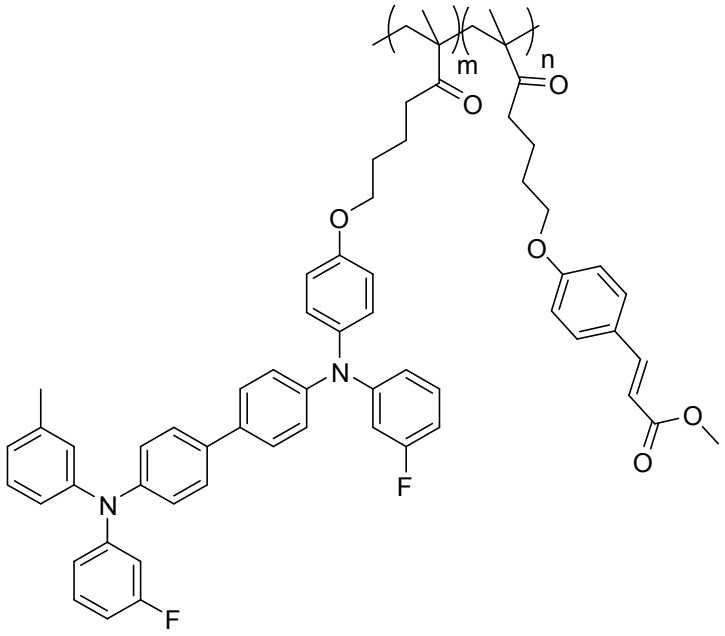

Figure 3.41. Structure of crosslinkable hole transport copolymer poly-TPD-F.

For this hybrid architecture, a hole transport layer containing cinnamate groups (above) was processed from toluene and crosslinked by UV exposure. Subsequently, the host polymer doped with either $Ir(ppy)_3$ (for green devices), $Ir(Fppy)_3$ (for blue devices), or FPt (for white devices) was solution processed from chlorobenzene. The remaining layers were deposited via vacuum deposition.

Table 3.9. Host Polymers for $Ir(ppy)_3$ Green Devices

Device	Polymer	EQE (%)[a]	LE (cd/A)[a]	Turn on (V)[b]
VI	**3.29**	5.2 ± 0.6	18 ± 2	~4
VII	**3.33**	0.3 ± 0.1	1 ± 1	~11
VIII	**3.37**	6.3 ± 0.5	21 ± 2	~5
IX	**3.39**	6.0 ± 0.9	20 ± 3	~5

[a] at luminance of 100 cd/m^2

[b] approximate turn on voltages taken from *L-V* curves at 10 cd/m^2

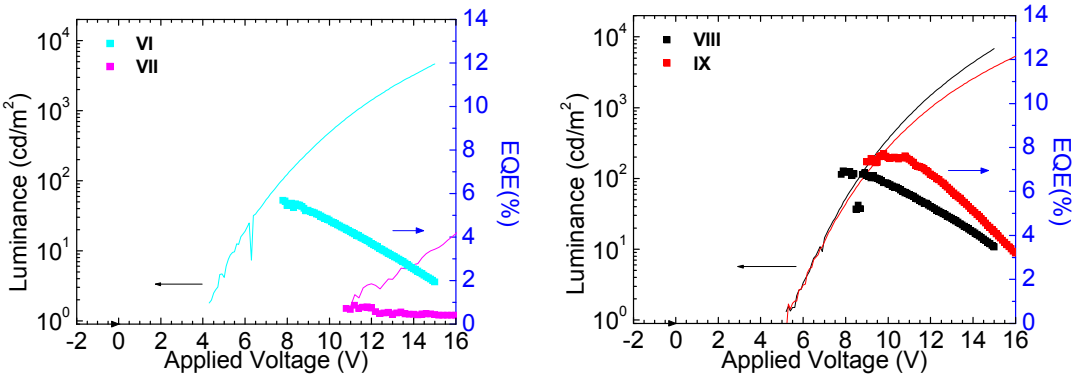

Figure 3.42. Luminance and external quantum efficiency as a function of applied voltage for devices VI and VII (left) and devices VIII and IX (right). Data courtesy of Dr. Andreas Haldi (Kippelen group).

Green devices demonstrated efficiencies (see table and figure directly above) in the range of 5 – 6 % with turn on voltages of ~ 4 or 5 V. A notable exception was device VII, which showed poor performance. A comparison to **PVK** devices reported by Vaeth, *et al.*[53] suggested the importance of ambipolar character in the emissive layer by comparing different devices. In a single layer device composed of PVK and $Ir(ppy)_3$ between the electrodes, the luminance efficiency was relatively low (5 cd/A at 1000 cd/m^2). Devices doped with the electron transport small-molecule PBD (2-(4-biphenylyl)-5-phenyl-1,3,4-oxadiazole) at 10 wt% increased the efficiency to 8.5% (30.1 cd/A at 150 cd/m^2). Although these device efficiencies were not as high, pursuit of better charge

balance might produce further improvements. Ambipolar transport materials are the subject of Chapter 4.

Table 3.10. Host Polymers for $Ir(Fppy)_3$ Blue Devices

Device	Polymer	EQE (%)[a]	Turn on (V)[b]
XI	**PVK**	0.8 ± 0.1	~4
XII	**3.29**	0.7 ± 0.1	~4

[a] at luminance of 100 cd/m^2
[b] approximate turn on voltages taken from *L-V* curves at 10 cd/m^2

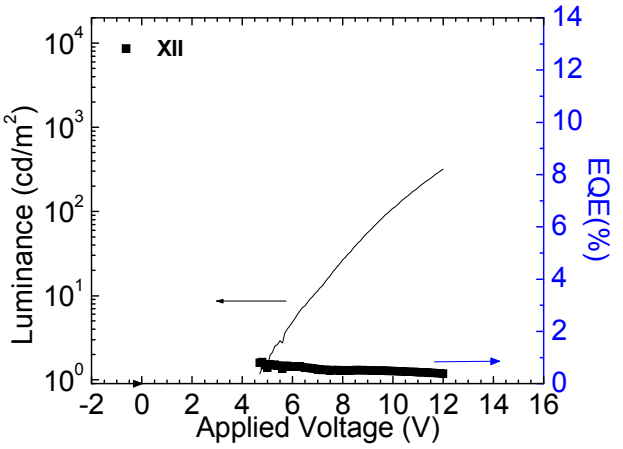

Figure 3.43. Luminance and external quantum efficiency as a function of applied voltage for devices XII. Data courtesy of Dr. Andreas Haldi (Kippelen group).

The PhOLED device data (see table and figure above) showed that for blue devices using the phosphor *fac*-tris[4,6-difluorophenyl]pyridiyl-N,C^2] iridium ($Ir(Fppy)_3$), polymer host **3.29** gave a best efficiency of 0.7%. A comparison device with **PVK** showed a similar external quantum efficiency of 0.8%. For **PVK**, it might be argued that the triplet energy is too low and consequently allows for triplet excitons to leak out of the emissive layer thereby limiting the efficiency. For triscarbazole, on the other hand, based on theoretical calculations and empirical measurement[46] an adequately

high triplet energy to host a blue emitter (at least as a small-molecule) was expected. The low efficiency might therefore result from an imbalance of the charge carriers within the emissive layer. In fact, Tsai *et al*.[46] reported devices containing vacuum-processed small-molecule triscarbazoles that acted as good hosts the blue-green emitter FIrpic (with efficiencies above 10% (at 100 cd/m^2)). Their device architectures employed TAZ (3-(4-biphenyl)-4-phenyl-5-(4-tert-butylphenyl)-1,2,4-triazole) as the electron-transport layer and hole-blocking layer in order to confine the recombination zone.[71,72] Therefore, issues of charge balance and recombination zone confinement within the emissive layer could play a role in the low efficiencies obtained.

White OLEDs (WOLEDs) using the phosphor FPt, which emits blue in dilute solution but shows excimer/aggregate emission in the solid state to afford near white emission were also studied.[39]

Table 3.11. Host Polymers for FPt White Devices

Device	Polymer	FPt (wt %)	EQE (%)[a]	LE (cd/A)[a]	Turn on (V)[b]	CRI
XIII	**3.35**	12-20	Short device lifetime (~2 s)			
XIV	**3.29**	15	1.5 ± 0.2	3 ± 1	~4	22
XV	**3.29**	18	1.5 ± 0.1	3 ± 1	~4.5	78
XVI	**3.37**	15	2.3 ± 0.2	5 ± 1	~5	74

[a] at luminance of 100 cd/m^2

[b] approximate turn on voltages taken from *L*-*V* curves

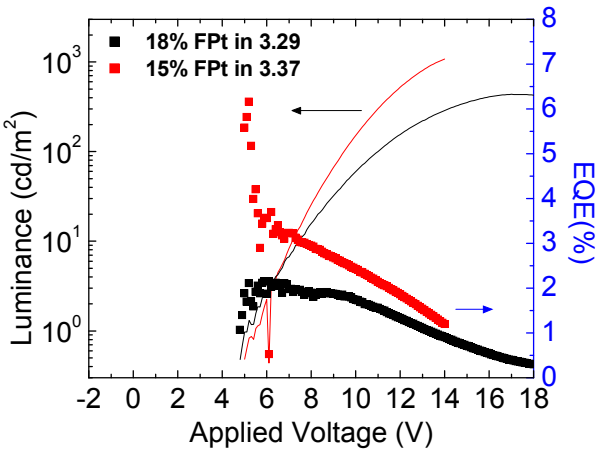

Figure 3.44. Luminance and external quantum efficiency as a function of applied voltage for devices XV (18 wt% FPt in polymer **3.29**) and XVI (15 wt% FPt in polymer **3.37**). Data courtesy of Dr. Andreas Haldi (Kippelen group).

Device XII represents a series made with polymer **3.35** and doped with different weight percentages of FPt. All **3.35** devices operated for only approximately two seconds, which precluded characterization of device parameters, except the electroluminescence spectra (see below).

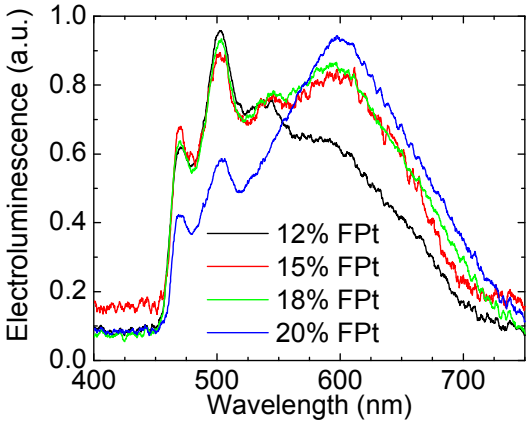

Figure 3.45. Electroluminescence spectra for Device XIII showing FPt doping effects (data courtesy of Dr. Andreas Haldi (Kippelen group)).

It is possible to observe the changes in the electroluminescence spectra for increasing amounts of FPt. In the lowest doping percent (by weight), less excimer/aggregate emission can be observed in the range near 600 nm. As the doping was increased to 20 wt%, the excimer emission increased while the monomeric blue emission peaks (just below 500 nm) started to decrease in intensity. Polymer **3.29** devices (XIV & XV) demonstrated efficiencies of 1.5% with notable effects in the color observed at different doping levels as can be seen from the electroluminescence spectra below.

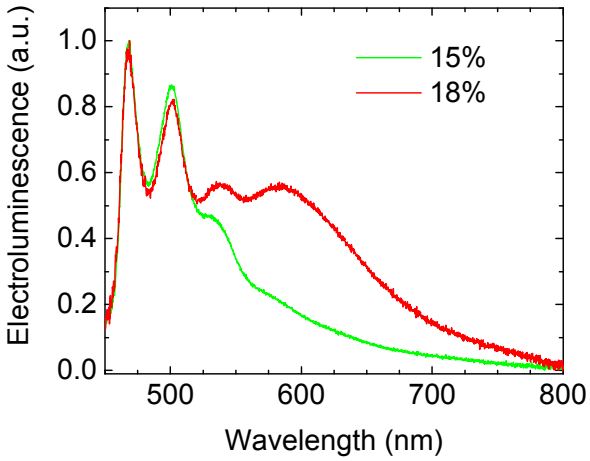

Figure 3.46. Electroluminescence spectra for Device XIV (green) and Device XV (red) showing FPt doping effects (data courtesy of Dr. Andreas Haldi (Kippelen group)).

At 15 wt% insufficient emission in the orange-red resulted in a color rendering index (CRI) of 22, which does not represent white emission. For reference, an incandescent light bulb has a defined CRI of 100.[43] Increasing the doping level to 18% improved the CRI significantly up to 78, which producing near white color. Device XVI, employing host polymer **3.37,** gave the best WOLED performance with an efficiency of 2.3% and a CRI of 74 (at only 15% FPt doping). The lower doping level needed to achieve near white emission may be a solubility effect, where FPt is less soluble in **3.37**

than **3.29** resulting in increased likelihood of excimer formation in device XVI. A single ambipolar side-chain copolymer (triphenylamine and oxadiazole-based) example[73] doped with small-molecule FPt with efficiencies below 1% has been reported. Another side-chain ambipolar terpolymer[74] incorporating an FPt-like side group attached to the polymer produced an EQE of 4.6% (luminance not reported) with a turn on voltage of 7.8 V. Small-molecule **mCP** as host in an FPt-based WOLED was reported by Adamovich *et al.*[38] with a maximum efficiency of 4.3% (11.3 cd/A at 500 cd/m^2) and 6.4% (17.0 cd/A at 1 cd/m^2) with the same CRI of 67 at both luminances. The efficiency of device XVI may therefore be considered promising for a device with polymer-based host, as compared with the fully sublimed literature example of **mCP**. The ambipolar literature example which produced an efficiency of 4.6% would suggest that better balance of charges may further improve results.

3.8. Conclusions

The goal of this chapter was to explore carbazole-based hole-transport materials attached as side-groups onto a polymer backbone. We have shown that several polymers incorporating different types of carbazole groups can be successfully synthesized. The syntheses were shown to be relatively simple and characterization of all precursors (where appropriate) was performed. For all polymers, glass transition temperatures above 100 °C were observed, which can impart a higher degree of layer stability to changes in OLEDs. In addition, decomposition temperatures were also found to be above 350 °C (for those polymers evaluated).

Measurements of the photophysical properties of the polymers were performed in order to establish their potential as host materials for PhOLEDs. The absorption of the materials was generally consistent with the reported absorption data of analogous small molecules. Essentially no shifts (< 2 nm) in the maxima were observed on going from solution spectra of the monomers or polymers to solid-state thin-films of the polymers. Fluorescence data showed that all polymers emitted in the blue or into the UV region of the spectrum. By comparison of the emission maxima, it was possible to observe bathochromic shifts of up to 40 nm relative to *9H*-carbazole fluorescence (reported around 350 nm). For some materials this was attributed to increased conjugation of the carbazole-based moiety (i.e. triscarbazole and CBP-type polymers) and was consistent with observed data reported in the literature for small-molecule analogues. In other materials, such as the mCP-type polymers (**3.38**, and **3.40**), the nature of the linker was found to affect the location of the peak significantly. Therefore, the type of linker group and its precise attachment were shown to modify the energy levels of the transport moiety and should be considered closely when designing side-chain transport polymers. Doping studies with the emitter FPt of polymers **3.30** and **3.36** demonstrated they could function as effective hosts with very high or essentially complete energy transfer when appropriately doped. This suggested these materials might act as good hosts for FPt under electroluminescent conditions.

Cyclic voltammetry measurements revealed that substitution of the carbazoles at the 3 and 6 positions afforded reversible redox properties for the first oxidation. Cyclic voltammetry and optical gap data were used to estimate the IP and EA of the monomers. Trends from comparisons across similar groups revealed that the substituents and the

nature of linker used to attach the transport moiety to the backbone can affect the levels. These findings suggest the IP and EA can be manipulated (if necessary) based on the appropriate choice of linker and/or substituents on the transport moiety.

A series of OLED devices fabricated in collaboration with the Kippelen group showed that particular polymers (**3.29**, **3.33**, **3.39**) could function as hole-transport materials. Polymer **3.29** in particular was found to work well and showed superior efficiency as compared to PVK. Measurement of the hole mobility of **3.29** is being pursued. Polymers **3.29**, **3.33**, **3.37**, and **3.39** were evaluated as host materials for the green emitter $Ir(ppy)_3$ and efficiencies up to 6% were achieved. For polymer-based hosts these efficiencies were deemed promising. Efficiencies may have been limited by poor charge balance within the emissive layer. A blue device (with emitter $Ir(Fppy)_3$ using polymer **3.29** gave a low efficiency (< 1%), which may have resulted from poor balance and/or confinement within the emissive layer. White OLEDs were also fabricated using the phosphor FPt. Polymers **3.29** and **3.37** were evaluated and the former gave an efficiency of 1.5%, while the latter gave a higher efficiency of 2.3%. These efficiencies are difficult to put into context due to lack of other work using side-chain polymers as hosts for FPt. As compared to **mCP** as a host for FPt, **3.37** gave approximately half the efficiency found for that device.

Overall, side-chain polymers were shown to be viable alternatives to small molecules for hole transport and hosting functions. For the most part, functionalization onto a polymer backbone, if done appropriately, can avoid significant modification of the transport group (as compared to the small-molecule analogue). The resulting polymers were all solution-processable materials and may well be used for simplified device

fabrication (with concurrent cost reduction). Future work for these materials should focus on the study of the several parameters. Measurement of hole mobilities would help to explain differences observed in certain hole transport devices. Phosphorescence spectra (in order to measure their respective triplet energies) would help to further elucidate the potential polymers as hosts for different emitters and/or as triplet exciton blockers (when used for hole transport layers). Finally, device lifetime studies would help to demonstrate effects from residual impurities expected to be present in polymers as compared to vacuum-processed layers.

3.9. References

(1) Seo, E. T.; Nelson, R. F.; Fritsch, J. M.; Marcoux, L. S.; Leedy, D. W.; Adams, R. N. *J. Am. Chem. Soc.* **1966**, *88*, 3498-3503.

(2) Adachi, C.; Tsutsui, T.; Saito, S. *Appl. Phys. Lett.* **1989**, *55*, 1489-1491.

(3) Adachi, C.; Tsutsui, T.; Saito, S. *Appl. Phys. Lett.* **1990**, *56*, 799-801.

(4) Adachi, C.; Tsutsui, T.; Saito, S. *Appl. Phys. Lett.* **1990**, *57*, 531-533.

(5) Adachi, C.; Tsutsui, T.; Saito, S. *Optoelectron. Devices Technol.* **1991**, *6*, 25-36.

(6) Tsutsui, T.; Adachi, C.; Saito, S. *Synth. Met.* **1991**, *41-43*, 1193-1196.

(7) O'Brien, D. F.; Burrows, P. E.; Forrest, S. R.; Koene, B. E.; Loy, D. E.; Thompson, M. E. *Adv. Mater.* **1998**, *10*, 1108-1112.

(8) Adachi, C.; Nagai, K.; Tamoto, N. *Appl. Phys. Lett.* **1995**, *66*, 2679-2681.

(9) Abkowitz, M.; Pai, M. *Philos. Mag. B* **1986**, *53*, 193-216.

(10) *Organic Light Emitting Devices. Synthesis, Properties and Applications*; Müllen, K.; Scherf, U., Eds.; Wiley-VCH Verlag GmbH & Co.: Weinheim, 2006.

(11) Han, E.; Do, L.; Niidome, Y.; Fujihira, M. *Chem. Lett.* **1994**, *23*, 969-972.

(12) Sheats, J. R.; Antoniadis, H.; Hueschen, M.; Leonard, W.; Miller, J.; Moon, R.; Roitman, D.; Stocking, A. *Science* **1996**, *273*, 884-888.

(13) Tokito, S.; Tanaka, H.; Noda, K.; Okada, A.; Taga, Y. *Appl. Phys. Lett.* **1997**, *70*, 1929-1931.

(14) Fenter, P.; Schreiber, F.; Bulovic, V.; Forrest, S. R. *Chem. Phys. Lett.* **1997**, *277*, 521-526.

(15) Shirota, Y. *J. Mater. Chem.* **2000**, *10*, 1-25.

(16) Van Slyke, S. A.; Chen, C. H.; Tang, C. W. *Appl. Phys. Lett.* **1996**, *69*, 2160-2162.

(17) Low, P. J.; Paterson, M. A. J.; Puschmann, H.; Goeta, A. E.; Howard, A. K.; Lamber, C.; Cherryman, J. C.; Tackley, D. R.; Leeming, S.; Brown, B. *Chem. Eur. J.* **2004**, *10*, 83-91.

(18) Kolb, E. S.; Gaudiana, R. A.; Mehta, P. G. *Macromolecules* **1996**, *29*, 2359-2364.

(19) Bellmann, E.; Shaheen, S. E.; Grubbs, R. H.; Marder, S. R.; Kippelen, B.; Peyghambarian, N. *Chem. Mater.* **1999**, *11*, 399-407.

(20) Shaheen, S. E.; Jabbour, G. E.; Kippelen, B.; Peyghambarian, N.; Anderson, J. D.; Marder, S. R.; Armstrong, N. R.; Bellmann, E.; Grubbs, R. H. *Appl. Phys. Lett.* **1999**, *74*, 3212-3214.

(21) Feast, W. J.; Peace, R. J.; Sage, I. C.; Wood, E. L. *Polym. Bull.* **1999**, *42*, 167-174.

(22) Tamada, M.; Koshikawa, H.; Yoshioka, T.; Usui, H.; Sato, H. *Polymer* **2000**, *41*, 5661-5667.

(23) Kido, J.; Hayase, H.; Hongawa, K.; Nagai, K.; Okuyama, K. *Appl. Phys. Lett.* **1994**, *65*.

(24) Baldo, M. A.; O'Brien, D. F.; You, Y.; Shoustikov, A.; Silbey, S.; Thompson, M. E.; Forrest, S. R. *Nature* **1998**, *395*, 151-154.

(25) O'Brien, D. F.; Baldo, M. A.; Thompson, M. E.; Forrest, S. R. *Appl. Phys. Lett.* **1999**, *74*, 442-444.

(26) Kozlov, V. G.; Parthasarathy, G.; Burrows, P. E.; Forrest, S. R.; You, Y.; Thompson, M. E. *Appl. Phys. Lett.* **1997**, *72*, 144-146.
(27) Baldo, M. A.; Lamansky, S.; Burrows, P. E.; Thompson, M. E.; Forrest, S. R. *Appl. Phys. Lett.* **1999**, *75*, 4-6.
(28) Adachi, C.; Kwong, R.; Forrest, S. R. *Org. Elect.* **2001**, *2*, 37-43.
(29) Watanabe, S.; Ide, N.; Kido, J. *Jap. J. Appl. Phys.* **2007**, *46*, 1186-1188.
(30) Ambrose, J. F.; Carpenter, L. L.; Nelson, R. F. *J. Electrochem. Soc.* **1975**, *122*, 876-894.
(31) Ambrose, J. F.; Nelson, R. F. *J. Electrochem. Soc.* **1968**, *115*, 1159-1164.
(32) He, J.; Liu, H.; Dai, Y.; Ou, X.; Wang, J.; Tao, S.; Zhang, X.; Wang, P.; Ma, D. *J. Phys. Chem. C* **2009**, *113*, 6761-6767.
(33) Takasu, I.; Mitzuno, Y.; Uchikoga, S.; Enomoto, S.; Sawabe, T.; Amano, A.; Wada, A.; Yoshida, J.; Ono, T. *Proc. of SPIE* **2009**, *7415*, 74150B-74151.
(34) Adachi, C.; Kwong, R. C.; Djurovich, P. I.; Adamovich, V.; Baldo, M. A.; Thompson, M. E.; Forrest, S. R. *Appl. Phys. Lett.* **2001**, *79*, 2082-2084.
(35) Low, P. J.; Paterson, M. A. J.; Yufit, D. S.; Howard, A. K.; Cherryman, J. C.; Tackley, D. R.; Brook, R.; Brown, B. *J. Mater. Chem.* **2005**, *15*, 2304-2315.
(36) Lei, G. T.; Wang, L. D.; Duan, L.; Wang, J. H.; Qui, Y. *Synth. Met.* **2004**, *144*, 249-252.
(37) Baldo, M. A.; Forrest, S. R. *Phys. Rev. B* **2000**, *62*, 10958-10966.
(38) Adamovich, V.; Brooks, J.; Tamayo, A.; Alexander, A. M.; Djurovich, P. I.; D'Andrade, B. W.; Adachi, C.; Forrest, S. R.; Thompson, M. E. *New J. Chem.* **2002**, *26*, 1171-1178.
(39) D'Andrade, B. W.; Brooks, J.; Adamovich, V.; Thompson, M. E.; Forrest, S. R. *Adv. Mater.* **2002**, *14*, 1032-1036.
(40) Ma, B.; Djurovich, P. I.; Thompson, M. E. *Coord. Chem. Rev.* **2005**, *249*, 1501-1510.
(41) Holmes, R. J.; Forrest, S. R.; Tung, Y.-J.; Kwong, R. C.; Brown, J. J.; Garon, S.; Thompson, M. E. *Appl. Phys. Lett.* **2003**, *82*, 2422-2424.
(42) Lee, J.; Lee, J.-I.; Song, K.-I.; Lee, S. J.; Chu, H. Y. *Appl. Phys. Lett.* **2008**, *92*, 133304.
(43) Williams, E. L.; Haavisto, K.; Li, J.; Jabbour, G. E. *Adv. Mater.* **2007**, *19*, 197-202.
(44) Su, S.-J.; Sasabe, H.; Takeda, T.; Kido, J. *Chem. Mater.* **2008**, *20*, 1691-1693.
(45) Zhang, Q.; Fu, Y. F.; Cheng, Y. X.; Su, G. P.; Ma, D. G.; Wang, L. X.; Jing, X. B.; Wang, F. S. *Synth. Met.* **2003**, *137*, 1111-1112.
(46) Tsai, M.-H.; Hong, Y.-H.; Chang, C.-H.; Su, H.-C.; Wu, C.-C.; Matoliukstyte, A.; Simokaitiene, J.; Grigalevicius, S.; Grazulevicius, J. V.; Hsu, C.-P. *Adv. Mater.* **2007**, *19*, 862-866.
(47) Kondakov, D. Y.; Pawlik, T. D.; Nichols, W. F.; Lenhart, W. C. *J. SID* **2008**, *16*, 37-46.
(48) Kondakov, D. Y.; Lenhart, W. C.; Nichols, W. F. *J. Appl. Phys.* **2007**, *101*, 024512.
(49) Partridge, R. H. *Polymer* **1983**, *24*, 748-754.

(50) Kido, J.; Hongawa, K.; Okuyama, K.; Nagai, K. *Appl. Phys. Lett.* **1993**, *63*, 2627-2629.
(51) Yang, M.-J.; Tsutsui, T. *Jpn. J. Appl. Phys.* **2000**, *39*, L828-L829.
(52) Kawamura, Y.; Yanagida, S.; Forrest, S. R. *J. Appl. Phys.* **2002**, *92*, 87-93.
(53) Vaeth, K. M.; Tang, C. W. *J. Appl. Phys.* **2002**, *92*, 3447-3453.
(54) Khalifa, M. B.; Vaufrey, D.; Bouazizi, A.; Tardy, J.; Maaref, H. *Mat. Sci. Eng. C* **2002**, *21*, 277-282.
(55) Jiang, X.; Liu, Y.; Song, X.; Zhu, D. *Synth. Met.* **1997**, *87*, 175-178.
(56) Grubbs, R. H.; Tumas, W. *Science* **1989**, *243*, 907-915.
(57) Schwab, P.; Grubbs, R. H.; Ziller, J. W. *J. Am. Chem. Soc.* **1996**, *118*, 100-110.
(58) Lamansky, S.; Djurovich, P. I.; Murphy, D.; Abdel-Razzaq, F.; Lee, H.-E.; Adachi, C.; Burrows, P. E.; Forrest, S. R.; Thompson, M. E. *J. Am. Chem. Soc.* **2001**, *123*, 4304-4312.
(59) Pollino, J. M.; Stubbs, L. P.; Weck, M. *Macromolecules* **2003**, *36*, 2230-2234.
(60) Wei, W.; Djurovich, P. I.; Thompson, M. E. *Chem. Mater.* **2010**, *22*, 1724-1731.
(61) Kaita, S.; Matsushita, K.; Tobito, M.; Maruyama, Y.; Wakatsuki, Y. *Macromol. Rapid Commun.* **2006**, *27*, 1752-1756.
(62) Zhou, L.; Zhang, H.; Deng, R.; Li, Z.; Yu, J.; Guo, Z. *J. Appl. Phys.* **2007**, *102*, 064504.
(63) Bonesi, S. M.; Erra-Balsells, R. *J. Lumin.* **2001**, *93*, 51-74.
(64) Tsuboi, T.; Murayama, H.; Yeh, S.-J.; Wu, M.-F.; Chen, C.-T. *Opt. Mater.* **2008**, *31*, 366-371.
(65) Park, T. J.; Jeon, W. S.; Park, J. J.; Kim, S. Y.; Lee, Y. K.; Jang, J.; Kwon, J. H. *Thin Solid Films* **2008**, *517*, 896-900.
(66) Song, J.-E.; Kim, B.-O.; Ha, Y. *Mater. Sci. Eng. C* **2004**, *24*, 191-194.
(67) Anderson, J. D.; McDonald, E. M.; Lee, P. A.; Anderson, M. L.; Ritchie, E. L.; Hall, H. K.; Hopkins, T.; Mash, E. A.; Wang, J.; Padias, A.; Thayumanavan, S.; Barlow, S.; Marder, S. R.; Jabbour, G. E.; Shaheen, S.; Kippelen, B.; Peyghambarian, N.; Wightman, R. M.; Armstrong, N. R. *J. Am. Chem. Soc.* **1998**, *120*, 9646-9655.
(68) Tsai, M.-H.; Lin, H.-W.; Su, H.-C.; Ke, T.-H.; Wu, C.-C.; Fang, F.-C.; Liao, Y.-L.; Wong, K.-T.; Wu, C.-I. *Adv. Mater.* **2005**, *18*, 1216-1220.
(69) Koene, B. E.; Loy, D. E.; Thompson, M. E. *Chem. Mater.* **1998**, *10*, 2235-2250.
(70) Pommerehne, j.; Vestweber, h.; Guss, W.; Mahrt, R. F.; Bassler, H.; Porsch, M.; Daub, J. *Adv. Mater.* **1995**, *7*, 551-554.
(71) Ichikawa, M.; Fujimoto, S.; Miyazawa, Y.; Koyama, T.; Yokoyama, M.; Miki, T.; Taniguchi, Y. *Org. Elect.* **2008**, *9*, 77-84.
(72) Gao, H.; Zhang, H.; Mo, R.; Sun, S.; Su, Z.-M.; Wang, Y. *Synthetic Metals* **2009**, *159*, 1767-1771.
(73) Ma, B.; Kim, B. J.; Deng, L.; Poulsen, D. A.; Thompson, M. E.; Frechet, J. M. J. *Macromolecules* **2007**, *40*, 8156-8161.
(74) Furuta, P. T.; Deng, L.; Garon, S.; Thompson, M. E.; Frechet, J. M. J. *J. Am. Chem. Soc.* **2004**, *126*, 15388-15389.

CHAPTER 4

Single-Molecule Ambipolar Transport Hosts

4.1. Introduction

This Chapter describes the synthesis and evaluation by thermal, photophysical, and electrochemical means of potential host materials for phosphorescent emitters containing both hole- and electron-transport moieties on a single molecule. Side-chain polymers of some of these molecules were also evaluated and OLEDs of some of the targets were explored as hosts for green and blue phosphors.

4.2. Introduction and Background

The reported mobilities of hole-transporting organic materials have been found to exceed those of electron-transport materials[1]; although exceptions are known.[2] As a result, an excess of charges (typically holes) may form within a given OLED device leading to decreased current efficiencies. In addition to relative mobilities, the injection barriers between the electrodes and the adjacent layer also affect the relative ratio of charge carriers within an given layer. In a device with an unbalanced number of carriers, recombination and emission may occur at the interfaces of hole and electron transport layers with accumulation of charged species that can have detrimental effects on device efficiency and stability.[3,4] If examined within the context of emissive layers for phosphorescent OLEDs, the imbalance therefore plays an important role in defining the recombination zone. In early PhOLEDs, emissive layers were comprised of unipolar charge transport materials, which inherently transport only one type of charge (hole or

electron) within the emissive layer. For such systems, the recombination zone would likely be confined to the area very near the interface. In such a narrowly-defined zone (see figure below), high concentrations of excitons may exist. While efficient recombination and emission may occur, the possibility of triplet exciton quenching events (through such processes as triplet-triplet annihilation[5]) or triplet exciton escape to adjacent organic layers without recombining on the phosphor are also possible; with the latter two processes reducing the performance of the device. In order to address some of the potential issues of narrow recombination zones, recent research has shifted toward the development of ambipolar host materials, which combine hole and electron transport moieties (by various approaches) that may lead to wider recombination zones which are shifted away from the interface.

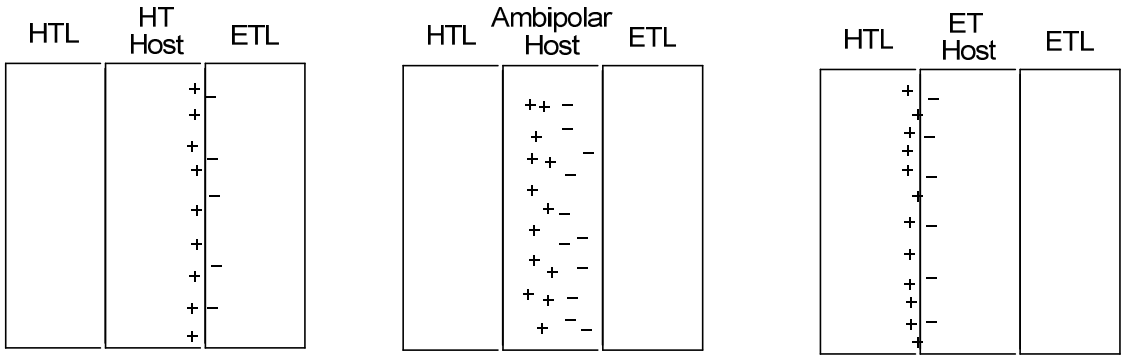

Figure 4.1. Simplified view of possible recombination zones for unipolar *vs*. ambipolar emissive layers.

In a study by Kim *et al*.[6] broad recombination zones were found to reduce the likelihood of triplet-exciton quenching events. Methods to achieve ambipolarity have, thus far, included the use of single molecule, copolymer, and blend approaches. For ambipolar materials, special attention must be given to avoiding formation of strong

charge-transfer states that can reduce the optical gap and the triplet energy, since these are important factors for energy transfer to phosphorescent emitters (see Chapter 1). Literature examples of such approaches combining carbazoles (see Chapter 3 introduction for further details) with oxadiazoles, triazoles, benzimidazoles, or pyridine are discussed below.

Oxadiazoles have been explored as electron transport materials since the early 1990s and include well-studied molecules such as 2-(4-biphenylyl)-5-(4-*tert*-butylphenyl)-1,3,4-oxadiazole (PBD)[7] and 1,3-bis-(*N,N*-t-butyl-phenyl)-1,3,4-oxadiazole (OXD-7).[8] In the pursuit of ambipolar molecules, combinations of oxadiazole and carbazole functionalities have been examined recently in the literature. The earliest known example of a molecule incorporating both carbazole and oxadiazole was reported by Guan *et al*.[9] in 2003. For molecule **4.1**, the thin-film fluorescence showed a maximum at 412 nm. In a fluorescent device (ITO/TPD/**4.1**/Alq_3/Mg:Ag (9:1)/Ag) a maximum power efficiency of 2.25 lm/W (at 15 V) was observed. From a molecular design perspective, the connectivity of the carbazole to oxadiazole group through a *para*-substituted geometry on a benzene when combined with the biphenyl group (on the opposite side of the oxadiazole), may give rise to extended conjugation across the length of the molecule. One finds, in general, that increased conjugation can reduce the magnitude of the optical gap relative to less conjugated systems.[10]

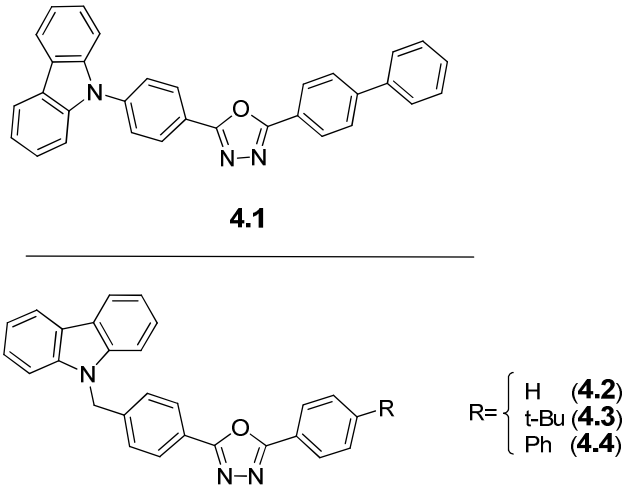

Figure 4.2. Carbazole and oxadiazole ambipolar molecules.

In 2006, Guan *et al*. reported the syntheses of molecules **4.2** – **4.4**.[11] These new molecules interrupted the conjugation between the carbazole and oxadiazole moieties by introducing an intervening sp^3-hybridized methanediyl group between the oxadiazole and carbazole. For **4.2** – **4.4**, the emission maxima were reported at 390, 394, and 410 nm (*vs.* 412 nm for **4.1**). Solid-state ionization potentials (IP) and electron affinities (EA) (estimated from cyclic voltammetry and onset of absorption data) of the molecules were all found to be near 6.1 eV and 2.6 eV, respectively. Comparison of **4.4** and **4.1**, showed that emission only shifted by 2 nm, which the authors did not address, but which suggested only a minimal effect from the disrupted conjugation between the carbazole and oxadiazole. The larger hypsochromic shift between **4.2** and **4.3** *vs.* **4.1** suggested the effect was due to removal of the phenyl substituent. Molecule **4.3** was evaluated as a host material in a PhOLED device with architecture: ITO/NPB/**4.3**:Ir(DBQ)$_2$(acac)/Alq$_3$ /Mg:Ag (9:1) (where DBQ = dibenzo[*f,h*]quinoxalinato and acac = acetylacetonate). At 4 wt% doping of the iridium emitter, a maximum power efficiency of 9.9 lm/W (EQE of

9.5%) at 5 V was obtained while an analogous 4,4'-*N,N'*-dicarbazole-biphenyl (**CBP**) device showed poorer performance (2.4 lm/W and 3.2% at 7 V), but the architecture incorporated a bathocuproine layer (BCP) (before the Alq_3 layer) and as such, a direct comparison could not be made. The authors suggested that the superior device properties observed with their molecule (vs. **CBP**) resulted from better balance of charge transport and higher charge recombination. Additional studies of the charge mobilities of the molecules would be required to support those conclusions.

Ma and co-workers[12] reported molecule **4.5** as an ambipolar host in 2008. By connecting the carbazole groups *ortho*- to oxadiazole across benzene groups, a twisted geometry (verified by x-ray crystallography), may have limited planarity and therefore shortened the length of π-conjugation across the molecule.

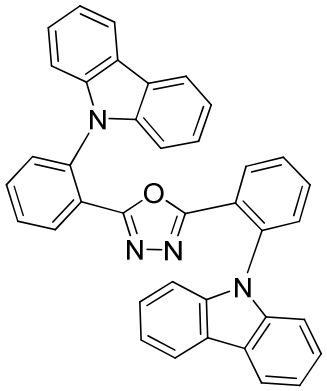

4.5

Figure 4.3. Carbazole and oxadiazole ambipolar molecule.

The molecule exhibited a glass transition temperature of 97 °C, reversible oxidation and reduction potentials, and solid-state IP and EA energies estimated at 5.6 and 2.6 eV (from cyclic voltammetry and absorption onset data). Although not addressed by the authors, the reversible oxidation observed was surprising, as unsubstituted

carbazoles generally demonstrate irreversible oxidations due to instability of the radical cation.[13] A fluorescence maximum of 434 nm (in chloroform) and triplet energy of 2.68 eV (measured from phosphorescence) were reported. The molecule was evaluated as a host for green ($Ir(ppy)_3$) and red ($(piq)_2Ir(acac)$) emitters (in devices: ITO/MoO_3/NPB/**4.5**:Emitter/BCP/Alq_3/LiF/Al). For a green device, a maximum EQE of 20.2% (77.9 cd/A and 59.3 lm/W) was recorded and for a red device, a maximum EQE of 18.5% (13.6 cd/A and 11.5 lm/W) was obtained. Overall, the authors reported a relatively straightforward ambipolar molecule with appropriate properties to host green and red emitters. A comparison to a *meta*- conjugated analogue of **4.5** would help to contrast the twist approach to the cross-conjugated approach in limiting conjugation. Other studies using triphenylamines and oxadiazole small molecules have been reported recently by the same group.[14,15]

Other heterocycles closely related to oxadiazoles, such as triazoles have also been used as electron transport groups. For example, 2-(4-biphenylyl)-5-(4-*tert*-butylphenyl)-1,2,4-triazole (TAZ) found by Kido and co-workers to be a good electron transport molecule and an efficient hole blocker.[16] Kim *et al*.[17] reported a series of molecules incorporating both carbazole and 1,2,4-triazoles as hosts for blue PhOLEDs.

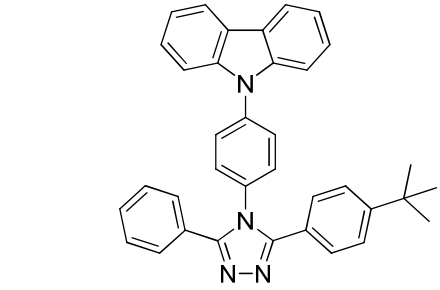

4.6

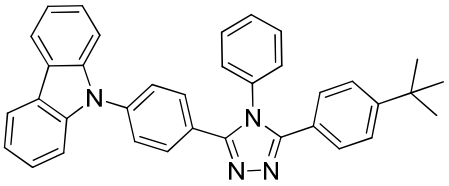

4.7

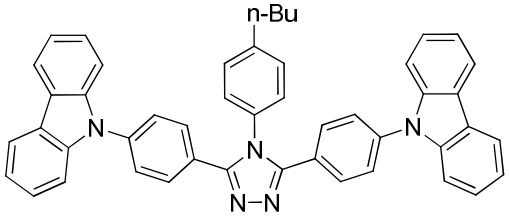

4.8

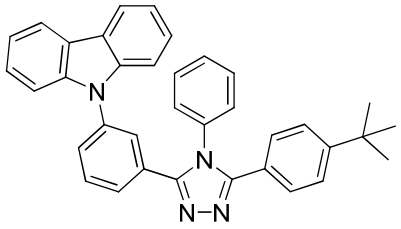

4.9

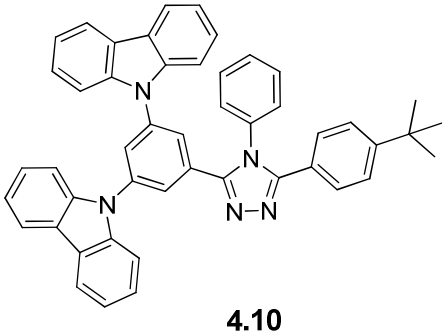

4.10

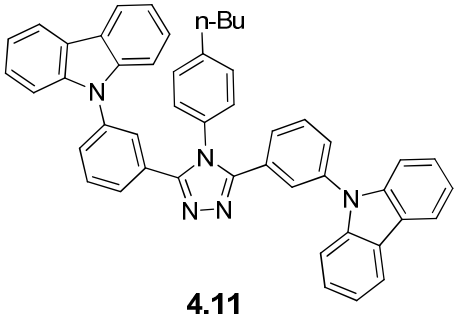

4.11

Figure 4.4. Carbazole and triazole ambipolar molecules.

Table 4.1 Molecular Properties **4.6-4.8**

molecule	E_T (eV)[a]	λ_{max}fluo (nm)[b]
4.6	3.01	345
4.7	2.82	379
4.8	2.82	385

[a] from phosphorescence at 77K ; [b] in chloroform at RT

In the report, the fluorescence and triplet energies of only the first three molecules were explicitly stated. In explaining the emission and triplet energy of **4.6**, the authors

argued that the dihedral angle between the phenyl carbazole and triazole was larger and limited conjugation. In comparison, when the same group was connected through the 3 and/or 5 positions on triazole (**4.7** and **4.8**), the angle was postulated to be smaller thereby permitting a higher level of conjugation and resulting in lower emission and triplet energies. For **4.9** – **4.11**, the triplet energies were only stated to be higher than 2.82 eV without specific values given. The authors attributed these energies to a more "kinked" structure without considering that the effect might originate from the *meta*- geometry of the connectivity. The photophysical data reported was not fully consistent with the authors' data interpretation, as the fluorescence and phosphorescence spectra, as shown, suggested **4.9 – 4.11** may have possessed triplet energies closer to that of **4.6**. The emission maxima of **4.10** and **4.11** revealed a slight bathochromic shift in the emission from combining the carbazoles onto a single side of the molecule. Contrasting **4.9** and **4.10** showed that having only one carbazole (as in **4.9**) afforded higher energy emission close to 350 nm. Therefore, the number of carbazoles and the details of how they are linked to an electron transport moiety can affect the emission (with a less obvious effect on the triplet energies). Only one example device using **4.11** was studied with an architecture comprised of ITO/PEDOT:PSS/NPB/**4.11** or **CBP**:FIrpic (6 wt%)/BAlq/LiF/Al. In the **4.11** device, a maximum luminance efficiency of 14.2 cd/A (at 1.1 mA/cm^2) was obtained while the **CBP** reference device gave values of 11.6 cd/A (at 0.11 mA/cm^2). Data on additional devices would have been helpful to further reveal the potential of the other hosts reported.

Another example of an ambipolar molecule incorporating a triazole was reported by Hong and co-workers[18] as a variant of the well-known **CBP** molecule.

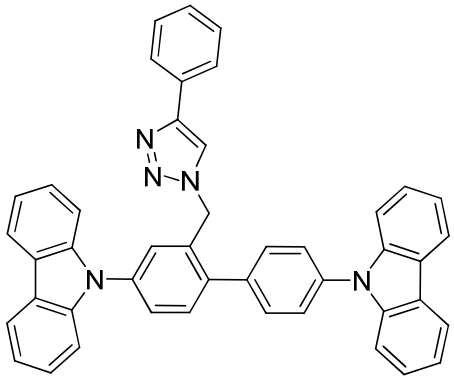

4.12

Figure 4.5. Carbazole and triazole ambipolar molecule.

The molecule had a triplet energy of 2.7 eV (determined from phosphorescence data at 77K) and IP and EA energies at 6.0 and 2.5 eV (estimated from cyclic voltammetry and the optical data). Compared to **CBP**, the triplet energy was increased by 0.15 eV. **4.12** also demonstrated a modest 3 nm blue shift to 362 nm, as compared to **CBP**, from the fluorescence spectra. The authors postulated that the modified properties were due to the electron-deficient nature of the triazole. It should be noted that there may also be an effect due twisting (resulting from the bulky triazole group) of the biphenyl core that could also contribute to these observations.

Table 4.2 Devices (ITO/CuPc/NPD/Host/ETL/LiF/Al)

Host	Emitter[a]	ETL	Max EQE (%)	Max PE (lm/W)	Max LE (cd/A)
4.12	FIrpic	BAlq	5.4	6.9	9
CBP	FIrpic	BAlq	4.2	6.3	7.5
4.12	$Ir(ppy)_3$	BAlq	7.2	6.5	19.9
CBP	$Ir(ppy)_3$	BAlq	3.7	3.3	10.2

[a] doped at 6 wt%

Blue (FIrpic) and green ($Ir(ppy)_3$) devices were prepared and comparison between **CBP** and **4.12** showed the latter molecule to be superior in both cases. Furthermore, additional devices using Alq_3 (data not shown) suggested that emission in **4.12** devices came strictly from the guest emitters in the emissive layer, while in **CBP** devices, emission from Alq_3 was observed (due to recombination at the interface from poor injection of electrons into **CBP**). It was shown that triazole could be used to impart ambipolar character to a CBP-type hole transport material. To further establish the usefulness of this molecule, additional studies (such as the molecular geometry) could provide insight into the origin of the higher triplet energy.

1,3,5-tris(*N*-phenylbenzimidazol-2-yl)benzene (**TPBI**; **4.13**) has been used as an electron transport material.[19] Carbazoles were utilized by Takizawa *et al*.[20] to develop an ambipolar variant of **TPBI**, molecule **4.14**.

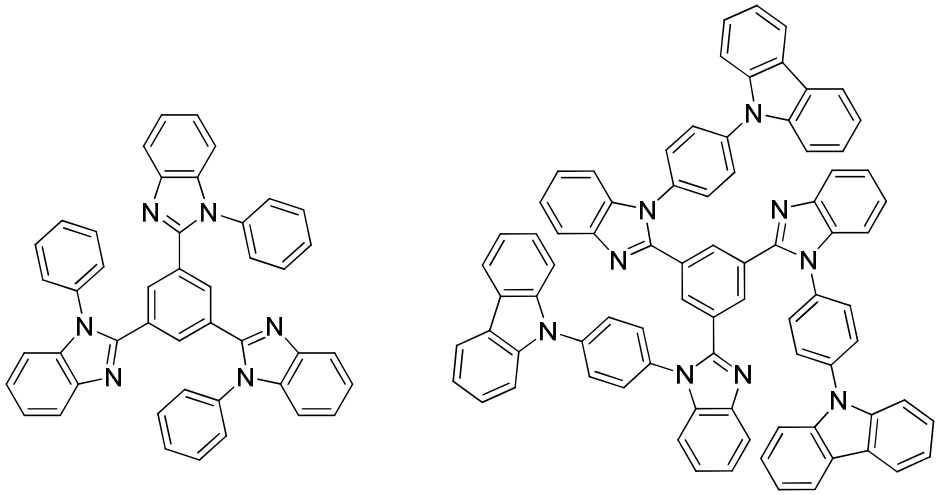

4.13 **4.14**

Figure 4.6. **TPBI** (**4.13**) and carbazole-functionalized TPBI-derivative (**4.14**).

Table 4.3 Molecular Properties **4.13** & **4.14**

molecule	λ_{max}fluo (nm)	E_T[a] (eV)	E_{ox}[b,c] (V)	E_{red}[b] (V)	HOMO[d] (eV)	LUMO[d] (eV)	H-L gap (eV)
TPBI (**4.13**)	373	2.67	1.23	-2.7	-6.0	-2.1	3.9
4.14	421	2.67	0.92	-2.7	-5.7	-2.1	3.6

[a] measured from phosphorescence (at 77K)
[b] obtained by differential pulse voltammetry (in CH_2Cl_2 *vs.* $FeCp_2^{+/0}$)
[c] irreversible process
[d] calculated from DFT calculations (B3LYP; 6-31G*)

The table above gives the properties of the molecules (a second variant molecule with diphenylamine in place of carbazole was also studied (not shown)). Comparison of the molecules showed that upon addition of the carbazole group, the fluorescence was red shifted and could be associated with the higher lying HOMO located on the carbazole moiety. The reduction potential and LUMO energy were not changed on introduction of the carbazole, due to the near complete isolation of the LUMO on the **TPBI** portion of the molecule (as shown by DFT calculations). Green devices were evaluated (ITO/NPD/4,4',4''-tris(*N*-carbazolyl)triphenylamine/**4.13** or **4.14**:Iridium(III) bis(2-phenylpyridinato-*N,C*$^{2'}$)acetylacetonate ($Ir(ppy)_2(acac)$) (6 wt%)/CsF/Al) and for host **4.13**, a maximum EQE of 4.7%, 18.8 cd/A, and 21.0 lm/W at 0.1 mA/cm^2 were observed. For **4.14**, a significant increase was observed with stated values of 14.0%, 48.2 cd/A, and 46.0 lm/W at 0.1 mA/cm^2. For the **TPBI** device, the electroluminescence data showed NPD emission, which was not observed for the ambipolar host device, presumably due to recombination at the interface. In the case of **4.14**, the recombination zone was shifted away from NPD due ease of hole injection and ambipolar transport within the new host. It was successfully shown that modification of **TPBI** could afford ambipolar host materials with concomitant reduction in the oxidation potential and no effect on the triplet energy.

Gong *et al*.[21] investigated a different combination of carbazole and benzimidazole as shown in the series of molecules below.

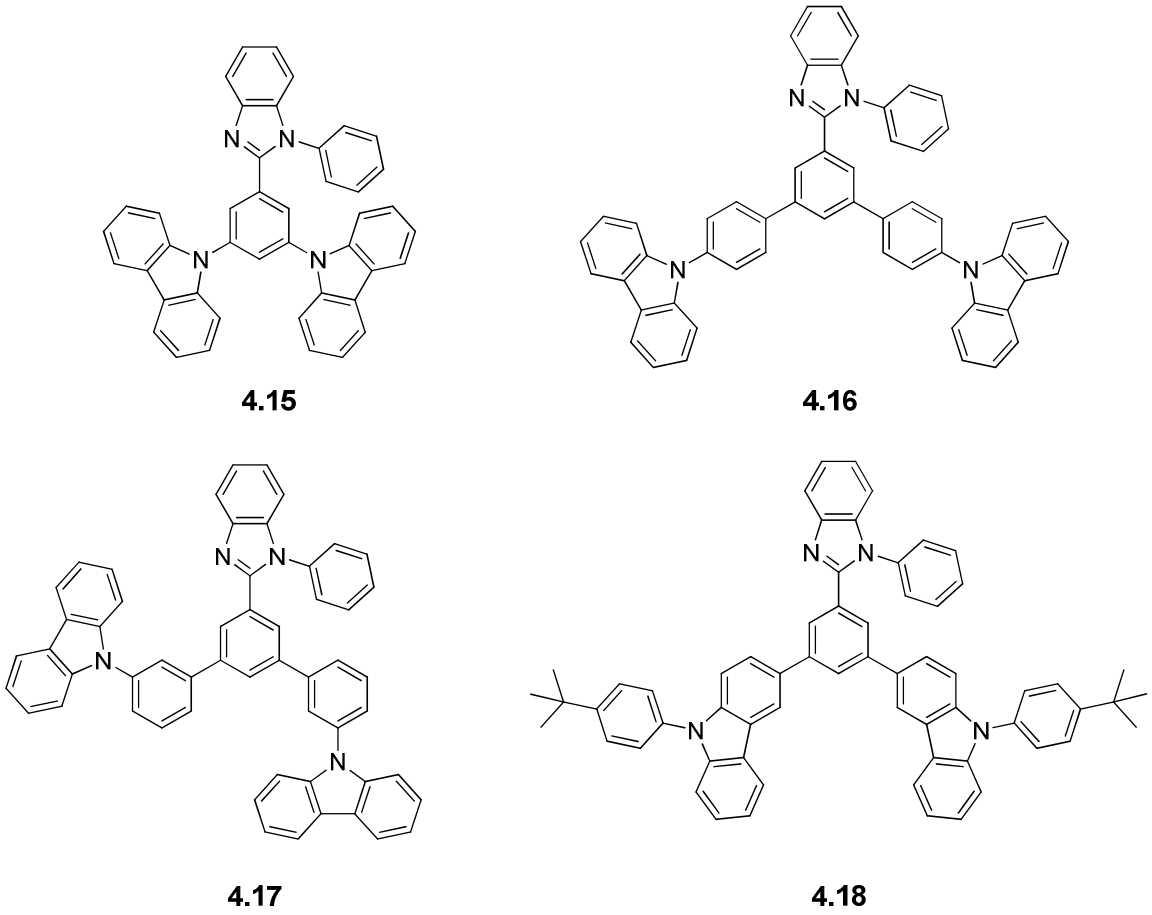

Figure 4.7. Carbazole and benzimidazole ambipolar molecules (**4.15**-**4.18**).

Table 4.4 Molecular Properties **4.15-4.18**

molecule	λ_{max}fluo (nm)[a]	E_T (eV)[b]	IP (eV)[c]	EA (eV)[c]
4.15	393	2.62	5.6	2.1
4.16	370	2.43	5.6	2.4
4.17	350,356	2.56	5.5	2.0
4.18	387	2.54	5.5	2.2

[a] measured in toluene
[b] measured from phosphorescence (at 77K)
[c] calculated from cyclic voltammetry and onset of absorption (for EA)

The authors explored several approaches to attachment of the carbazoles. Fluorescence spectroscopy revealed that introduction of a phenyl spacer (as in **4.16** and

4.17) induced a hypsochromic shift, attributed to reduction of charge transfer between the benzimidazole and carbazole moieties; with a stronger effect observed for *meta*-conjugated **4.17**. Attachment at the 3 (or 6) position of carbazole, as in **4.19**, did not decouple the groups as strongly. The highest E_T was found for **4.15** (mCP-like) while **4.16** (with the carbazole *para*- on the phenyl spacer) had the lowest triplet energy at 2.43 eV. For **4.17** and **4.18** the relative decrease was smaller (2.56 and 2.54 eV, respectively). Despite the blue shifts observed in fluorescence for **4.16** or **4.17**, the triplet energies were noted to decrease. Oxidation potentials were found to be irreversible and no reductions were observed (in dichloromethane). Green devices (ITO/MoO_3/NPB/**4.15** – **4.18**:$Ir(ppy)_3$ (9 wt%)/TPBI/LiF/Al) demonstrated that **4.15** and **4.18** gave the lowest EQEs (7.7 and 7.0%), while **4.16** gave a better efficiency of 12.7% (despite its lower triplet energy). The best device was obtained using host **4.17** with an efficiency of 18.7% (73.4 lm/W, 70.2 cd/A) at 12.1 V. DFT calculations showed that **4.16** and **4.17** had more isolated HOMO and LUMO orbitals which the authors suggested could impart improved overall hole- and electron-transport ability and explain the superior device performance.

Pyridine has also been explored as an electron transport group in combination with carbazole. Molecules **4.19** and **4.20**, were reported by Su *et al*.[22] to afford hosts with expected ambipolarity.

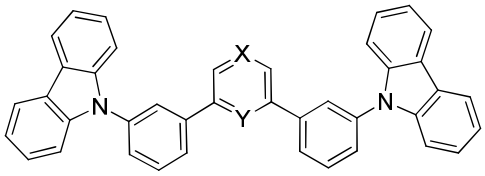

X=CH, Y=N **4.19**

X=N, Y=CH **4.20**

Figure 4.8. Carbazole and pyridyl-based ambipolar molecules (**4.19** and **4.20**).

As compared to **CBP** (E_T = 2.56 eV[12]), introduction of a pyridine unit between the biphenyl core was shown to increase the triplet energy of 2.71 eV for both molecules. The higher E_T could be attributed to reduced π-conjugation from the *meta*- substitution across the pyridine. The ambipolarity of the molecules was evaluated by constructing devices with the architecture: ITO/NPD/**4.19**, **4.20**, or **CBP**/Alq_3/LiF/Al. Electroluminescence data showed no emission that could be attributed to **4.19**, **4.20**, or **CBP** (for thin 10 nm layers). For **4.20**, the majority of the emission could be attributed to the NPD with some emission from Alq_3, while for **4.19** emission originated almost equally from those respective layers. In the case of the **CBP** device, the emission came exclusively from Alq_3. These results were interpreted as showing that **CBP** transports holes predominantly, that **4.20** transported both holes and electrons (but electrons preferentially), and that **4.19** transported both charges in a much more balanced manner. No explanation was offered for these differences. As hosts for blue (FIrpic), complex devices were fabricated (ITO/poly(arylene amine ether sulfone)-containing tetraphenylbenzidine (doped with tris(4-bromophenyl)aminium hexachloroantimonate/ 2,2'-bis(m-di-p-tolylaminophenyl)- 1,1'-biphenyl/**4.19** or **4.20**:FIrpic(11 wt%)/3,5,3',5'-tetra (m-pyrid-3-yl)phenyl-[1,1']-biphenyl/LiF/Al) that gave efficiencies of 22.6% (34.5 lm/W) for **4.19** and 17.9% (24.1 lm/W) for **4.20** (both at 1,000 cd/m^2). Theoretical calculations to provide insight into the HOMO and LUMO spatial distributions would have been useful in understanding the differences between the ambipolar hosts.

In 2001, Forrest and co-workers[23] reported that **CBP** (**4.21**) demonstrated ambipolar transport properties. This was deduced from devices fabricated with and

without a bathocuproine (BCP) electron transport layer that showed that the **CBP** device without the BCP layer was more efficient by 4%. Although the report was suggestive of some extent of electron transporting capability, in all likelihood **CBP** should still behave as predominantly hole transporting molecule. Jeon *et al*.[24] explored this finding further by introducing additional phenyl rings (see **4.22** and **4.23**).

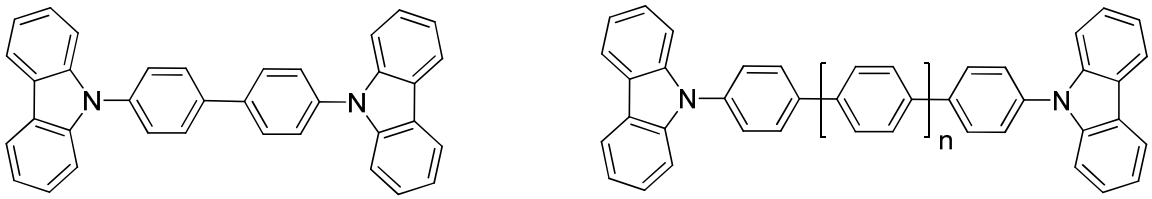

4.21

4.22 (n = 1)
4.23 (n = 2)

Figure 4.9. CBP and CBP-like ambipolar molecules (**4.21**-**4.23**).

The extended structures exhibited red shifted emission as would be expected from extension of the π-system. It was precisely this extension that was argued to afford the ambipolarity, as the multiple phenyl ring system was suggested to increase the electron transport capability (although this was not studied). Devices with structures ITO/NPB/**CBP**, **4.22**, or **4.23**:$Ir(ppy)_3$ (8 wt%)/BAlq/Alq_3/LiF/Al were studied. Within this group of materials, **4.22** was found to be the best host material with a maximum power efficiency of 16.3 lm/W, while **CBP** and **4.23** had values of 13.2 and 8.8 lm/W, respectively. The inferior performance of **4.23** was suggested to result from a suspected lower triplet energy (vs. **4.22**), but this was not verified. The effectiveness of the extension approach discussed may be inherently limited. Further increases in the number of bridging phenyl groups would likely reduce the optical gap more and would limit the

usefulness of such materials as hosts in PhOLEDs; although the examples shown may still be useful as hosts for green or red emitters.

A copolymer approach to achieve ambipolarity was explored by Chen and co-workers.[25] The approach gave the flexibility to adjust the relative content of the transport groups, which is not possible for same-molecule systems discussed earlier.

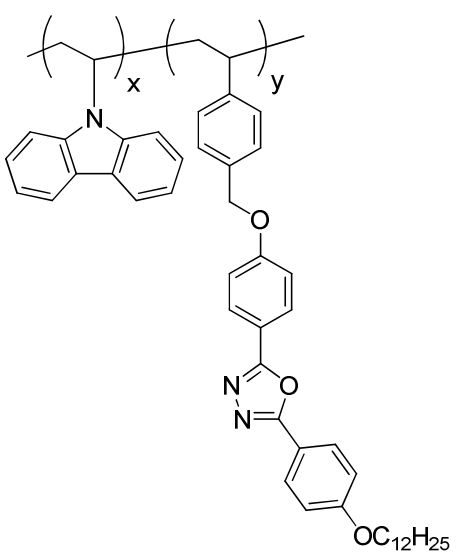

	x	:	y
4.24	0.88		0.12
4.25	0.84		0.16
4.26	0.80		0.20
4.27	0.64		0.36
4.28	0.45		0.55

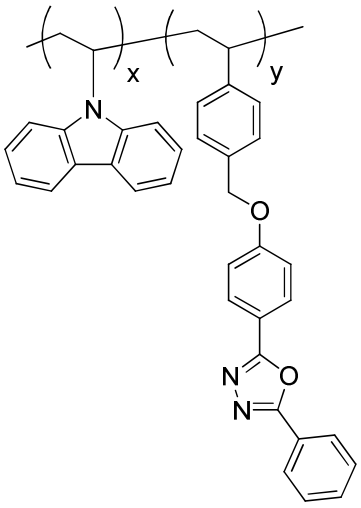

4.29 x = 0.80 & y = 0.20

Figure 4.10. Carbazole and oxadiazole ambipolar copolymers (**4.24**-**4.29**).

The absorption spectra recorded were dependent on the relative composition but maxima could be attributed to the PVK and oxadiazole groups from looking at the differences between spectra. Cyclic voltammetry (of polymers coated on carbon electrode) showed that progressively higher oxadiazole content increased the oxidation potential (from 0.63 to 0.77 V) and the IP as well. It is not immediately clear why the oxidation potential would change, unless the carbazole behaves differently (perhaps due

to some interaction with oxadiazole) at different ratios. Electron affinities (obtained from the IP and optical gap) showed a similar trend. For green devices (ITO/PEDOT:PSS/**PVK** or copolymers:$Ir(ppy)_3$/BCP/Ca/Al), **4.25** gave the best luminance efficiency of 17.9 cd/A (at 32 mA/cm^2). **PVK** and **4.28** gave the lowest efficiencies at 2.0 (at 62 mA/cm^2) and 7.4 cd/A (at 26 mA/cm^2), while the remaining copolymers have efficiencies higher than 10 cd/A. The electroluminescence showed that for all hosts the emission was strictly from the emitter which indicated good energy transfer and as such may indicate an appropriately high triplet state (at least as compared to the emitter). Copolymers **4.26** and **4.29** showed different efficiencies and the lower efficiency of the latter was attributed to poorer solubility of the emitter (as studied by AFM). The approach reported showed that the copolymer approach could yield solution-processable host layers with ease of layer processing and the ability to tune the ambipolar properties. Further investigation on polymer composition (i.e. random vs. di-block), morphological stability, and lifetime studies would have been useful. In a similar approach to the one discussed, additional examples of copolymers containing triphenylamine and oxadiazole groups have also been explored.[26-30]

4.3. Goals for Chapter 4

The research aims of this chapter were to design and evaluate new ambipolar host materials by combining hole (carbazole) and electron (oxadiazole or triazole) transport groups onto a single molecule. Single molecule ambipolar targets were pursued because they can be used as vacuum-processable materials or converted to solution-processable

polymers. In addition, polymers containing a single ambipolar side-chain unit may not suffer from potential phase segregation issues[31] that can be observed in ambipolar hosts layers achieved through polymer blends or copolymers.

Development of synthetic approaches and studies of the photophysical, thermal, and electrochemical properties of these potentially ambipolar molecules are discussed. In addition, experimentally determined triplet energies (for selected molecules), examples of side-chain polymers, and OLED devices are reported.

4.4. Design Rationale and Synthesis of Ambipolar Small-Molecules and Side-chain Polymers

In this section we focus on the design rationale and specifics of synthesis of these materials. Specific experimental details are given in Chapter 2. Discussions of thermal, photophysical, and electrochemical properties in addition to evaluation of polymers in OLED devices are included in subsequent sections of this chapter.

For the targets pursued, combination of carbazole with an electron transport heterocycles (oxadiazole or triazole) was pursued. In the pursuit of high triplet energy molecules, that may serve as hosts for blue emitters (i.e. FIrpic), molecules were designed that would limit the strength of charge-transfer states (between the carbazole and electron transport heterocycles) by such approaches as *meta*- conjugation, spacer groups, and possibly originating from twisting within the molecules to break planarity.

Two oxadiazole and carbazole targets were pursued by synthesis of an mCP-like derivative. **S3.11** was coupled with carbazole via an Ullmann reaction and then the

methyl ester was reacted with hydrazine under reflux to yield the hydrazide molecule **S4.1**.

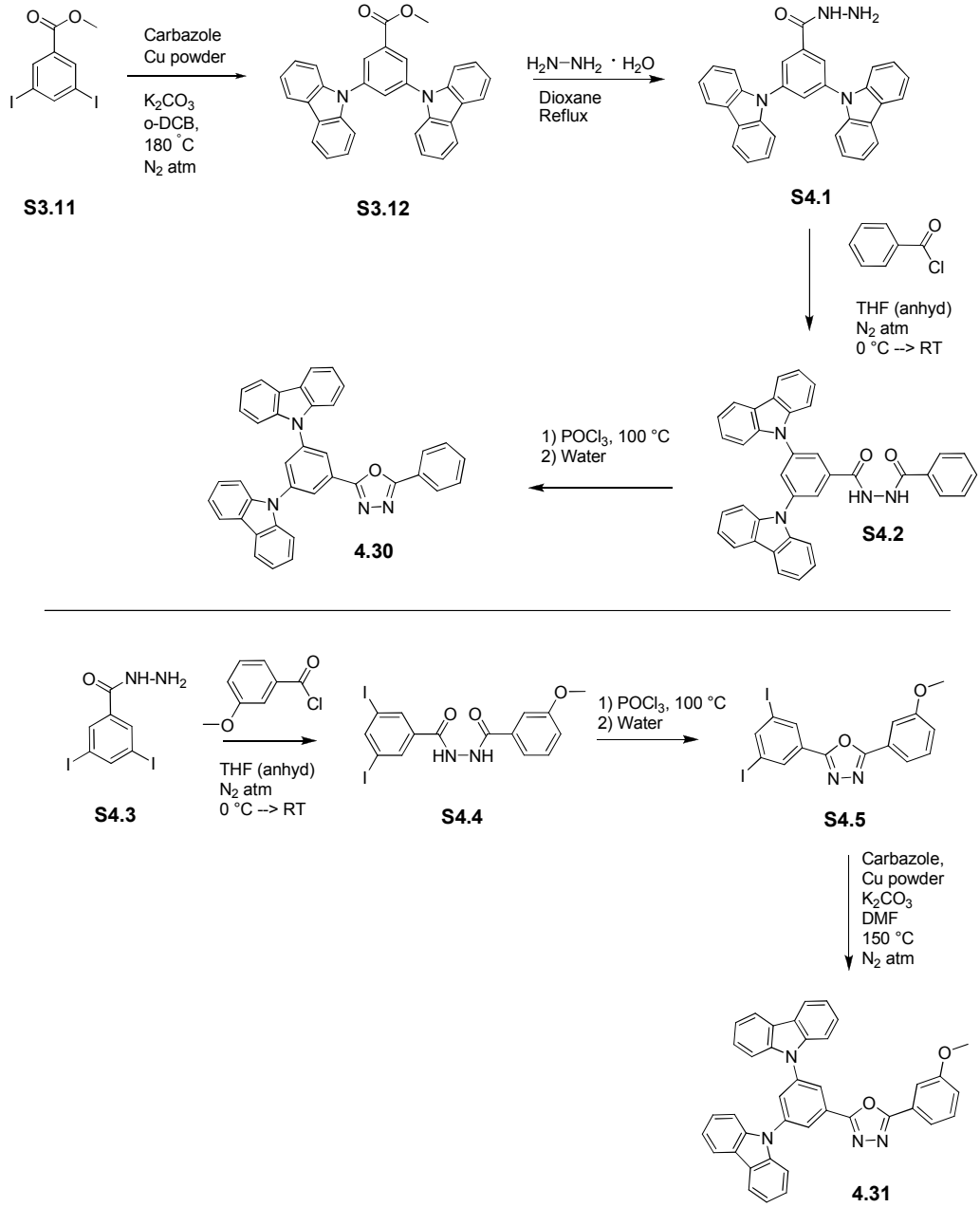

Scheme 4.1. Synthesis of oxadiazole-based ambipolar small-molecules **4.30** and **4.31**.

Hydrazide **S4.1** was reacted with benzoyl chloride and in the subsequent step phosphorus oxychloride was used to to yield the oxadiazole small-molecule **4.30**. The second target was started by formation of hydrazide **S4.4** from the diiodo material, **S4.3**. After formation of the oxadiazole (**S4.5**), Ullmann coupling conditions were used to functionalize the iodo- positions with carbazole to yield **4.31**. It was proposed that having the oxadiazole *meta*- to the carbazoles (on a benzene ring) would limit the extent of conjugation between the groups and lower the likelihood of forming charge-transfer states that could reduce the transport gap and red-shift the emission.

From **4.31**, functionalization of the ambipolar host with a norbornene monomer was pursued by deprotection of the methoxy group with boron tribromide and then reaction with a bromoalkyl norbornene derivative. The monomer was polymerized by ring opening metathesis polymerization (ROMP) with Grubbs' initiator (first generation). Obtaining the polymer version was pursued for the ability to solution process layers of the host in order to compare differences between the small-molecule and polymer-based OLED devices with the same ambipolar transport moiety.

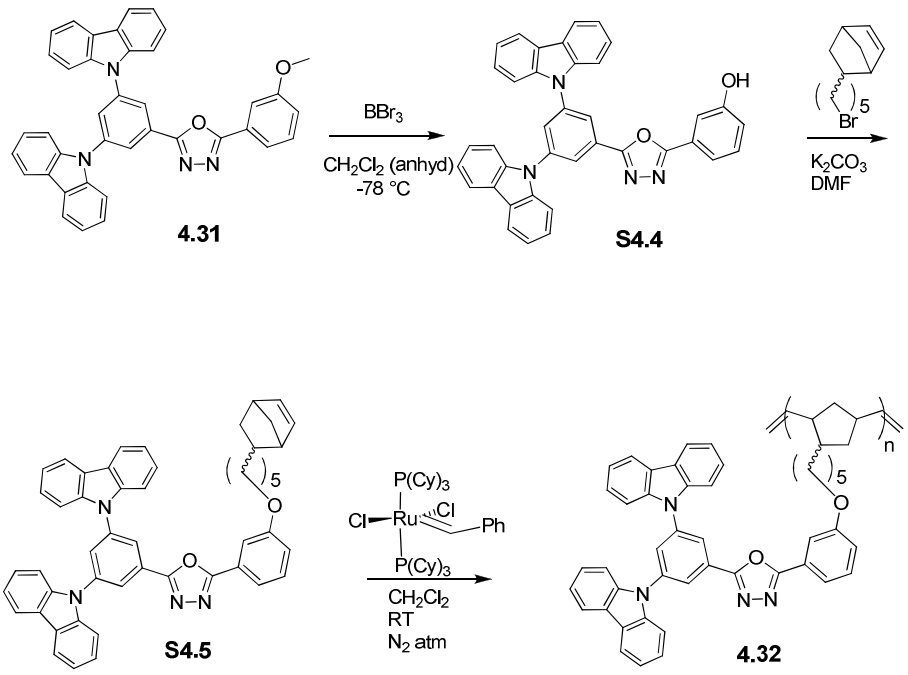

Scheme 4.2. Synthesis of oxadiazole-based ambipolar side-chain polymer **4.32**.

Work by Kido and co-workers[22] showed that a phenyl spacer between a pyridine and carbazole could be used to achieve ambipolarity (see introduction). The phenyl spacer may serve to limit charge transfer between the electron- and hole-transport groups. Although a recent study employing a phenyl spacer has been reported[21] (between benzimidazoles and carbazole groups), no such study has been performed for molecules containing oxadiazoles or triazoles. Therefore, molecule **4.33** was designed for this purpose. The synthesis was started by formation of hydrazide **S4.8**; from reaction of methyl 3,5-dibromobenzoate and hydrazine. The intermediate was then reacted with 3-methoxybenzoyl chloride to afford **S4.9**.

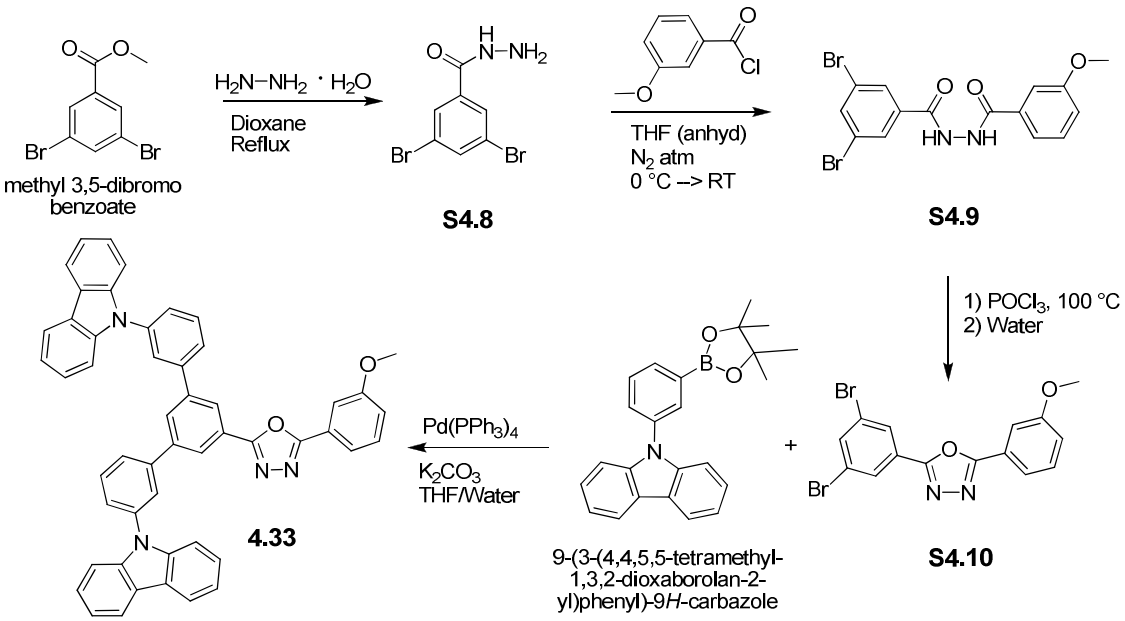

Scheme 4.3. Synthesis of oxadiazole-based ambipolar small-molecule **4.33**.

Phosphorus oxychloride induced cyclization of hydrazide **S4.9** to yield the oxadiazole followed by Suzuki coupling to form the final target **4.33**. The synthesis was intentionally designed to permit the flexibility of synthesizing molecule **4.31** directly from this intermediate by Ullmann coupling to *9H*-carbazole.

The deprotection of the methoxy group with boron tribromide of **4.33** and subsequent reaction with the norbornene derivative were used to obtain monomer **S4.11** which was polymerized with Grubbs' first generation catalyst.

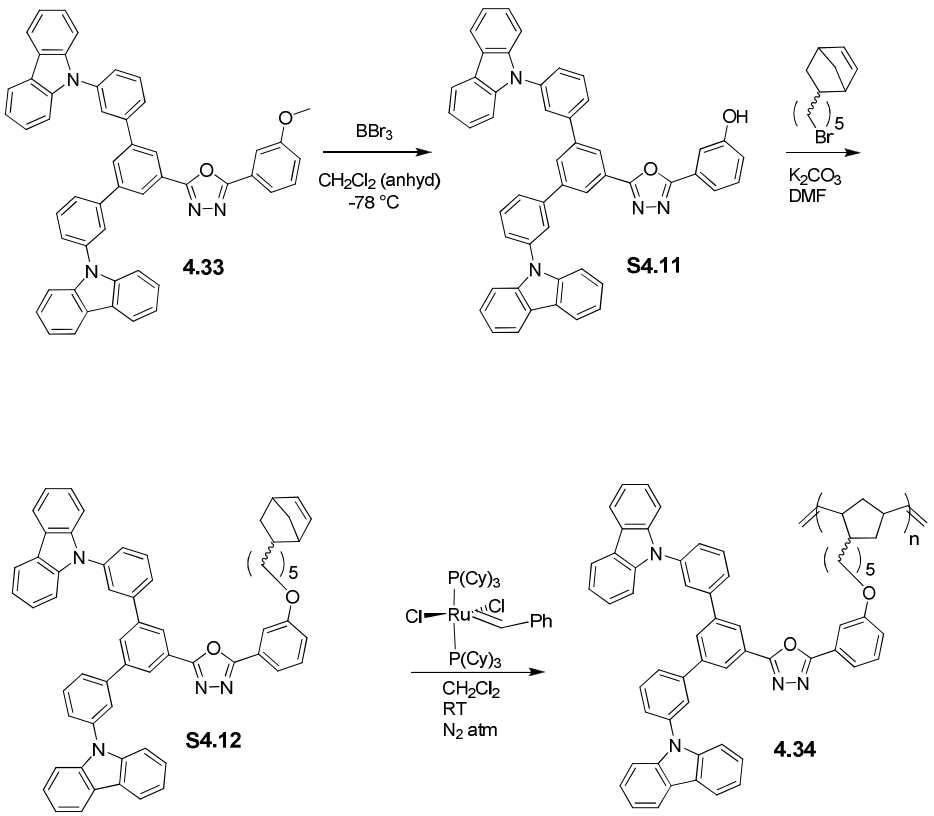

Scheme 4.4. Synthesis of oxadiazole-based ambipolar side-chain polymer **4.34**.

A variant of the above target (**4.35**) incorporating a single phenyl-carbazole peripheral group was pursued in order to study what effect might result on going from a one-to-one ratio of transport moieties *vs*. a two-to-one ratio (as used in the preceding target **4.33**). The synthesis of a small-molecule was accomplished through analogous methods to those already discussed.

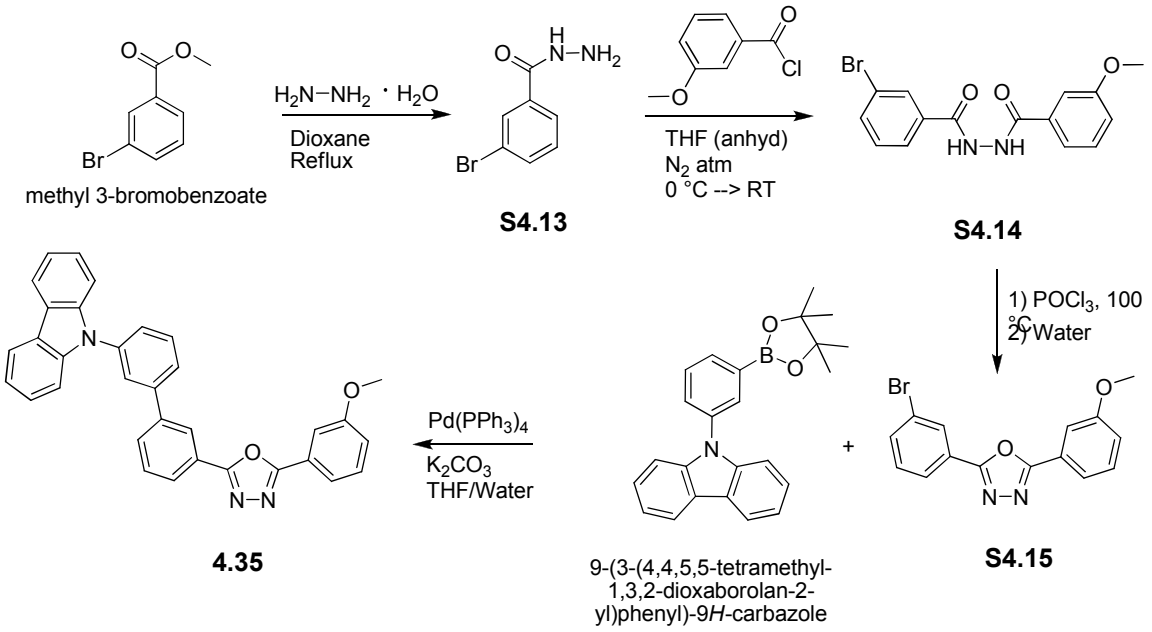

Scheme 4.5. Synthesis of oxadiazole-based ambipolar small-molecule **4.35**.

1,2,4-Triazole is another example of an electron transporting heterocycle explored in the organic electronics literature. A comparative study of oxadiazole and triazole was pursued for some of the ambipolar hosts. The triazole heterocycle could be obtained in lieu of the oxadiazole via two alternative pathways. Initially, the top pathway, performed with $POCl_3$ or PCl_3 and aniline in a single step, yielded either only oxadiazole or very low yields of the triazole. The reaction was modified based on the literature[32,33] and it was observed that pre-reaction of the aniline with phenyl phosphorodichloridate (for one hour), followed by addition of the hydrazide would yield the triazole in 50 – 60% yields. The oxadiazole was typically observed as a by-product, due to intramolecular ring closure originating from one of the hydrazide oxygen atoms.

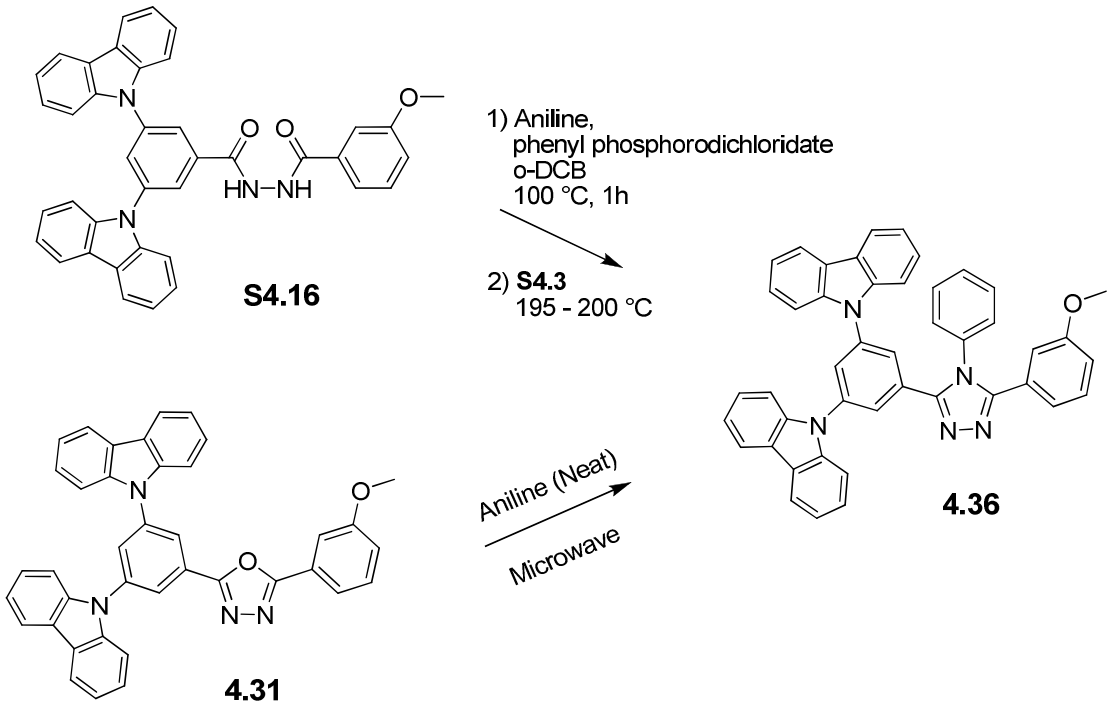

Scheme 4.6. Synthesis of triazole-based ambipolar small-molecule **4.36**.

A second pathway explored to obtain the triazole target was the conversion of the oxadiazole to the triazole in neat aniline under microwave conditions. The reaction was based on a literature[34] report in which under conventional (hot plate) heating in a pressure vessel the conversion was observed. Successful conversion of **4.31** in neat aniline to the triazole target (**4.36**) was achieved in ~ 30-50% yields, although the conversion still required reaction times of several hours at ~ 200 °C. This type of conversion could be used to convert other oxadiazole molecules to triazole for comparison purposes. The methoxy group of **4.36** was deprotected and functionalized with to afford a norbornene monomer and polymerized by ROMP to yield polymer **4.37**.

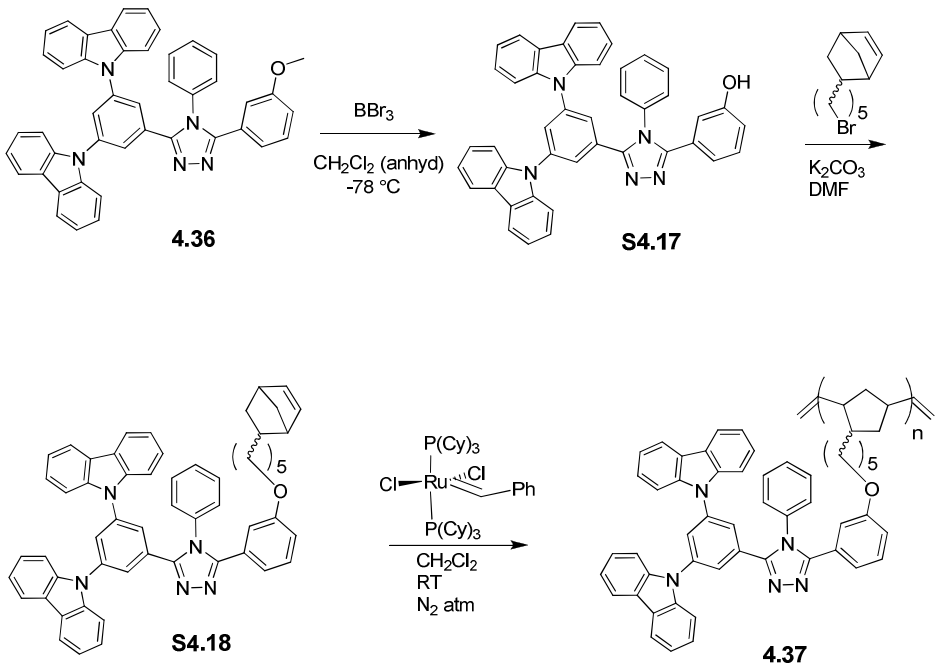

Scheme 4.7. Synthesis of triazole-based ambipolar side-chain polymer **4.37**.

A phenyl spaced target (analogous to **4.36**) was designed to investigate the effect, if any, the group would have on coupling between the carbazole and triazole moieties. Hydrazide **S4.9** was used to form the triazole and the final target was obtained by coupling to the boronic ester carbazole-derivative.

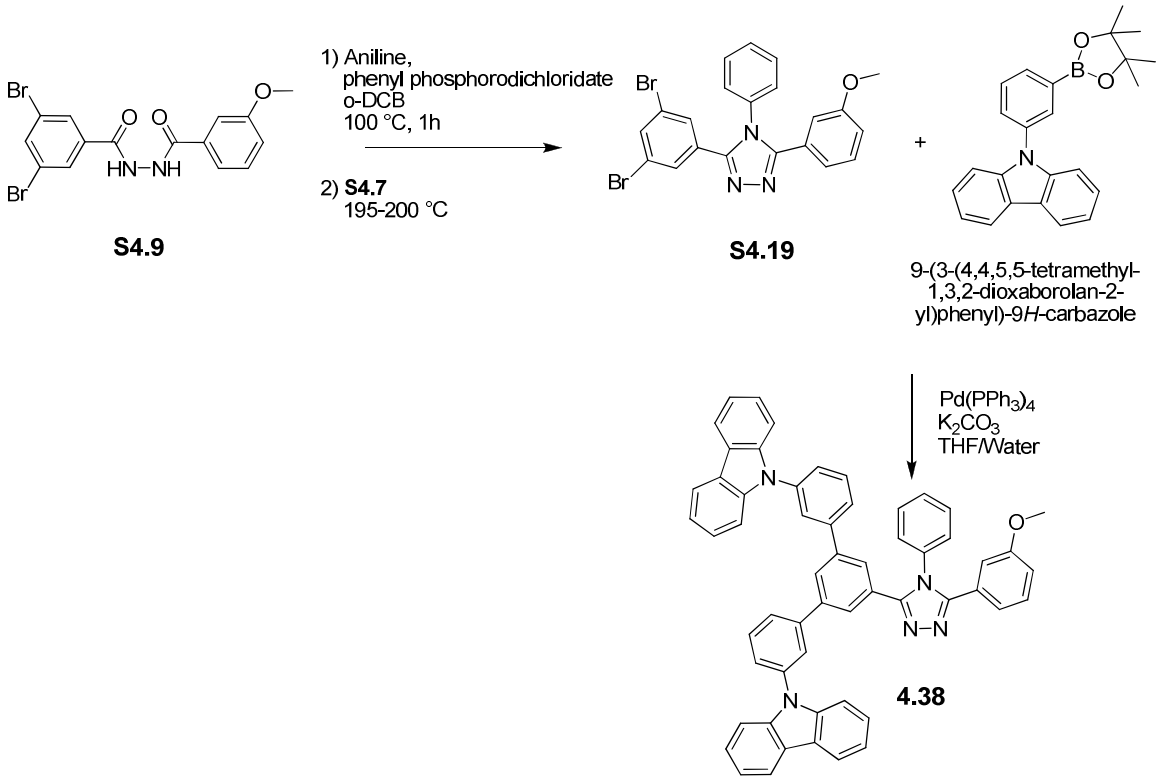

Scheme 4.8. Synthesis of triazole-based ambipolar small-molecule **4.38**.

Deprotection of the methoxy group to a hydroxyl group allowed for functionalization (as shown in the scheme below) of the molecule at the deprotected group to yield a norbornene monomer which was subsequently polymerized via ROMP.

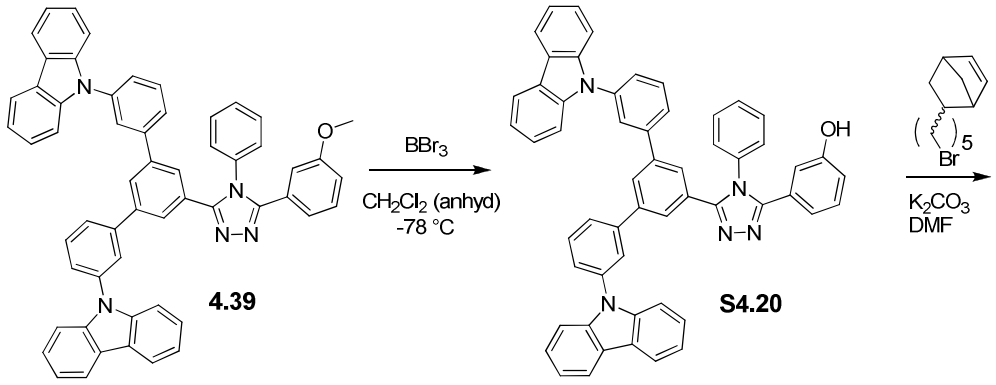

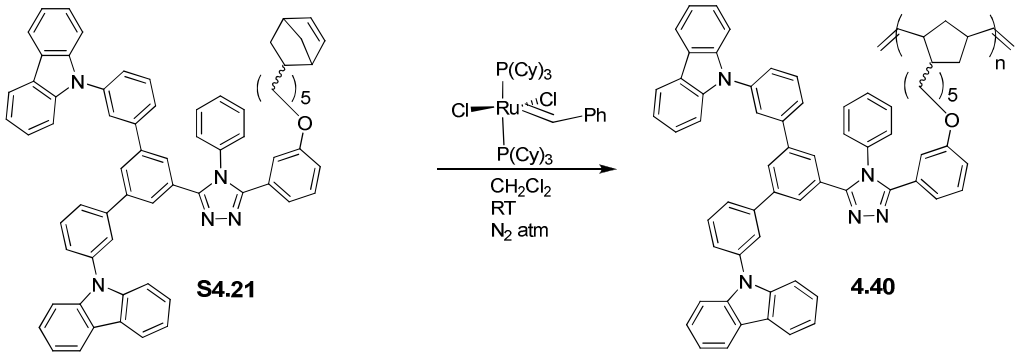

Scheme 4.9. Synthesis of triazole-based ambipolar side-chain polymer **4.40**.

All intermediates and ambipolar targets were characterized by ^{1}H NMR, ^{13}C NMR, mass spectrometry, and elemental analysis. For the polymers, ^{1}H NMR, gel permeation chromatography, and elemental analyses were performed. It is recognized that the polymers will not possess the level of purity achievable for the small-molecules (purified by chromatography). Full details are given in Chapter 2.

In summary, the small-molecule targets were designed to probe the effects of the different electron-transport heterocycles, the effects of a phenyl-spacer (to potentially decouple the hole- and electron- transport moieties), and the ratio of the transport groups. In addition, side-chain polymers were synthesized in order to study whether these molecules could be converted into solution-processable hosts without greatly affecting the properties of the ambipolar moieties.

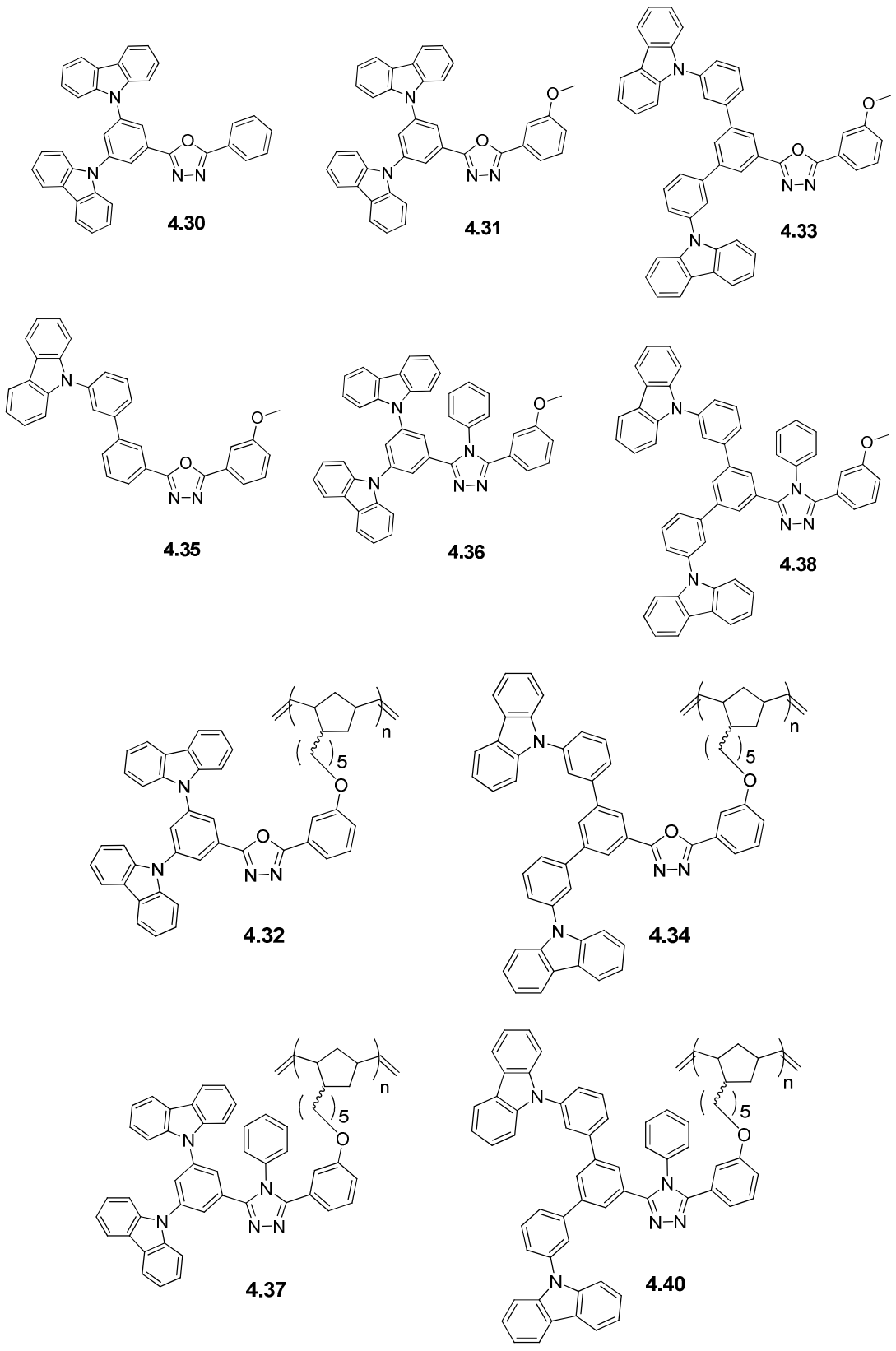

Figure 4.11. Summary of small molecules and polymers synthesized.

4.4.1 Thermal and Polymer Properties

Table 4.5 Thermal and Polymer Properties

Sample	M_w (kDa)[a]	M_n (kDa)[a]	PDI[a]	T_g (°C)[b]	T_c (°C)[b]	T_m (°C)[b]	T_d (°C)[c]
4.30	–	–	–	118.9	192.5	260.6	430.8
4.31	–	–	–	110.3	172.6	266.5	414.1
4.36	–	–	–	122.2	Not observed	248.9	417.6
4.33	–	–	–	122.3	Not observed	Not observed	433.4
4.38	–	–	–	132.7	Not observed	205.2	446.5
4.35	–	–	–	68.1	Not observed	131.9	391.7
4.32	60.0*	35.0*	1.71	157.5	Not observed	Not observed	412.0
4.37	22.9	15.8	1.45	169.3	Not observed	Not observed	418.9
4.40	29.0	19.3	1.50	161.6	Not observed	Not observed	428.9
4.34	37.7	19.5	1.94	160.8	Not observed	Not observed	423.0

[a] Calculated from gel permeation chromatography (in THF) vs. polystyrene standards

* in chloroform

[b] Determined from differential scanning calorimetry (10 °C/min)

[c] Determined from thermogravimetric analysis (at 5% weight loss)

For the small molecules and polymers, the data recorded from differential scanning calorimetry showed that all the samples (except **4.35**) possessed glass transitions above 100 °C; which are desirable for the stability of OLED device operation. Melting transitions were observed for all small molecules (except for **4.33**) and were observed to be above 200 °C (except for **4.35**). In addition, the melting transitions were observed only in the first scan and followed by glass transitions in the second scan; with the exception of **4.30** and **4.31**, where the glass transition, melting transition, and crystallization event were all observed in the same (second) heating. The presence of crystallization events for these molecules suggested that the materials may possess a mixed glassy and crystalline state, but their glass transitions should still be sufficiently high to permit use in OLED devices. The decomposition temperatures (at 5% weight

loss) for the small-molecules and polymers were found to be near or above 400 °C (except for **4.35**).

4.5. Photophysical Properties

4.5.1. UV-vis. Absorption Studies

The following figures show the normalized absorption at room temperature of the small-molecules in solution. Table 4.6 shows a summary of the absorption maxima of the spectra acquired.

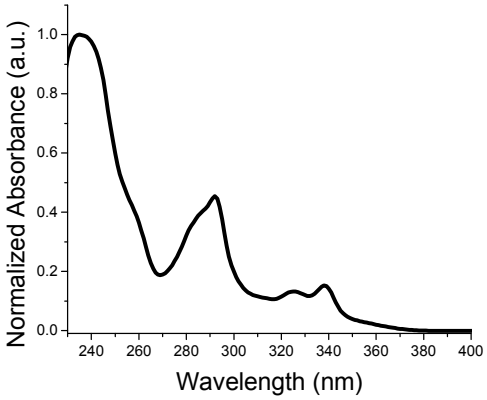

Figure 4.12. Room temperature UV-vis. absorption of **4.30** (in CH_2Cl_2).

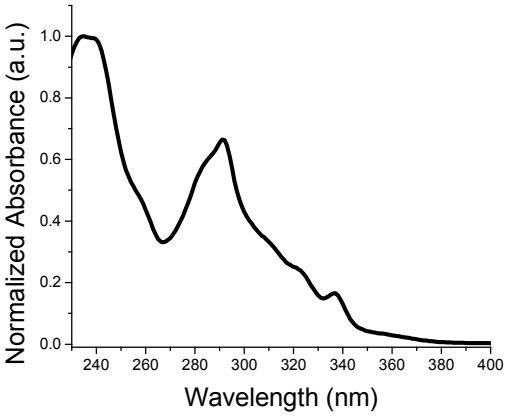

Figure 4.13. Room temperature UV-vis. absorption of **4.31** (in CH_2Cl_2).

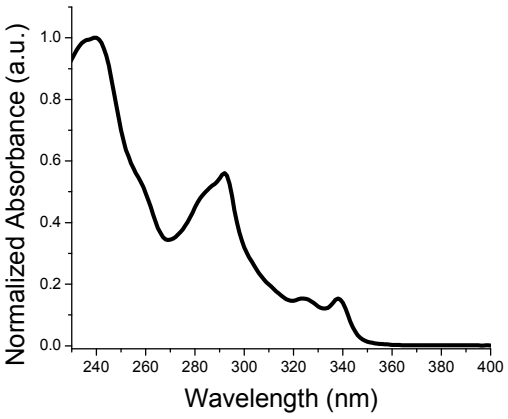

Figure 4.14. Room temperature UV-vis. absorption of **4.36** (in CH_2Cl_2).

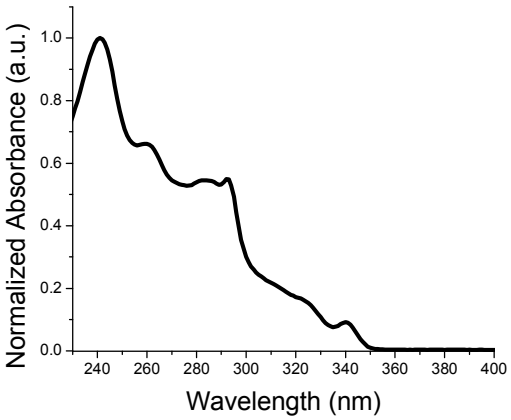

Figure 4.15. Room temperature UV-vis. absorption of **4.33** (in CH_2Cl_2).

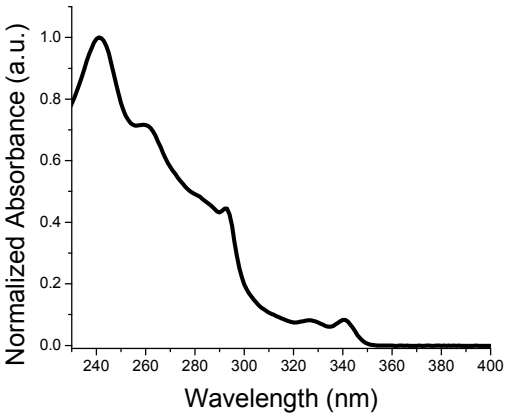

Figure 4.16. Room temperature UV-vis. absorption of **4.38** (in CH_2Cl_2).

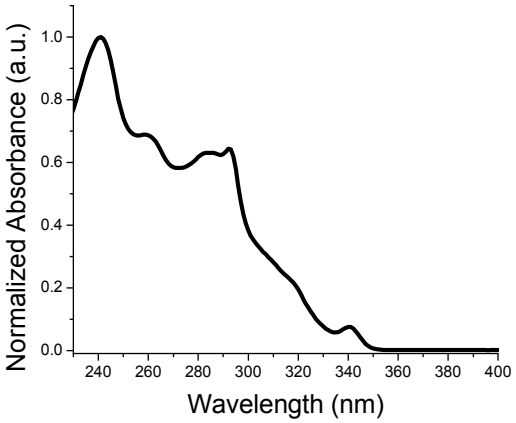

Figure 4.17. Room temperature UV-vis. absorption of **4.35** (in CH_2Cl_2).

Table 4.6 UV-vis. Properties (in solution)

Sample	λ_{max} (nm)[a]	Approx. Abs. Onset (nm)
4.30	235, 292, 325, 338	382
4.31	235, 291, 337	384
4.36	240, 292, 325, 338	363
4.33	241, 260, 283, 292, 340	354
4.38	241, 259, 292, 327, 340	356
4.35	241, 260, 284, 292, 339	356

[a] Measured at room temperature in dichloromethane

For all small-molecules, maxima *ca*. 240, 290, and 340 nm were observed. It was shown in a study by Bonesi *et al*.[35] that *9H*-carbazole and certain derivatives of carbazole absorb at these characteristic wavelengths (in solution and solid-state), originating from $\pi \rightarrow \pi^*$ transitions. Therefore, these may be assigned to carbazole moieties in the molecules.

Comparison of the oxadiazole-type molecules, **4.30** and **4.31**, showed a change in the spectral shape and relative strength of absorption between 275 – 350 nm for the two compounds, which implied an effect from the methoxy substituent. A more notable

observation was a weak absorption tail extending out beyond 350 nm that produced a red-shifted onset of absorption for both of these compounds to approximately 380 nm (as compared to the other molecules). Such an effect was observed in mCP-type polymers containing an electron withdrawing ester group on the benzene (to which the carbazoles were attached; see Chapter 3). In these molecules, a stronger charge-transfer effect between the carbazole and oxadiazole groups may explain the lower energy absorption. Triazole-based molecule **4.35** was found to be quite similar to **4.30**, but onset of absorption was closer to 360 nm suggesting charge-transfer effects may be weaker. The absence of the tail in absorption may originate from weaker donor-acceptor interaction between the triazole group (due to lower electronegativity of nitrogen) and carbazole and/or from a potential twisting effect between the moieties that disrupts planarity. Theoretical calculations on oxadiazole and triazole molecules, **4.31** and **4.36**, indicated that the ground-state geometry for the triazole should be more twisted out of plane from the phenyl group with peripheral carbazoles.

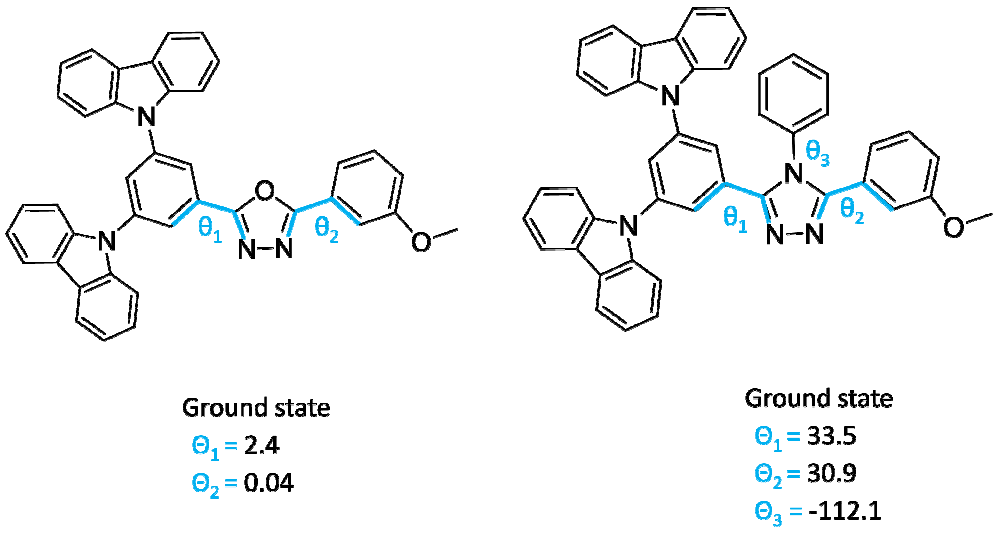

Figure 4.18. Dihedral angles for ground-state of **4.31** (left) and **4.36** (right) calculated from DFT (B3LYP/6-31G**). (Data courtesy of the Brédas group).

For the ambipolar molecules with a phenyl spacer, **4.33** and **4.35** (oxadiazole-based), and **4.38** (triazole-based) absorptions between 250 and 290 were noted with maxima occurring near 260 and 280 nm. For the oxadiazole-type molecules, onset of absorption was below 360 nm, with no evidence of a tail suggesting that the spacer may indeed weaken charge-transfer between the transport moieties (as compared to non-spaced molecules). For **4.38**, only a minor blue shift (< 10 nm) in onset was observed indicating the spacer did not have as large an effect.

4.5.2 Fluorescence and Phosphorescence Studies

Fluorescence of the small-molecules (in solution) and of thin-film of the polymers on glass substrates were obtained. The spectra shown in the figures below:

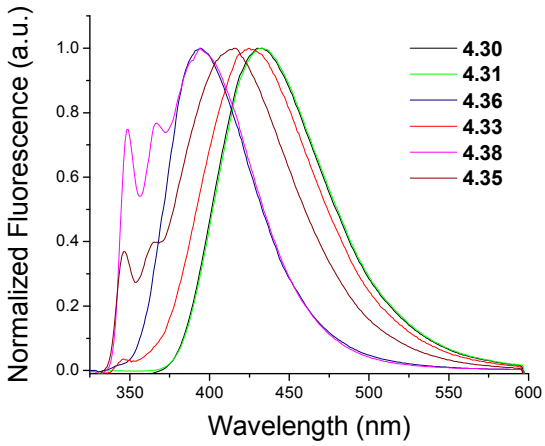

Figure 4.19. Room temperature fluorescence of all ambipolar small-molecules (in CH_2Cl_2; excitation at 300 nm).

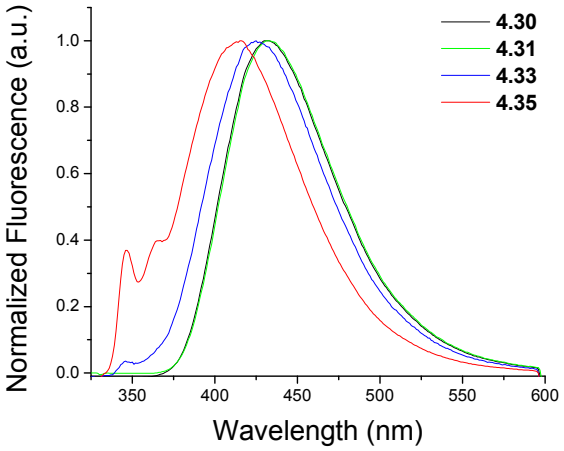

Figure 4.20. Comparison of room temperature fluorescence of oxadiazole-based small-molecules (in CH_2Cl_2; excitation at 300 nm).

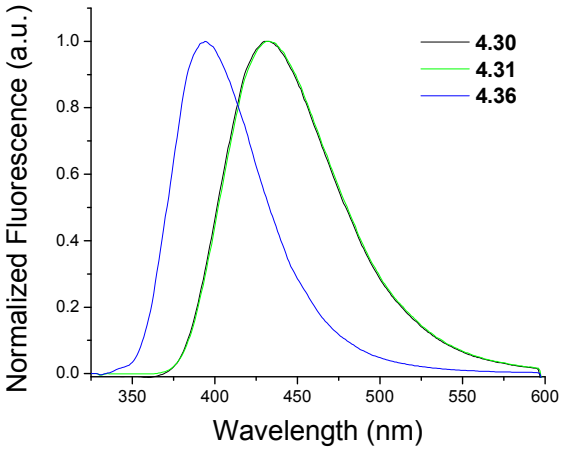

Figure 4.21. Comparison of room temperature fluorescence of non-phenyl spaced oxadiazole-based and triazole-based small-molecules (in CH_2Cl_2; excitation at 300 nm).

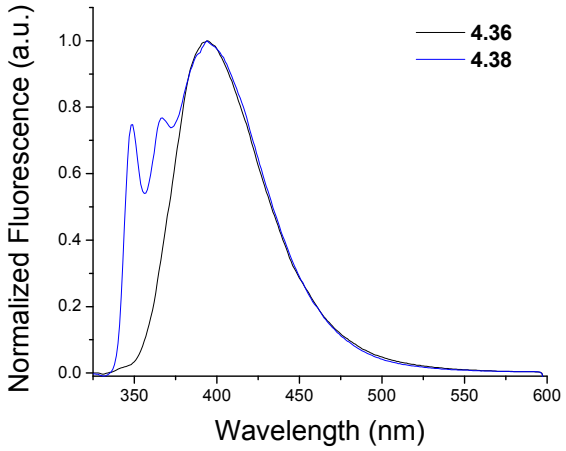

Figure 4.22. Comparison of room temperature fluorescence of triazole-based small-molecules (in CH_2Cl_2; excitation at 300 nm).

Table 4.7 Fluorescence of Small Molecules

Polymer	λ_{max}fluo (nm)
4.30	431
4.31	432
4.36	395
4.33	346*, 425
4.38	349, 367, 394
4.35	347, 365, 416

[a] dichloromethane at room temperature; excitation at 300 nm
* weak emission

All solution fluorescence measurements demonstrated that the molecules examined have emission in the blue region of the spectrum. For molecules, **4.30** and **4.31** demonstrated similar emission with a single maximum near 430 nm. Changing the heterocycle to triazole, as in **4.36**, resulted in an emission peak at 395 nm. As compared to **4.30** and **4.31**, the notable blue shift in emission (~ 35 nm) likely originates from a weaker electron affinity resulting in a wider optical gap (supported by electrochemical

data; vide infra); due to the presumably poorer electron accepting properties of triazoles vs. oxadiazoles.

Introduction of a phenyl spacer in the oxadiazole-type results in molecules that exhibited a modest hypsochromic shift and what may be a very weak emission (relative to the maximum) for molecule **4.33**. Interestingly, **4.35** (with a single phenyl spaced carbazole) showed a more complex and structured emission and a stronger hypsochromic shift to 416 nm with evident peaks at 347 and 365 nm. The structured emission of the phenyl-spaced molecules was investigated (see below). The peaks near 340 and 360 nm were conjectured to originate from the emission of phenyl carbazole portion of the molecule, as *N*-phenylcarbazole has reported emission peaks at 346 and 359 nm (in CH_2Cl_2).[35]

The introduction of the phenyl spacer in triazole-type targets, as in **4.38**, showed a maximum emission of 394 nm with additional peaks at 349 and 367 nm. Again, these were presumed to originate from the phenyl carbazole portion of the molecule. Comparing **4.36** to **4.38**, the broad emission maxima were found to be the same.

In order to study the origin of the structured emission spectra observed in some of the samples, excitation spectra were obtained for molecules **4.35** and **4.38**.

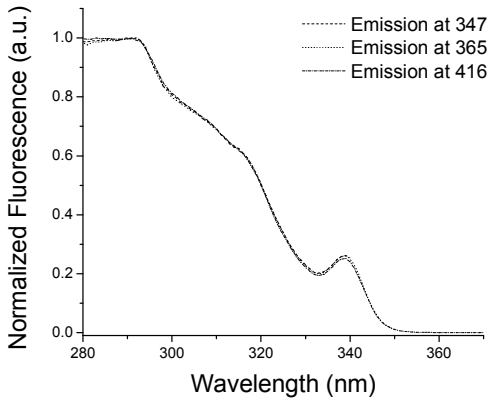

Figure 4.23. Excitation spectra of **4.35** (in CH_2Cl_2).

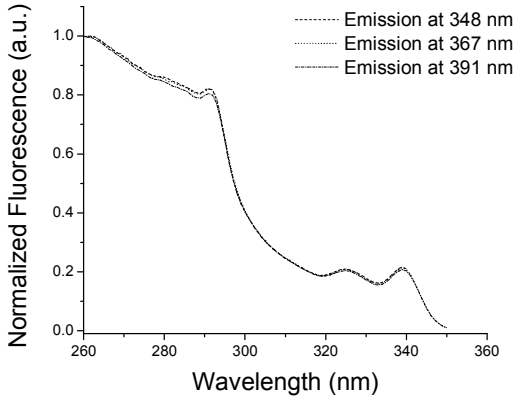

Figure 4.24. Excitation spectra of **4.38** (in CH_2Cl_2).

In both cases, the excitation spectra (taken at or near the maxima of emission of the molecules) indicated that emission originated from the same species; based on their similarity. In addition, the shapes of the spectra were noted to conform to those observed for absorption of the respective molecules. These data do not support the possibility that the peaks originated from an impurity or some other source. As the structured emission also showed lower energy broad emission peaks (assumed to originate from the charge-transfer state between carbazole and oxadiazole), an investigation of solvent polarity

effects was performed. Emission spectra were obtained for **4.33**, **4.35**, and **4.38** in cyclohexane and the data were as follows:

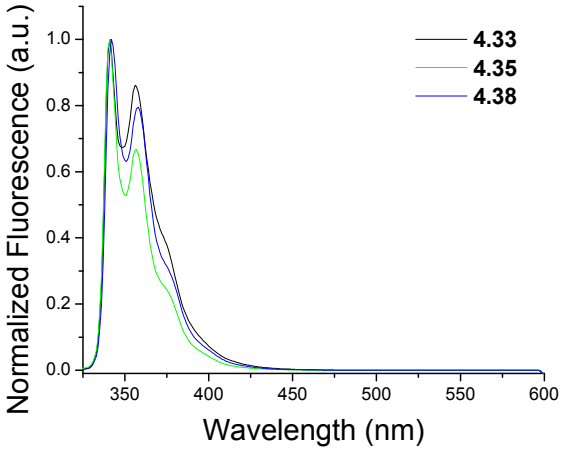

Figure 4.25. Comparison of room temperature fluorescence of phenyl-spaced molecules (in cyclohexane; excitation at 300 nm).

In all cases, the broad charge-transfer type emission peaks observed in dichloromethane were no longer observed and the maxima were all found to agree with the reported maxima of *N*-phenylcarbazole[35]; supporting the assumption that the structured emission observed originates from that component of the molecule. The spectrum of **4.38** taken in highly polar acetonitrile resulted in notable suppression of the structured emission peaks (although incomplete), while the broad charge-transfer type emission shifted to lower energy (maxima at 416 nm). For these molecules, therefore, the nature of the emission was found to be solvatochromic. Emission was found to originate from different excited states, either from the *N*-phenylcarbazole-type component or the from the charge-transfer state between carbazole donor and the electron heterocycle acceptor. Theoretical studies are planned to gain further insight into the origin of the dual fluorescence.

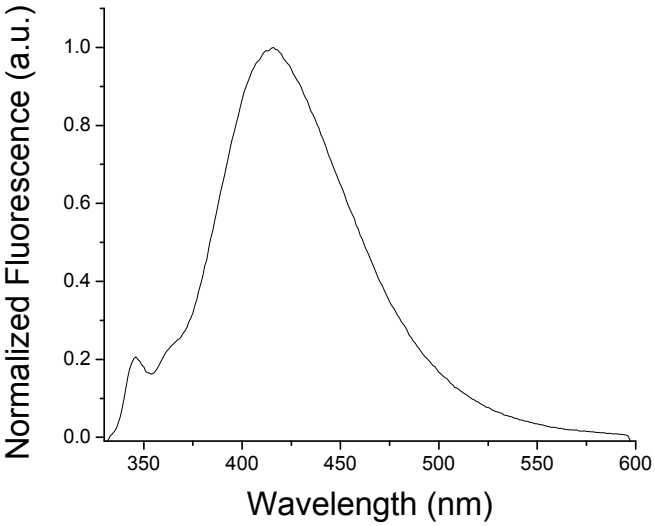

Figure 4.26. Comparison of room temperature fluorescence of **4.38** (in acetonitrile; excitation at 300 nm).

For the analoguous side-chain polymers, fluorescence of thin-films were obtained at room temperature. The thin-films were spin-coated onto glass slides from dichloromethane solutions (10 mg/mL).

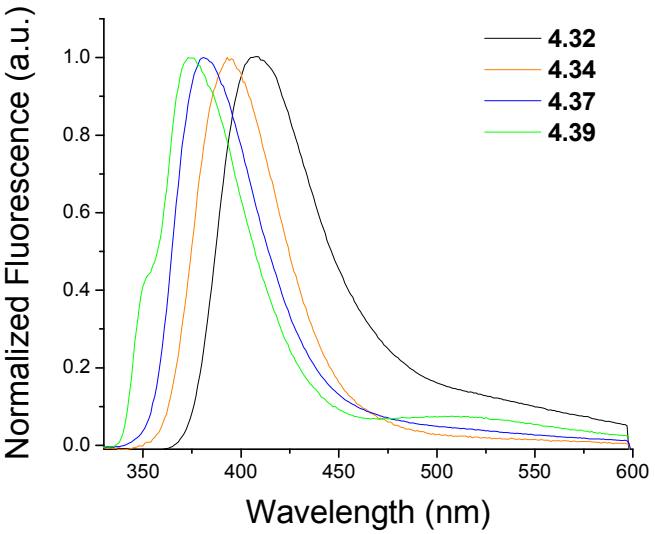

Figure 4.27. Room temperature fluorescence of ambipolar polymers as thin-films on glass (excitation at 300 nm).

Table 4.8 Fluorescence of Polymers (thin-films)

Polymer	λ_{max}fluo (nm)
4.32	408
4.37	381
4.34	394
4.40	374

[a] thin-films on glass; excitation at 300 nm

As compared to the small molecules in solution, all the thin-films were blue shifted between 15 – 25 nm (*vs.* the broad maxima observed in dichloromethane). It may be inferred that the solid-state film environment is less polar which may account for the effect. For **4.40**, thin-film emission showed a small shoulder near 350 nm which is consistent with the dual emission noticed in solution.

Phosphorescence studies of analogous compounds **4.31** (oxadiazole-based) and **4.37** (triazole-based) were performed by Solvay S.A. (by Dr. Jean-Pierre Catinat) and the spectra produced were found to be as follows:

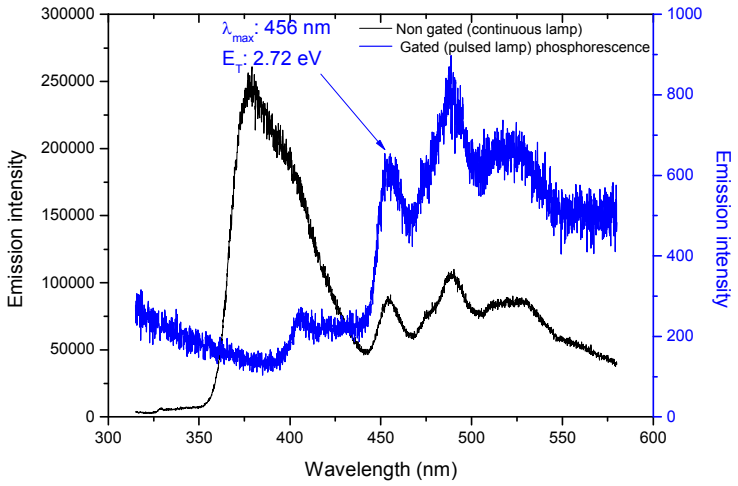

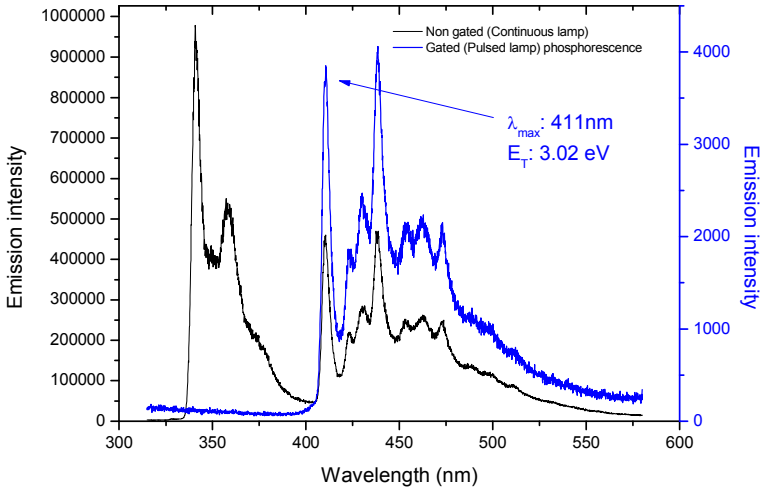

Figure 4.28. Phosphorescence (non-gated and gated) of **4.31** (top) and **4.36** (below) at 77K in 2-methyltetrahydrofuran (excitation at 300 nm).

From the gated phosphorescence spectra it was possible to estimate the adiabatic triplet state energy of the ambipolar molecules. The measured values revealed that **4.31** possessed an adiabatic E_T of 2.7 eV and **4.37** an E_T of 3.0 eV.

Table 4.9 Experimental and Calculated Triplet Energies

Molecule	E_T exp (eV)	E_T calc (eV)[b]
4.31	2.72[a]	2.63
4.37	3.02[a]	3.16
FIrpic	2.62[c]	2.70

[a] measured by phosphorescence (77K in 2-MeTHF)
[b] calculated by TDDFT (B3YLP/6-31G*)
[c] from reference [36]

Good agreement was found between the calculated energy values and trends determined from the calculations (provided by Dr. Lingyun Zhu in the Brédas group) to those measured experimentally. Furthermore, we can attribute the 0.3 eV increase in

triplet energy observed for **4.37** to the change from the oxadiazole to the triazole heterocycle. In either case, the triplet energy measured should prove adequate for hosting high triplet energy emitters for blue OLEDs (such as FIrpic).

4.6. Electrochemical Studies and Energy Level Estimations

The redox properties of the small-molecules were studied by cyclic voltammetry. The voltammograms are shown below and specific experimental details are given in Chapter 2.

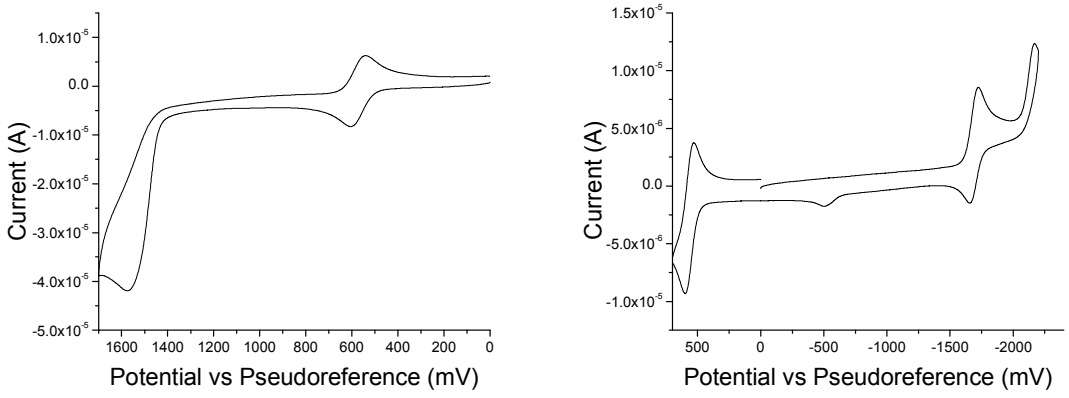

Figure 4.29. Cyclic voltammograms of **4.30** in dimethylformamide (vs. $FeCp_2^+$/ $FeCp_2$). Left: Oxidation; Right: Reduction.

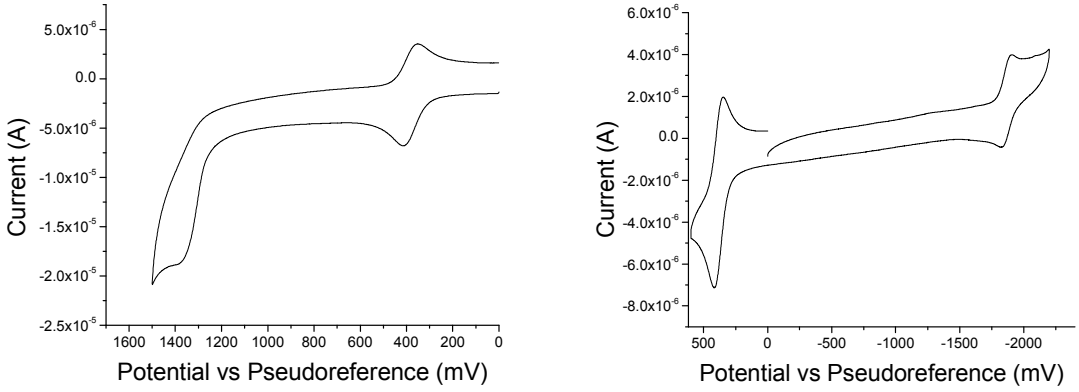

Figure 4.30. Cyclic voltammograms of **4.31** in dimethylformamide (vs. $FeCp_2^+$/ $FeCp_2$). Left: Oxidation; Right: Reduction.

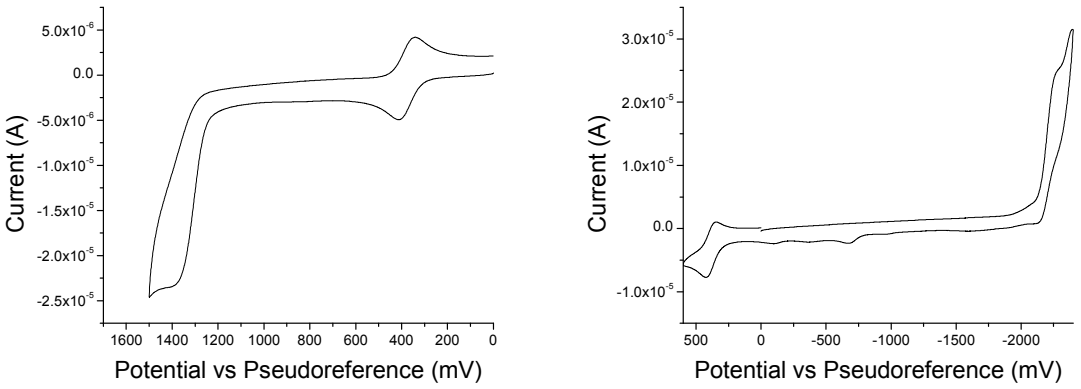

Figure 4.31. Cyclic voltammograms of **4.36** in dimethylformamide (vs. $FeCp_2^+$/ $FeCp_2$). Left: Oxidation; Right: Reduction.

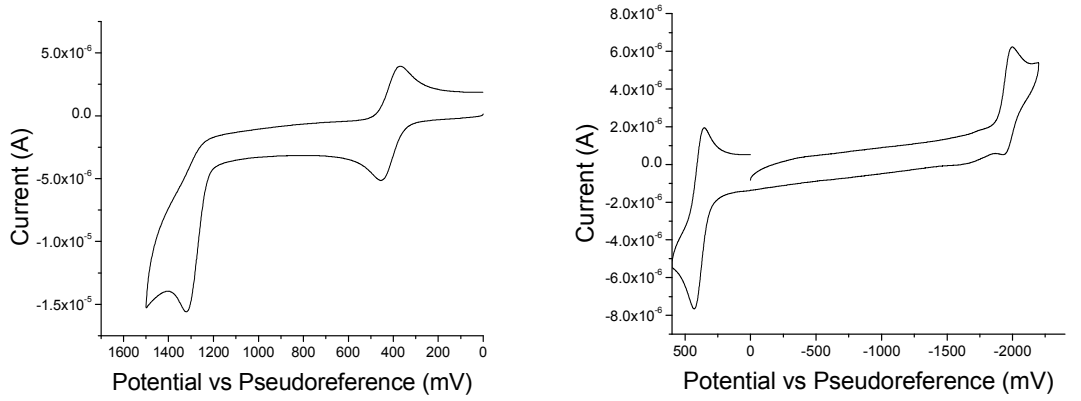

Figure 4.32. Cyclic voltammograms of **4.33** in dimethylformamide (vs. $FeCp_2^+$/ $FeCp_2$). Left: Oxidation; Right: Reduction.

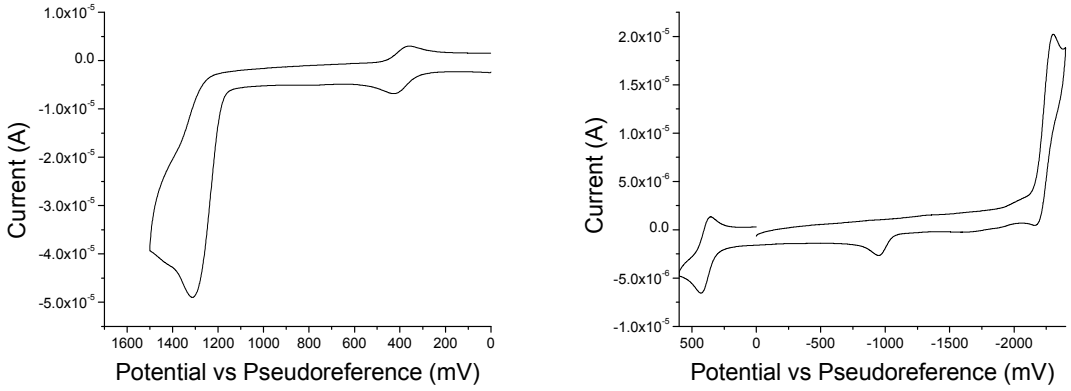

Figure 4.33. Cyclic voltammograms of **4.38** in dimethylformamide (vs. $FeCp_2^+$/ $FeCp_2$). Left: Oxidation; Right: Reduction.

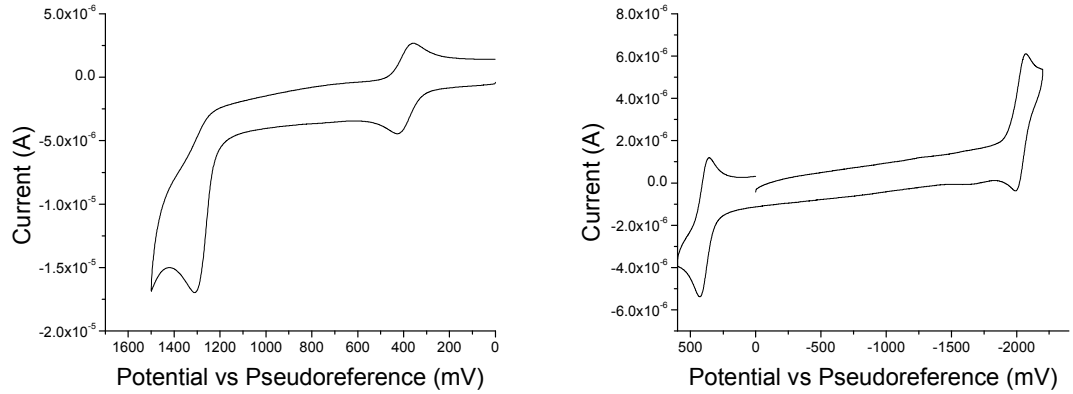

Figure 4.34. Cyclic voltammograms of **4.35** in dimethylformamide (vs. $FeCp_2^+$/ $FeCp_2$). Left: Oxidation ; Right: Reduction.

For all compounds, oxidations (vs. $FeCp_2^+$/ $FeCp_2$) were found to be fully irreversible and E_{ox} was assumed to be approximately equal to $E_{1/2}^{+/0}$ (for the first oxidation). For some compounds, reductions were reversible (or quasireversible) while others were found to be irreversible and $E_{1/2}^{0/-}$ was calculated from the maxima and minima of the reduction potential waves. For the irreversible reductions, E_{red} was assumed to be approximately equal to $E_{1/2}^{0/-}$.

The oxidation potentials measured for the ambipolar small molecules were all irreversible which was expected based on our experience with mCP-like groups (see Chapter 3) and the instability of radical cations of unsubstituted carbazoles.[13] The first oxidations were all quite close occurring near 1.0 V. A slight decrease was observed for the phenyl-spaced molecules (**4.33**, **4.35**, and **4.38**) that suggested that greater donor-acceptor separation might have an effect due to reduction of the electron-withdrawing effects from the electron transport heterocycle on carbazole.

The reduction potentials of the molecules were much more varied and found to be irreversible. The oxadiazole-type molecules **4.30** and **4.31** had reduction potentials of ~ -2.3 V with no measurable effect from the methoxy group on the latter molecule. The phenyl-spaced oxadiazole-based examples (**4.33** and **4.35**) were found to be slightly more difficult to reduce with reduction potentials *ca*. -2.4 V. Finally, the triazole-type molecules (**4.37** and **4.39**) were the most difficult to reduce with reduction potentials of ~ -2.7 V. In some reduction voltammograms (for **4.30**, **4.36**, and **4.38**), additional oxidation events were noted on the return scan between 0 and -1000 mV. These small peaks typically represent the oxidation events of new chemical specie(s) that can form during the redox process.

Table 4.10 Redox Properties and IP and EA Estimates

Sample	$E_{1/2}^{+/0}$ (V)[a,b]	$E_{1/2}^{0/-}$ (V)[a,b]	~ IP (eV)[c]	~ EA (eV)[c]
4.30	1.00	-2.25*	5.80	2.55
4.31	1.03	-2.25*	5.83	2.55
4.36	1.03	-2.67	5.83	2.13
4.33	0.92	-2.40	5.72	2.40
4.38	0.92	-2.70	5.72	2.10
4.35	0.92	-2.42*	5.72	2.38

[a] determined by cyclic voltammetry (vs. ferrocenium/ferrocene) ;
[b] for irreversible processes (assumed E_{ox} and $E_{red} \approx E_{1/2}^{+/0}$ and $E_{1/2}^{0/-}$)
[c] calculated from IP = ${}^{1}E_{1/2}$ + 4.8 and EA = ${}^{-1}E_{1/2}$ + 4.8
* reversible/quasireversible process

The redox data was used to estimate the ionization potential (IP) and electron affinity (EA) using the approximation that the solid-state ferrocenium/ferrocene couple relative to the vacuum level is reported at 4.8 eV.[37] Values were calculated from the equations IP = $E_{1/2}^{+/0}$ + 4.8 and EA = $E_{1/2}^{0/-}$ + 4.8. A study by Djurovich *et al*.[38] found that reduction potentials correlate with an r^2 of 0.92 to the inverse photoelectron spectroscopy (IPES) measured electron affinities. Therefore, the EA values estimated from the reduction potentials are in all likelihood superior to EAs estimated from the optical gap and IP. In estimations of EA from the IP plus the optical gap, the optical gap does not represent the transport gap (defined as difference between the IP and the EA energies) due to the exciton binding energy. As a result of the energy difference between the optical gap and the transport gap (up to 1 eV), the EAs estimated from the optical gap, therefore, do not represent the true EA.[39] The estimated values of the molecules are shown in the figure below for ease of comparison.

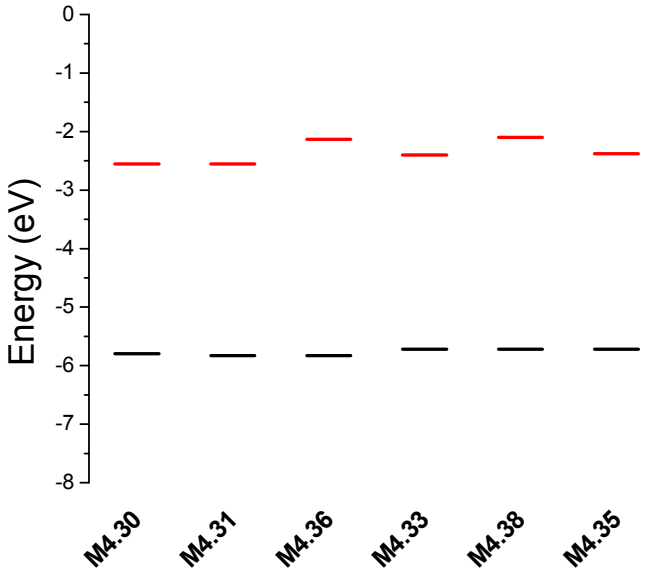

Figure 4.35. Energy diagram showing estimated IP(−) and EA(−) of ambipolar small-molecules.

The estimated IP levels were found to be quite similar for all the ambipolar molecules, suggesting that the HOMO is localized on the carbazole moieties of the molecules. The estimated EA levels of **4.30** and **4.31** were found to be the same at ~2.55 eV. The EAs of molecules **4.33** and **4.35** were smaller by ~0.15 eV and ~0.17 eV and may originate from a minor conjugation effect from the phenyl spacer group to the oxadiazole. For the triazole-based molecules, the estimated EAs were further reduced to ~2.1 eV which could be explained on the basis of the nitrogen in place of the oxygen resulting in poorer electron accepting properties for triazole. In a theoretical study by DFT (B3LYP/6-31+G*) of the molecules 2,5-diphenyl-1,3,4-oxadiazole and 3,5-diphenyl-4*H*-1,2,4-triazole reported by Jansson *et al*.[40] a similar decrease in the adiabatic electron affinity was calculated on exchanging oxadiazole to triazole (by ~ 0.3 eV).

4.7. OLED Devices of Selected Ambipolar Hosts

4.7.1 OLED Devices based on Host **4.30**

OLED devices were fabricated by Dr. Dengke Cai of the Kippelen group in the School of Electrical and Computer Engineering. Two different device architectures were explored with green or blue emitters. For all devices, all layers were vacuum processed (unless noted otherwise).

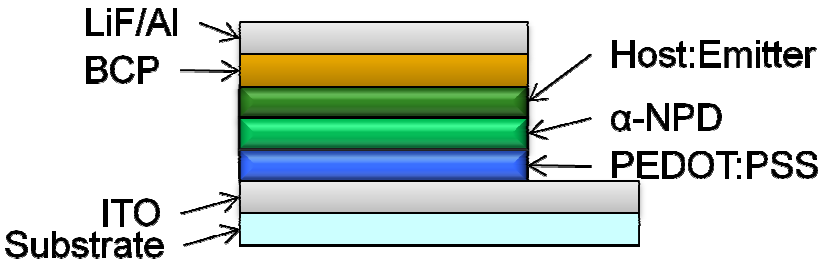

Figure 4.36. OLED device architecture I for study of host **4.30** (or **4.31**).

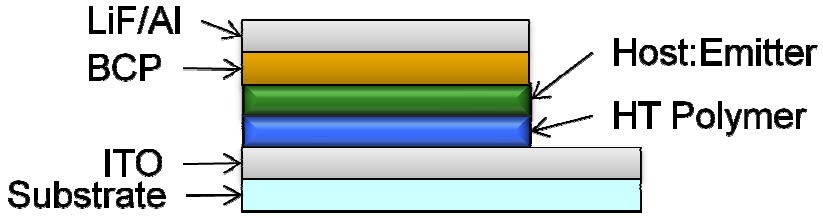

Figure 4.37. OLED device architecture II for study of host **4.30**.

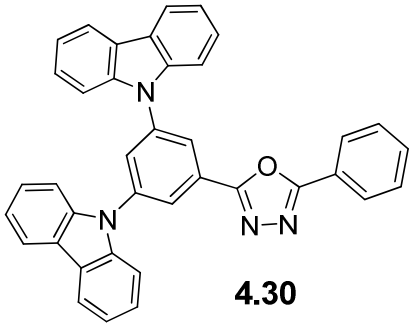

4.30

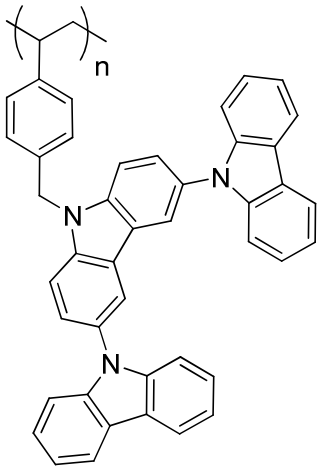

HT polymer

Figure 4.38. Ambipolar host **4.30** (right) and HT polymer (for architecture II devices).

Table 4.11. Host **4.30** for $Ir(ppy)_3$ devices with Architecture I

Device	Doping (wt%)	L (cd/m^2)	EQE (%)	LE (cd/A)	Turn on (V)[a]
A	6	100	14.6	43.1	2.7
	6	1,000	12.2	39.2	2.7
	6	10,000	8.8	30.3	2.7
	6	70,000	3.5	13	2.7
B	9	100	12.7	43	2.8
	9	1,000	11.2	38.9	2.8
	9	10,000	7.8	26.9	2.8
	9	70,000	4.1	14.7	2.8

[a] turn on voltages taken from *L-V* curves at 10 cd/m^2

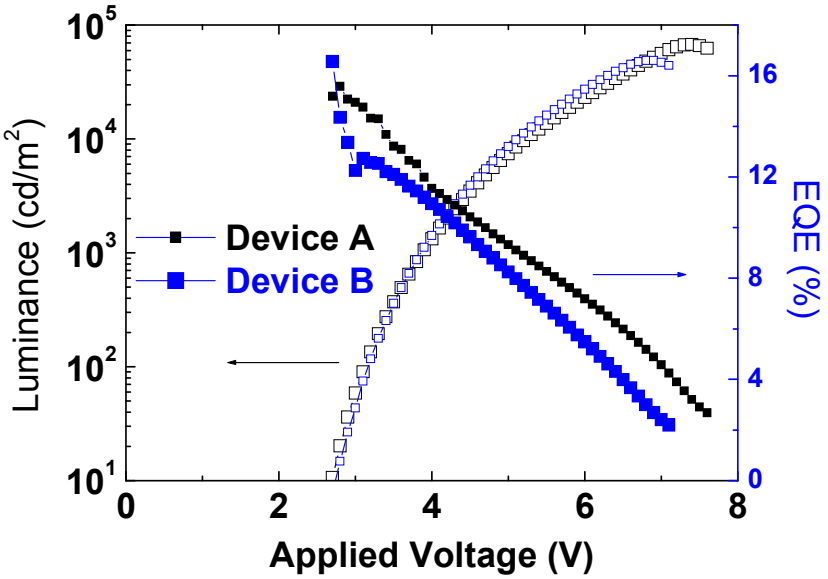

Figure 4.39. Luminance and external quantum efficiency as a function of applied voltage for devices A & B. Data courtesy of Dr. Dengke Cai (Kippelen group).

Devices with host **4.30** (based on architecture I) exhibited a maximum EQE of 14.6% at 100 cd/m^2. Decreased efficiencies were observed at higher brightnesses consistent with roll-off effects.[41] An increase in the doping level of the $Ir(ppy)_3$ resulted in decreased performance and a very slight increase in the turn on voltages. The decreased efficiency may be the result of increased concentration quenching events at higher doping levels (through triplet-triplet annihilation).

Architecture II with a solution-processed hole transport polymer (see figure 4.32 above) was also studied. The results were as follows:

Table 4.12. Host **4.30** for $Ir(ppy)_3$ devices with Architecture II

Device	Doping (wt%)	L (cd/m^2)	EQE (%)	LE (cd/A)	Turn on (V)[a]
C	6	100	16.6	56.8	3.0
	6	1,000	15.6	53.5	3.0
	6	10,000	11.9	40.8	3.0
D	9	100	13.2	44.6	3.3
	9	1,000	12.4	42.3	3.3
	9	10,000	8.8	30.0	3.3

[a] turn on voltages taken from *L-V* curves at 10 cd/m^2

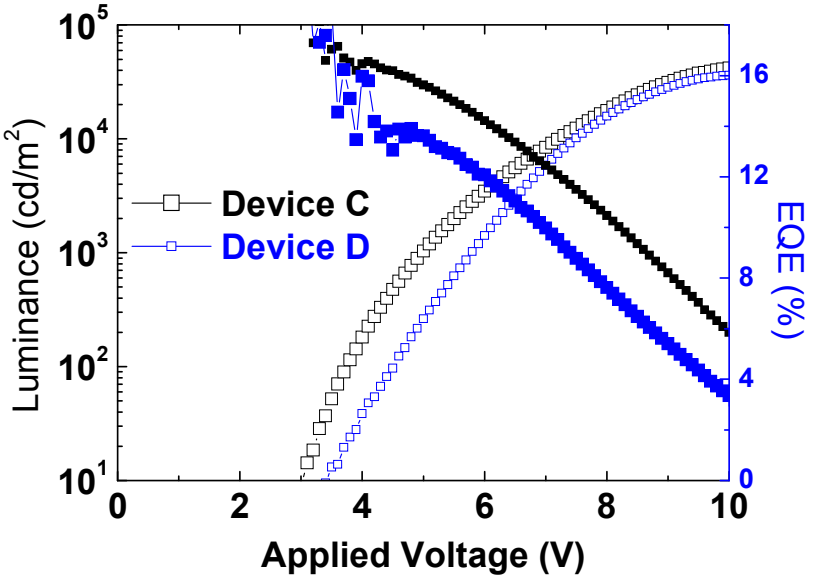

Figure 4.40. Luminance and external quantum efficiency as a function of applied voltage for devices C & D. Data courtesy of Dr. Dengke Cai (Kippelen group).

Although devices with this architecture were found to be slightly more efficient than those with architecture I, the difference was not remarkable. Increased doping level of the emitter was again noted to produce devices with decreased efficiencies presumably due to concentration quenching.

Blue FIrpic devices were also fabricated with either architecture III or IV as shown in the figures:

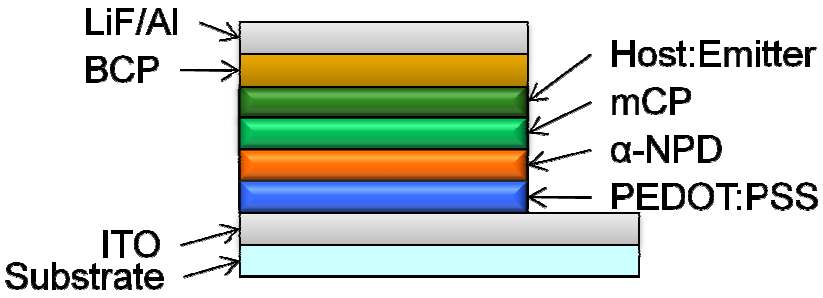

Figure 4.41. OLED device architecture III for study of host **4.30** (or **4.36**).

Table 4.13. Host **4.30** for FIrpic devices with Architecture III

Device	mCP thickness (nm)	L(cd/m^2)	EQE (%)	LE (cd/A)	PE (lm/W)	Turn on (V)[a]
E	5	100	0.66	2.24	–	3.2
	5	1,000	0.71	2.42	–	3.2
	5	10,000	0.51	1.8	–	3.2
F	10	100	2.4	7.5	–	3.1
	10	1,000	2.2	7.6	–	3.1
	10	10,000	1.6	5.5	–	3.1
G	15	100	11.4	39	35	3.0
	15	1,000	10.9	37.1	27.5	3.0
	15	10,000	3.7	13	6.7	3.0

[a] turn on voltages taken from *L-V* curves at 10 cd/m^2

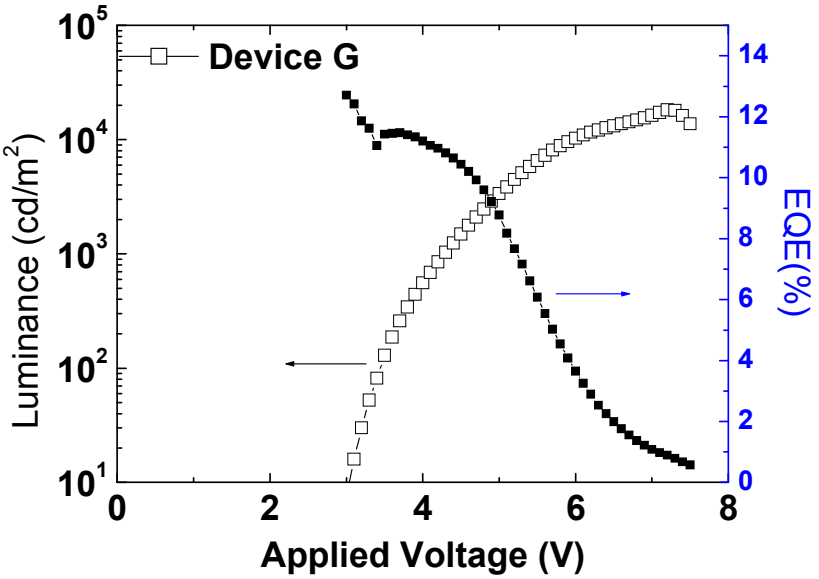

Figure 4.42. Luminance and external quantum efficiency as a function of applied voltage for device G. Data courtesy of Dr. Dengke Cai (Kippelen group).

The effect of introducing **mCP** as a triplet exciton blocker to confine the emission zone was studied and the effect on device performance (with architecture III) were notable. At 5 nm of **mCP** thickness, very low efficiency devices were obtained that were improved by doubling the **mCP** layer thickness to 10 nm. The best blue devices were obtained with an mCP thickness of 15 nm with a maximum EQE of 11.4% at 100 cd/m^2. The efficiency did not drop significantly at a higher brightness of 1,000 cd/m^2 remaining near 11%. At 10,000 cd/m^2, the efficiency dropped to 3.7%. The luminance and EQE curves are shown in the figure above.

Blue devices with architecture IV incorporated a solution-processed HT polymer (see figure 4.32) were also studied.

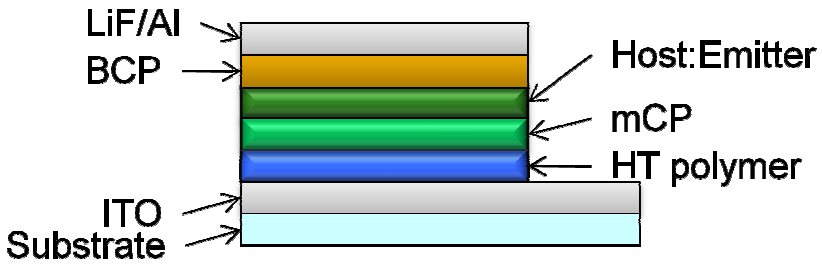

Figure 4.43. OLED device architecture IV for study of host **4.30** (or **4.36**).

Table 4.14. Host **4.30** for FIrpic (10 wt%) devices with Architecture IV

Device	mCP thickness (nm)	L(cd/m^2)	EQE (%)	LE (cd/A)	PE (lm/W)	Turn on (V)[a]
H	no mCP	100	12.7	43.2	39.2	3.0
	no mCP	1,000	11.2	38.7	28.6	3.0
	no mCP	10,000	5.4	18.7	9.5	3.0
I	no mCP*	100	6.2	21.1	14.7	–
	no mCP*	1,000	5.1	17.4	8.8	–
J	5	100	11.3	39.1	35.1	3.1
	5	1,000	9.6	32.8	23.7	3.1
	5	10,000	2.9	9.9	4.6	3.1

[a] turn on voltages taken from *L-V* curves at 10cd/m^2
* 15 wt% emitter

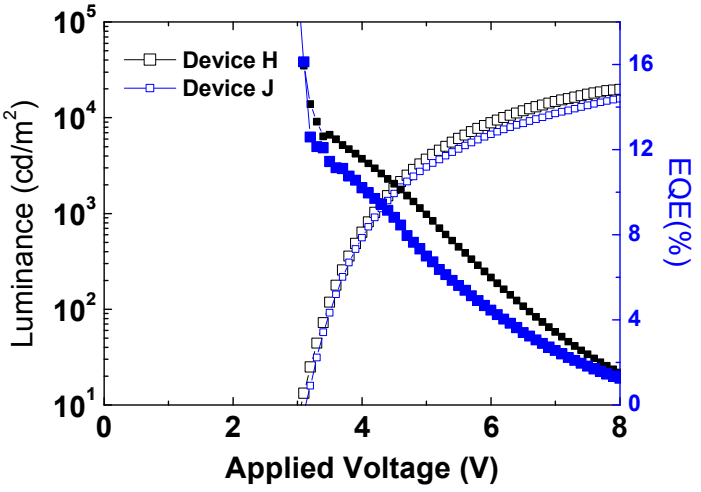

Figure 4.44. Luminance and external quantum efficiency as a function of applied voltage for devices H & J. Data courtesy of Dr. Dengke Cai (Kippelen group).

For devices with this architecture, the effect of a layer of **mCP** as a triplet exciton blocker was also evaluated. For a device with no **mCP** layer (at 10 wt% emitter doping), a maximum EQE of 12.7% at 100 cd/m^2 was recorded and were slightly superior to those observed with architecture III (with 15 nm of **mCP**). The use of **mCP** in the prior blue devices with architecture III was predicated on its ability to act as a triplet exciton blocker. This rationale was based on the low triplet energy of α-NPD (reported to be ~2.3 eV)[42], while that of **mCP** is much higher (~2.9 eV).[43] It is possible that the HT polymer used in architecture IV may possess a sufficiently high triplet energy to preclude the need for a separate triplet exciton blocking layer. A device with a thin layer of **mCP** demonstrated slightly poorer device performance. Increasing the doping level to 15 wt% of FIrpic (with no **mCP** layer) resulted in a reduction in efficiency by approximately half and was attributed to concentration quenching.

4.7.2. OLED Devices based on Host **4.31**

Green devices with host **4.31** were also evaluated with architecture I and were found to similar device performance as compared to host **4.30** with the same architecture.

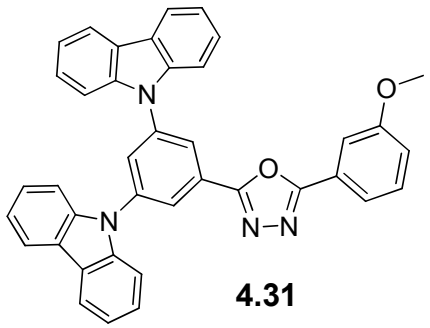

4.31

Figure 4.45. Ambipolar host **4.31**.

Table 4.15 Host **4.31** for $Ir(ppy)_3$ device with Architecture I

Doping (wt%)	L (cd/m^2)	EQE (%)	Turn on (V)[a]
6	100	15.0	2.8
6	1,000	13.5	2.8
6	10,000	10.5	2.8

[a] turn on voltages taken from *L-V* curves at 10 cd/m^2

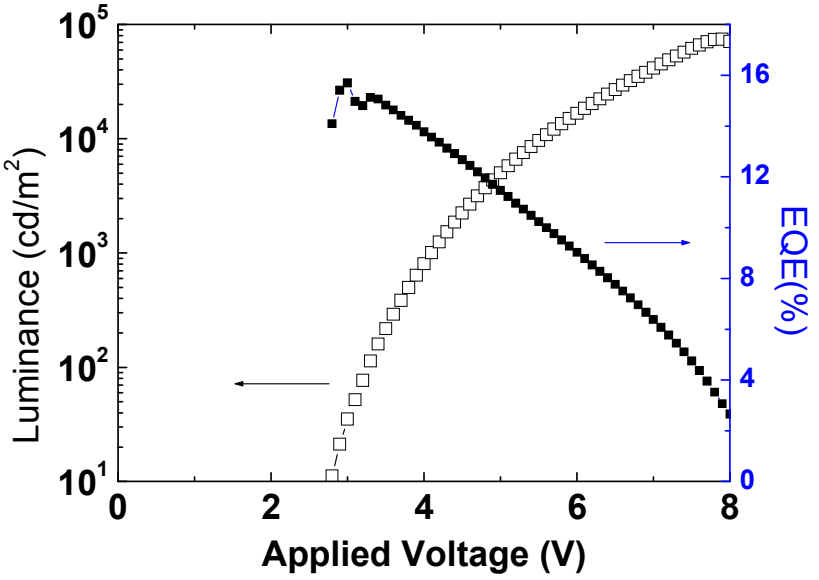

Figure 4.46. Luminance and external quantum efficiency as a function of applied voltage for devices A & C. Data courtesy of Dr. Dengke Cai (Kippelen group).

Slightly higher efficiencies were observed for host **4.31**, but it was difficult to attribute any high degree of significance to the observed values. The minor efficiency differences observed, therefore, might be attributed to batch effects, as the devices were fabricated at different times.

4.7.3 OLED Devices Based on Host **4.36**

Blue devices with triazole-based host **4.36** were studied using either architectures III or IV. The device efficiencies are shown in the tables below.

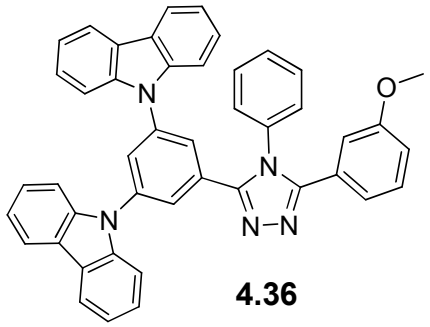

4.36

Figure 4.47. Ambipolar host **4.36**.

Table 4.16 Host **4.36** for FIrpic blue device with Architecture III (with 15 nm mCP layer)

Doping (wt%)	L (cd/m^2)	EQE (%)	LE (cd/A)	PE (lm/W)	Turn on (V)[a]
10	100	6.6	36.1	32.4	3.1
10	1,000	6.7	36.9	25.7	3.1
10	10,000	4.9	27.2	14.3	3.1

[a] turn on voltages taken from *L-V* curves at 10 cd/m^2

Table 4.17 Host **4.36** for FIrpic blue device with Architecture IV (with 15 nm mCP layer)

Doping (wt%)	L (cd/m^2)	EQE (%)	LE (cd/A)	PE (lm/W)	Turn on (V)[a]
10	100	5.2	17.7	16.4	3.0
10	1,000	8.9	30.4	21.6	3.0
10	10,000	8.4	28.8	14.8	3.0

[a] turn on voltages taken from *L-V* curves at 10 cd/m^2

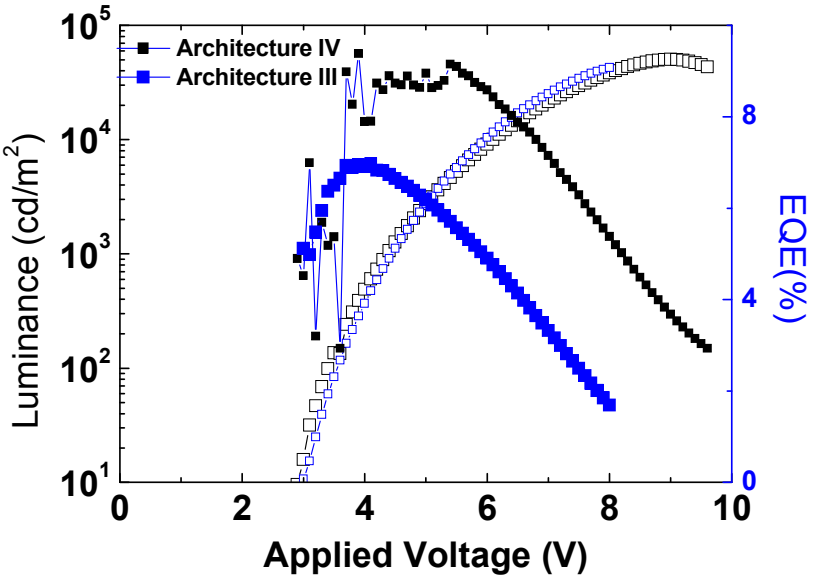

Figure 4.48. Luminance and external quantum efficiency as a function of applied voltage for **4.36** devices with architectures III or IV. Data courtesy of Dr. Dengke Cai (Kippelen group).

For a device with architecture III (with a 15 nm mCP layer), the efficiency at 100 cd/m^2 was approximately half the values obtained using **4.30** in an analogous architecture. At 1,000 cd/m^2, the device efficiency remained stable but at 10,000 cd/m^2 the efficiency reduced to 4.9%. A device with architecture IV (with a 15 nm **mCP** layer) gave an efficiency of 5.2% at 100 cd/m^2 but interestingly demonstrated higher EQEs of 8.9 and 8.4% at higher luminance levels of 1,000 and 10,000 cd/m^2. The LE and PE values of 28.8 cd/A and 14.8 lm/W were also the highest obtained for any of the blue devices measured at 10,000 cd/m^2. As noted before, this device contained an **mCP** layer. For host **4.30**, the use of a 5 nm layer of **mCP** actually reduced the device performance significantly and no **mCP** produced the best device (see Table 4.14). Therefore, the values obtained for architecture IV with **4.37** may not represent the maximum

efficiencies that could be obtained and a device without **mCP** should be fabricated for comparison.

4.8. Conclusions

It was shown that several examples of potentially ambipolar small molecules containing both carbazole (hole transport) and either oxadiazole or triazole (electron transport) heterocycles could be synthesized successfully. The syntheses of these targets required multiple steps but several common precursors (amongst some of the targets) facilitated the syntheses. For the triazole targets, issues of oxadiazole formation, as the major product, were addressed. The design of these molecules incorporated approaches to reduce the likelihood of charge-transfer between the hole and electron transport moieties by *meta*- conjugation or the addition of spacers. Solution-processable hosts, were pursued by functionalization of certain small molecules with a norbornene group followed by ring opening metathesis polymerization. These polymers were processed as thin-films and their fluorescence was studied.

The photophysical properties of the ambipolar materials were examined. The UV-vis. data revealed that absorption was mostly associated with the carbazole groups. For some of the oxadiazole-based molecules, evidence of charge-transfer was observed in the spectra that could be reduced by modification (i.e., by introduction of a phenyl spacer) to increase the distance between the donor and acceptor moieties. Fluorescence spectra for the molecules (in solution) showed that they were all blue in emission. The triazole-type hosts emitted at higher energies than the oxadiazole-type hosts due to the difference in the EA energies between the two heterocycles studied (see estimated EA energies in

figure 4.29). For the oxadiazole molecules, **4.33** and **4.35**, the introduction of a phenyl spacer produced hypsochromic shifts (~0.05 – 0.1 eV) in the emission maximum, as compared the non-spaced molecules (**4.30** and **4.31**). Such an effect could originate from reduced interaction of the carbazole and oxadiazole groups. In the case of the triazoles, comparison of **4.36** to the phenyl spaced analogue **4.38** showed that the spacer group did not produce any shift in the emission maximum. In addition, dual fluorescence was observed in the phenyl-spaced molecules that was studied by excitation spectra and spectra obtained in solvents of different polarities. Thin-films of the polymeric analogues of some of the small-molecules were obtained by spin-coating and blue emission was observed. Phosphorescence at 77 K for molecules **4.31** and **4.36** showed that the triazole possessed a higher triplet energy (by ~0.3 eV) *vs*. that of **4.31**, which was ~2.7 eV. Both hosts should still have sufficiently high triplet energies to host blue emitters. Therefore, the type of heterocycle used in these molecules can offer some control of the triplet energy.

Cyclic voltammetry measurements showed that the oxidation potential of the ambipolar targets were all irreversible and approximately similar (~ 1.0 V). The reduction potentials were notably affected by the nature of the electron transport heterocycle. In the case of triazole-type molecules, the reductions were observed to be more difficult than those of the oxadiazole-type molecules by up to ~ 0.45 V. To a lesser extent, the reduction potential for the oxadiazole-type molecules was noted to increase by ~ 0.15 V upon insertion of a phenyl spacer. The same effect was not observed for the triazoles.

Molecules **4.30**, **4.31**, and **4.36** were used as vacuum-processed hosts in green and blue PhOLED devices (fabricated by the Kippelen group) with a variety of architectures (vide supra). For these devices, efficiencies up to 16.6% (for green) and 12.7% (for blue) were obtained in unoptimized devices suggesting that the ambipolar molecules may be promising host materials. Gong *et al.*[21] reported a green device with an ambipolar host and a maximum EQE of 18.7% using a fully vacuum-processed architecture. The best blue device using an ambipolar host was reported by Su *et al.*[22] with a maximum EQE of 22.6%, but the architecture could be considered complex.

Molecules containing moieties combining hole and electron transport groups were designed, synthesized, and studied for use as hosts for phosphorescent emitters. From the studies, it is possible to draw some general conclusions about the modifications used in these types of molecules as summarized below.

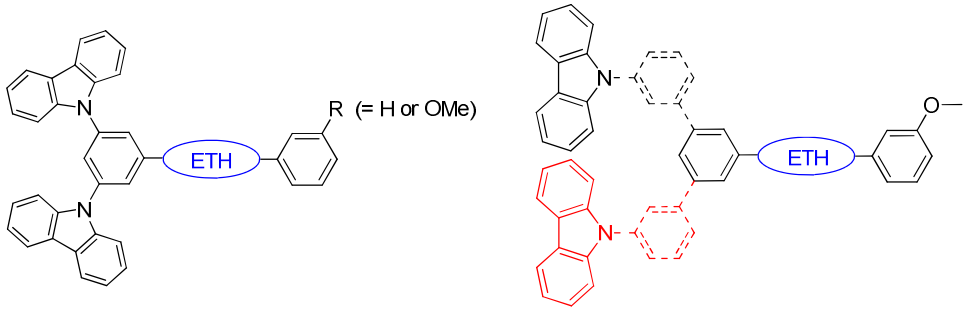

Molecular Modification	Observed Effect
ETH: Oxadiazole *vs.* Triazole	Can influence electron affinity and triplet energy
Phenyl Spacer	Can decrease strength of donor-acceptor interaction
One arm *vs.* Two arms	Modifies emission maximum

Figure 4.49. Summary of molecular modifications and their effects on hosts (where ETH is an electron transport heterocycle).

Although it was shown that the charge transport groups could be successfully combined onto a single molecule, additional studies on the mobilities (hole and electron) should be examined to ascertain how well each carrier is transported. Work on additional OLED devices using the remaining untested small-molecules and polymers should also be pursued.

4.9. References

(1) Naka, S.; Okada, H.; Onnagawa, H.; Yamaguchi, Y.; Tsutsui, T. *Synth. Met.* **2000**, *111-112*, 331-333.

(2) So, F.; Krummacher, B.; Mathai, M. K.; Poplavskyy, D.; Choulis, S. A.; Choong, V.-E. *J. Appl. Phys.* **2007**, *102*, 091101.

(3) Kondakov, D. Y.; Sandifer, J. R.; Tang, C. W.; Young, R. H. *J. Appl. Phys.* **2002**, *93*, 1108-1119.

(4) Brutting, W.; Riel, H.; Beierlein, T.; Riess, W. *J. Appl. Phys.* **2001**, *89*, 1704-1712.

(5) Baldo, M. A.; Adachi, C.; Forrest, S. R. *Phys. Rev. B* **2000**, *62*, 10967-10977.

(6) Kim, S. H.; Jang, J.; Yook, K. S.; Lee, J. Y. *Appl. Phys. Lett.* **2008**, *92*, 023513.

(7) Adachi, C.; Tsutsui, T.; Saito, S. *Appl. Phys. Lett.* **1989**, *55*, 1489-1491.

(8) Hamada, Y.; Adachi, C.; Tsutsui, T.; Saito, S. *Jpn. J. Appl. Phys.* **1992**, *31*, 1812-1816.

(9) Guan, M.; Bian, Z. Q.; Zhou, Y. F.; Li, F. Y.; Li, Z. J.; Huang, C. H. *Chem. Commun.* **2003**, *2003*, 2708-2709.

(10) *Physics of Organic Semiconductors*; Brutting, W., Ed.; Wiley-VCH Verlag GmbH & Co. : Weinheim, 2005.

(11) Guan, M.; Chen, Z. Q.; Bian, Z. Q.; Liu, Z. W.; Gong, Z. L.; Baik, W.; Lee, H. J.; Huang, C. H. *Org. Elect.* **2006**, *7*, 330-336.

(12) Tao, Y.; Wang, Q.; Yang, C.; Wang, Q.; Zhang, Z.; Zou, T.; Qin, J.; Ma, D. *Angew. Chem. Int. Ed.* **2008**, *47*, 8104-8107.

(13) Ambrose, J. F.; Nelson, R. F. *J. Electrochem. Soc.* **1968**, *115*, 1159-1164.

(14) Tao, Y.; Wang, Q.; Ao, L.; Zhong, C.; Qin, J.; Yang, C.; Ma, D. *J. Mater. Chem.* **2010**, *20*, 1759-1765.

(15) Tao, Y.; Wang, Q.; Shang, Y.; Yang, C.; Ao, L.; Qin, J.; Ma, D.; Shuai, Z. *Chem. Commun.* **2009**, 77-79.

(16) Kido, J.; Ohtaki, C.; Hongawa, K.; Okuyama, K.; Nagai, K. *Jpn. J. Appl. Phys.* **1993**, *32*, L917-L920.

(17) Kim, J. H.; Yoon, D. Y.; Kim, J. W.; Kim, J.-J. *Synth. Met.* **2007**, *157*, 743-750.

(18) Kim, M. K.; Kwon, J.; Kwon, T.-H.; Hong, J.-I. *New J. Chem.* **2010**, *34*, 1317-1322.

(19) Gao, Z.; Lee, C. S.; Bello, I.; Lee, S. T.; Chen, R.-M.; Luh, T.-Y.; Shi, J.; Tang, C. W. *Appl. Phys. Lett.* **1999**, *74*, 865-867.

(20) Takizawa, S.; Montes, V. A.; Anzenbacher, J., P. *Chem. Mater.* **2009**, *21*, 2452-2458.

(21) Gong, S.; Zhao, Y.; Yang, C.; Zhong, C.; Qin, J.; Ma, D. *J. Phys. Chem. C* **2010**, *114*, 5193-5198.

(22) Su, S.-J.; Sasabe, H.; Takeda, T.; Kido, J. *Chem. Mater.* **2008**, *20*, 1691-1693.

(23) Adachi, C.; Kwong, R.; Forrest, S. *Org. Elect.* **2001**, *2*, 37-43.

(24) Jeon, J. Y.; Park, T. J.; Jeon, W. S.; Park, J. J.; Kwon, J. H.; Lee, J. Y. *Chem. Lett.* **2007**, *36*, 1156-1157.

(25) Yeh, K.-M.; Lee, C.-C.; Chen, Y. *J. Polym. Sci.: Part A: Polym. Chem.* **2008**, *46*, 5180-5193.

(26) Debeaux, M.; Thesen, M. W.; Schneidenbach, D.; Hopf, H.; Janietz, S.; Kruger, H.; Wedel, A.; Kowalsky, W.; Johannes, H.-H. *Adv. Funct. Mater.* **2009**, *19*, 1-10.

(27) Furuta, P. T.; Deng, L.; Garon, S.; Thompson, M. E.; Frechet, J. M. J. *J. Am. Chem. Soc.* **2004**, *126*, 15388-15389.

(28) Ma, B.; Kim, B. J.; Deng, L.; Poulsen, D. A.; Thompson, M. E.; Frechet, J. M. J. *Macromolecules* **2007**, *40*, 8156-8161.

(29) Suzuki, M.; Tokito, S.; Sato, F.; Igarashi, T.; Kondo, K.; Koyama, T.; Yamaguchi, T. *Appl. Phys. Lett.* **2005**, *86*, 103507.

(30) Tsuchiya, K.; Kasuga, H.; Kawakami, A.; Taka, H.; Kita, H.; Ogino, K. *J. Polym. Sci.: Part A: Polym. Chem.* **2009**, *48*, 1461-1468.

(31) Bozano, L. D.; Carter, K. R.; Lee, V. Y.; Miller, R. D.; DiPietro, R.; Scott, J. C. *J. Appl. Phys.* **2003**, *94*, 3061-3068.

(32) Chiriac, C. I. *Rev. Roum. Chem.* **1982**, *27*, 645-649.

(33) Chiriac, C. I. *Rev. Roum. Chem.* **1983**, *28*, 977-980.

(34) Levin, Y. A.; Skorobogatova, M. S. *Chem. Hetero. Comp.* **1967**, *3*, 266-267.

(35) Bonesi, S. M.; Erra-Balsells, R. *J. Lumin.* **2001**, *93*, 51-74.

(36) Adachi, C.; Kwong, R. C.; Djurovich, P. I.; Adamovich, V.; Baldo, M. A.; Thompson, M. E.; Forrest, S. *Appl. Phys. Lett.* **2001**, *79*, 2082-2084.

(37) Pommerehne, j.; Vestweber, h.; Guss, W.; Mahrt, R. F.; Bassler, H.; Porsch, M.; Daub, J. *Adv. Mater.* **1995**, *7*, 551-554.

(38) Djurovich, P. I.; Mayo, E. I.; Forrest, S.; Thompson, M. E. *Org. Elect.* **2009**, *10*, 515-520.

(39) Hill, I. G.; Kahn, A.; Soos, Z. G.; Pascal Jr., R. A. *Chem. Phys. Lett.* **2000**, *327*, 181-188.

(40) Jansson, E.; Jha, P. C.; Agren, H. *Chem. Phys.* **2006**, *330*, 166-171.

(41) Giebink, N. C.; Forrest, S. R. *Phys. Rev. B* **2008**, *77*, 235215.

(42) Goushi, K.; Kwong, R.; Brown, J. J.; Sasabe, H.; Adachi, C. *J. Appl. Phys.* **2004**, *95*, 7798-7802.

(43) Ren, X.; Li, J. L.; Holmes, R. J.; Djurovich, P. I.; Forrest, S.; Thompson, M. E. *Chem. Mater.* **2004**, *16*, 4743-4747.

CHAPTER 5

Crosslinkable Solution-Processed OLED Layers

5.1. Introduction

Side-chain polymers containing a triscarbazole hole transport group and different crosslinkable co-monomers in addition to a small molecule triscarbazole functionalized with a crosslinkable moiety were synthesized. For these materials, the groups chosen for study (based on literature precedence) included thermally and/or photochemically initiated crosslinkable moieties such as benzocyclobutenes, trifluorovinyl ethers, oxetanes, or styrenes. The resistance to solvent damage of the thin films of these materials was evaluated (by UV-vis., ellipsometry, and atomic force microscopy) and a study of rapid thermal processing (RTP) was explored as means to significantly reduce the time required to crosslink/insolubilize the films.

5.2. Introduction and Background

Vacuum-deposited organic small molecules have thus far been used to produce the highest efficiency OLED devices due to ease of fabrication of well-defined multilayers and the high levels of purity obtained. Despite this, vacuum deposition can be broadly described as a time-consuming and expensive process that becomes more difficult when fabricating layers on large-area substrates.[1] In contrast, solution-based layers may be more affordable to process and are generally more amenable to large area substrates. One concern for solution processing, especially for polymers, has been that such higher molecular-weight materials, are typically more difficult to purify as

compared to sublimed or column purified small molecules. This is especially concerning as high purity is very desirable for long-lifetime devices.

Yet another concern of solution processed layer has been that deposition of a subsequent layer can damage or destroy the preceding layer (should the processing solvent also dissolve the preceding layer). In an effort to avoid this negative effect, materials and solvents have been explored that do not dissolve preceding layers by way of an "orthogonal solvent" approach. Several groups have explored this approach but the method has been found to be limited by the need to design materials with very specific solubilities in particular sets of solvents.[2-6] Another approach for achieving solution-processed multilayers that avoid damage of preceding layers has been to incorporate reactive substituents onto organic materials (small molecule or polymer-based) for charge transport or hosting molecules that can be reacted via thermal, light, or chemical initiation and effectively crosslink the layer. Crosslinking can effectively insolubilize a layer and prevents damage from subsequently processed layer. The diagram below shows a simplified visual representation of the process.

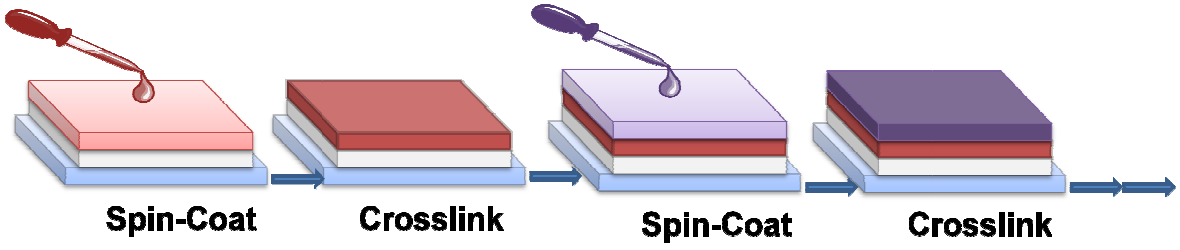

Figure 5.1. Schematic showing how crosslinking permits solution processing of multilayer OLEDs.

An examination of several approaches for crosslinking is provided below. We have purposely focused on reports that are most relevant to the work discussed in this Chapter and therefore not all examples known are discussed.

Trifluorovinylether (TFVE) group undergoes a [2+2] cycloaddition to yield a coupled hexafluorocyclobutane moiety at temperatures near or above 200 °C.[7] However, as the process yields a dimer, more than two TFVE groups must be incorporated into small molecules in order to ensure crosslinking or in the case of polymers, they must be included as a freely available side group.

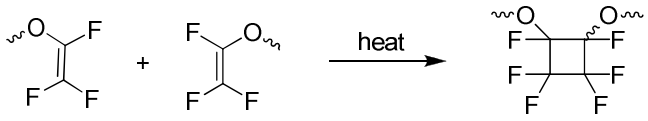

Figure 5.2. Thermal 2+2 cycloaddition of a trifluorovinyl ether.

A report by Niu *et al*.[8] used TFVEs on a hole-transport polymer **5.1** showed that it could be crosslinked at 235 °C for 40 min and used in conjunction with another TFVE-functionalized small molecule, tris(trifluorovinylethyl)-functionalized tris(carbazolyl) triphenylamine (**5.2**) in an OLED with the architecture: ITO/**5.1**(20 nm)/**5.2**/EML/TPBI/Al (where the EML was a solution-processed blend layer of PVK and TPBI with an iridium emitter). The crosslinked materials permitted successful fabrication of a three-layered device where the two crosslinked layers facilitated hole injection into the EML. An maximum EQE of 3% was observed, while for an analogous device without **5.2**, a much lower EQE of 1.24% was obtained and attributed to a larger hole injection barrier from **5.1** directly into the emissive layer.

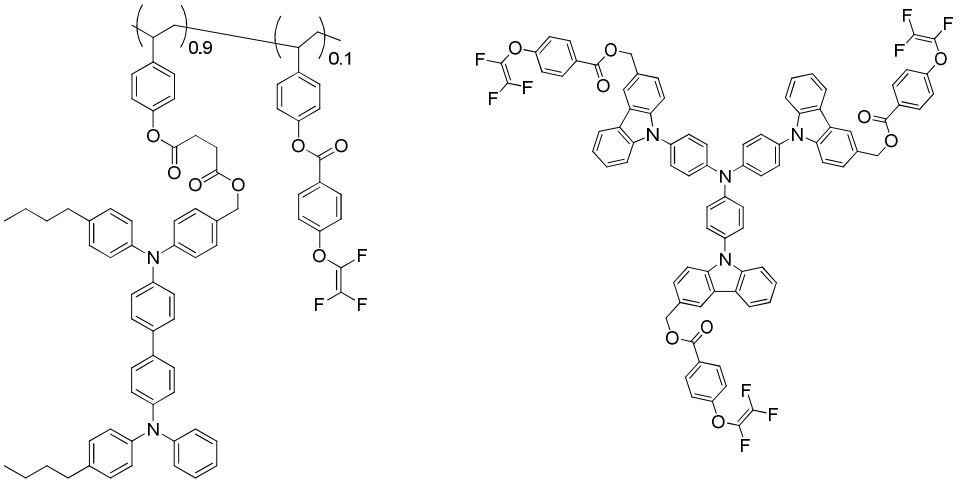

5.1 **5.2**

Figure 5.3. Hole transport materials **5.1** and **5.2** with trifluorovinylether crosslinking groups.

Another example of a TFVE-functionalized hole-transport molecule was reported by Lim *et al*.[9] Crosslinking was achieved by heating layers of **5.3** to 230 °C for 2 h. AFM images of the crosslinked films revealed surfaces that were smoother than those compared to a PEDOT-PSS layer (0.47 nm vs. 1.15 nm, respectively). An OLED with the architecture: ITO/**5.3**/PFO/Ba/Al (PFO = Poly(9,9-dioctylfluorenyl-2,7-diyl)) was compared to an equivalent device with PEDOT-PSS. The device with crosslinkable **5.3** had superior luminance efficiency (0.132 cd/A vs. 0.091 cd/A (for PEDOT-PSS device)). The long heating time and concomitant high temperature required for crosslinking could may be a problematic and limiting factor for TFVE.

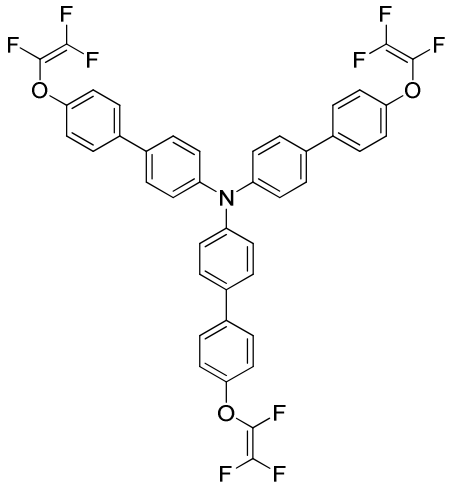

5.3

Figure 5.4. A tris(trifluorovinyl)-functionalized triphenylamine **5.3**.

The benzocyclobutene (BCB) group has also been studied for the purposes of thermal crosslinkability. The BCB group typically requires heating to 200 °C or above, and irreversibly forms a dibenzocyclooctadiene ring via cycloaddition.[1,10]

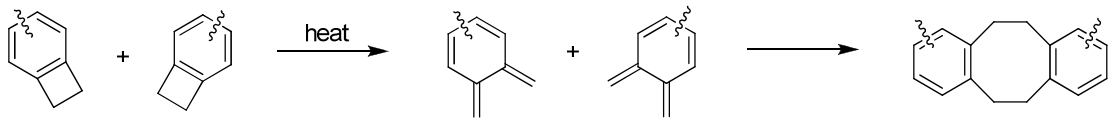

Figure 5.5. Benzocyclobutene thermally initiated crosslinking.

Fréchet and co-workers[11] side-chain copolymer, **5.4**, with hole transport and BCD side-groups (Figure 17). Copolymer **5.4** (n:m = 90:10) was crosslinked by heating to between 180 and 250 °C (but was found to be completely unreactive at temperatures below 150 °C). DSC, UV-vis., and AFM studies of the material are summarized in Figure 18. The UV-vis. spectra revealed differences between the heating times of 2 h vs. 4 h on the solubility in chloroform. Two hours of heating were found to be inadequate to completely insolubilize the copolymer layer. Devices with architecture

ITO/**5.4**/Alq_3/LiF/Al, with and without **5.4**, or TPD in place of **5.4** were tested and the devices showed emission from the Alq_3 component. EQE were essentially the same between the crosslinked and un-crosslinked devices (near 0.7%), but were slightly less efficient as compared to the small molecule TPD device (*ca*. 0.89% efficiency). Another OLED with the architecture: ITO/crosslinked-**5.4**/EML/BCP/LiF/Al (where the EML was a bipolar polymer with oxadiazole and triphenylamine side chains doped with an Ir phosphor; BCP = bathocuproine) was fabricated, as well as a device without any hole-transport layer (for comparison purposes). An EQE of 6.4% was obtained without any hole-transport layer as compared to an EQE of 10.4% when crosslinked **5.4** was introduced and could be attributed to better exciton confinement and localization of the recombination zone near or on the emissive layer. BCB groups were shown to yield crosslinked layers without significantly adverse effects on device performance and were shown to successfully allow the fabrication of more efficient devices with two solution-processed layers (in the phosphorescent device examples). A limitation for the use of BCB groups may result from the need for high temperature and long heating times required to achieve successful insolubilization of the layers.

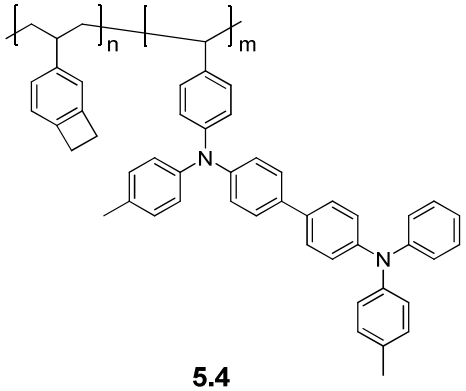

5.4

Figure 5.6. Benzocyclobutene-bis(diarylamino)biphenyl co-polymer **5.4**.

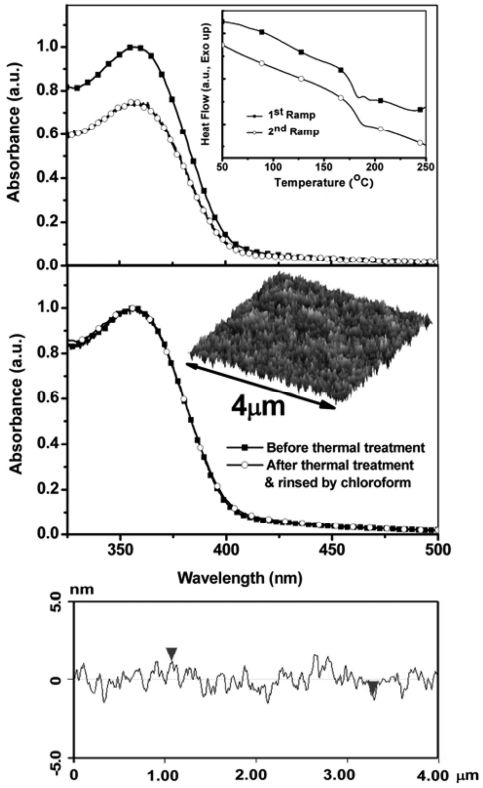

Figure 5.7. UV-vis. spectra of **5.4** before (dark squares) and after washing with chloroform following crosslinking (open circles) for 2h (top) and 4h (bottom); top inset shows DSC of **5.4** and bottom shows an AFM image of the crosslinked film. Reprinted with permission from ref. 11. Copyright 2007 American Chemical Society.

Styrenes can undergo radical polymerization by a thermally initiated process and therefore offer another avenue for crosslinking for OLED applications. In the case of small molecules are typically functionalized with at least two styrene groups. For polymers, crosslinking may be achieved by incorporating styrene end groups or as side groups. In all, styrene chemistry does not require any added reagents for processing and virtually no side products (beyond those associated with chain termination events) are expected. As in other examples of thermal crosslinking care must be taken to assure that the electroactive species does not react with the propagating polymer chain.

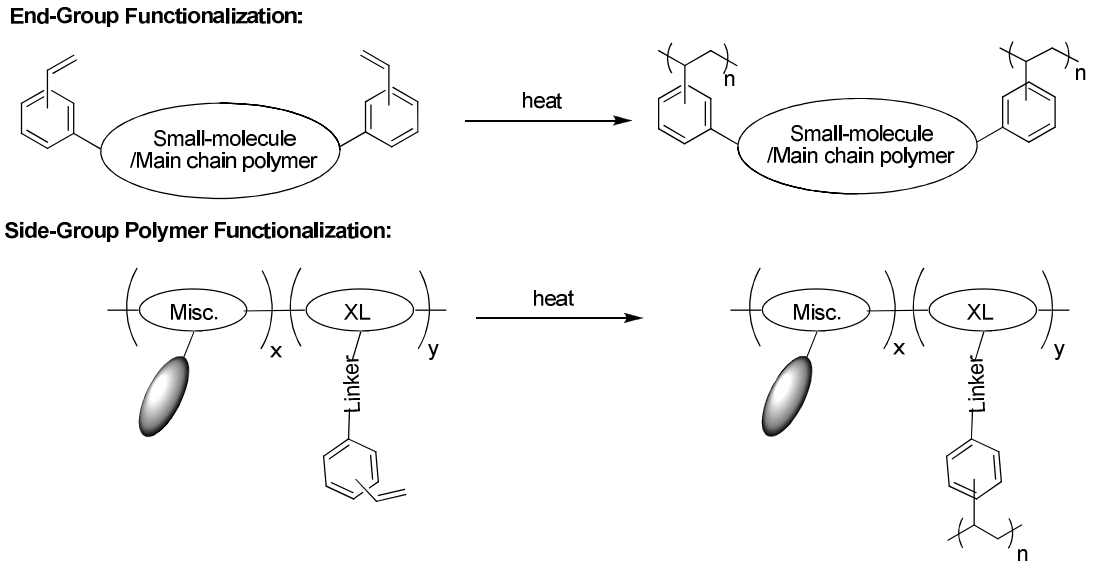

Figure 5.8. Thermally initiated crosslinking of styrene-functionalized molecules and polymers.

Jen and co-workers[12] reported on a di(styrene)-functionalized tris(carbazolyl) triphenylamine derivative, **5.5**. Crosslinking was evaluated by DSC, UV-vis., and AFM studies and it was found that isothermal heating of thin films of **5.5** at 180 °C could fully crosslink the material; layers heated to 160 °C for 30 min failed to crosslink fully. White OLEDs (ITO/PEDOT:PSS(60 nm)/crosslinked-**5.5**(15-34 nm)/EML (30 nm)/TPBI(25 nm)/CsF/Al (EML = blend of blue-, green-, and red-emitting transition-metal phosphors with PVK; TPBI = 1,3,5-tris(*N*-phenylbenzimidazol-2-yl)benzene)) were fabricated and devices were shown to have stable emission with near-white color (Table 5.1). Devices with and without **5.5** as an interlayer between PEDOT-PSS and the emissive layer, showed that improved performance was observed in **5.5** devices that the authors attributed to enhanced hole injection. As it was not possible to compare devices with a crosslinked *vs*. uncrosslinked layer of **5.5**, the effect of the thermal treatment needed to insolubilize on device performance could not be ascertained.

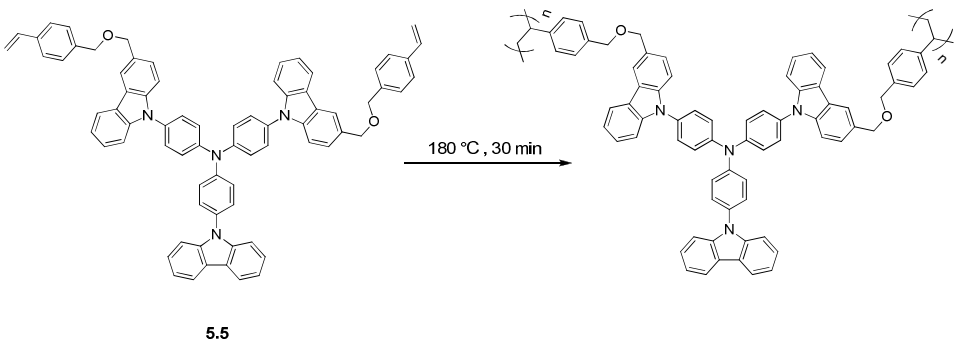

Figure 5.9. Crosslinking of a styrene-functionalized tris(carbazolyl) triphenylamine derivative.

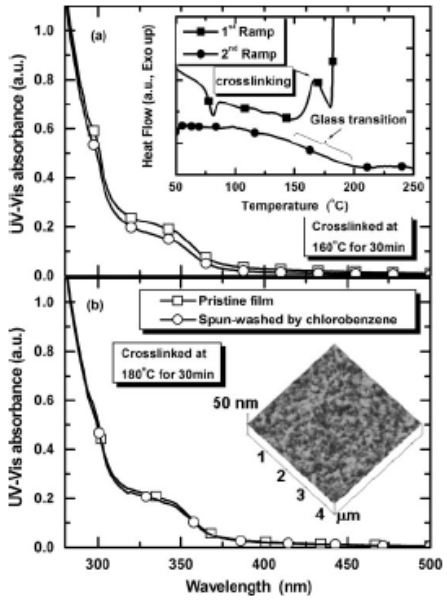

Figure 5.10. (a) Pre- and post-washing UV-vis. of **5.5** crosslinked at 160 °C; inset shows DSC of (1st ramp) non-crosslinked and (2nd ramp) crosslinked **5.5**. (b)Pre- and post-washing UV-vis. of **5.5** crosslinked at 180 °C; inset shows AFM post-crosslinking. Reproduced from ref. 12. Copyright Wiley-VCH Verlag GmbH & Co. KGaA. Reproduced with permission.

Table 5.1. Data for OLEDs with various thicknesses of **5.5**.

hole-transport material	None	**5.5**		
		15 nm	25 nm	34 nm
Device No.	1	2	3	4
Max η_{ext} (%)	2.07	4.01	5.85	5.2
power efficiency @ 800 cd/m^2 (lm/W)	2.08	4.56	5.59	3.74

Small molecule styrene-functionalized bis(diarylamino)biphenyl derivatives **5.6-5.10** were reported by Jen and co-workers[13] and films of these molecules were crosslinked at 170 °C for 30 min with good resistance to exposure to chlorobenzene; annealing at 150 °C resulted in reduced resistance near 85%. Molecule **5.6** could only be polymerized and not crosslinked. Layers of these molecules were studied by AFM and found to be smooth and defect-free. Devices were fabricated with architecture: ITO/PEDOT:PSS/crosslinked-**5.7-5.10**/PFBT5/CsF/Al, where PFBT5 served as the electron-transport and emissive layer (see Table 2 for devices and their performances). The crosslinked hole-transport materials were found to improve device performance as compared to a device with no such layer; attributed to enhanced hole injection into the emissive layer. A higher crosslinking temperature of 230 °C for **5.10** was explored but resulted in decreased performance. The authors suggested that the higher temperature may have damaged the PEDOT-PSS layer as a possible explanation of the decrease. It was shown that bis(styrene)-functionalized materials could be crosslinked in 30 min and at temperatures lower than those needed for other thermal crosslinking chemistries discussed earlier (vide supra).

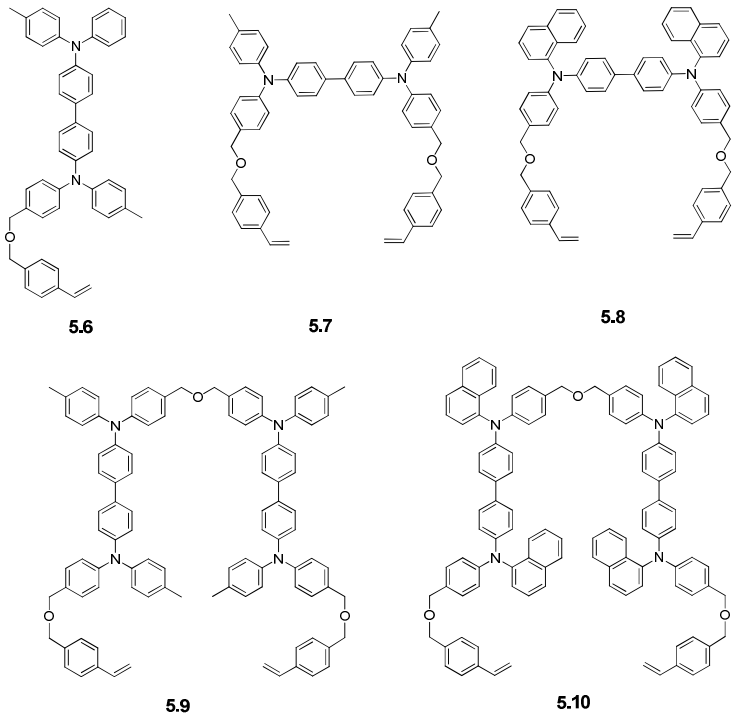

Figure 5.11. Crosslinkable styrene-functionalized bis(diarylamino)biphenyl derivatives **5.6** – **5.10**.

Table 5.2. Data for OLEDs using styrene-functionalized bis(diarylamino)biphenyl hole-transport materials.

Material	EQE (%)	Luminance Efficiency (cd/A)
None	0.72	2.42
5.7	1.78	6.29
5.8	2.92	9.45
5.9	2.15	7.56
5.10	3.2	10.8
5.10[a]	0.99	3.51

[a]crosslinked at 230 °C for 30 min; all others 180 °C for 30 min

Cinnamates and chalcones are other examples of groups that dimerize through a [2+2] cycloaddition and do so upon exposure to ultraviolet radiation.[14,15] As these groups absorb at *ca*. 290 nm and *ca*. 345 nm, electroactive materials functionalized with these

crosslinkers should not absorb near or at these wavelengths in order to both maximize the crosslinking process and avoid any damage induced from photodecomposition. The crosslinking process for cinnamate is shown in the figure below.

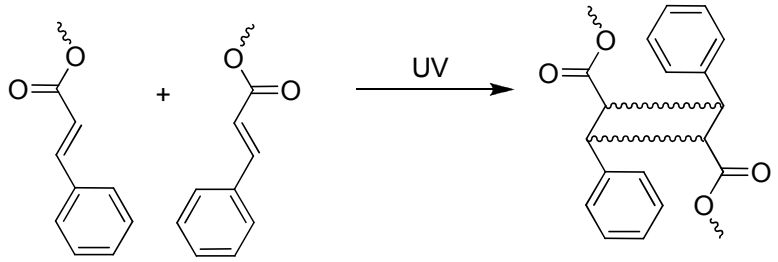

Figure 5.12. [2 + 2] Cycloaddition of cinnamates.

In 2002, Zhang *et al.*[16] demonstrated the synthesis of copolymers containing cinnamate (**5.11**) or chalcone (**5.12**) side groups.

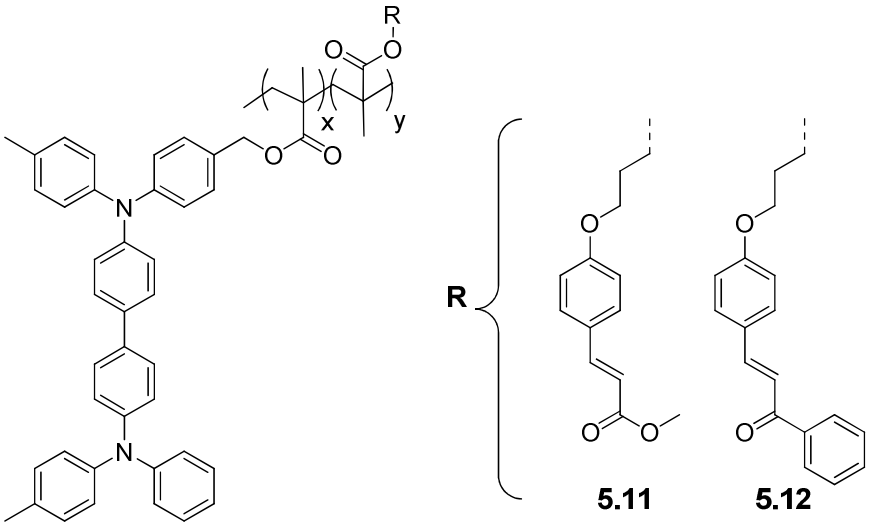

Figure 5.13. Crosslinkable copolymers of bis(diarylamino)biphenyl and cinnamate or chalcone methacrylates.

UV-vis. studies showed that for different UV exposure times showed overall decreased absorption in the near-UV that was attributed to the cycloaddition reaction. For a homopolymer without crosslinkable groups, the absorption spectrum was unchanged and taken as evidence of stability against photodecomposition. UV-vis. spectra of the before and after tetrahydrofuran washing were obtained as evidence of solvent resistance. OLEDs with architecture: ITO/**5.11** or **5.12**/Alq_3/Mg (with or without crosslinking) were prepared and devices were found to be less efficient when crosslinked, despite no evidence of damage to the hole-transport groups from UV exposure reported.

In follow up work to that discussed above a series of substituted TPD-like derivatives as side groups on an acrylate copolymer with a crosslinkable co-monomer were demonstrated.[17]

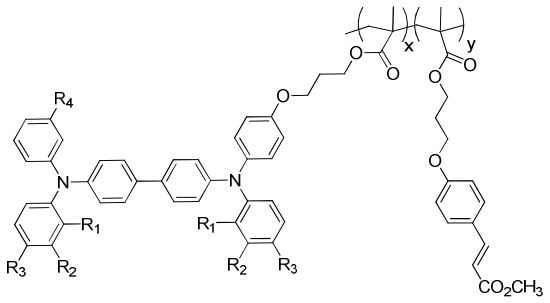

(target x = 0.7 and y = 0.3)

polymer	R_1	R_2	R_3	R_4
5.13	H	Me	H	H
5.14	H	H	OMe	Me
5.15	H	F	H	Me
5.16	F	H	F	Me

Figure 5.14. Methacrylate bis(diarylamino)biphenyl-cinnamate copolymers **5.13** – **5.16**.

AFM showed essentially no changes for the crosslinked films after annealing at 160 °C, while vapor-deposited TPD changed significantly at only 80 °C (presumably due to crystallization). OLED devices with a general architecture: ITO/**5.13-5.16**/Alq_3/Mg:Ag were fabricated. EQE for devices with copolymer **5.15** were evaluated as a function of UV exposure per unit of area which showed that EQE was stable up to a dose of 25mJ/cm^2 at 350 nm. At higher doses, the EQEs were found to decrease more significantly. Crosslinked two-layer devices (ITO/**5.14**/(**5.13 or 5.15**)/Alq_3/Mg:Ag) demonstrated superior EQEs relative to single-layer crosslinked hole-transport layer devices; attributed to an easier hole injection cascade from ITO into the lower-IP polymer, then the higher-IP polymer, and finally into the Alq_3 layer (as compared to the first devices with only one crosslinked layer). Device lifetime studies were carried out and for polymers **5.13-5.16** device half-lifetimes of 681, 1575, 1849, and 840 s when crosslinked were reported. A half lifetime value of 1550 s was found for an uncrosslinked **5.14**. An analogous control device with vapor-deposited TPD had a half lifetime of 36000 s. Clearly the devices have poorer lifetimes as compared to vacuum-processed layers, but compared among themselves (uncrosslinked to crosslinked), the process (when optimized) does not adversely affect OLED lifetime. Polymer **5.15** has been used in other OLED devices and reports, as a crosslinkable hole-transport material onto which either a polymeric electron-transport[18] or emissive[19-21] layer can be solution-processed.

Oxetanes can undergo cationic ring-opening polymerization (CROP) to form linear polyethers.[22]

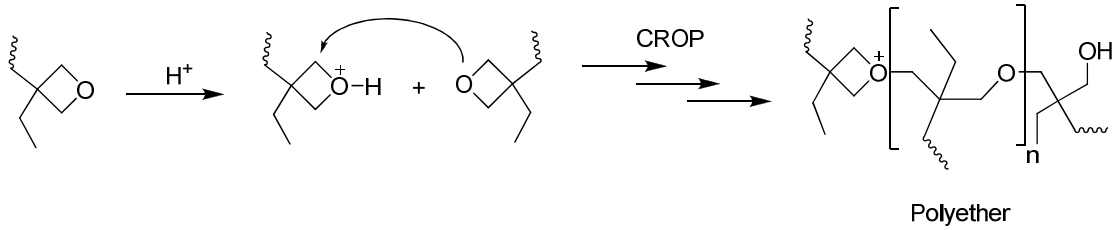

Figure 5.15. Cationic polymerization of oxetanes.

This process can be initiated by the addition of UV photoacid-generators (such as diaryliodonium or triarylsulfonium salts) that show strong absorptions in the UV (e.g., 235 nm for Ph_3S^+,[23] and can be red-shifted through substitution[24]), resulting in photodecomposition of the compound and the formation of a strong acid. We also note that protons can be generated when UV photoacid-generators decomposition are sensitized (through an electron-transfer process) by dyes (or electroactive organic compounds) with longer absorption wavelengths.[24-26]. Potential advantages of oxetane crosslinking include low shrinkage and the relatively high polymerization rates.[27-29] Among the disadvantages of the approach are the likelihood for protons or oxonium species to remain after the crosslinking process; these may then diffuse to other layers under the influence of an electric field and could have detrimental effects on performance. In addition, for OLED applications, care must be taken that the organic electroactive materials used are not reactive/sensitive to strong acids.

The earliest known use of oxetanes for crosslinking for OLEDs was made in 1999 by Bayerl *et al.*.[28] Bis(diarylamino)biphenyl molecules were modified with either short or extended oxetane groups were synthesized (**5.17** and **5.18**). Films of **5.17** or **5.18** on ITO (with 1 wt % of a photoacid – 4-(thiophenoxyphenyl) diphenylsulfonium hexafluoroantiomoate) were crosslinked by UV exposure (1 min at 302 nm). DSC

showed the disappearance of glass transition events upon crosslinking. Two devices were fabricated with polymer **5.17**, one non-crosslinked and one crosslinked, in a simple device that consisted of ITO/**5.17**/Al. An increased current maximum (by 15 ×) was observed for the crosslinked device, as opposed to the non-crosslinked device. A second type of device tested the resistance of the crosslinked layer by processing an emissive layer atop (architecture: ITO/crosslinked-**5.17**/EML/Ca (EML = blend of poly(-methylstyrene, PBD, and perylene)). This second device emitted blue light (at 2000 cd/m^2) under continuous operation.

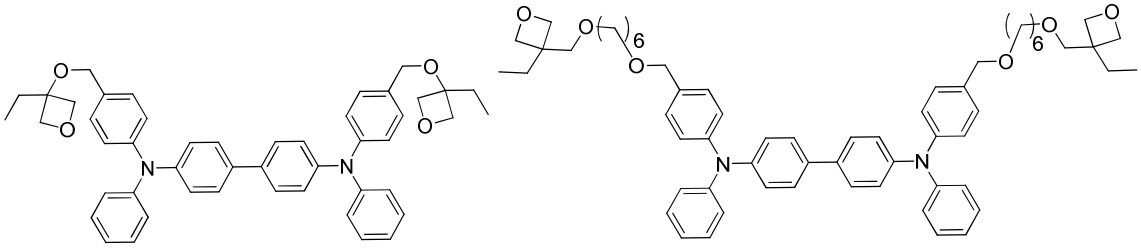

5.17 **5.18**

Figure 5.16. Oxetane-functionalized bis(diarylamino)biphenyl derivatives **5.17** and **5.18**.

Nuyken *et al*.[30] reported a series of diamine derivatives functionalized with oxetanes. A sulfonium salt photoinitiator was used to crosslink the films as confirmed by solvent resistance as substantiated by essentially no change in the UV-vis. absorption. OLED devices (architecture: ITO/**5.19** or **5.20**/Ca) were fabricated with a single active layer. In addition, a copolymer containing hole-transport and oxetane groups as side-groups was also evaluated (see **5.21**; Figure 5.18). For the copolymer, the oxetane co-monomer was stated to adversely affect the hole-transport properties due to dilution of the transport functionality.

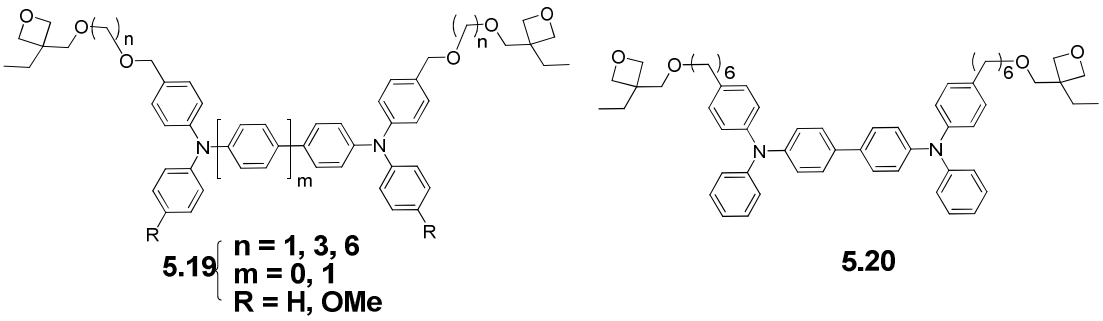

Figure 5.17. Oxetane-functionalized bis(diarylamino)oligophenylene derivatives **5.19** and **5.20**.

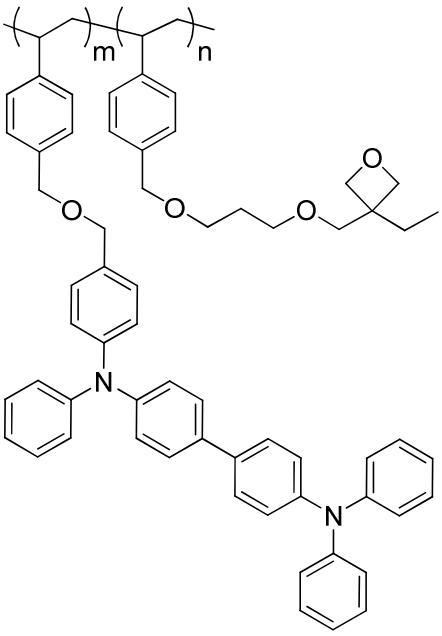

Figure 5.18. Oxetane-bis(diaryalmino)biphenyl copolymer **5.21**.

Other side-chain copolymers were explored by Bacher *et al*.[31] containing various types of hole-transporting diamines with an oxetane co-monomer (see figure 5.15). Glass transition events were found (by DSC) to occur below 100 °C for these polymers. In the presence of a photoacid generator (doped at 1 wt %), films of the polymers were exposed to UV irradiation (10 s at 366 nm). The films were subsequently cured (at 150 °C). This

post-irradiation cure was found to be essential as in the absence of this step the viscosity of the films limited the effective reaction rate of the oxetane groups. In other words, the films had to be heated above their glass transition temperatures in order to permit sufficient freedom of motion for the oxetanes to react with one another at a high enough rate. OLEDs with the architecture: ITO/**5.22-5.29**/Ag were prepared in addition to a reference device prepared with the crosslinkable diamine derivative **5.30** (see figure 5.20). The copolymer devices all higher turn-on voltages vs. **5.30** device; attributed to lower overall proportion of the hole transporting diamine for the copolymers as compared to the small molecule.

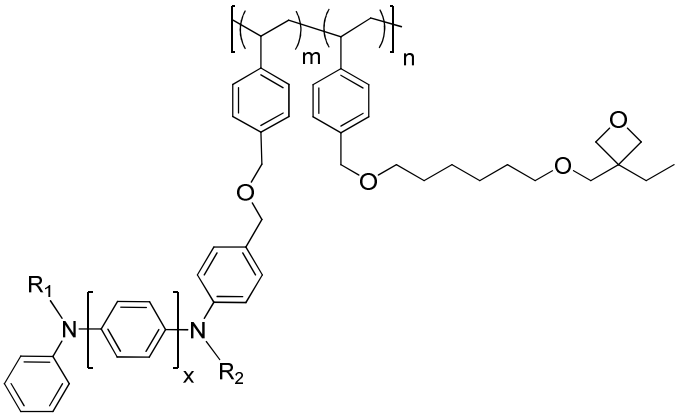

Name	x	R_1	R_2	(m:n)
5.22	1	Phenyl	Phenyl	(1:1)
5.23	1	Phenyl	Phenyl	(3:1)
5.24	2	Phenyl	Phenyl	(1:1)
5.25	2	Phenyl	Phenyl	(3:1)
5.26	2	1-Napthyl	1-Napthyl	(1:1)
5.27	2	1-Napthyl	1-Napthyl	(3:1)
5.28	2	1-Napthyl	Phenyl	(1:1)
5.29	2	1-Napthyl	Phenyl	(3:1)

Figure 5.19. Co-polymers **5.22 – 5.29** containing oxetane and bis(diarylamino)biphenyl or bis(diarylamino)benzene groups in the side chains.

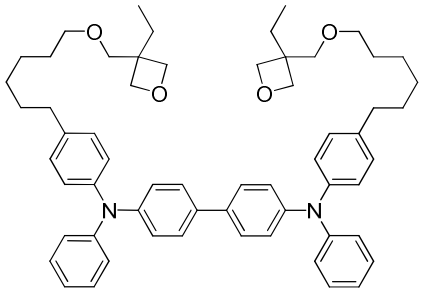

5.30

Figure 5.20. Small molecule oxetane-functionalized bis(diarylamino)biphenyl **5.30**.

Meerholz and co-workers[32] studied **5.30** (above), **5.31**, and **5.32** as crosslinkable hole-transport layers. PVK, Ir phosphors, and oxadiazole-derivatives were solution-processed on the crosslinked layers and good performance was obtained for devices fabricated. A green device demonstrated a best EQE of 18.8% (depending on conditions) with two crosslinked layers consisting of a hole-injection layer of crosslinked **5.32** (doped with $NOSbF_6$) and a second layer of crosslinked **5.32**. A comparable red device gave a best efficiency of 13%. Blue devices were also studied but were not comparable to the above devices (due to a difference in host materials) and exhibited a notably lower EQE of 5.7%. The authors attributed the lower efficiency of the blue devices to poor triplet exciton confinement.

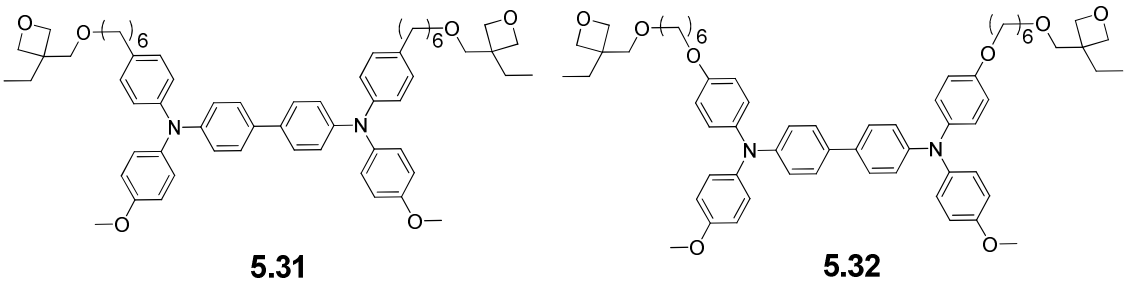

5.31 **5.32**

Figure 5.21. Additional examples of oxetane-functionalized bis(diarylamino)biphenyl derivatives, **5.31** and **5.32**.

5.3. Goals of Chapter 5

Triscarbazole-based hole transport copolymers incorporating crosslinkable side-groups such as benzocyclobutene, trifluorovinyl ether, and oxetane were synthesized. The crosslinkable groups were chosen based on literature precedence and were known to dimerize or polymerize under thermal and/or photochemical conditions. Crosslinked layers of the copolymers were evaluated for changes in layer thickness (by ellipsometry) and changes to surface morphology (by atomic force microscopy (AFM)) after harsh solvent exposure. In addition, rapid thermal processing was explored as method to reduce the processing times for some of the copolymers. In addition to the copolymers, an example of a triscarbazole-based hole transport small molecule functionalized with a crosslinkable bis(styrene) moiety was also synthesized and studied by rapid thermal processing and atomic force microscopy. Some examples of OLED devices were also fabricated and studied.

5.4. Crosslinkable Copolymers

5.4.1. Design rationale and Synthesis

Benzocyclobutene (BCB) has been used by Fréchet and co-workers[11] in crosslinkable copolymers (see introduction section) that required several hours (≥ 4) of heating above 200 °C to produce insolubilized thin films. Crosslinking reactions on those time scales would likely not be considered amenable for crosslinking needed in commercial device applications. One of the goals of the work presented here was to explore approaches that would reduce the time required for crosslinking. Two styrene-type monomers of benzocyclobutene were synthesized for this purpose. The first coupled

a vinyl group directly to the benzocyclobutene group (via Suzuki coupling) to afford an equivalent styrene monomer (**5.33**) to that used in the literature.

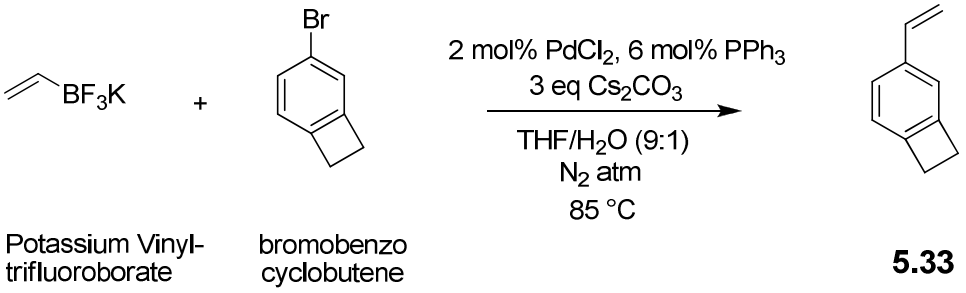

Scheme 5.1. Synthesis of benzocyclobutene styrene monomer **5.33**.

A second BCB-type monomer (**5.34**) was designed with a spacer that extended the benzocyclobutene away from the styrene (and consequently from the polymer backbone) based on the expectation that the extension would facilitate the likelihood for two BCB groups to more readily find and react with one another during the thermal crosslinking step.

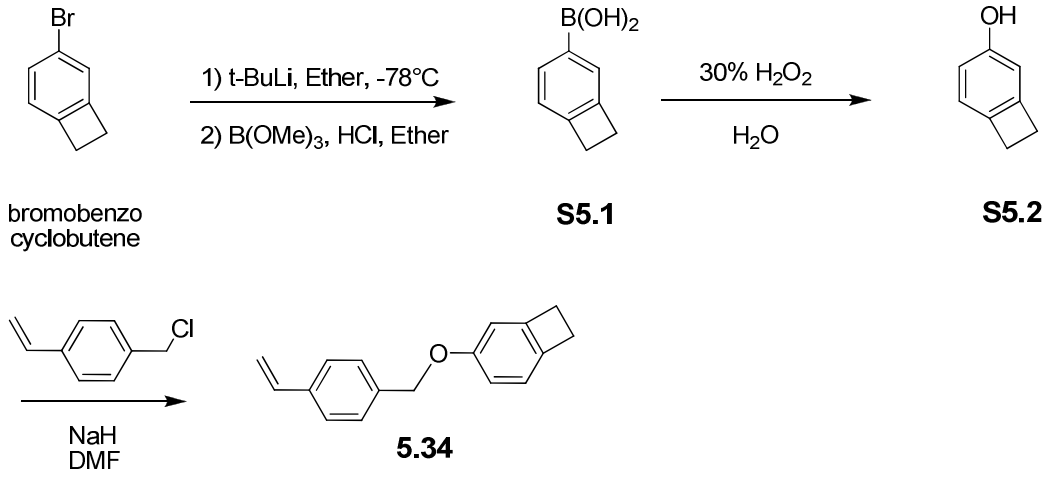

Scheme 5.2. Synthesis of extended-chain benzocyclobutene styrene monomer **5.34**.

The extended benzocyclobutene monomer was synthesized by conversion of the bromo-group of the commercially available starting material into a hydroxy group followed by coupling with 4-vinylbenzyl chloride.

A second thermally crosslinkable group chosen for study was based on the work of Jen and co-workers[9,12] on the trifluorovinylether (TFVE) group. A monomer was formed by Suzuki coupling of the bromo- TFVE group with potassium vinyltrifluoroborate to afford **5.35**.

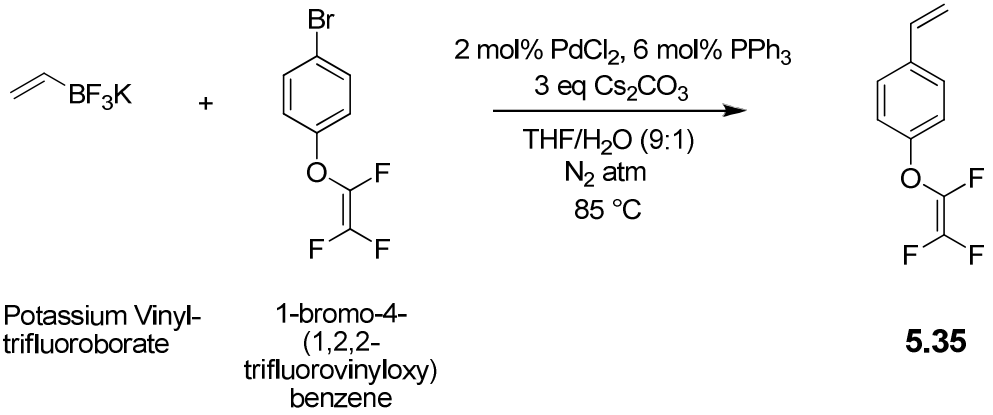

Scheme 5.3. Synthesis of trifluorovinylether styrene monomer **5.35**.

Oxetane groups were also chosen for study based on side-chain copolymers and small molecules containing the group as reported by Meerholz and co-workers.[28,30-33] The oxetane-containing hole transport materials reported were crosslinked by the decomposition of an acid generator (under UV irradiation) that would generate protons that initiated the cationic ring opening polymerization of the oxetane groups. For the copolymers examples, the mole percent of oxetane co-monomer incorporated was 25 or 50% mol %. At those levels, a dilution effect of the active hole transport group was

postulated to limit the efficiencies of the OLED devices. The same monomer used in the above studies was synthesized to afford **5.36** as shown below.

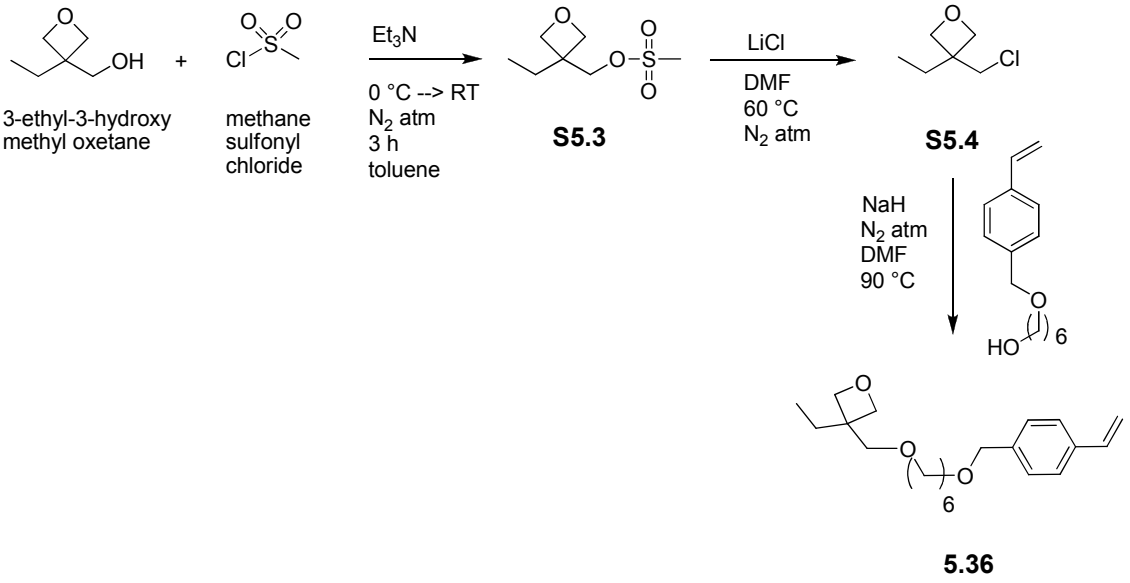

Scheme 5.4. Synthesis of oxetane styrene monomer **5.36**.

A hole-transport co-monomer based on the triscarbazole group (see Chapter 3) was chosen for the styrene-based crosslinkable monomers already described. By using the same transport co-monomer for all the crosslinkable copolymers it was possible to more easily focus on the effects from the crosslinking groups. Triscarbazole intermediate, **S3.3**, was reacted with 4-vinylbenzyl chloride to afford the hole transport monomer **S5.6**.

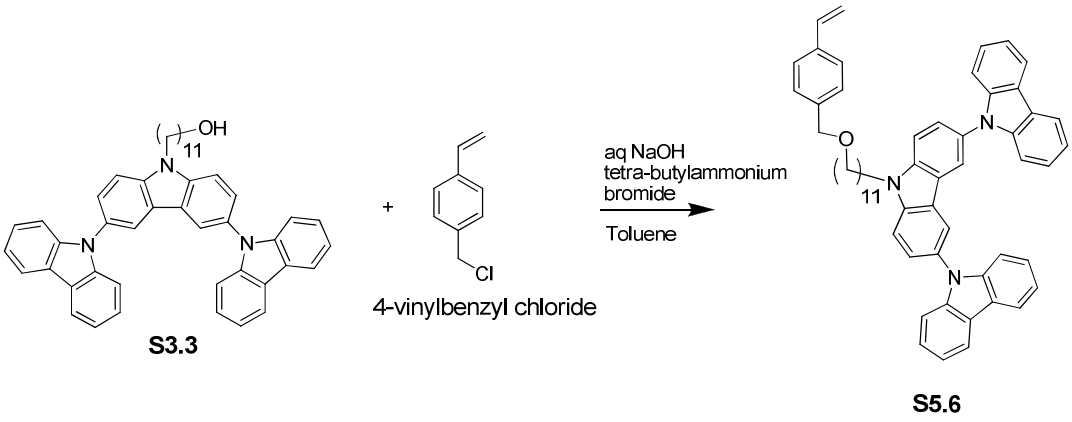

Scheme 5.5. Synthesis of triscarbazole styrene monomer **S5.6**.

Co-monomer **S5.6** was copolymerized with the crosslinkable co-monomers (**5.33**, **5.34**, **5.35**, and **5.36**) using azobisisobutyronitrile (AIBN) as an initiator at 60 °C under inert atmosphere for approximately one week. The following schemes show the copolymers synthesized and their target ratios.

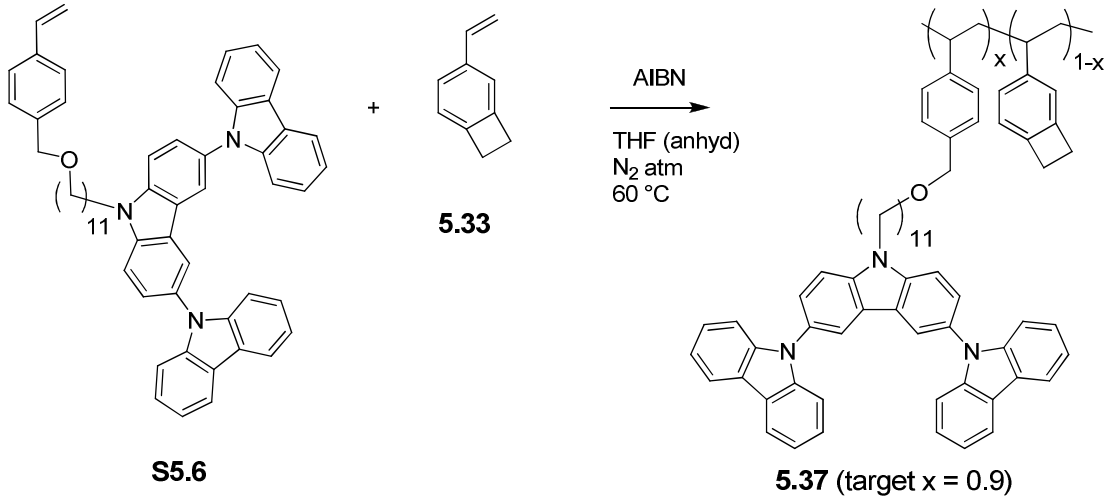

Scheme 5.6. Synthesis of triscarbazole-benzocyclobutene copolymer **5.37**.

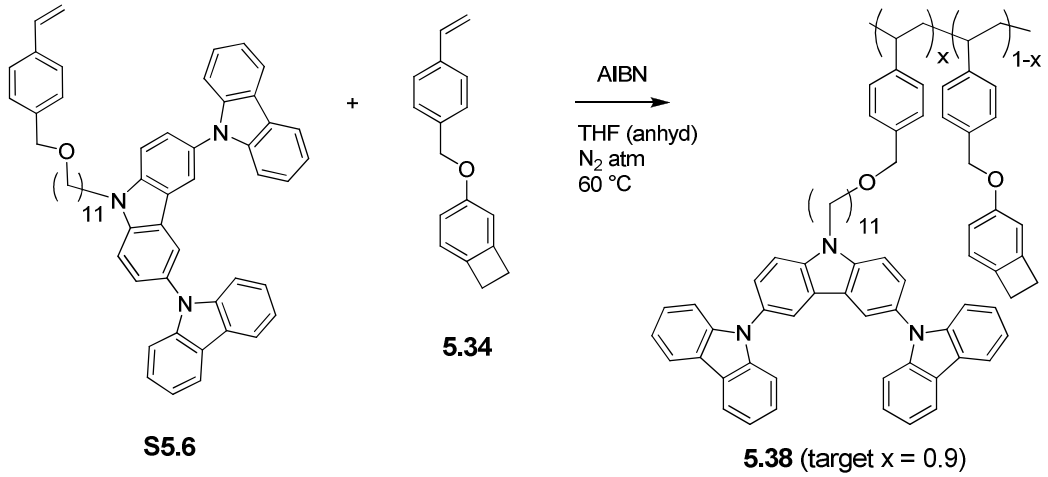

Scheme 5.7. Synthesis of extended-chain triscarbazole-benzocyclobutene copolymer **5.38**.

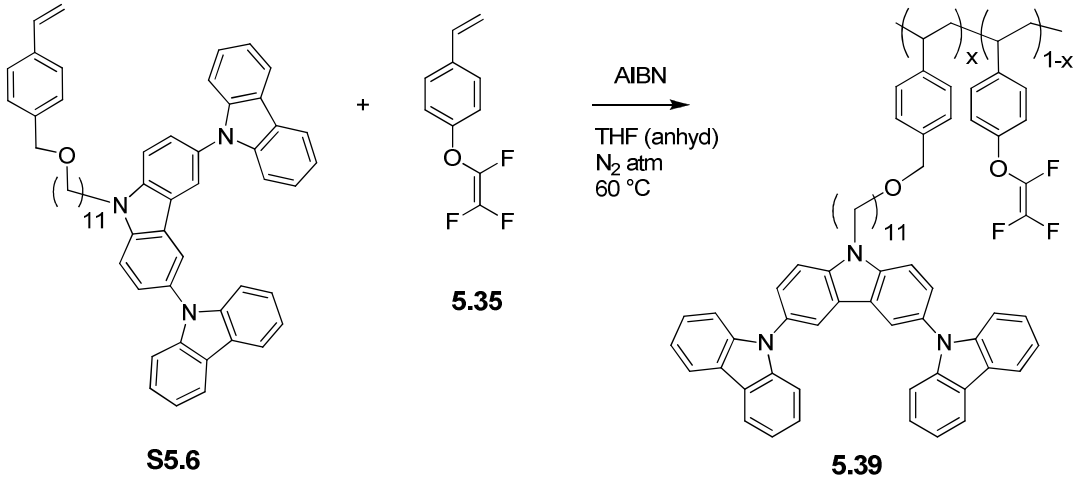

Scheme 5.8. Synthesis of triscarbazole-trifluorovinylether copolymer **5.39**.

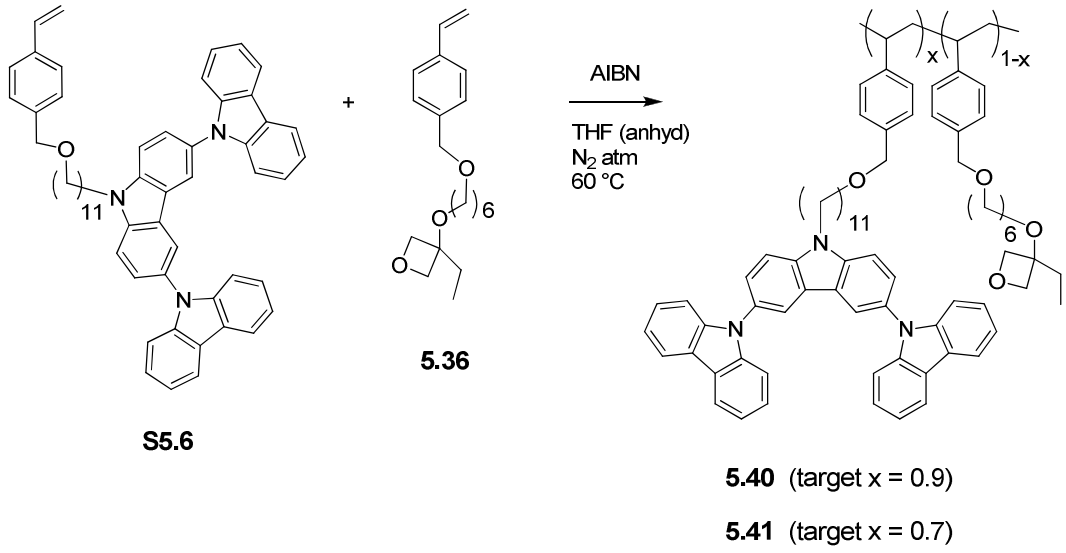

Scheme 5.9. Synthesis of triscarbazole-oxetane copolymers **5.40** and **5.41**.

For copolymer **5.41**, the elemental analysis data suggested that the incorporation may have been closer to x = 0.8.

For all copolymers discussed, purification was performed by multiple precipitations (≥ 3×) into a poor solvent (typically methanol or acetone) followed by characterization by ^{1}H NMR, gel permeation chromatography (GPC), and elemental analysis. Complete conditions for the syntheses shown above are reported in Chapter 2.

5.4.2. Polymer and Thermal Properties

Table 5.3 Copolymer Properties

Polymer	M_w (kDa)[a]	M_n (kDa)[a]	PDI[a]	T_g (°C)[b]	T_d (°C)[c]
5.37	31.1	9.2	3.4	–	391.1
5.38	23.9	10.4	2.3	126.4	382.1
5.39	22.8	6.9	3.3	131.3	435.2
5.40	12.7	7.4	1.7	119.6	392.3
5.41	25.7	7.4	3.5	100.1	372.8

[a] Calculated from gel permeation chromatography (in chloroform or THF) *vs*. polystyrene standards

[b] Determined from differential scanning calorimetry

[c] Determined from thermogravimetric analysis (at 5% weight loss)

"-" denotes not determined

5.4.3. Crosslinking Studies of Benzocyclobutene Copolymers (**5.37** and **5.38**)

Thin films of benzocyclobutene-containing copolymer (**5.37**) were prepared by spin coating (experimental details included in Chapter 2) on glass slides and processed under various conditions. The thin films on glass slides were tested for solvent resistance either by a *dip test*, whereby the films were soaked in chloroform (for different amounts of time) or by a *spin coat test*, whereby chloroform was processed atop the film (for 60 sec at 1000 rpm). The former test was considered to be harsher while the latter test was more likely to replicate the conditions a given layer would be subjected to during the deposition of a subsequent layer (from solution). UV-vis. measurements were used to qualitatively examine the resistance of the thin films as a function of changes in absorption.

Non-crosslinked control thin films were prepared as controls and absorption data (see figure below) demonstrated no resistance to solvent exposure. Other thin films were heated on a hot plate (under inert atmosphere) at 200 °C for 120 or 240 minutes. For

samples heated for 120 minutes, UV-vis. (not shown) absorption decreased but stabilized indicating some level of crosslinking; based on stabilization of the absorption signal upon continued exposure to solvent with no appreciable change or reduction in the absorption after 1 min of dipping the film. The highest qualitative resistance was observed for thin films crosslinked for 240 minutes at 200 °C, as shown in the absorption spectra below.

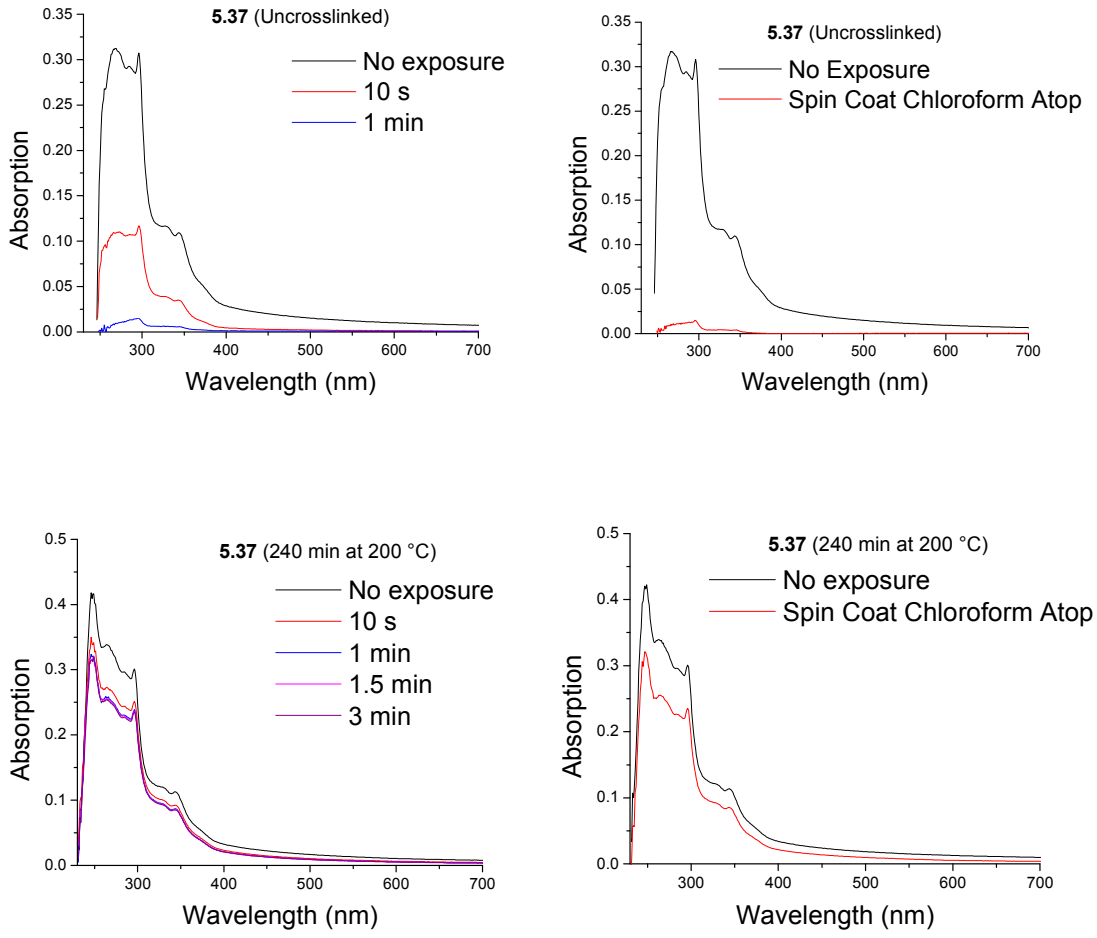

Figure 5.22. UV-vis. study of thin film on glass of copolymer **5.37**. Top left: Uncrosslinked (*dip test*) Top right: Uncrosslinked (*spin coat test*) Bottom left: Crosslinked 240 min at 200 °C (*dip test*) Bottom right: Crosslinked 240 min at 200 °C (*spin coat test*).

Based on the results for copolymer **5.37**, an extended BCB monomer, **5.34**, was developed that might reduce the temperature or time required for insolubilization. UV-vis. spectra of thin films of copolymer **5.38** heated at 175 and 200 °C for 30, 60, 120, and 240 minutes indicated no appreciable layer resistance to solvent attack; absorption decayed rapidly to baseline upon solvent exposure. At 230 °C, the absorbance of the thin films stabilized at approximately 50 % of the original signal when heated for 60 or 120 min. Films heated for 240 min, were the most resistant with ~ 80% of their absorbance signal being retained even after minutes of soaking in chloroform. In comparison, the results for **5.38** indicated no measurable improvement to the results obtained for thin films of copolymer **5.37**.

Differential scanning calorimetry (DSC) was used to examine copolymer **5.38** and demonstrated a melt transition at 167 °C followed by a broad exothermic event in the 230 – 300 °C range (with a maximum near 270 °C) consistent with benzocyclobutene dimerization reactions.[34] The peak was noted to disappear on second heating with only a glass transition event noted.

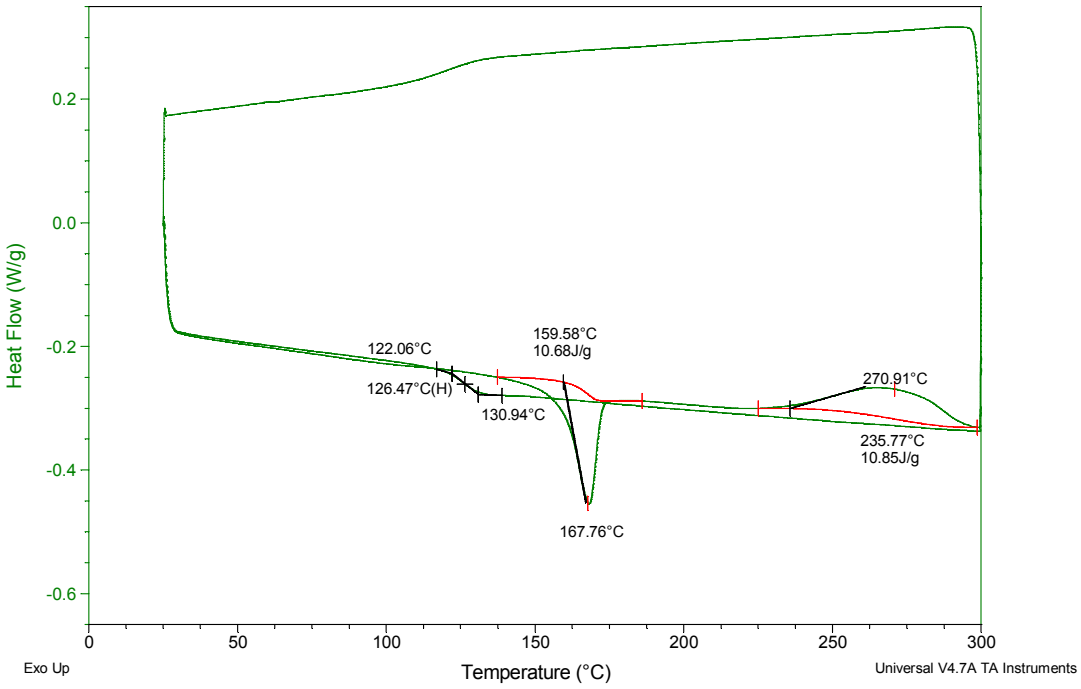

Figure 5.23. Differential scanning calorimetry of copolymer **5.38** (first heating showing melt and exothermic transitions and second heating showing only glass transition).

Based on the DSC data, new thin films of **5.38** were prepared and evaluated when crosslinked at 300 °C on a hot plate under nitrogen atmosphere. The increased heating temperature increased the rate of the crosslinking and UV-vis. data showed that for all films > 80% of the absorption signal was retained for all crosslinking times evaluated (30, 60, 90, and 120 min) and under all solvent exposure times.

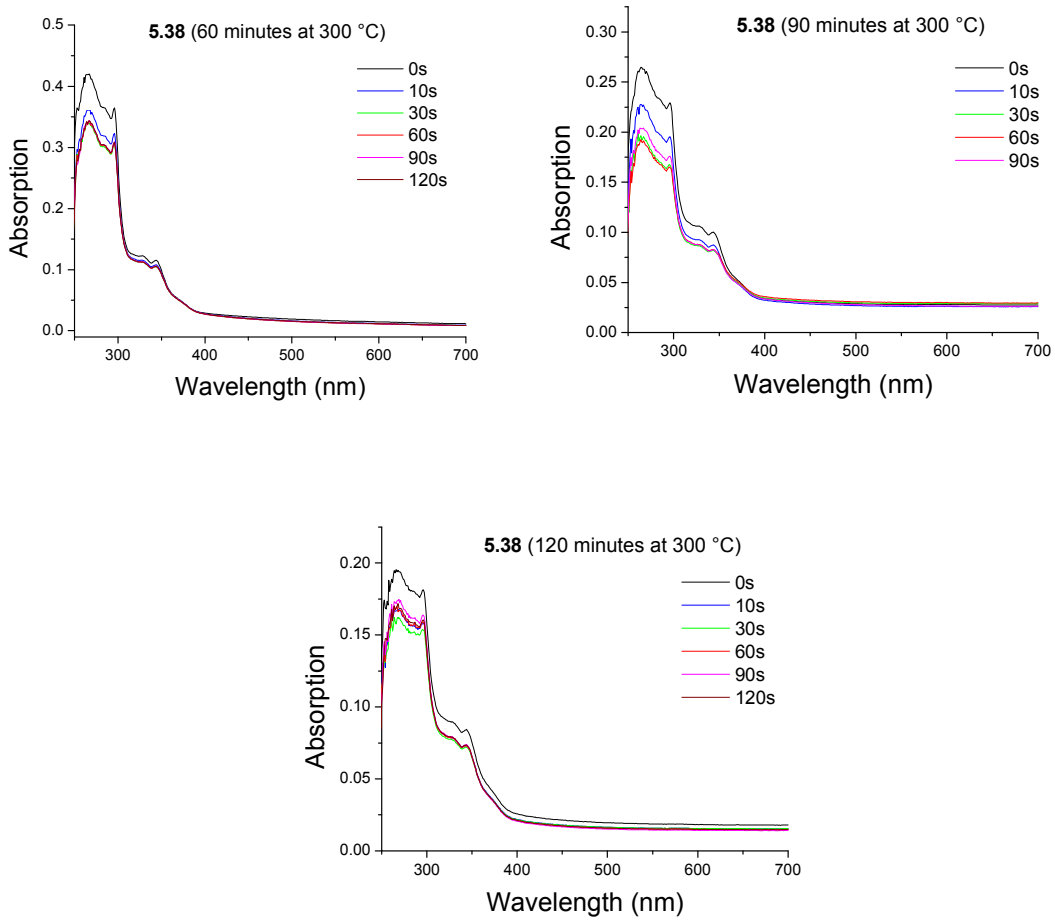

Figure 5.24. UV-vis. study of thin film on glass of copolymer **5.38**. Top left: Crosslinked 60 min at 300 °C. Top right: Crosslinked 90 min at 300 °C. Bottom: Crosslinked 120 min at 300 °C. All evaluated by *dip coat test* in chloroform for various lengths of time.

The results showed that the higher heating temperature was useful in reducing the processing times and resulted in higher resistances at shorter heating times, but that some decay in absorption signal always occurred. In order to further reduce the heating times, an alternative heating approach based on rapid thermal processing (see below) was explored.

Rapid thermal processing (RTP) can be used to very rapidly and uniformly heat samples to temperatures in excess of 1000 °C with high intensity lamps and is most commonly used for wafer processing for semiconductor applications. In 2007, Ouaknine *et al*.[35] demonstrated that RTP could be used to cure 200 mm films of benzocyclobutene in as little as five minutes depending on the conditions set. RTP was therefore chosen as an alternative method (*vs.* hot plate) for heating of thermal crosslinkable thin films of copolymer **5.38** (and other copolymers; see discussion below) with the goal of reducing processing times below the 30 minute mark. To the best of our knowledge, RTP has not been previously explored for processing of crosslinkable layers intended for OLEDs.

Thin films of **5.38** were spin-coated onto silicon (SiO_2/Si) substrates and evaluation by RTP (for this and other materials, was performed by Dr. Jassem Abdallah). In order to evaluate the RTP process, a processing profile was designed that included a nitrogen purge, heating, and cooling steps (see Chapter 2 for RTP profiles) for a total time of 41 minutes needed for processing. For the initial testing of RTP, ramp rates of 20 and 10 °C min^{-1} were used to achieve a maximum temperature of 300 °C in 21 minutes, followed by a dwell (or soak time) at the maximum temperature for 10 minutes. Two thin films of the copolymer were processed and monitored for changes in thickness after exposure to chloroform by the previously defined *dip* (film 1) or *spin coat* (film 2) *tests*. The thickness measurements were obtained by ellipsometry.

Table 5.4 Processing Steps and Measured Thicknesses (by ellipsometry)

Step	Description	Film 1 Thickness (nm)	Film 2 Thickness (nm)
1	After spin coating and fast drying	13.8	12.7
2	After RTP Process (see Profile I)	11.0	11.6
3	After chloroform exposure (*dip* or *spin coat test*)	15.1	14.8
4	After 5 min drying at 90 °C	14.3	13.8
5	After 30 min drying at 120 °C	13.2	12.5
6	After overnight vacuum bake at 120 °C	12.4	12.4

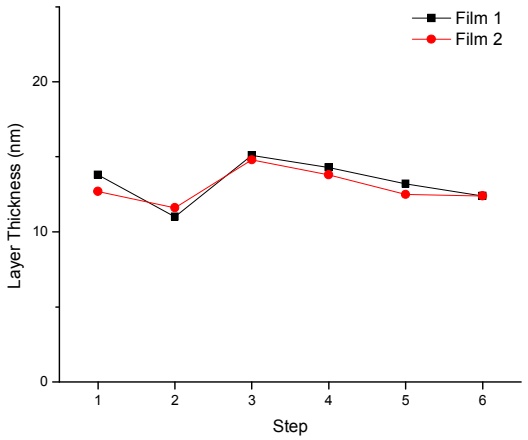

Figure 5.25. Layer thicknesses of thin films of copolymer **5.38** processed by RTP (Profile I). (where Film 1 was evaluated by the *dip test* and Film 2 was evaluated by the *spin coat test*).

Immediately after the RTP process, the thicknesses were noted to decrease which was attributed to densification of the thin films due to crosslinking. After chloroform exposure, the thin films were noted to increase in their thickness implying a swelling process likely due to penetration of the crosslinked material by the solvent. Following several drying steps, the films returned to a thickness consistent with the pre-exposure films. Overall, the ellipsometry data showed that the thicknesses of the films did not change and was considered evidence of crosslinking of copolymer **5.38**.

Atomic force microscopy (AFM) was used to study the surface morphology of the thin films of **5.38** after the RTP process and then after solvent exposure in order to evaluate for evidence of damage to the surface (i.e. pitting (holes formed by solvent attack) or increased roughness). The root mean square (rms) value for each film, calculated by the AFM software, was equal to the standard deviation of the height differences from the mean height (always defined as zero in AFM measurements). Hence, a larger rms value indicates a larger average surface roughness. The AFM image below (representative of films 1 and 2 after RTP, but prior to any solvent exposure) showed that smooth uniform films with a low rms value (below 1 nm) were obtained. Additional images at different spots of the film were taken (not shown).

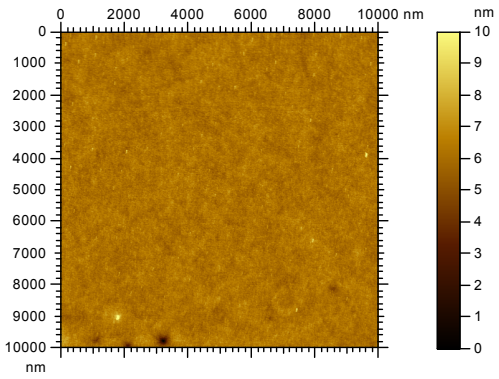

Figure 5.26. Representative AFM images of films of **5.38** after RTP. rms = 0.39 nm. (Image courtesy of Anthony Giordano).

Film 1 was soaked in chloroform for 60 s and the AFM image (below) taken after drying showed that the rms value did not increase significantly. It was noted that some defects were present for the soaked film.

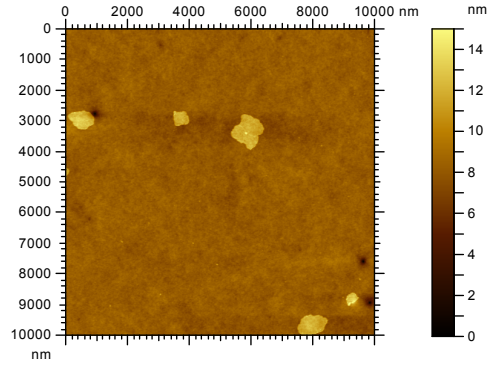

Figure 5.27. AFM of thin film 1 of **5.38** after solvent exposure (*dip test*). rms = 0.53 nm. (Image courtesy of Anthony Giordano).

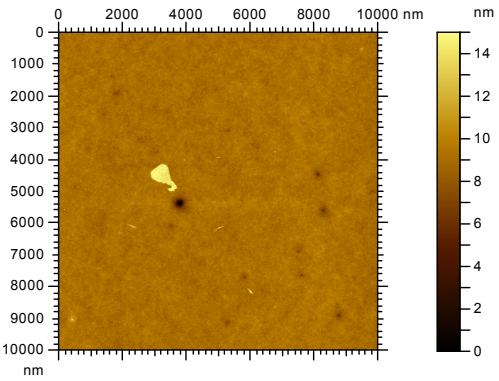

Figure 5.28. AFM of thin film 2 of **5.38** after solvent exposure (*spin coat test*). rms = 0.53 nm. (Image courtesy of Anthony Giordano).

Film 2 was evaluated to solvent resistance by spin coating chloroform directly on top of the thin film. The AFM image (above) taken after drying, showed that the surface remained generally smooth and uniform (as compared to the pre-exposure film). Less surface defects were observed (as in the dipped film), presumably due to the decreased time of the solvent exposure resulting in less damage to the surface.

A second RTP profile (II) was evaluated with faster ramp rates (150 and 50 °C min^{-1}) in order to reduce the time needed to reach 300 °C (as compared to RTP profile I). In addition, the dwell time was reduced to five minutes (from 10 minutes in profile I). For profile II, the total processing time was reduced by half (19.4 minutes total). The number of heating steps (after solvent exposure) was also reduced. Ellipsometry determined thicknesses for a single thin film on silicon substrate (SiO_2/Si) of **5.38** was processed by profile II were as follows:

Table 5.5 Processing Steps and Measured Thicknesses (by ellipsometry)

Step	Description	Thickness (nm) -
1	After spin coating and fast drying	22.2
2	After RTP Process	20.3
3	After chloroform exposure (*spin coat test*)	24.6
4	After overnight vacuum bake at 120 °C	19.9

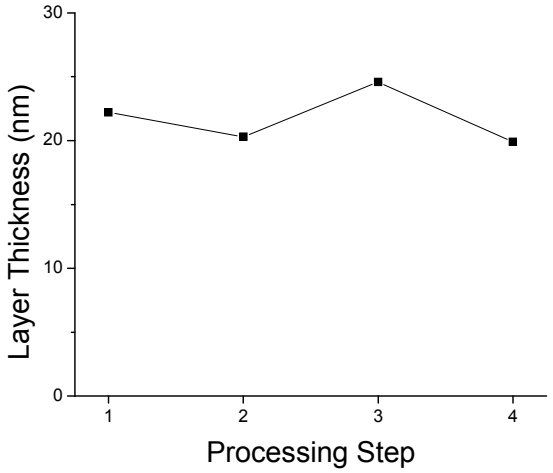

Figure 5.29. Layer thicknesses (as measured by ellipsometry) of thin films of copolymer **5.38** after processing steps 1-4.

The ellipsometry measurements showed that the thickness of the thin film remained stable over the different processing steps. As in the first RTP evaluation, evidence of film swelling was noted in the third step, but the solvent could be driven off by a drying step. AFM images of the films (pre- and post- solvent exposure) were as follows:

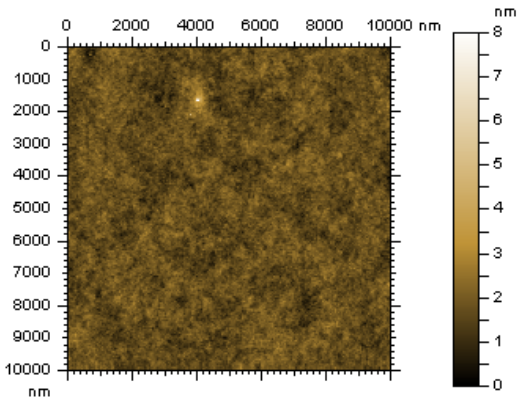

Figure 5.30. Representative AFM image of thin film of **5.38** after RTP. rms = 0.39 nm. (Image courtesy of Benjamin Wunsch)

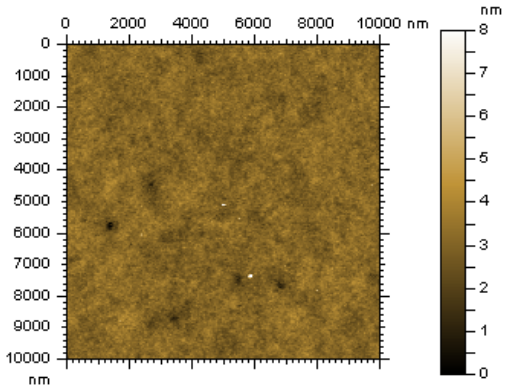

Figure 5.31. AFM of thin film of **5.38** after solvent exposure (*spin coat test*). rms = 0.53 nm. (Image courtesy of Benjamin Wunsch)

Comparison of the pre-solvent exposure film to the post-exposure film showed no significant changes in rms values or evidence of surface damage from the solvent.

Based on the results for copolymer **5.38**, at least for the conditions used, it was found that rapid thermal processing (RTP) may offer an alternative heating approach that could permit rapid crosslinking of thin films of benzocyclobutene-containing copolymers for OLED layers. As compared to a copolymer containing benzocyclobutene reported by

Fréchet and co-workers[11] requiring up to 6 hours of heating, RTP was shown to reduce the processing time, at least for the copolymer tested, down to as low as five minutes of heating.

5.4.4. Crosslinking Studies of Trifluorovinylether (TFVE) Copolymer (**5.39**)

Thin films of trifluorovinyl ether-containing copolymer (**5.39**) were prepared on glass slides by spin coating (experimental details included in Chapter 2) and processed (under various conditions). The thin films were tested for solvent resistance by either a *dip test* or *spin coat test* (with chloroform) as already described. UV-vis. measurements were used to qualitatively examine the solvent resistance of the thin films, as a measure of changes observed in the absorption spectra upon solvent exposure.

Absorption spectra of non-crosslinked control thin films of **5.39** demonstrated no resistance to solvent exposure as did thin films heated on a hot plate (under inert atmosphere) for 40 minutes at 200 or 230 °C. For thin films crosslinked for 240 minutes at 230 °C, approximately 80% of the absorption signal was retained even after several minutes of chloroform exposure.

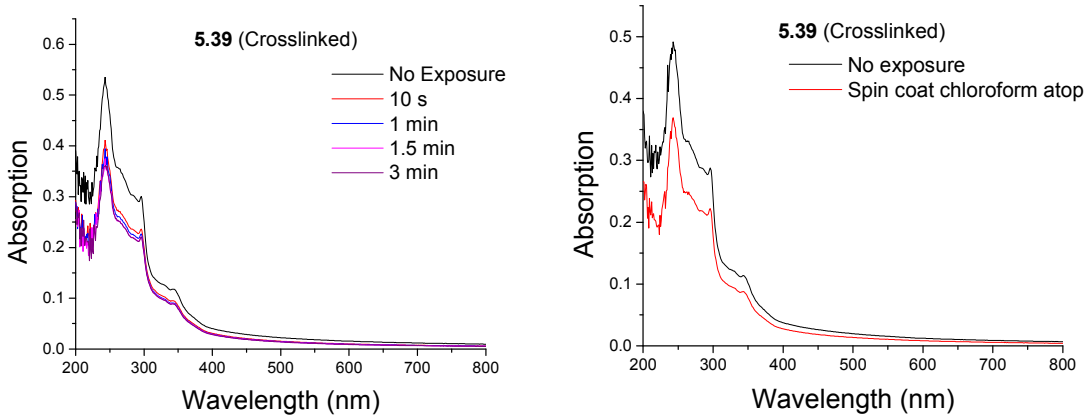

Figure 5.32. UV-vis. study of thin film on glass of copolymer **5.39**. Left: Crosslinked 240 minutes at 230 °C (*dip test*) Right: Crosslinked 240 minutes at 230 °C (*spin coat test*).

As with the BCB copolymer, RTP was also studied as a means to crosslink copolymer **5.39**. A thin film of **5.39** spin-coated onto a silicon (SiO_2/Si) substrate was processed using RTP profile III with a 10 minute dwell time at 300 °C and a total processing time of 21 minutes.

Table 5.6 Processing Steps and Measured Thicknesses (by ellipsometry)

Step	Description	Thickness (nm)
1	After spin coating and fast drying	17.5
2	After RTP Process	13.9
3	After chloroform exposure (*spin-coat test*)	26.1
4	After overnight vacuum bake at 120 °C	17.1

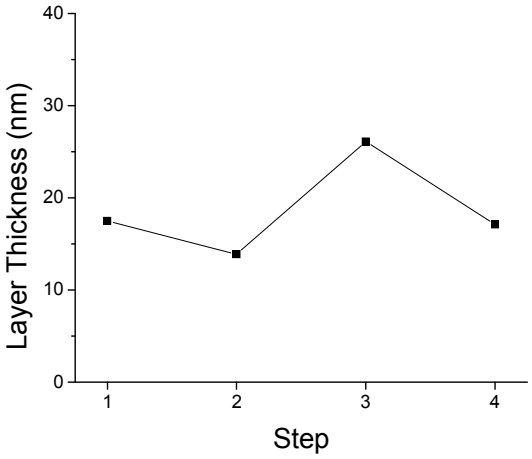

Figure 5.33. Layer thicknesses (as measured by ellipsometry) of thin films of copolymer **5.39** after processing steps 1-4.

Ellipsometry data showed the layer thickness of the thin film decreased after the RTP step and that the solvent exposure step produced an increase in the thickness (that was eliminated after drying the film). An AFM image of the thin film taken before solvent exposure had a small rms value that did not change notably upon solvent exposure (see second AFM image).

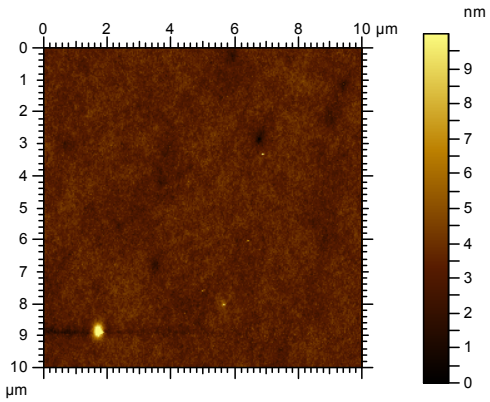

Figure 5.34. AFM image of thin film of **5.39** after RTP. rms = 0.55 nm. (Image courtesy of Benjamin Wunsch)

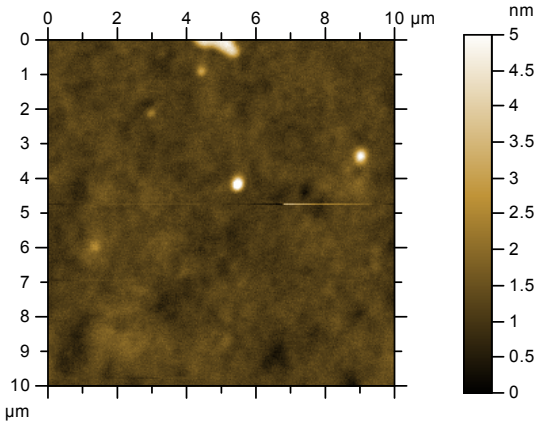

Figure 5.35. AFM of thin film of **5.39** after solvent exposure (*spin coat test*). rms = 0.53 nm. (Image courtesy of Benjamin Wunsch)

Overall, RTP was used to reduce the heating time required to insolubilize a thin film of **5.39** to as low as 10 minutes. In comparison to the literature, a copolymer containing a TFVE group reported by Jen and co- workers[8] required 40 minutes to produce insolubilized films.

5.4.5. Crosslinking Studies of Oxetane Copolymers (**5.40** and **5.41**)

Oxetane-functionalized copolymer **5.40** (containg 10 mol% of the oxetane co-monomer) was doped with varying percentages (0.75 or 1.0 wt%) of a photoacid generator and thin films (on glass) were spin coated (see chapter 2 for details). Photoacid generators, like the aryliodonium salt used here (see below), generate protons upon irradiation of light of a particular wavelength (depending on their chemical structure)[36] and can be used to initiate the cationic ring opening polymerization of the oxetanes (see Introduction section).

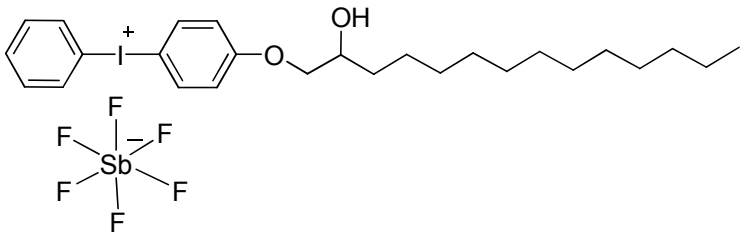

Figure 5.36. 4-((2-Hydroxytetradecyl)oxy)-phenyl)phenyliodonium hexafluoroantimonate, Photoacid Generator (PAG).

Under initial testing conditions, decomposition of the doped PAG was attempted using a handheld UV lamp (broad band emission with λ_{max} = 366 nm), held at a distance of approximately one inch above the thin films for either 1 or 3 minutes. The films were then soft-cured at 85 °C for 1 minute and then baked for 15 min at 200 °C. UV-vis. spectra were taken before and after the spin coating chloroform onto the films are shown below.

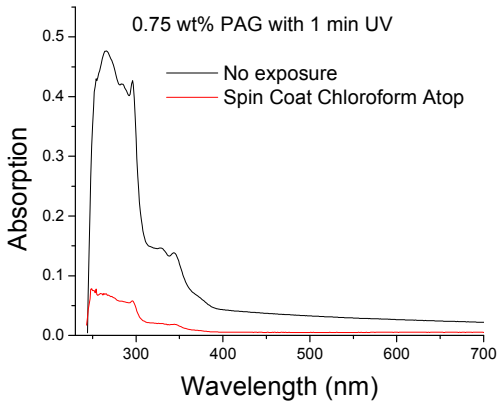

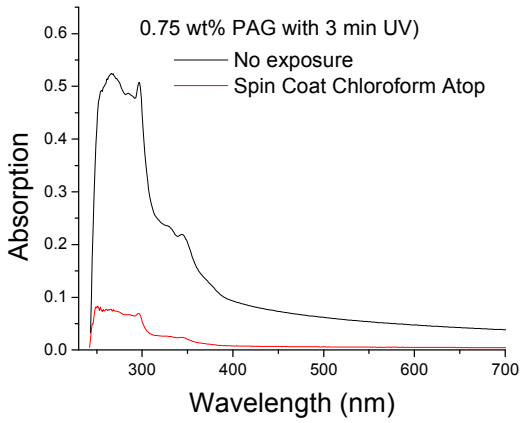

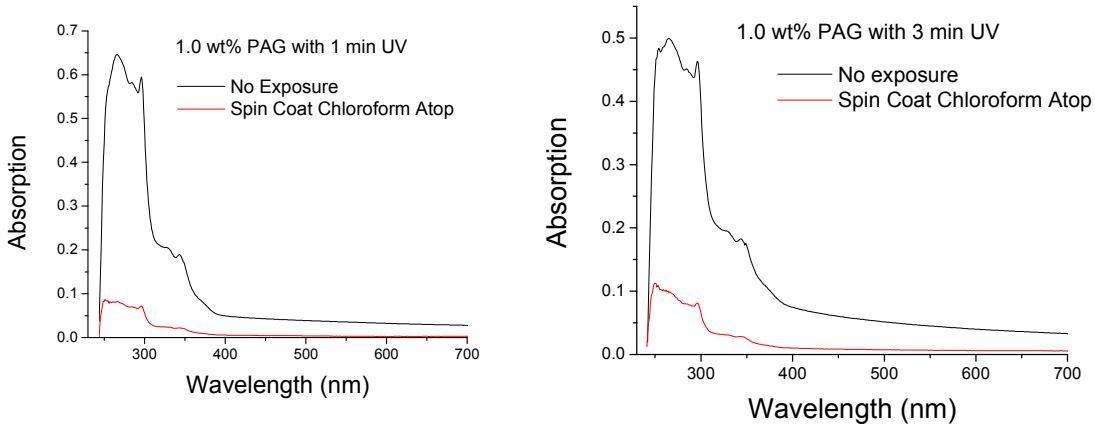

Figure 5.37. Above) UV-vis spectra of **5.40** (0.75 wt% PAG) exposed to 1 or 3 min UV irradiation. Below) UV-vis spectra of **5.40** (1.0 wt% PAG) exposed to 1 or 3 min UV irradiation.

The absorption spectra showed that regardless of PAG doping level or ultraviolet exposure time, the absorption decayed significantly after exposure indicating either a low level of crosslinking or no crosslinking. The poor results may have originated from a variety of sources including (1) too low doping levels of PAG (2) insufficient UV intensity from a handheld lamp or (3) too low mole percentage of oxetane co-monomer incorporated into the copolymer.

As discussed in the introduction, a literature example of a side-chain copolymer containing oxetane (as reported by Meerholz and co-workers) incorporated the oxetane co-monomer at 25 or 50 mol%; much higher than for copolymer **5.40**. Therefore, copolymer **5.41** was synthesized with a higher mole percent composition of the oxetane co-monomer, in order to address the possibility that the oxetane content was too low. For subsequent crosslinking evaluations, other potential issues were explored by increasing

the doping level of the PAG to 2 wt% and changing the UV irradiation source to the photoreactor.

Thin films of copolymer **5.41** doped with 2 wt% of the PAG were spin-coated onto glass slides, exposed to UV irradiation in a photoreactor (with lamps at λ_{max} of 253 or 300 nm for 10 or 60 seconds), and analyzed for resistance to the solvent chloroform by UV-vis. The results showed that for all films, regardless of conditions, the absorption signal decayed after exposure and no appreciable solvent resistance was attained indicating unsuccessful crosslinking of the films.

Due to the unsuccessful crosslinking of copolymer **5.41** via UV initiation, alternative initiation of the PAG was explored. It is known that under sufficient heating, aryliodonium salts decompose and produce acids; and can be considered thermoacid generators (TAGs).[37] In order to evaluate the potential use of TAGs for oxetane copolymers, a preliminary evaluation of the copolymer (neat) and the copolymer doped with the TAG (see figure below) was conducted by differential scanning calorimetry.

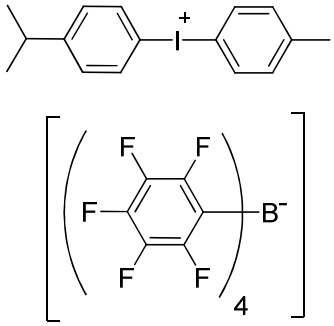

Figure 5.38. 4-isopropyl-4'-methyldiphenyl iodonium tetrakis(pentafluorophenyl) borate, Thermoacid Generator (TAG).

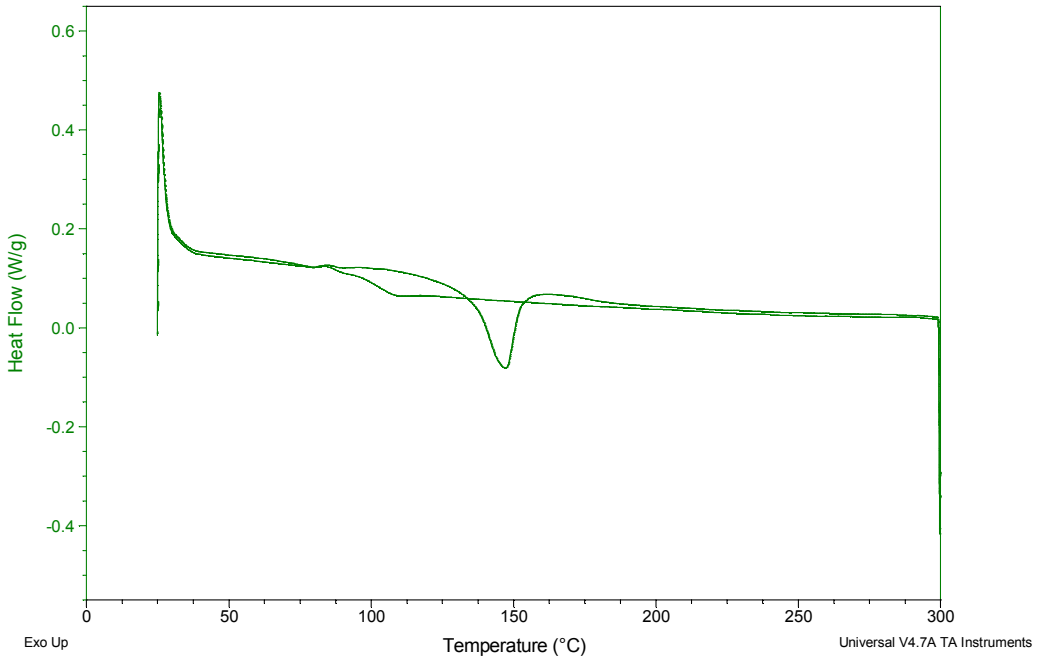

Figure 5.39. Differential scanning calorimetry of **5.41** (neat) showing a melting (first heating) and glass transition (second heating) event.

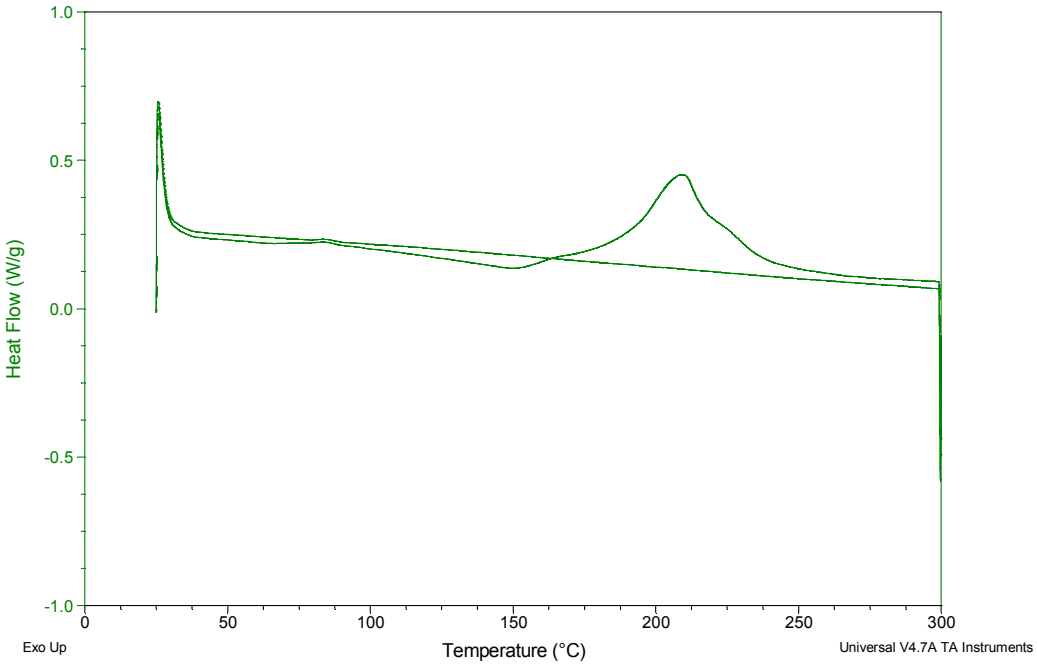

Figure 5.40. Differential scanning calorimetry of **5.41** (5 wt% TAG loading) showing a broad exothermic peak.

Comparison of the DSCs of the neat copolymer and the copolymer doped with 5 wt% of the TAG showed the appearance of a broad exothermic event between 150 – 250 °C (maximum at 209 °C) on the first heating cycle that was no longer observed for the second. In addition, no glass transition was observed on the second heating of the doped copolymer. The changes were tentatively attributed to the crosslinking of the copolymer.

Three thin films of **5.41** (doped with 7 wt% of the TAG) were spin-coated onto silicon (SiO_2/Si) substrates and heated by RTP (see RTP profile IV in Chapter 2) with a heating ramp rate of 60 °C min^{-1} and a soak temperature of 200 °C. In addition to RTP, two additional thin films were heated (covered by a watch glass) on hot plate (under nitrogen atmosphere) at 175 and 210 °C, under inert atmosphere.

Table 5.7 Processing Steps and Measured Thicknesses (by ellipsometry)

Step	**Description**	**Thickness (nm) - RTP**	**Thickness (nm) - HP-210 °C**	**Thickness (nm) - HP-175 °C**
1	After spin coating and fast drying	93.9	85.3	81.9
2	I) RTP process at 200 °C II) 20 min at 210 °C on hot plate III) 30 min at 175 °C on hot	86.6	81.1	78.6
3	After chloroform exposure (*spin-coat test*)	88.6	83.8	78.8
4	After overnight vacuum bake at 120 °C	87.8	81.4	76.7

where HP denotes hot plate

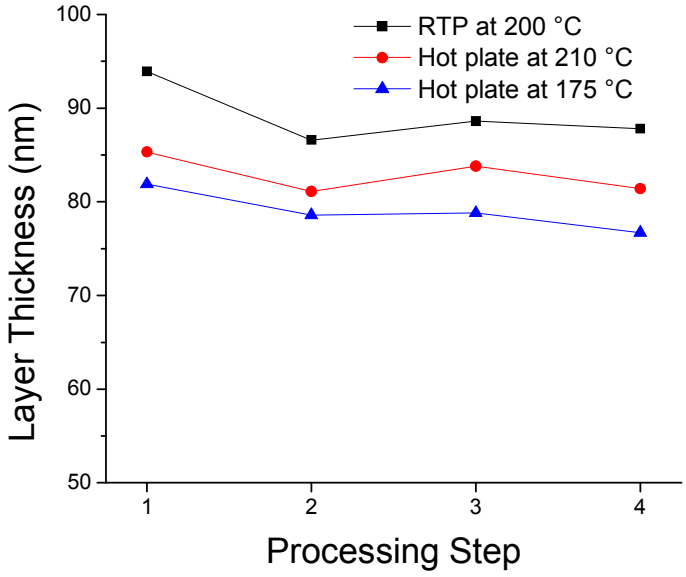

Figure 5.41. Layer thicknesses (as measured by ellipsometry) of thin films of copolymer **5.41** (7 wt% loading of TAG) after processing steps 1-4.

Measurements of the layer thickness showed they did not change substantially after solvent exposure and drying. In the figure below, a representative AFM image of three films after the crosslinking process (by either RTP or hot plate) is shown for the surfaces produced. For both the thin films processed by RTP and on the hot plate at 210 °C, the surfaces remained smooth and essentially defect free after solvent exposure.

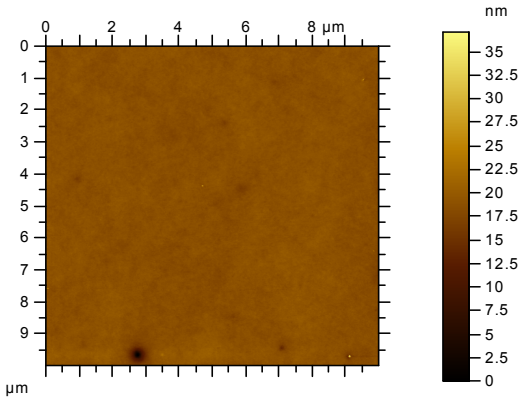

Figure 5.42. Representative AFM image of thin film of **5.41** after RTP or hot plate heating. rms = 0.65 nm. (Image courtesy of Benjamin Wunsch)

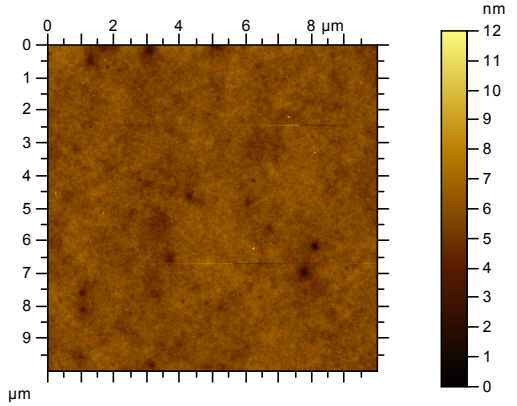

Figure 5.43. AFM of thin film of **5.41** (processed by RTP) after solvent exposure (*spin coat test*). rms = 0.51 nm. (Image courtesy of Benjamin Wunsch)

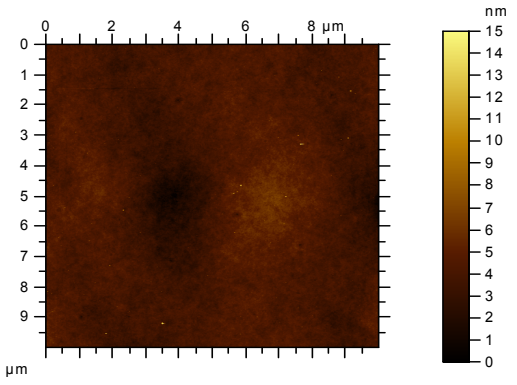

Figure 5.44. AFM of thin film of **5.41** (processed on a hot plate at 210 °C) after solvent exposure (*spin coat test*). rms = 0.81 nm. (Image courtesy of Benjamin Wunsch)

For the thin film processed at the lowest temperature of 175 °C, signs of pitting damage were noted on the AFM image (below) that suggested that the crosslinking level of the film was not sufficiently high to afford uniform resistance to solvent attack. At the lower heating temperature, the rate of crosslinking was lower and non-uniform crosslinking may have occurred permitting nucleation and growth of pin holes. Based on the observation, temperatures around or below 175 °C are inadequate to fully insolubilize thin films of copolymer **5.41** that can resist damage when exposed to harsh solvent treatment.

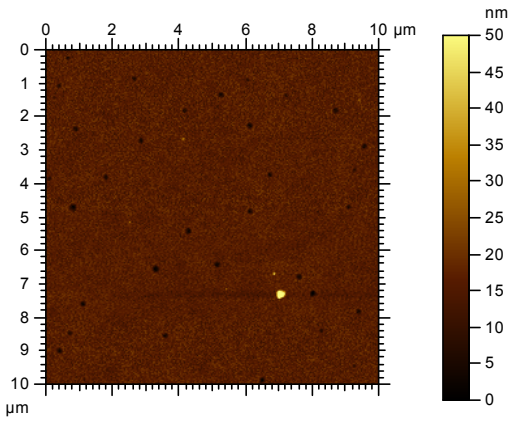

Figure 5.45. AFM of thin film of **5.41** (processed on a hot plate at 175 °C) after solvent exposure (*spin coat test*). rms = 2.56 nm. (Image courtesy of Benjamin Wunsch)

Based on the prior results, thin films of TAG doped copolymer **5.40** were evaluated using RTP and hot plate conditions in order to determine if they would crosslink. Earlier attempts to crosslink **5.40** by UV initiation alone were unsuccessful (vide supra). Thin films of **5.40** doped with 6 wt% of the TAG were spin-coated onto silicon (SiO_2/Si) substrates and heated by RTP (with 150 and 100 °C min^{-1} ramp rates) or

on a hot plate (covered by a watch glass) at 190 °C; under nitrogen atmosphere. In both processes, the thin films were heated for 15 minutes.

Table 5.8. Processing Steps and Measured Thicknesses (by ellipsometry)

Step	**Description of Processing Step**	**Thickness (nm) - RTP**	**Thickness (nm) - HP-190 °C**
1	After spin coating and fast drying	58.0	61.4
2	I) RTP process at 190 °C II) 15 min at 190 °C on hotplate	56.1	58.4
3	After chloroform exposure (*spin-coat test*)	54.2	56.8
4	After overnight vacuum bake at 120 °C	55.2	56.4

where HP denotes hot plate

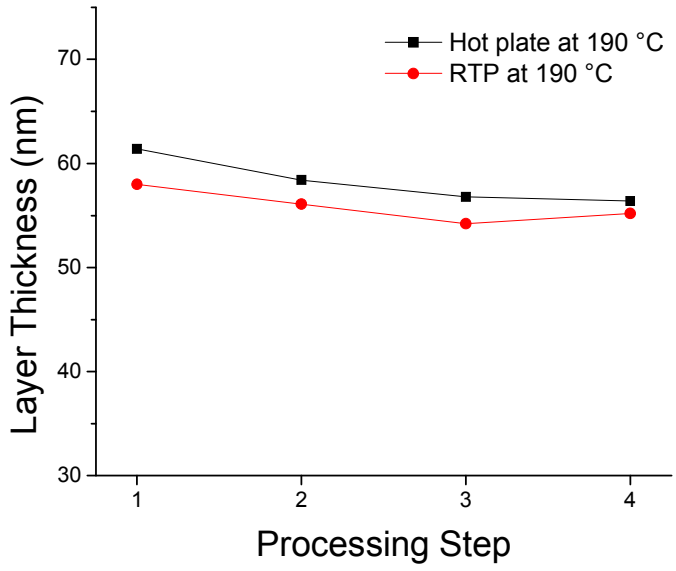

Figure 5.46. Layer thicknesses (as measured by ellipsometry) of thin films of copolymer **5.40** (6 wt% loading of TAG) heated by hot plate or RTP after processing steps 1-4.

Ellipsometry determined film thicknesses were observed to be stable after solvent exposure. AFM images of the surfaces after solvent exposure showed that the films had low roughness with rms values near or below 1 nm. For the film processed by RTP some minor surface defects were noted, while the hot plate processed film had less defects by comparison.

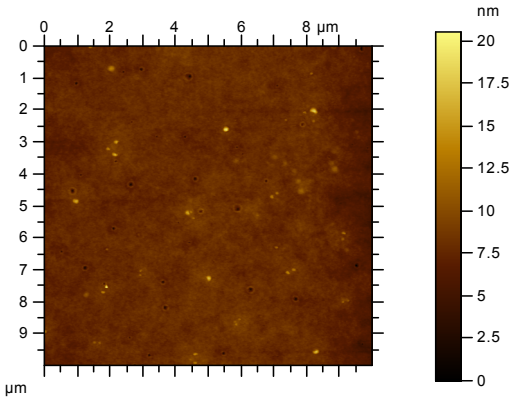

Figure 5.47. AFM of thin film of **5.40** (processed by RTP) after solvent exposure (spin coat test). rms = 0.75 nm. (Image courtesy of Benjamin Wunsch)

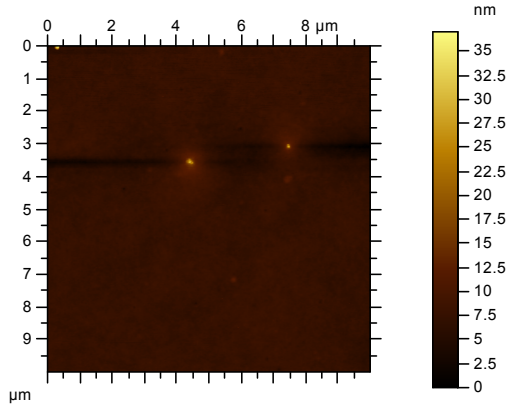

Figure 5.48. AFM of thin film of **5.40** (processed on a hot plate at 175 °C) after solvent exposure (spin coat test). rms = 0.98 nm. (Image courtesy of Benjamin Wunsch)

As reported by Meerholz and co-workers,[31] the side-chain copolymers used in those studies contained high levels of the oxetane co-monomer which lead to dilution of the

hole transport functionality (see Introduction). In the case of copolymer **5.40**, it was possible to show that a lower level of co-monomer (10 mole percent) was sufficient to afford insolubilized thin films when doped with the TAG and crosslinked under thermal initiation conditions.

In the studies discussed above, the thermoacid generator (TAG) was doped at levels of 6 and 7 wt% of the copolymer. The decomposition of acid generators are known to leave by-products[37] and might interfere with OLED device performance. Therefore, a study of thin films with reduced doping levels of the TAG was pursued with lower levels of 0.5, 1, and 2 wt% of the TAG. Doped thin films of **5.40** were spin-coated onto silicon (SiO_2/Si) substrates and covered films were heated on a hot plate at 200 °C for 30 minutes. A control sample with no TAG was also evaluated.

Upon spin-coating, thin films on silicon dioxide (SiO_2/Si) were formed at all the specified doping levels of the TAG. Interestingly, as the films were heated, dewetting of the surface was observed (visually) for three of the four samples. The film surfaces were examined by optical microscopy as shown:

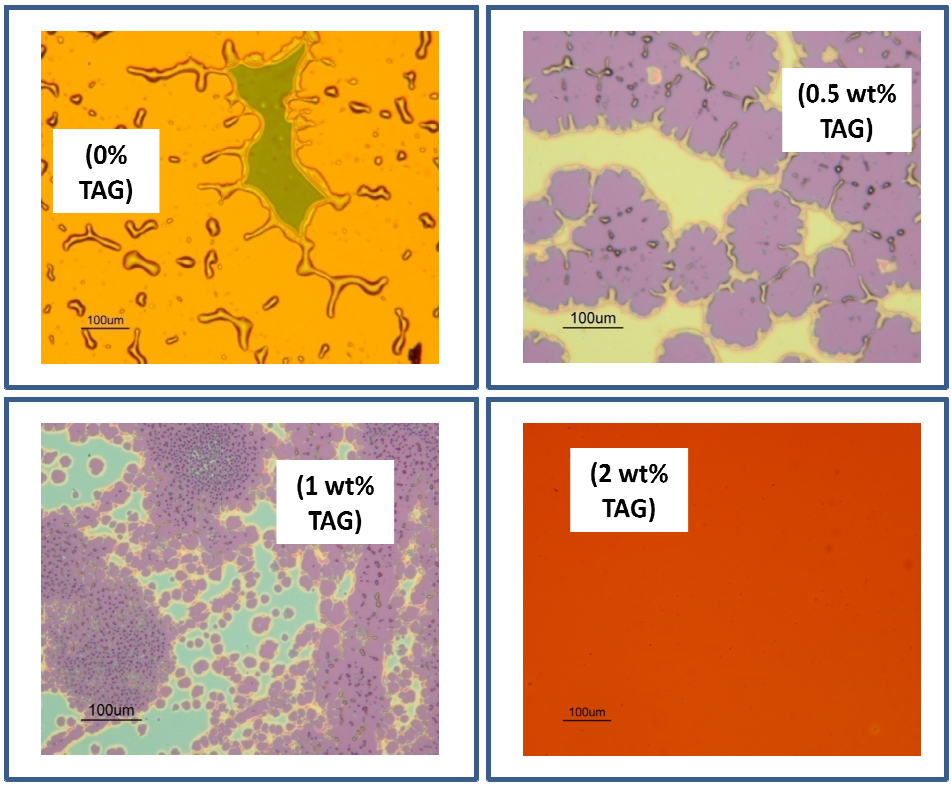

Figure 5.49. Optical microscopy images films of copolymer **5.40** (doped with 0, 0.5, 1, and 2 wt% TAG) on intrinsic SiO_2/Si after heat treatment at 200 °C. (Images courtesy of Jassem Abdallah)

For the thin film with no TAG loading, dewetting (defined below) of the copolymer was observed after heating to 200 °C. Likewise, the thin films with 0.5 and 1 wt% loading of TAG also showed evidence of partial dewetting upon heating. For the 2 wt% TAG doped film, the image suggested that no dewetting had occurred.

The process of dewetting a surface occurs when a material that is processed onto a substrate breaks up (by forming holes initially) and eventually forms droplets of the material on the substrate.[38] Studies of coatings on substrates have found that thin films (i.e. of a polymer) minimize their free energy by exposing the lowest surface energy material (either the substrate or the polymer) to the ambient surrounding[39]; a process that can be described by the spreading coefficient, *S*:

$$S = \gamma_s - (\gamma_c + \gamma_{cs}) \quad (5.1)$$

where γ_s and γ_c represent the surface free energy of the substrate and coating, and γ_{cs} represents the interfacial energy between the two. For cases where the surface energy of the coating is lower than of the substrate, films are stable, while in the case where they are higher, films are unstable and dewet.[40] For intrinsic silicon dioxide (without any modification), the surface energy has been reported at 64 mJ/cm^2 .[41]

For the films of copolymer **5.40** studied by optical microscopy, wetting of the silicon substrate at room temperature produced uniform thin films. It was only upon heating that the dewetting or partial dewetting was observed for three of the four films. The phenomenon of dewetting of polystyrene thin films taken above their glass transition temperatures has been reported.[40,42] Presumably, these thin films gain sufficient chain mobility to form holes and dewet. As copolymer **5.40** had a glass transition temperature of 119.6 °C, the dewetting observed at high temperatures may be consistent with heating beyond the copolymer's glass transition. Interestingly, it was noted that the films of **5.40** with 0.5 and 1 wt% loading of the TAG showed only partial dewetting, implying that crosslinking was occurring concurrently with the dewetting process; but not rapidly enough to fully insolubilize the films. As evidence that the residual surface material was crosslinked, it was observed that this material could not be removed by washing with solvent.

In order to address the issue of dewetting, Dr. Jassem Abdallah and I considered raising the surface free energy of the intrinsic silicon (Si/SiO_2) substrate by soaking them in piranha solution (70:30 (v/v) = sulfuric acid:hydrogen peroxide) followed by thorough washing with deionized water and acetone. The surface energy of piranha treated silicon

dioxide has been reported in the range of 72 – 77 mJ/cm^2.[43] Thin films of **5.40** were spin-coated onto the treated substrates (doped with 0.5 and 1 wt% TAG) and heated at 200 °C for 30 min (covered on a hot plate under inert atmosphere). Optical microscopy of the thin films revealed that for the control film (with no TAG loading) partial dewetting still occurred, but to a lesser extent, as compared to non-piranha treated substrates. For the 0.5 and 1 wt% films, no dewetting was observed, in contrast to the earlier thin films that partially dewet intrinsic silicon dioxide.

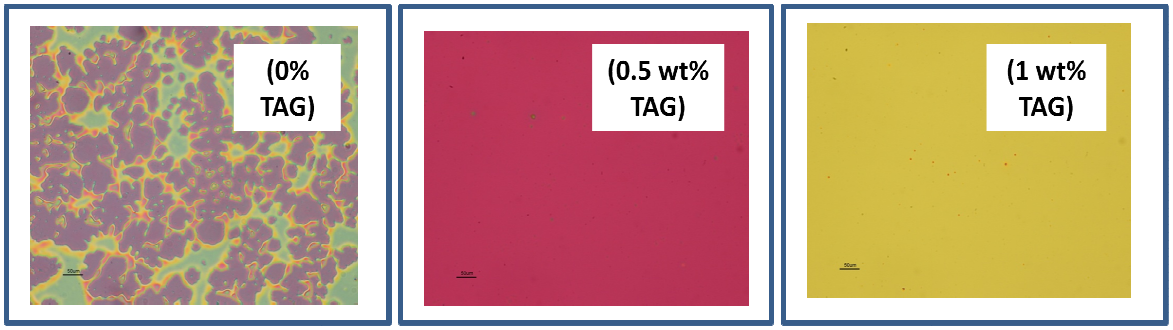

Figure 5.50. Optical microscopy images films of copolymer **5.40** (doped with 0, 0.5, and 1 wt% TAG) on piranha-treated SiO_2/Si after heat treatment at 200 °C. (Images courtesy of Jassem Abdallah)

The thicknesses of the thin films with 0.5 and 1 wt% TAG doping were measured by ellipsometry.

Table 5.9. Processing Steps and Measured Thicknesses (by ellipsometry)

Step	**Description of Processing Step**	**Thickness (nm) – 1.0 wt% TAG**	**Thickness (nm) – 0.5 wt% TAG**
1	After spin coating and fast drying	53.2	59.6
2	Film (on piranha treated substrate) heated for 30 min (covered) on hot plate at 200 °C	53.3	58.6
3	After chloroform exposure (*spin-coat test*) and drying at 60 °C	44.5	50.4
4	After drying at 120 °C	42.0	48.2

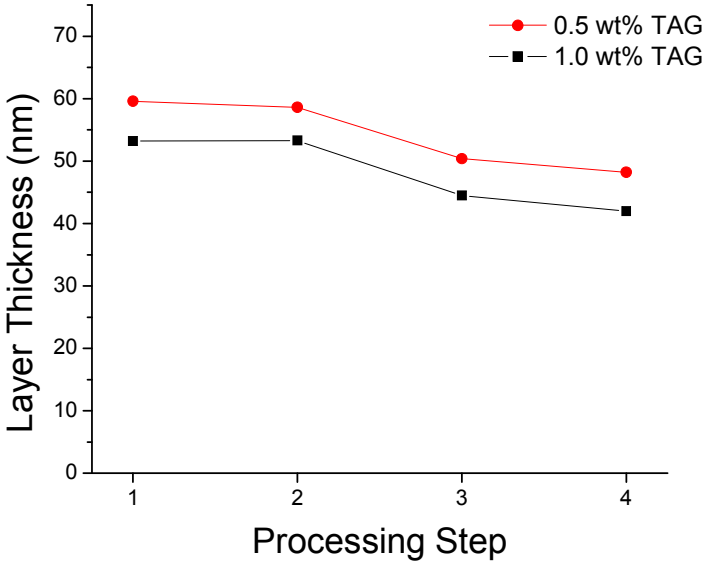

Figure 5.51. Layer thicknesses (as measured by ellipsometry) of thin films of copolymer **5.40** (with 0.5 or 1.0 wt% TAG loading) on piranha treated substrates.

At the lower doping levels of TAG, the measurements showed a loss of thickness of ~ 10 nm; an approximate loss of 20% of the surface thickness. The decrease can be attributed to the reduction of the TAG doping level. An AFM image of the thin film doped at the lowest level of 0.5 wt% after solvent exposure and drying was found to be smooth (rms = 0.47 nm) with no evidence of surface damage.

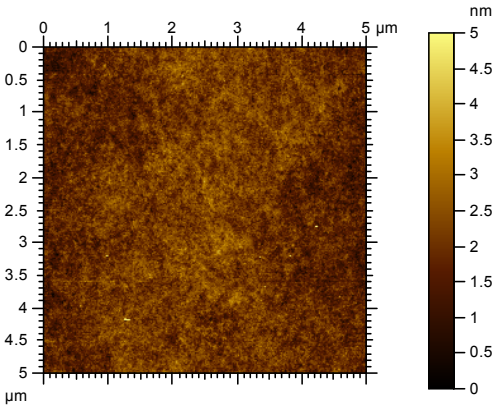

Figure 5.52. AFM of thin film of **5.40** (0.5 wt% TAG) on piranha treated silicon substrate after solvent exposure (spin coat test). rms = 0.47 nm. (Image courtesy of Benjamin Wunsch)

Despite the observed loss in film thickness observed, it was shown that thin films of **5.40** doped with TAG levels as low as 0.5 wt% could be insolubilized with approximately 80% thickness retention.

5.5. Crosslinkable Small Molecule

5.5.1. Design Rationale and Synthesis for Crosslinkable Small Molecule

In the previous sections, crosslinkable copolymers were used to achieve insolubilized thin films. In this section, discussion on a crosslinkable small molecule is presented based on a bis(styrene) approach. A few literature examples of bis-styrene functionalized small molecules for OLEDs have been reported for crosslinking.[12,13] These materials can typically be crosslinked in thirty minutes to one hour at temperatures near 200 °C. The advantage of such an approach (*vs*. that of a polymer) stems from the ability to use well-purified (i.e. by chromatography) small molecules. Based on the triscarbazole hole transport group evaluated in the copolymers above, a crosslinkable triscarbazole small molecule was synthesized. It was conceived that the bulk of the triscarbazole group plus the bis(styrene) functionality might produce a solution-processable small molecule.

Conversion of 3,5-dimethoxyphenylmagnesium chloride to 1-iodo-3,5-dimethoxybenzene was performed as the first step using iodine. The iodo- intermediate was coupled to triscarbazole (obtained from Solvay, S.A.) by Ullmann coupling and then the methoxy groups were deprotected with boron tribromide to afford intermediate **S5.9**.

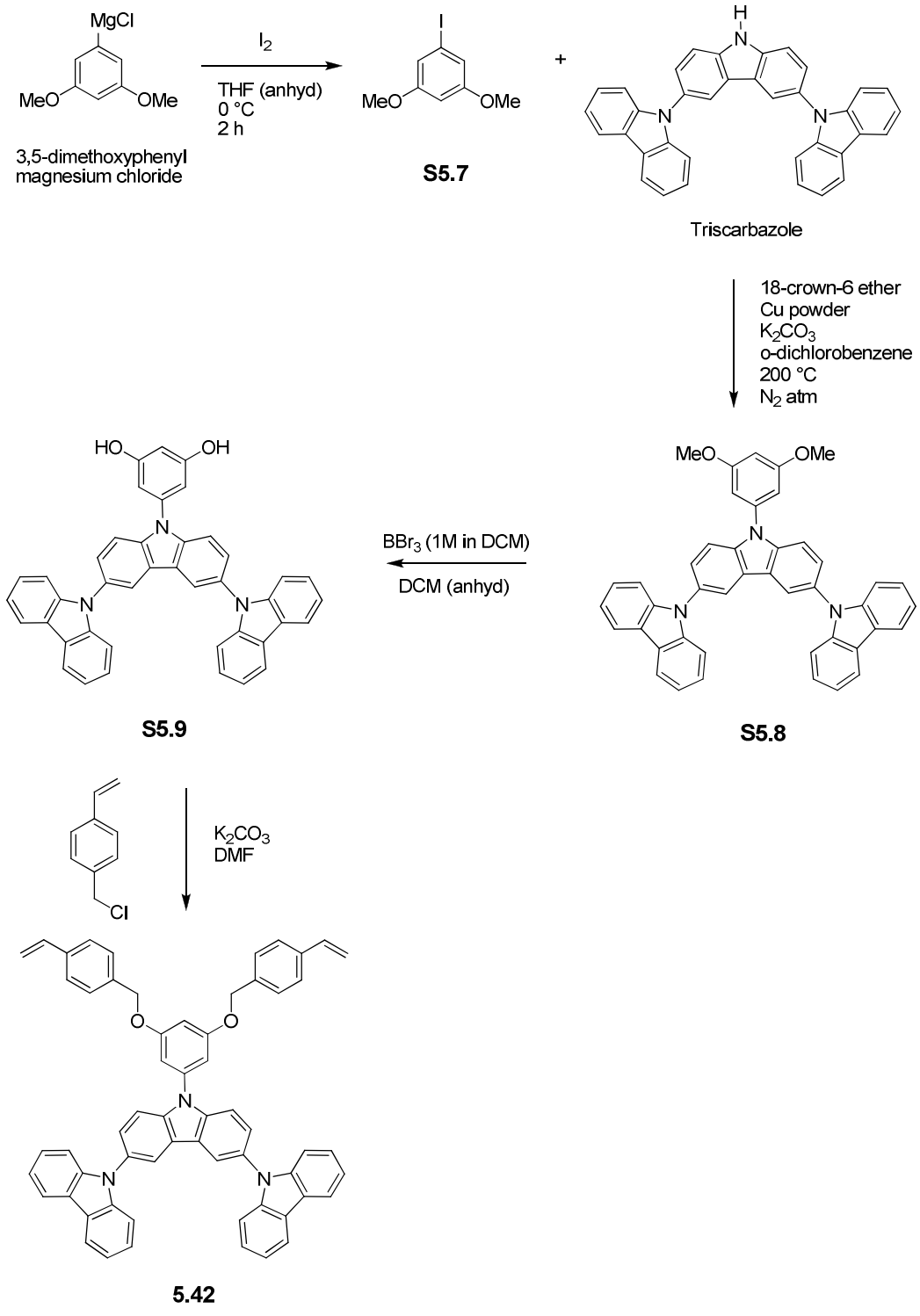

Scheme 5.10. Synthesis of bis(styrene) triscarbazole small molecule **5.42**.

S5.9 was subsequently reacted with 4-vinylbenzyl chloride to afford the final bis(stryrene) functionalized target **5.42**, which was purified by column chromatography.

Full synthetic details for the above syntheses (including characterization data) may be found in Chapter 2.

5.5.2 Crosslinking Studies of Bis(styrene) Triscarbazole **5.42**

Attempts to process thin films from solution of small molecule **5.42** onto intrinsic silicon dioxide (SiO_2/Si) proved unsuccessful due to room temperature dewetting (see earlier discussion on dewetting). Issues of wettability may be caused due to the low polarity of organic materials which can result in incompatibilities when they are processed onto high surface energy surfaces (like those of oxides).[44] Therefore, in order to improve the wettability of **5.42**, we explored surface modifiers to treat the intrinsic silicon substrate. The two modifiers chosen were benzylphosphonic acid (**BPA**) and a pentafluorinated benzylphosphonic acid (**F5BPA**).[44,45]

BPA **F5BPA**

Figure 5.53. Surface modifiers (**BPA** and **F5BPA**) used for silicon dioxide substrates.

On the **BPA** and **F5BPA** treated silicon substrates, thin films were obtained successfully. A thin film was processed by RTP (see profile VI) with a 15 min dwell time at 200 °C on BPA-treated silicon.

Table 5.10. Processing Steps and Measured Thicknesses (by ellipsometry)

Step	Description	Film Thickness (nm) -
1	After spin coating and fast drying	34.4
2	After RTP Process	33.1
3	After chloroform exposure (*spin-coat test*)	45.1
4	After overnight vacuum bake at 120 °C	35.8

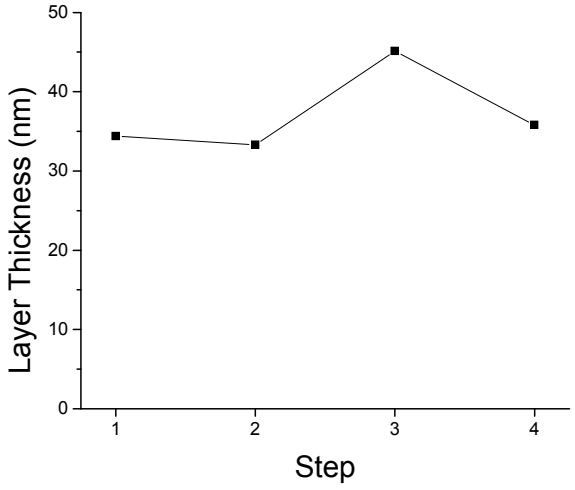

Figure 5.54. Layer thicknesses (as measured by ellipsometry) of thin films of bis(styrene) triscarbazole, **5.42**.

Ellipsometry measurements showed that the thickness of the film did not change significantly after solvent exposure and drying. An AFM image taken before solvent exposure showed that the film had a small rms value and was free of obvious defects.

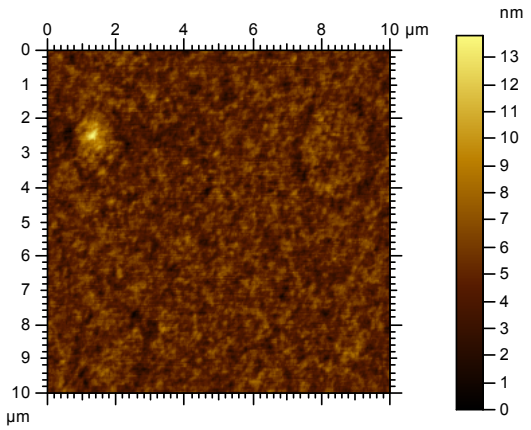

Figure 5.55. Representative AFM image of thin film of **5.42** after RTP. rms = 1.14 nm. (Image courtesy of Benjamin Wunsch)

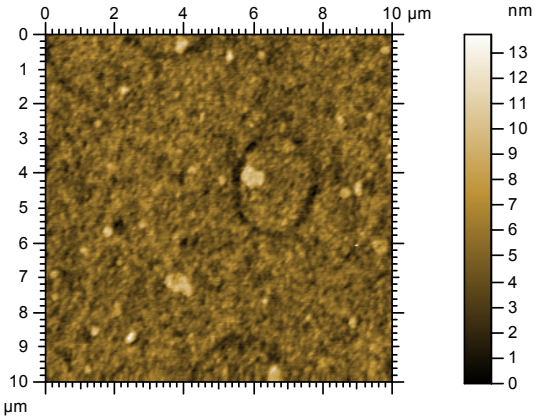

Figure 5.56. AFM of thin film of **5.42** after solvent exposure (spin coat test). rms = 1.25 nm. (Image courtesy of Benjamin Wunsch)

The AFM image of the film taken after solvent exposure and drying (above), showed some minor defects. **5.42** was shown to be crosslinkable despite some evidence of surface damage. Surface roughness did not increase significantly (as compared to the pre- solvent exposure film) and sufficient evidence of solvent resistance was observed. Using RTP, heating times as short as 15 minutes were shown to be effective in producing

insolubilized thin films; further time reductions may yet be possible. In order to evaluate the small molecule as a hole-transport material, OLED devices were fabricated.

5.6. Example OLED Devices

Devices reported here were fabricated by Dr. Dengke Cai (Kippelen group, School of Computer and Electrical Engineering). Crosslinkable small molecule bis(styrene) triscarbazole was tested as a hole-transport (HT) material in OLED devices. Green devices were fabricated based on the architecture:

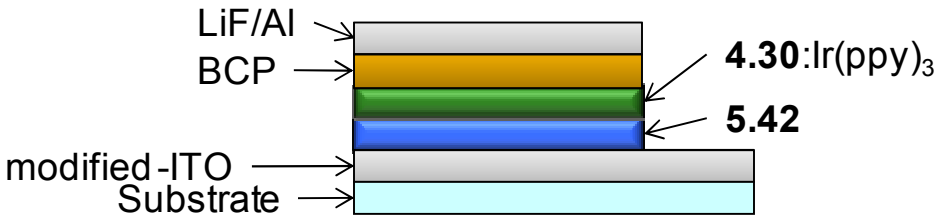

Figure 5.57. Green OLED architecture for testing crosslinkable small molecule, **5.42**.

Ambipolar small molecule **4.30** (see Chapter 4) was used as the host material. For the purposes of comparison, two devices were prepared. In the first device, the HT layer composed of **5.42** was spin-coated onto **F5BPA**-modified-ITO (see figure 5.52) and the subsequent layers were vacuum-deposited on top. In the second device the layer of **5.42** was crosslinked at 200 °C for 30 minutes.

Table 5.11. Green $Ir(ppy)_3$ devices

Device	Doping (wt%)	HT Material	L (cd/m^2)	EQE (%)	Turn on (V)[a]
A	6	**5.42**[b]	100	5.6	3.9
	6	**5.42**[b]	1,000	4.8	3.9
B	6	**5.42**[c]	100	1.9	2.9
	6	**5.42**[c]	1,000	4.3	2.9

[a] turn on voltages taken from *L-V* curves at 10 cd/m^2

[b] uncrosslinked

[c] crosslinked on hot plate (200 °C for 30 min; inert atmosphere)

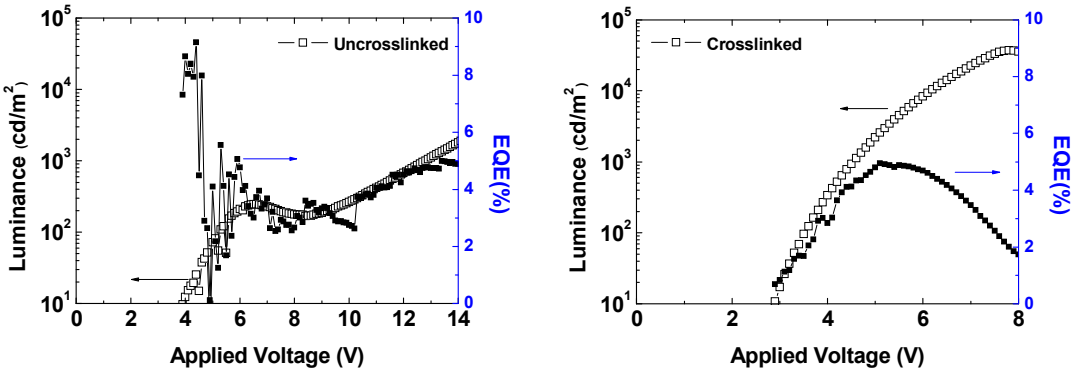

Figure 5.58. Luminance and external quantum efficiency as a function of applied voltage for uncrosslinked device A (left) and crosslinked device B. Data courtesy of Dr. Dengke Cai (Kippelen group).

From the luminance and EQE data for the devices shown in the figure above, it is clear that the uncrosslinked device showed inconsistent curves that might be indicative with damage to the hole-transport layer. Although the emissive layer was vacuum deposited, the layer may have suffered damage under device operation. Its possible that damage to the layer occurred under operation but further investigation would be required. It is likely that the EQE values calculated from the data for device A are not representative of the true value. The crosslinked device showed luminance and EQE

curves that were less irregular, but overall decreased EQE of 1.9% at a luminance of 100 cd/m^2 was found. Interestingly, the efficiency for the crosslinked device increased at a higher brightness of 1,000 cd/m^2. For the crosslinked device, the insolubilized layer may be resistant to changes during device operation. Another notable change between the devices was the observed decrease by ~1 V in the turn-on voltage for device B. Of course, it is difficult to explain these observations based on preliminary test devices and additional studies are warranted.

A series of blue devices were fabricated that evaluated the ability to solution-process the host layer directly onto the crosslinked hole transport layer composed of small molecule **5.42**. For devices with the architecture shown below, the host was comprised of a blend of the homopolymers **p-TCZ** and **p-OXD** (provided by Dr. Xuyang He). For the devices fabricated on **F5BPA**-modified ITO, the layer of **5.42** was crosslinked at 200 °C for 30 min before processing of the blended emissive layer.

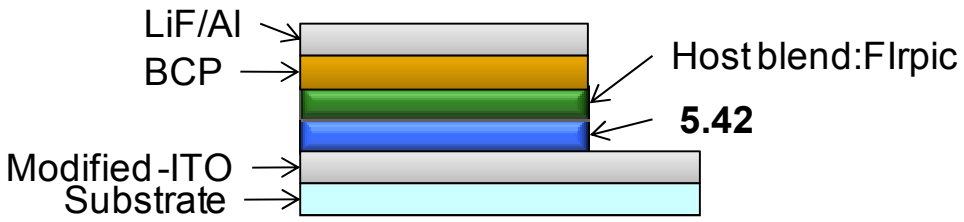

Figure 5.59. Blue OLED architecture for testing crosslinkable small molecule, **5.42**.

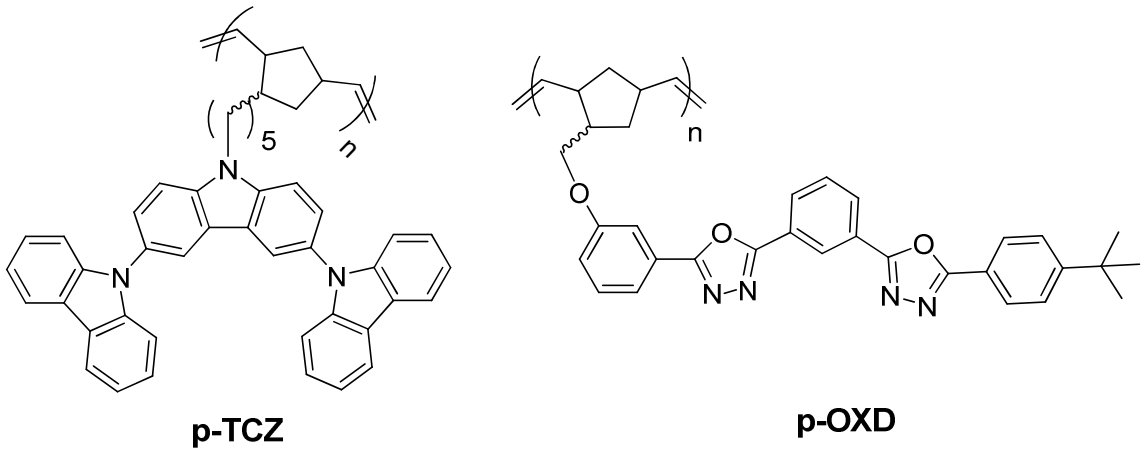

Figure 5.60. Triscarbazole homopolymer (**p-TCZ**) and oxadiazole homopolymer (**p-OXD**).

Table 5.12. Blue Firpic devices with crosslinked **5.42** HT layer

Device	Doping (wt%)	Host Blend[a]	L (cd/m^2)	EQE (%)
A	6	**p-TCZ:p-OXD** = 60:40	100	1.4
	6	**p-TCZ:p-OXD** = 60:40	1,000	0.59
B	6	**p-TCZ:p-OXD** = 50:50	100	3.3
	6	**p-TCZ:p-OXD** = 50:50	1,000	3.4
C	6	**p-TCZ:p-OXD** = 40:60	100	5.5
	6	**p-TCZ:p-OXD** = 40:60	1,000	4.8

[a] Blends given in wt%:wt% composition

Overall, the device efficiencies were noted to be highly dependent on the composition ratio of the ambipolar blend of polymers used; for the best device, efficiencies as high as 5.5% were obtained. The performance obtained for blue device (C) was the highest with an EQE of 5.5 at a luminance of 100 cd/m^2 and was considered promising.

5.7. Conclusions

Several triscarbazole-based hole transport copolymers containing different crosslinkable thermal groups (including benzocyclobutene or trifluorovinyl ether) were synthesized and characterized. These copolymers were evaluated for crosslinking by different heating methods including hot plate and rapid thermal processing (RTP). For the BCB copolymers (**5.37** and **5.38**), under hot plate heating, UV-vis. studies showed thin films had to be heated for several hours at 230 °C to show high levels of solvent resistance (~ 80%), which could be reduced from hours to approximately 30 minutes by increasing the hot plate temperature to 300 °C (with up to ~90% resistance). In order to further decrease the processing time, RTP was used to rapidly achieve and hold the thin films (of copolymer **5.38**) at 300 °C. Using RTP, heating for as little as five minutes was found to be sufficient to afford very high insolubilization of thin films of the BCB-containing copolymer. For the trifluorovinyl ether copolymer (**5.39**) preliminary studies on a hot plate heating required up to four hours of heating (at 230 °C) to produce solvent resistance (~ 80%). RTP was also used to process films of **5.39**, which reduced the heating time to only ten minutes. For the RTP studies, changes in layer thicknesses and surface roughness were monitored by ellipsometry and AFM at different steps.

Two triscarbazole-based hole transport copolymers containing different mole percentages (~10 or ~30%) of an oxetane co-monomer were synthesized and characterized. These copolymers (**5.40** and **5.41**) were doped with acid generators but several attempts to initiate the decomposition of the acid generator by UV irradiation to crosslink the oxetanes proved unsuccessful and alternative means to initiate crosslinking were pursued through the use of thermoacid generatora (TAG). Heating of the TAG

doped (7 wt%) thin films either by RTP or on a hot plate (for times between 15 – 30 minutes) produced insolubilized layers (confirmed by ellipsometry and AFM). Reduction of the TAG doping level was pursued and issues of layer dewetting upon heating were observed for levels less than 2 wt%; presumably due to competition between the dewetting process and the crosslinking reaction. Surface treatment of the silicon substrate (with piranha solution) was performed in order to raise its surface free energy and counteract the dewetting. On the treated surfaces, thin films that did not dewet could be obtained with TAG doping levels as low as 0.5 wt%. At lower doping levels, the layers were noted to decrease by ~ 20%, but were observed by AFM to remain generally smooth.

A new bis(styrene) triscarbazole-based small molecule (**5.42**) was synthesized and evaluated as a crosslinkable material. Issues of dewetting were encountered when processing **5.42** at room temperature onto silicon substrates. By treatment of the substrates with benzyl phosphonic acid modifiers, it was possible to produce thin films that could be insolubilized by RTP with 15 minutes of heating at 200 °C. PhOLEDs were fabricated using **5.42** as a hole transport layer for blue and green devices with promising efficiencies were obtained, but additional devices might produce additional improvements. The bis(styrene) substituent employed could also be incorporated into other small molecules to afford other potentially crosslinkable small molecules.

Overall, several crosslinkable materials were evaluated and crosslinked by rapid thermal processing that permitted insolubilization of thin films on substrates in 5 – 15 minutes. In addition, the side-chain functionalized crosslinkers developed could be combined with other charge transport-type co-monomers. Future work for these materials

should focus on testing RTP processed thin films in OLED devices to further explore the potential effects of the process on the thin films might have on device performance.

5.8. References

(1) So, F.; Kido, J.; Burrows, P. *MRS Bulletin* **2008**, *33*, 663-669.

(2) Hwang, M.-Y.; Hua, M.-Y.; Chen, S.-A. *Polymer* **1999**, *40*, 3233-3235.

(3) Ma, W.; Iyer, P. K.; Gong, X.; Liu, B.; Moses, D.; Bazan, G. C.; Heeger, A. J. *Adv. Mater.* **2005**, *17*, 274-277.

(4) Zhang, Y.; Huang, F.; Chi, Y.; Jen, A. K.-Y. *Adv. Mater.* **2008**, *20*, 1565-1570.

(5) Garcia, A.; Yang, R.; Jin, Y.; Walker, B.; Nguyen, T.-Q. *Appl. Phys. Lett.* **2007**, *91*, 153502.

(6) Zhang, Y.; Huang, F.; Jen, A. K.-Y.; Chi, Y. *Appl. Phys. Lett.* **2008**, *92*, 063303.

(7) Ji, J.; Narayan-Sarathy, S.; Neilson, R. H.; Oxley, J. D.; Babb, D. A.; Rondan, N. G.; Smith Jr., D. W. *Organometallics* **1998**, *17*, 783-785.

(8) Niu, Y.-H.; Liu, M. S.; Ka, J.-W.; Jen, A. K.-Y. *Appl. Phys. Lett.* **2006**, *88*, 093505.

(9) Lim, B.; Hwang, J.-T.; Kim, J. Y.; Ghim, J.; Vak, D.; Noh, Y.-Y.; Lee, S.-H.; Lee, K.; Heeger, A. J.; Kim, D.-Y. *Org. Lett.* **2006**, *8*, 4703-4706.

(10) Cava, M. P.; Deana, A. A. *J. Am. Chem. Soc.* **1959**, *81*, 4266.

(11) Ma, B.; Lauterwasser, F.; Deng, L.; Zonte, C. S.; Kim, B. J.; Fréchet, J. M. J. *Chem. Mater.* **2007**, *19*, 4827-4832.

(12) Niu, Y.-H.; Liu, M. S.; Ka, J.-W.; Bardeker, J.; Zin, M. T.; Schofield, R.; Chi, Y.; Jen, A. K.-Y. *Adv. Mater.* **2007**, *19*, 300.

(13) Cheng, Y.-J.; Liu, M. S.; Zhang, Y.; Niu, Y.; Huang, F.; Ka, J.-W.; Yip, H.-L.; Tian, Y.; Jen, A. K.-Y. *Chem. Mater.* **2008**, *20*, 413-422.

(14) Nakayama, Y.; Matsuda, T. *J. Polym. Sci. A* **1992**, *30*, 2451-2457.

(15) Rehab, A.; Salahuddin, N. *Polymer* **1999**, *40*, 2197-2207.

(16) Zhang, Y.-D.; Hreha, R. D.; Jabbour, G. E.; Kippelen, B.; Peyghambarian, N.; Marder, S. R. *J. Mater. Chem.* **2002**, *12*, 1703-1708.

(17) Domercq, B.; Hreha, R. D.; Zhang, Y.-D.; Larribeau, N.; Haddock, J. N.; Schultz, C.; Marder, S. R.; Kippelen, B. *Chem. Mater.* **2003**, *15*, 1491-1496.

(18) Zhan, X.; Haldi, A.; Yu, J.; Kondo, T.; Domercq, B.; Cho, J.-Y.; Barlow, S.; Kippelen, B.; Marder, S. R. *Polymer* **2009**, *50*, 397-403.

(19) Cho, J.-Y.; Domercq, B.; Barlow, S.; Suponitsky, K. Y.; Li, J.; Timofeeva, T. V.; Jones, S. C.; Hayden, L. E.; Kimyonok, A.; South, C. R.; Weck, M.; Kippelen, B.; Marder, S. R. *Organometallics* **2007**, *26*, 4816-4829.

(20) Kimyonok, A.; Domercq, B.; Haldi, A.; Cho, J.-Y.; Carlise, J. R.; Wang, X.-Y.; Hayden, L. E.; Jones, S. C.; Barlow, S.; Marder, S. R.; Kippelen, B.; Weck, M. *Chem. Mater.* **2007**, *19*, 5602-5608.

(21) Haldi, A.; Kimyonok, A.; Domercq, B.; Hayden, L. E.; Jones, S. C.; Marder, S. R.; Weck, M.; Kippelen, B. *Adv. Funct. Mater.* **2008**, *18*, 3056-3062.

(22) Crivello, J. V.; Falk, B.; Zonca, M. R. *J. Polym. Sci. A* **2004**, *42*, 1630.

(23) Dektar, J. L.; Hacker, N. P. *J. Am. Chem. Soc.* **1990**, *112*, 6004.

(24) Pappas, S. P.; Pappas, B. C.; Gatechair, L. R.; Jilek, J. H. *Polym. Photochem.* **1984**, *5*, 1.

(25) Dektar, J. L.; Hacker, N. P. *J. Photochem. Photobio. A* **1989**, *46*, 233.

(26) Crivello, J. V.; Bulut, U. *J. Polym. Sci. A* **2005**, *43*, 5217.

(27) Nuyken, O.; Bohner, R.; C, E. *Macromol. Symp.* **1996**, *107*, 125.
(28) Bayerl, M. S.; Braig, T.; Nuyken, O.; Müller, D.; Groß, M.; Meerholz, K. *Macromol. Rapid Commun.* **1999**, *20*, 224-228.
(29) Sangermano, M.; Giannelli, S.; Acosta Ortiz, R.; Berlanga Duarte, M. L.; Rueda Gonzalez, A. K.; Garcia Valdez, A. E. *J. Appl. Polym. Sci* **2009**, *112*, 1780.
(30) Nuyken, O.; Bacher, E.; Braig, T.; Fáber, R. M., F.; Rojahn, M.; Wiederhirn, V.; Meerholz, K.; Müller, D. *Des. Monomers Polym.* **2002**, *5*, 195-210.
(31) Bacher, E.; Bayerl, M. S.; Rudati, P.; Reckefuss, N.; Müller, C. D.; Meerholz, K.; Nuyken, O. *Macromolecules* **2005**, *38*, 1640-1647.
(32) Yang, X.; Müller, D.; Neher, D.; Meerholz, K. *Adv. Mater.* **2006**, *18*, 948-954.
(33) Müller, C. D.; Falcou, A.; Reckefuss, N.; Rojahn, M.; Wiederhirn, V.; Rudati, P.; Frohne, H.; Nuyken, O.; Becker, H.; Meerholz, K. *Nature* **2003**, *421*, 829-833.
(34) Tan, L.-S.; Venkatasubramanian, N.; Mather, P. T.; Houtz, M. D.; Benner, C. L. *J. Polym. Sci. A Poly. Chem.* **1998**, *36*, 2637-2651.
(35) Ouaknine, M.; Malik, I. J.; Odera, M.; Ishigaki, T.; Ueda, T.; Fukada, T.; Yoo, W. S.; Soussan, P.; Muller, P. *Microelect. Eng.* **2007**, *84*, 2646-2652.
(36) Shirai, M.; Tsunooka, M. *Bull. Chem. Soc. Jpn.* **1998**, *71*, 2483-2507.
(37) McEwen, W. E.; DeMassa, J. W. *Heteroatom Chem.* **1996**, *7*, 349-354.
(38) Reiter, G. *Phys. Rev. Lett.* **1992**, *68*, 75-78.
(39) Oslanec, R.; Costa, A. C.; Composto, R. J. *Macromolecules* **2000**, *33*, 5505-5512.
(40) Carroll, G. T.; Sojka, M. E.; Lei, X.; Turro, N. J.; Koberstein, J. T. *Langmuir* **2006**, *22*, 7748-7754.
(41) Kawai, A.; Nagata, H.; Morimoto, H.; Takata, M. In *Surface Modification Technologies VII*; Sudarshan, T. S., Ishizaki, K., Takata, M., Kamata, K., Eds. 1994, p 343-353.
(42) Al Akhrass, S.; Ostaci, R.-V.; Grohens, Y.; Drockenmuller, E.; Reiter, G. *Langmuir* **2008**, *24*, 1884-1890.
(43) Janssen, D.; De Palma, R.; Verlaak, S.; Heremans, P.; Dehaen, W. *Thin Solid Films* **2006**, *2006*, 1433-1438.
(44) Hotchkiss, P. J.; Li, H.; Paramonov, P. B.; Paniagua, S. A.; Jones, S. C.; Armstrong, N. E.; Bredas, J.-L.; Marder, S. R. *Adv. Mater.* **2009**, *21*, 1-6.
(45) Paniagua, S. A.; Hotchkiss, P. J.; Jones, S. C.; Marder, S. R.; Mudalige, A.; Marrikar, F. S.; Pemberton, J. E.; Armstrong, N. E. *J. Phys. Chem. C* **2008**, *112*, 7809-7817.

Chapter 6

Conclusions and Future Work

6.1. Summary of Conclusions

The aim of this thesis was to develop solution-processable charge-transport materials for applications in organic light-emitting diodes (OLEDs). In pursuit of this aim, different areas were studied including the development of hole-transporting side-chain polymers in Chapter 3. The design and synthesis of new ambipolar small-molecules and polymers was investigated in Chapter 4. Finally, issues concerning solution-processing of multilayers was addressed in Chapter 5 by developing several hole-transport copolymers and an example of a small-molecule incorporating different types of crosslinking functionalities.

In Chapter 3, a series of hole-transporting side-chain homopolymers were studied. Carbazole-based groups inspired by the organic electronics literature were successfully functionalized as side groups onto norbornene monomers. Examples of hole-transporting side-chain polymers reported in the literature have mostly been based on arylamine-type groups (such as **TPD** and **TPA**), which have triplet energies below 3.4 eV. Low triplet energies may limit the usefulness of hosts derived from these groups for high triplet energy emitters (> 3.5 eV). As part of the study, additional carbazole-based groups with reported high triplet energies (up ~ 4 eV) including triscarbazole and **mCP** were chosen as side-groups. High triplet energy polymers could be useful not only as hosts for phosphorescent emitters but also as hole-transport layers with triplet exciton blocking properties.

Examination of the UV-vis. spectra of the monomers synthesized showed that the majority had comparable absorption characteristics to the reported data for their small molecule analogues and suggesting the moieties remained largely unaffected by their attachment to norbornene. For monomers **3.36** and **3.38**, evidence of a weak charge-transfer state was observed and attributed to an electron-withdrawing effect from an ester type linker chain used to attach the mCP-type moiety to the norbornene monomer. Solid-state thin-film photoluminescence of the polymers were likewise consistent with the emission data for analogous small molecules, with the exception of mCP-type polymers **3.37** and **3.38** (with an ester group linker attached to the **mCP** benzene). For these polymers, a notable red shift in emission (~ 0.4 eV) was observed as compared to the **mCP** small molecule. mCP-type polymer **3.35** (with a different linker) had an emission maximum similar to **mCP** which implied the effect was originating from the linker. Oxidation potentials examined by cyclic voltammetry were in the range of 0.5 – 1.0 V. Monomers with oxidations closer to 0.5 V (with triscarbazole, carbazole, and CBP side-groups) could afford solution-processable hole-transport layers with easier of hole injection from the anode. The mCP-type polymers with higher oxidation potentials *ca*. 1.0 V may be better suited as host layers. For polymers with carbazoles blocked at the 3,6 positions (**3.28**, **3.32**, **3.42**, and **3.44**) reversible first oxidations were observed and attributed to prevention of carbazole-carbazole dimerization events. The increased electrochemical stability of the radical cations formed in solution could lead to carbazole-based side-chain polymers with similar resistance to dimerization events under OLED device operation and improve device stability/lifetime. It is noted that **PVK** and other arylamine-type side-chain polymers, possess irreversible oxidations. For CBP-type

polymer **3.41**, evidence of a reversible oxidation was observed that was in contrast to reports of irreversible oxidations noted for the small-molecule **CBP** and tentatively attributed to stabilization by the linker attached to one of the carbazoles of the radical cation formed on the same moiety. Based on these studies, the choice of linker and the substituent groups attached to the carbazole transport moiety can be used to tune the photophysical and electrochemical properties of the charge-transport side-chain polymer, if desired. Otherwise, attachment with minimal effects on the properties of the transport moiety could also be achieved.

OLED devices (fabricated in collaboration with Dr. Andreas Haldi of the Kippelen group) employing a few of the polymers as solution-processed hole-transport or host layers produced devices with promising efficiencies. As hole-transport layers external quantum efficiencies as high as 18.5% could obtained with polymer **3.29** (with all subsequent layers processed from vacuum). The ability to reduce the number of layers processed from vacuum has the potential to simplify the fabrication process and may likewise reduce the cost. As solution-processed host layers, some of the polymers produced external quantum efficiencies of ~1 for blue, 2 – 3% for white, and up to 6% for green OLEDs. For green devices, it was shown that solution-processed host layers were practical in producing high efficiencies. We also note that these layers were processed onto a solution-processed and crosslinked hole-transport layer thereby requiring that only the electron transport and cathode be vacuum deposited. Although encouraging device results were obtained, questions remained as to whether further improvement of unipolar polymers as hosts would be possible. This was based on the view that improving the balance of charge carriers with the emissive layer might lead to

better recombination efficiency and a potentially larger recombination zone shifted away from the transport layer interfaces.

Chapter 4 sought to address some of the perceived limitations of unipolar hosts by development of new ambipolar small-molecules containing carbazole groups in combination with either oxadiazole or triazole (electron-deficient heterocycles).

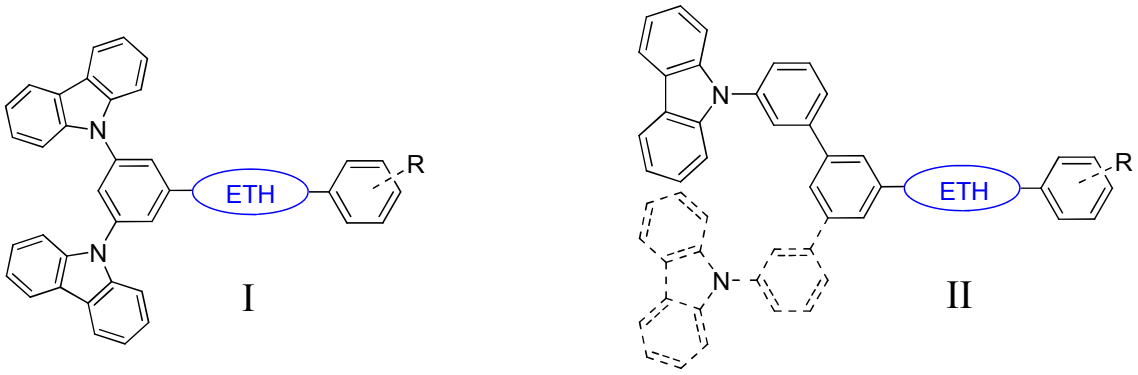

Figure 6.1. Ambipolar small-molecule design types: **I** and **II** (where ETH = electron transport heterocycles (oxadiazole or triazole) and R = H or methoxy).

For these molecules, *meta*- conjugation (across benzene group(s)) was chosen to minimize charge-transfer interactions between the hole- and electron- transport moieties. Strong interactions have the potential to reduce the optical gap and triplet energy. The effect of introducing a phenyl spacer to further decouple the transport groups was also explored. In order to obtain solution-processable ambipolar materials, the small-molecules synthesized were converted to norbornene monomers and subsequently to polymers.

The absorption spectra of type I oxadiazole small molecules showed evidence of a weak charge-transfer state between oxadiazole and carbazole. Upon introduction of a phenyl spacer (type II) the oxadiazole-containing molecules showed a hypsochromically shifted onset by ~ 0.25 eV. This effect was attributed to weaker coupling between the

carbazole and oxadiazole groups. For the triazole based molecules, the absorption onsets were similar (~ 360 nm) for both types of molecular designs. In these molecules, the triazole and carbazole may be sufficiently decoupled due to the twist of the former (see Chapter 4), even in the type I design, that the introduction of the phenyl spacer has no appreciable effect on the onset. Solution photoluminescence showed that the emission maxima of the polymers were in the range of 390 – 430 nm, suggesting these molecules might function as hosts for high energy emitters such as FIrpic. The triazole-based ambipolar molecules emitted at higher energies than the oxadiazole equivalent molecules, with maxima just below 400 nm. For the oxadiazole molecules, introduction of a phenyl spacer induced blue shifts of up to 0.1 eV in the emission maximum, as compared to the non-spaced molecules. The spacer group had no appreciable effect on the emission maxima between type I or type II triazole molecules. Interestingly, dual emission was noted in the type II molecules incorporating either oxadiazole or triazole. The effect was most significant for the triazole molecule with evidence of emission from both a charge-transfer excited state and a more localized excited state (attributed to the phenyl carbazole portion of the molecule) with two structured emission peaks in the range of 340-360 nm. Additional theoretical studies are planned to investigate the more complex emission. Comparing the design approaches (I *vs*. II) on the basis of the emission data showed that the introduction of the phenyl spacer could be used to produce hypsochromic shifts in emission maxima for the oxadiazole-based targets. The approach might also prove useful with other ETHs. Solid-state fluorescence spectra of the side-chain polymers possessed emission maxima that were moderately blue-shifted compared to solution. Measurement of phosphorescence at 77K permitted calculation of the triplet

energies of oxadiazole and triazole molecules with type I design. The triplet energies were estimated to be ~2.7 eV for the former and ~3 eV for the latter. The 0.3 eV difference indicated that the choice of electron transport heterocycle plays an important role in determination of the triplet energy. Cyclic voltammetry measurements revealed very similar oxidation potentials for all the ambipolar molecules *ca*. 1.0 V. The similarity in the oxidation potentials amongst all the targets suggests the HOMO is located on the carbazoles. The reduction potentials showed moderate changes upon introduction of the phenyl spacer while comparison between analogous molecules with oxadiazole and triazole heterocycles showed much greater differences. In both cases the data implied that the LUMO is very likely localized on the ETH groups, with perhaps some delocalization into the peripheral phenyls. For the triazole-containing targets, the reductions were more difficult by ~ 0.4 V (as compared to oxadiazole-containing molecules *ca*. -2.3 eV). While changing the ETH from oxadiazole to triazole resulted in blue shift of the emission and a higher triplet energy, the increase in the reduction potential of the triazole-based molecules suggests they may act as poorer electron acceptors.

Type I oxadiazole and triazole-containing small-molecules were evaluated as vacuum-processed hosts for green and blue PhOLED devices (by Dr. Dengke Cai of the Kippelen group). For these devices, efficiencies up to 16.6% (for green) and 12.7% (for blue) were obtained in unoptimized devices using oxadiazole type I hosts, suggesting that these ambipolar molecules are promising host materials. Test devices incorporating the remaining untested ambipolar small molecules and polymers are planned.

Chapter 5 explored a series of crosslinkable materials that could be processed from solution. Crosslinking was evaluated in order to facilitate processing of multilayers

without damaging or destroying the prior solution deposited layer(s). Several triscarbazole-based hole transport materials including copolymers and an example of triscarbazole small-molecule containing different thermally crosslinkable groups (including benzocyclobutene, trifluorovinyl ether, and styrenes) were synthesized. These materials were spin-coated as thin-films and different heating methods (including hot plate and rapid thermal processing (RTP)) were applied to insolubilize the films. Although heating for several hours (up to 4) on a hot plate (at temperatures below 250 °C) was shown to produce solvent resistant films, the need for several hours was considered a limiting factor to utilizing crosslinking for commercial OLED layer fabrication. In order to decrease the heating times required, rapid thermal processing was examined as a means to very rapidly and uniformly heat the crosslinkable thin-films. Using this method, it was found that heating for as short as five minutes could produce bulk insolubilization of the crosslinkable copolymers and small-molecule. Two additional triscarbazole-based hole transport copolymers containing oxetane group co-monomers were also synthesized and studied as crosslinkable materials. When doped with thermoacid generators and heated (200 °C), thin-films of these copolymers produced insolubilized thin-films. Layer dewetting upon heating above the glass transition temperature was observed for TAG doping levels below 2 wt% and attributed to a faster rate of dewetting *vs*. crosslinking. Raising the surface free energy of the substrate was used to counteract the dewetting process and for treated surfaces, TAG doping levels as low as 0.5 wt% were shown to be effective at producing insolubilized layers, although some loss of thickness of approximately 20% was observed. Some preliminary devices were fabricated by Dr. Dengke Cai using the small molecule bis(styrene) triscarbazole

with promising results, further studies on all the crosslinkable materials developed in devices are required in order to better understand the feasibility and effects of crosslinking on device performance.

In conclusion, the work discussed in this thesis showed that solution-processable side-chain polymers could be used effectively as hole-transport or host layers in phosphorescent OLEDs. It was also shown that new small-molecules (and side-chain polymers incorporating these molecules) with combined hole and electron transport groups possessed photophysical and electrochemical properties suggestive of their potential as ambipolar hosts for high triplet energy guest emitters. OLED devices incorporating these molecules further showed that these materials were indeed promising hosts for high E_T emitters. Finally, a variety of crosslinkable materials were shown to successfully form insolubilized layers on reduced time scales (30 min or less) by thermal treatment using RTP. Overall, each of the areas explored in Chapters 3, 4, and 5 provided valuable insight into the development of new types of charge-transport molecules and side-chain charge-transport polymers. Furthermore, the solution-processability of the polymers could be used to reduce the number of layers that have to be processed by vacuum sublimation. Hybrid devices with solution-processed hole and host layers (as studied in Chapter 3) further demonstrated that practical efficiencies (up to 6%) could be achieved that might be viewed as competitive against fully vacuum-processed hosts. While the efficiencies for polymer-based OLED may never match those of vacuum-processed devices, the reduction in processing time and fabrication costs for polymers may outweigh the reduction in efficiencies. Despite the encouraging findings, additional

studies are warranted including lifetime determination in order to further establish the usefulness of side-chain charge-transport polymers.

6.2. Future Work

Short-term future work for the materials discussed above should include an examination of the charge transport mobilities in order to determine any effects from attachment of the charge-transport moieties as side groups as well as on the polymers obtained. For the ambipolar hosts, determination of the hole and electron mobilities would useful in elucidating the relative balance of the carriers in the emissive layer. Further examination of the triplet energies of the hosts and polymers should also be performed. For the crosslinkable materials additional devices should be fabricated to study the effects of crosslinking on performance. Lastly, device lifetime studies would be highly valuable as little can be said about the long-term performance and stability of any of the devices discussed above.

Based on the promising results found for side-chain polymers, future work could include development and studies of side-chain polymers combining different monomer groups, linkers, and charge transport moieties. New hole-, electron-, or ambipolar as side-groups could be functionalized onto monomer groups and used to produce various types of charge-transport polymers.

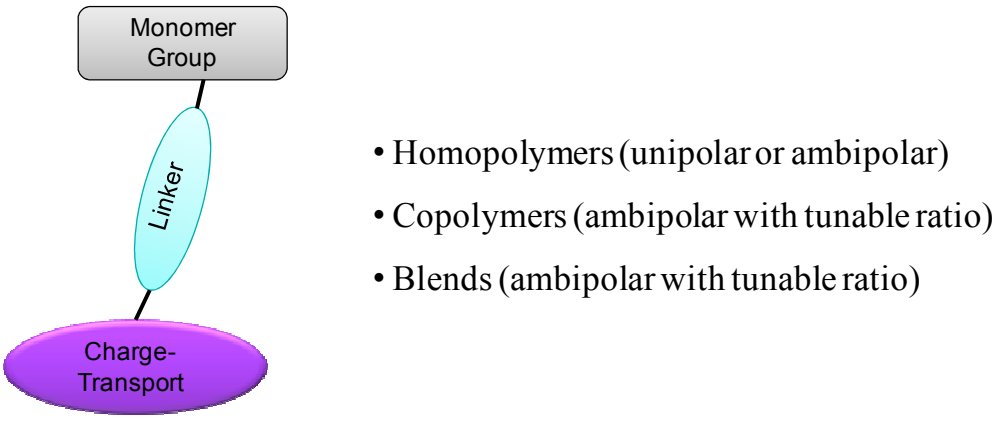

Figure 6.2. Representative side-chain monomer (where the charge-transport group represents either a hole-, electron-, or ambipolar-type moiety) and the potential uses of such monomers.

In addition to unipolar or ambipolar homopolymers containing a single type of transport group, copolymers or blends of homopolymers could also be used to achieve ambipolar emissive layers. One possible advantage of copolymers and blends might be the ability to tune the ratio of the charge-transport groups leading to better charge balance or permitting some influence on the location (and/or size) of the recombination zone. Despite the potential advantages, additional complications such as phase segregation could arise in these copolymer/blend systems which are currently being studied by Dr. Xuyang He in our group.

Further work on ambipolar single molecules might investigate modification of the triazole group at the phenyl substituent in order to improve the electron transport properties of the heterocycle. In addition, combinations of carbazoles with other electron-deficient groups, such as triazine, pyrimidine, and borane-containing groups, could result in new ambipolar hosts with improved electron transport properties, while retaining sufficiently high triplet energies suitable for hosting blue emitters. These new

ambipolar molecules could be used as vacuum-processable hosts or converted to solution-processable polymers.

With respect to crosslinking, the side-chain co-monomers developed and studied in Chapter 5 could be easily copolymerized with different charge transport co-monomers to afford new types of crosslinkable layers. The bis(styrene) group used in the small-molecule triscarbazole target might also be incorporated into other potentially solution-processable small-molecules for use as host or charge transport materials. Furthermore, evaluation of the performance of RTP crosslinked layers in actual OLED devices would also be of interest.